FORCE Technology

Project No. and Title of Report:					
ONRII187 01 **PMM model test with DDG51 including uncertainty assessment**					
Client: ONR			***Client's Ref.:***		
Author(s): Claus D. Simonsen			***Date:*** 3/19/2004 ***Approved by:***		
A					
Revision	***Description***	***By***	***Checked***	***Approved***	***Date***
Keywords: PMM test, experimental uncertainty assessment			***Classification:*** □ **Open** □ **Internal** □ **Confidential**		

Classification and approval:

Classification: Open

Definitions:

Public

The document may be freely distributed after successful review by and with the Client given the Client's permission.

Confidential for the duration of the project:

As for Confidential, but only for the duration of the project. After final Project Approval by the Client, status for reports classified Confidential for the duration of the project are automatically downgraded to Public.

Confidential:

The document is for the use of the Client and FORCE, and shall not be used or disclosed to third parties without the unanimous agreement between the partners and the Client.

Client:

ONR

Partners:

FORCE Technology, Department of Maritime Industry (DMI)
Hjortekærsvej 99
DK 2800 Lyngby
Denmark

phone: + 45 72 15 77 00
fax: + 45 72 15 77 01
e-mail: cds@force.dk

IOWA Institute of Hydraulic Research (IIHR)
College of Engineering, The University of Iowa
Iowa City, Iowa
USA

Distribution list:

No. 1 nn
No. 2 nn
No. 3 nn
No. 4 nn
No. 5 nn
No. 6 nn
No. 7 nn
No. 8 nn
No. 9 nn
No. 10 nn

Document history:

Issue	Date	Initials	Revised pages	Status / Changes implemented
001	27.10.2003	CDS		Preliminary draft issue
002	25.11.2003	CDS		Update on data reduction equations
003	24.02.2004	CDS		Inclusion of experimental results
004	19.03.2004	CDS		Final update

Authors:

Claus Daniel Simonsen

Lyngby March 19th 2004

LIST OF CONTENTS: **PAGE:**

1. Introduction

The present report deals with the work required in order to 1) assess the experimental uncertainties related to the Planar Motion Mechanism (PMM) test, 2) provide PMM data for comparison with PMM data from the IIHR towing tank and 3) validate CFD codes. The scope is to develop a procedure for the uncertainty assessment, which can be used in connection with measurements of the integrated forces acting on ship models using the PMM apparatus. The procedure only covers the measured hydrodynamic forces. This means that uncertainties related to the traditional maneuvering coefficients and their application in connection with maneuvering simulations are not dealt with.
To test the procedure it is applied to a PMM test with a 4-meter model of the *DDG51 frigate*. Normally, the PMM testing in FORCE Technology's towing tank is conducted with 7 to 8 meter models, so the present model is close to the lower limit of the model sizes to be used for PMM tests. This is both with respect to mounting the PMM equipment in the model and to be able to measure forces of a reasonable magnitude. However, with the choice of benchmark ship in the present project, the 4-meter model has to be used.
Finally, it must be noted that the uncertainty analysis covered in the present report is mostly related to the conventional Planar Motion Mechanism. Consequently, some aspects may be somewhat different for mechanisms having separated X-, Y- and PHI-carriages.

2. Facility

The PMM tests are conducted in FORCE Technology's towing tank in Lyngby, Denmark. The towing tank is 240m long, 12m wide and 5.5m deep.

3. Model

The applied model is a 1:35.48 scale model of the hull of the *DDG51 frigate*. The full scale and model scale hull particulars are given in Table 3.1. The test is conducted with the bare hull appended with bilge keels only.

The DDG51 frigate			
		Ship	Model
Scale	-	1 : 1	1 : 35.48
L_{PP}	m	142.00	4.0023
L_{WL}	m	142.18	4.0083
B_{WL}	m	19.10	0.5382
T_m	m	6.16	0.1736
∇	m^3	8472	0.1897
Δ	Ton	8684	0.1897
C_b	-	0.506	0.506

Table 3.1. Full scale and model scale particulars

4. Test conditions

The considered experimental test conditions cover a set of tests, which are representative for a standard 1st quadrant PMM test and which can be used for assessment of the experimental uncertainty for representative conditions.
The PMM testing technique enables various test conditions to be studied individually. The conditions, which are considered in this work, are “pure drift”, “pure sway”, “pure yaw” and “yaw and drift”. The first is a static test, meaning that the model is towed in the same steady condition through the tank, while the three remaining tests are dynamic, i.e. the model is oscillating. The contents of the tests can be summarized as follows:

“**Pure drift**”:
The model travels through the tank in oblique flow due to a given drift angle β.

“**Pure sway**”:
The model travels through the tank on straight ahead course while it is oscillated from side to side. With u, v and r being the surge velocity, the sway velocity and the yaw rate in the ships local coordinate system, the pure sway motion can also be expressed in terms of the velocities, i.e. $u = U_C$ (carriage speed), $r = 0$ and v oscillates harmonically.

“**Pure Yaw**”:
The model travels through the tank while it performs a pure yaw motion, where it is forced to follow the tangent of the oscillating path. In terms of velocities this means that $v = 0$, while r and u oscillate harmonically. u oscillates, since the carriage speed in the present set-up is constant.

“**Yaw and drift**”:
The model travels through the tank, while it performs a pure yaw motion as described above. However, a fixed and preset drift angle is overlaid on the motion in order to obtain a drift angle relative to the tangent of the oscillating path. In terms of velocities this means that $v \neq 0$, but constant, while r and u oscillate harmonically.

For all of the above conditions, the tests will be conducted according to FORCE’s standard PMM testing procedures. This means that the model will be constrained in roll but free to heave and pitch. Further, Three approach speeds corresponding to the Froude numbers: $Fr = 0.138$, $Fr = 0.280$ and $Fr = 0.410$ are tested. The test programs for the three speeds, including repeat tests for uncertainty assessment are shown in Appendix A.

5. Measured quantities

For all of the conditions outlined in Section 4, the quantities listed in Table 5.1 are measured during each run, as is standard practice in DMI PMM tests. Measurements 0 through 5 provide the instantaneous operating conditions for the ship and 6 through 9 provide the resultant forces.

All forces are measured in a coordinate system following the ship, meaning that *X*-components act in the longitudinal direction of the ship and *Y*-components perpendicular

to this direction. The yaw moment is taken with respect to the mid-ship position at $L_{pp}/2$. All hydrodynamic forces and moments presented in the present work are non-dimensionalized by the following data reduction equations

$$X' = \frac{F_{X_{Hydro}}}{0.5\rho U^2 A_0}, \quad Y' = \frac{F_{Y_{Hydro}}}{0.5\rho U^2 A_0}, \quad N' = \frac{M_{Z_{Hydro}}}{0.5\rho U^2 A_0 L_{pp}} \tag{5.1}$$

where ρ is the water density. $U = \sqrt{u^2 + v^2}$ is the ship speed. It is constant in the static test, but it varies in the dynamic test. A_0 is the lateral underwater area defined as $A_0 = L_{pp} T_m$. L_{pp} and T_m are the length between perpendiculars and the mean draft, respectively. Furthermore L_{pp} is used as characteristic arm for the yaw moment.

ID	Quantity	Sampling frequency [Hz]
0	Ship speed	5
1	Sinkage, forward	45
2	Sinkage, aft	45
3	PMM cosine	45
4	PMM sine	45
5	PMM rpm	5
6	X-force, forward	45
7	X-force, aft	45
8	Y-force, forward	45
9	Y-force, aft	45

Table 5.1. Overview of measured quantities.

6. Brief description of the PMM motion generation

As mentioned above the PMM test consists of static and dynamic motions. In the static case, the motion is purely dependent of the carriage speed U_C and the specified drift angle β relative to the towing direction. The different static drift cases are obtained as a combination of the carriage speed and the specified angles. See Figure 6.1.

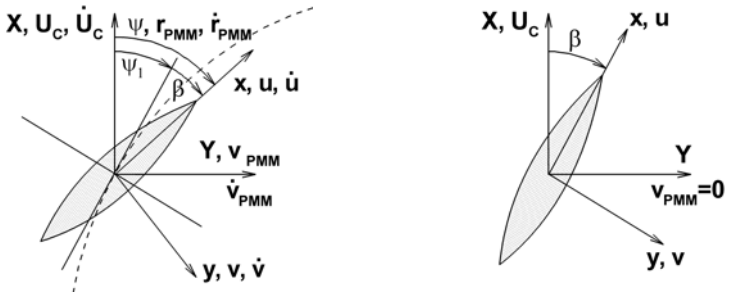

Dynamic PMM Static PMM

Figure 6.1. Definition of tests and motion parameters.

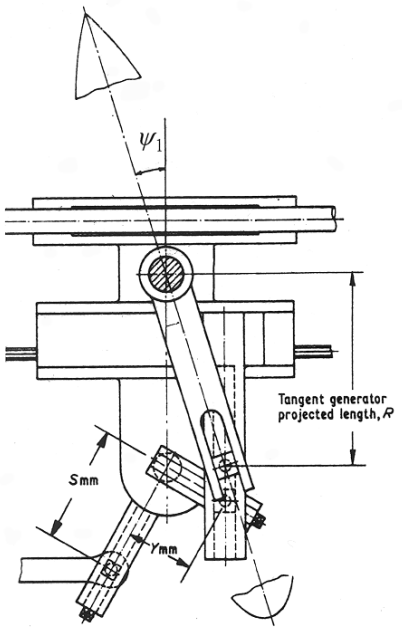

Figure 6.2. Scotch yoke type mechanism.

In the dynamic PMM test the applied cyclic motion is generated by means of a Scotch yoke type mechanism, see Figure 6.2. The idea is to construct a prescribed motion in which the heading, ψ, the surge, u, the sway, v, and yaw, r, velocities and the surge, $\dot{u}$, sway, $\dot{v}$, and yaw, $\dot{r}$, accelerations (in the ships local (x, y) coordinate system) are known to any given time. The motion is composed by means of 1) the carriage speed, U_C, 2) a PMM generated oscillating translation of the model from side to side (perpendicular to the towing direction) defined by the velocity v_{PMM} and the acceleration $\dot{v}_{PMM}$, 3) a PMM generated horizontal rotation from side to side of the model around the mid-ship position, defined by the angular velocity r_{PMM} and the angular acceleration $\dot{r}_{PMM}$ and 4) a drift angle β if the yaw and drift condition is considered. See Figure 6.1. The time dependent motion parameters above can basically be described by means of four quantities. These are the sway crank amplitude, S_{mm}, the yaw crank amplitude Y_{mm}, the number of PMM rotations per minute, N and the projected length of the tangent generator fork, R. The following relations are used (Chislett and Wagner Smitt, 1973):

Heading:

$$\psi = \psi_1 + \beta = -\arctan\left(\frac{Y_{mm}}{R}\cos\left(\frac{2\pi N}{60}t\right)\right) + \beta = -\arctan(a\cos(\omega t)) + \beta \qquad [rad] \tag{6.1}$$

Yaw rate:

$$r_{PMM} = \frac{Y_{mm}}{R}\left(\frac{2\pi N}{60}\right)\sin\left(\frac{2\pi N}{60}t\right)\frac{1}{1+\left(\frac{Y_{mm}}{R}\cos\left(\frac{2\pi N}{60}t\right)\right)^2} = a\omega\sin(\omega t)\frac{1}{1+(a\cos(\omega t))^2} \tag{6.2}$$

Yaw acceleration:

$$\dot{r}_{PMM} = \frac{Y_{mm}}{R}\left(\frac{2\pi N}{60}\right)^2 \cos\left(\frac{2\pi N}{60}t\right)\left[\frac{1+\left(\frac{Y_{mm}}{R}\right)^2\left(1+\sin^2\left(\frac{2\pi N}{60}t\right)\right)}{\left(1+\left(\frac{Y_{mm}}{R}\cos\left(\frac{2\pi N}{60}t\right)\right)^2\right)^2}\right] = a\omega^2\cos(\omega t)\left[\frac{1+a^2(1+\sin^2(\omega t))}{\left(1+(a\cos(\omega t))^2\right)^2}\right] \tag{6.3}$$

Transverse translation:

$$\eta_{PMM} = -2S_{mm}\sin\left(\frac{2\pi N}{60}t\right) = -2S_{mm}\sin(\omega t) \tag{6.4}$$

Transverse velocity:

$$v_{PMM} = -2\frac{2\pi N}{60}S_{mm}\cos\left(\frac{2\pi N}{60}t\right) = -2\omega S_{mm}\cos(\omega t) \tag{6.5}$$

Transverse acceleration

$$\dot{v}_{PMM} = 2\left(\frac{2\pi N}{60}\right)^2 S_{mm}\sin\left(\frac{2\pi N}{60}t\right) = 2\omega^2 S_{mm}\sin(\omega t) \tag{6.6}$$

where $a = Y_{mm}/R$ and $\omega = (2\pi N)/60$.

It must be noted that the yaw rate and acceleration are the same in the global and local coordinate systems for all conditions, i.e. $r = r_{PMM}$ and $\dot{r} = \dot{r}_{PMM}$. For the sway velocity and acceleration it is different. In pure sway $v = v_{PMM}$ and $\dot{v} = \dot{v}_{PMM}$, but in pure yaw and yaw and drift $v \neq v_{PMM}$ and $\dot{v} \neq \dot{v}_{PMM}$ so transformations are required. This is described later in the report. Finally, for the pure yaw condition the following relation must be satisfied in order to obtain the correct motion where the models center plane is tangent to traveled path:

$$S_{mm} = \frac{U_0}{2R}\frac{60}{2\pi N}Y_{mm} = \frac{U_0}{2\omega R}Y_{mm} \tag{6.7}$$

7. Uncertainty analysis

Following the approach in (ITTC 1999a and b) the uncertainty assessment, which covers both precision and bias limits, will be based on the data reduction equations for the forces and moments. In the present application, the equations used in the maneuvering community (5.1), will be used.

When the forces are measured during the test, they include both hydrodynamic forces and inertial forces related to the mass of the model, so in order to extract the hydrodynamic component only, it is necessary to subtract the inertial contributions from

the measured quantity. Based on the equations of motion of a ship in 3 degrees of freedom in the ships coordinate system (Chislett, 1990) one has

$$-F_{X_{measured}} + F_{X_{hydro}} = M(\dot{u} - rv - X_G r^2 - Y_G \dot{r}) \tag{7.1}$$

$$-F_{Y_{measured}} + F_{Y_{hydro}} = M(\dot{v} + ru - Y_G r^2 + X_G \dot{r}) \tag{7.2}$$

$$-M_{Z_{measured}} + M_{Z_{hydro}} = I_Z \dot{r} + M(X_G(\dot{v} + ru) - Y_G(\dot{u} - rv)) \tag{7.3}$$

If the hydrodynamic components in these equations are isolated and inserted into (5.1) one has the following data reduction equations

$$X' = \frac{F_{X_{measured}} + M(\dot{u} - rv - X_G r^2 - Y_G \dot{r})}{0.5\,\rho U^2 T_m L_{pp}} \tag{7.4}$$

$$Y' = \frac{F_{Y_{measured}} + M(\dot{v} + ru - Y_G r^2 + X_G \dot{r})}{0.5\,\rho U^2 T_m L_{pp}} \tag{7.5}$$

$$N' = \frac{M_{Z_{measured}} + I_Z \dot{r} + M(X_G(\dot{v} + ru) - Y_G(\dot{u} - rv))}{0.5\,\rho U^2 T_m L_{pp}^2} \tag{7.6}$$

where $F_{X_{measured}}$, $F_{Y_{measured}}$ and $M_{Z_{measured}}$ are the measured total *X*- and *Y*-forces and the measured yaw moment, respectively. ρ is the water density and U is the model speed defined as $U = \sqrt{u^2 + v^2}$. u and v are the surge and sway velocities, respectively and r is the yaw rate. Finally, the dots above the velocity quantities indicate the corresponding accelerations. T_m and L_{pp} are the mean draft and the length between perpendiculars. M and I_Z are the mass and moment of inertia of the model, i.e. of the model itself, the gauges and the ballast weights. X_G and Y_G are the *X*- and *Y*-distances from the center of gravity of the model to the point, which the model rotates around. The equations (7.4) to (7.6) are applied to the dynamic tests, but if static tests are considered, i.e. when the yaw rate and the surge, sway and yaw accelerations are zero, the equations reduce to

$$X' = \frac{F_{X_{measured}}}{0.5\,\rho U^2 T_m L_{pp}} \tag{7.7}$$

$$Y' = \frac{F_{Y_{measured}}}{0.5\,\rho U^2 T_m L_{pp}} \tag{7.8}$$

$$N' = \frac{M_{Z_{measured}}}{0.5\,\rho U^2 T_m L_{pp}^2} \tag{7.9}$$

where $U = \sqrt{(U_c \cos(\beta))^2 + (-U_c \sin(\beta))^2} = U_C$, i.e. the carriage speed.

Based on the multiple test approach, the total uncertainty for the average (calculated on the basis of a number of repeated tests) *X*- and *Y*-forces and yaw moment are given by

$$U_{\bar{X}'}^2 = B_{X'}^2 + P_{\bar{X}'}^2 \tag{7.10}$$

$$U_{\bar{Y}'}^2 = B_{Y'}^2 + P_{\bar{Y}'}^2 \tag{7.11}$$

$$U_{\bar{N}'}^2 = B_{N'}^2 + P_{\bar{N}'}^2 \tag{7.12}$$

where *B* and *P* are the bias (systematic errors) and precision (random errors) limits, respectively. (ITTC 1999a and b). Expressions for the individual components are described in the following sections.

7.1 Limitations of the present method

Before the methods for estimation of the errors are described, the limitations and assumptions of the method will be listed:

1: It must be noted that the present work is focused on the force level only. This means that the uncertainties are estimated only for the coefficients defined above and that the uncertainties related to the traditional hydrodynamic derivatives and their influence on later full scale maneuvering simulations are not considered.

2: The theory presented below is to be applied for static drift tests and for dynamic pure sway, pure yaw and combined yaw and drift tests.

3: The considered results from each run are not the instantaneously measured values, but either mean values or faired values. For the static tests this means that the forces and moments are mean values, which are obtained as an average of the instantaneously measured values from each run. For the dynamic tests the resulting time varying forces and moments for one motion period are obtained by fairing with Fourier series consisting of eight harmonics. The fairing is based on the four to five periods, which are measured in each run. The uncertainty introduced via the static averaging and the dynamic fairing is not considered in the present work.

4: The effect of roll is not considered, so the model is fixed with zero heel angle, $\varphi = 0$. Consequently, the uncertainty analysis does not include this degree of freedom. However, this also means that the analysis does not account for errors in the upright position, i.e. if the heel angle is not exactly zero. In order to account for this effect is necessary to go back and redo the presented analysis based on the equations of motion including roll and heel.

5: In the theory presented below, it is assumed that the model movement is based on pure harmonic motions. However, if this is not the case, the uncertainty analysis should be extended in order to investigate how deviations from the pure harmonic motions influence the results.

6: In the present analysis the carriage acceleration is assumed to be zero. Therefore, uncertainties related to acceleration of the carriage, which is introduced via variations in the carriage speed during the run, are not accounted for.

7: The uncertainty related to time is also included in the uncertainty analysis. It may be possible to do it differently, but the way it is done in this context is to introduce time via the motion parameters. This means that time does not directly appear in the influence coefficients for the data reduction equations. Instead, it is indirectly included as an additional uncertainty component in the time varying motion parameters. The idea is to treat time as an input variable in the expressions for the motion parameters, similar to the PMM settings for instance, and then derive the influence coefficients by differentiation of these expressions with respect to time.

8: As seen in Section 5, the carriage speed is sampled with a frequency of 5 Hz, while the forces are sampled with 45 Hz. Therefore, if two subsequent speed measurements are made at t_0 and t_1 there will be a time lack between the speed measurement at t_0 and the following 7 force measurements taken between t_0 and t_1. In order to overcome this problem and obtain speeds, which correspond to the times for which the forces are measured, linear interpolation is applied. The effect of this interpolation is not considered in the uncertainty analysis.
Another time lack, which is much smaller than the one previously described, occurs during the scan of the channels. If the sampling frequency is 45 Hz, the time period between two samples will be $\Delta t = 1/45$ second. In the beginning of this time period the channels are scanned one after the other and then nothing happens until it is time for the next sampling. The time assigned to all the channel readings within the sample will be the same, but there will be a time lack between the scan of the first and last channel for instance. However, since the present test only involves 10 channels, this time lack is small, so no correction is performed. Instead, the effect is accounted for by means of an uncertainty in time. In the following uncertainty analysis it is assumed that the scanning takes place during the first $1/10\Delta t = 0.0022$ seconds of the time between two samples. This number is then used as the uncertainty in time.

9: Sinkage at AP and FP is presented in the report, but no bias error estimates are made for these quantities. Though, data to be used for precision limit estimates is available from the repeat test program, so the sinkage is presented with the precision limits based on this data.

7.2 Definition of bias limits

The bias limits will be assessed based on a study of the measuring system. According to (ITTC 1999a) they can be estimated on the basis of

$$B_r^2 = \sum_{i=1}^{J} \theta_i^2 B_i^2 + 2\sum_{i=1}^{J-1}\sum_{k=i+1}^{J} \theta_i \theta_k B_{ik} \tag{7.13}$$

where θ_i is the influence coefficient defined by

$$\theta_i = \frac{\partial r}{\partial X_i} \tag{7.14}$$

B_i are the bias limits in X_i and B_{ik} are the correlated bias limits in X_i and X_k

$$B_{ik} = \sum_{\alpha=1}^{L} (B_i)_\alpha (B_k)_\alpha \tag{7.15}$$

where L is the number of correlated bias error sources that are common for measurement of variables X_i and X_k.

The bias error for each variable in the data reduction equation may consist of a number of bias errors, so in order to calculate the combined bias error the root-sum-square is used

$$B_i^2 = \sum_{k=1}^{J} (B_i)_k^2 \tag{7.16}$$

i is the number of the considered variable in the data reduction equation.

7.2.1 Non-dimensional longitudinal force, X'

For the dynamic tests the bias limit equation for X' is given by (7.13)

$$\begin{aligned} B_{X'}^2 = {} & \theta_{F_{X\,measured}}^2 B_{F_{X\,measured}}^2 + \theta_\rho^2 B_\rho^2 + \theta_{T_m}^2 B_{T_m}^2 + \theta_{L_{pp}}^2 B_{L_{pp}}^2 + \theta_M^2 B_M^2 + \theta_{X_G}^2 B_{X_G}^2 + \theta_{Y_G}^2 B_{Y_G}^2 + \\ & \theta_u^2 B_u^2 + \theta_{\dot{u}}^2 B_{\dot{u}}^2 + \theta_v^2 B_v^2 + \theta_r^2 B_r^2 + \theta_{\dot{r}}^2 B_{\dot{r}}^2 \end{aligned} \tag{7.17}$$

In this expression it is assumed that none of the variables are correlated. The influence coefficients are found from applying (7.14) on (7.4).

$$\theta_{F_{X\,measured}} = \frac{\partial X'}{\partial F_{X_{measured}}} = \frac{2}{\rho(u^2+v^2)T_m L_{pp}} \tag{7.18}$$

$$\theta_\rho = \frac{\partial X'}{\partial \rho} = \frac{-2\,(F_{X_{measured}} + M(\dot{u} - rv - X_G r^2 - Y_G \dot{r}))}{\rho^2(u^2+v^2)T_m L_{pp}} \tag{7.19}$$

$$\theta_{T_m} = \frac{\partial X'}{\partial T_m} = \frac{-2\,(F_{X_{measured}} + M(\dot{u} - rv - X_G r^2 - Y_G \dot{r}))}{\rho(u^2+v^2)T_m^2 L_{pp}} \tag{7.20}$$

$$\theta_{L_{pp}} = \frac{\partial X'}{\partial L_{pp}} = \frac{-2\,(F_{X_{measured}} + M(\dot{u} - rv - X_G r^2 - Y_G \dot{r}))}{\rho(u^2+v^2)T_m L_{pp}^2} \tag{7.21}$$

$$\theta_M = \frac{\partial X'}{\partial M} = \frac{2(\dot{u} - rv - X_G r^2 - Y_G \dot{r})}{\rho(u^2+v^2)T_m L_{pp}} \tag{7.22}$$

$$\theta_{X_G} = \frac{\partial X'}{\partial X_G} = \frac{-2Mr^2}{\rho(u^2+v^2)T_m L_{pp}} \tag{7.23}$$

$$\theta_{Y_G} = \frac{\partial X'}{\partial Y_G} = \frac{-2M\dot{r}}{\rho(u^2+v^2)T_m L_{pp}} \tag{7.24}$$

$$\theta_u = \frac{\partial X'}{\partial u} = \frac{-4u\,(F_{X_{measured}} + M(\dot{u} - rv - X_G r^2 - Y_G \dot{r}))}{\rho(u^2+v^2)^2 T_m L_{pp}} \tag{7.25}$$

$$\theta_{\dot{u}} = \frac{\partial X'}{\partial \dot{u}} = \frac{2M}{\rho(u^2+v^2)T_m L_{pp}} \tag{7.26}$$

$$\theta_v = \frac{\partial X'}{\partial v} = \frac{2}{\rho(u^2+v^2)T_m L_{pp}}\left[-Mr - \frac{2v\left(F_{X_{measured}} + M(\dot{u} - rv - X_G r^2 - Y_G \dot{r})\right)}{(u^2+v^2)}\right] \tag{7.27}$$

$$\theta_r = \frac{\partial X'}{\partial r} = \frac{-2M(v + 2X_G r)}{\rho(u^2+v^2)T_m L_{pp}} \tag{7.28}$$

$$\theta_{\dot{r}} = \frac{\partial X'}{\partial \dot{r}} = \frac{-2MY_G}{\rho(u^2+v^2)T_m L_{pp}} \tag{7.29}$$

For the static tests the bias limit is defined as

$$B_{X'}^2 = \theta_{F_{X\,measured}}^2 B_{F_{X\,measured}}^2 + \theta_\rho^2 B_\rho^2 + \theta_{T_m}^2 B_{T_m}^2 + \theta_{L_{pp}}^2 B_{L_{pp}}^2 + \theta_{U_C}^2 B_{U_C}^2 \tag{7.30}$$

where the influence coefficients are found by applying (7.14) on (7.7).

$$\theta_{F_{X\,measured}} = \frac{\partial X'}{\partial F_{X_{measured}}} = \frac{2}{\rho U_C^2 T_m L_{pp}} \tag{7.31}$$

$$\theta_\rho = \frac{\partial X'}{\partial \rho} = \frac{-2\,F_{X_{measured}}}{\rho^2 U_C^2 T_m L_{pp}} \tag{7.32}$$

$$\theta_{T_m} = \frac{\partial X'}{\partial T_m} = \frac{-2\,F_{X_{measured}}}{\rho U_C^2 T_m^2 L_{pp}} \tag{7.33}$$

$$\theta_{L_{pp}} = \frac{\partial X'}{\partial L_{pp}} = \frac{-2\,F_{X_{measured}}}{\rho U_C^2 T_m L_{pp}^2} \tag{7.34}$$

$$\theta_{U_C} = \frac{\partial X'}{\partial U_C} = \frac{-4\,F_{X_{measured}}}{\rho U_C^3 T_m L_{pp}} \tag{7.35}$$

7.2.2 Non-dimensional transverse force, Y'

The bias limit equation for Y' is given by application of (7.13) under the assumption that the variables are not correlated

$$\begin{aligned} B_{Y'}^2 = {} & \theta_{F_{Y\,measured}}^2 B_{F_{Y\,measured}}^2 + \theta_\rho^2 B_\rho^2 + \theta_{T_m}^2 B_{T_m}^2 + \theta_{L_{pp}}^2 B_{L_{pp}}^2 + \theta_M^2 B_M^2 + \theta_{X_G}^2 B_{X_G}^2 + \theta_{Y_G}^2 B_{Y_G}^2 + \\ & \theta_u^2 B_u^2 + \theta_v^2 B_v^2 + \theta_{\dot{v}}^2 B_{\dot{v}}^2 + \theta_r^2 B_r^2 + \theta_{\dot{r}}^2 B_{\dot{r}}^2 \end{aligned} \tag{7.36}$$

In this expression the influence coefficients are found by applying (7.14) on (7.5)

$$\theta_{F_{Y\,measured}} = \frac{\partial Y'}{\partial F_{Y_{measured}}} = \frac{2}{\rho(u^2+v^2)T_m L_{pp}} \tag{7.37}$$

$$\theta_\rho = \frac{\partial Y'}{\partial \rho} = \frac{-2\,(F_{Y_{measured}} + M(\dot{v}+ru-Y_G r^2 + X_G\dot{r}))}{\rho^2(u^2+v^2)T_m L_{pp}} \tag{7.38}$$

$$\theta_{T_m} = \frac{\partial Y'}{\partial T_m} = \frac{-2\,(F_{Y_{measured}} + M(\dot{v}+ru-Y_G r^2 + X_G\dot{r}))}{\rho(u^2+v^2)T_m^2 L_{pp}} \tag{7.39}$$

$$\theta_{L_{pp}} = \frac{\partial Y'}{\partial L_{pp}} = \frac{-2\,(F_{Y_{measured}} + M(\dot{v}+ru-Y_G r^2 + X_G\dot{r}))}{\rho(u^2+v^2)T_m L_{pp}^2} \tag{7.40}$$

$$\theta_M = \frac{\partial Y'}{\partial M} = \frac{2\,(\dot{v}+ru-Y_G r^2 + X_G\dot{r})}{\rho(u^2+v^2)T_m L_{pp}} \tag{7.41}$$

$$\theta_{X_G} = \frac{\partial Y'}{\partial X_G} = \frac{2M\dot{r}}{\rho(u^2+v^2)T_m L_{pp}} \tag{7.42}$$

$$\theta_{Y_G} = \frac{\partial Y'}{\partial Y_G} = \frac{-2Mr^2}{\rho(u^2+v^2)T_m L_{pp}} \tag{7.43}$$

$$\theta_u = \frac{\partial Y'}{\partial u} = \frac{2}{\rho(u^2+v^2)T_m L_{pp}}\left[Mr - \frac{2u(F_{Y_{measured}} + M(\dot{v}+ru-Y_G r^2 + X_G\dot{r}))}{(u^2+v^2)}\right] \tag{7.44}$$

$$\theta_v = \frac{\partial Y'}{\partial v} = \frac{-4v(F_{Y_{measured}} + M(\dot{v}+ru-Y_G r^2 + X_G\dot{r}))}{\rho(u^2+v^2)^2 T_m L_{pp}} \tag{7.45}$$

$$\theta_{\dot{v}} = \frac{\partial Y'}{\partial \dot{v}} = \frac{2M}{\rho(u^2+v^2)T_m L_{pp}} \tag{7.46}$$

$$\theta_r = \frac{\partial Y'}{\partial r} = \frac{2M(u-2Y_G r)}{\rho(u^2+v^2)T_m L_{pp}} \tag{7.47}$$

$$\theta_{\dot{r}} = \frac{\partial Y'}{\partial \dot{r}} = \frac{2MX_G}{\rho(u^2+v^2)T_m L_{pp}} \tag{7.48}$$

For the static tests the bias limit is defined as

$$B_{Y'}^2 = \theta_{F_{Y\,measured}}^2 B_{F_{Y\,measured}}^2 + \theta_\rho^2 B_\rho^2 + \theta_{T_m}^2 B_{T_m}^2 + \theta_{L_{pp}}^2 B_{L_{pp}}^2 + \theta_{U_C}^2 B_{U_C}^2 \tag{7.49}$$

where the influence coefficients are found by applying (7.14) on (7.8).

$$\theta_{F_{Y\,measured}} = \frac{\partial Y'}{\partial F_{Y_{measured}}} = \frac{2}{\rho U_C^2 T_m L_{pp}} \tag{7.50}$$

$$\theta_{\rho} = \frac{\partial Y'}{\partial \rho} = \frac{-2\ F_{Y_{measured}}}{\rho^2 U_C^2 T_m L_{pp}} \tag{7.51}$$

$$\theta_{T_m} = \frac{\partial Y'}{\partial T_m} = \frac{-2\ F_{Y_{measured}}}{\rho U_C^2 T_m^2 L_{pp}} \tag{7.52}$$

$$\theta_{L_{pp}} = \frac{\partial Y'}{\partial L_{pp}} = \frac{-2\ F_{Y_{measured}}}{\rho U_C^2 T_m L_{pp}^2} \tag{7.53}$$

$$\theta_{U_C} = \frac{\partial Y'}{\partial U_C} = \frac{-4\ F_{Y_{measured}}}{\rho U_C^3 T_m L_{pp}} \tag{7.54}$$

7.2.3 Non-dimensional yaw moment, N'

The bias limit equation for N' is given by

$$B_{N'}^2 = \theta_{M_{Z\,measured}}^2 B_{M_{Z\,measured}}^2 + \theta_{\rho}^2 B_{\rho}^2 + \theta_{T_m}^2 B_{T_m}^2 + \theta_{L_{pp}}^2 B_{L_{pp}}^2 + \theta_{I_Z}^2 B_{I_Z}^2 + \theta_{X_G}^2 B_{X_G}^2 + \theta_{Y_G}^2 B_{Y_G}^2 + \theta_u^2 B_u^2 + \theta_{\dot{u}}^2 B_{\dot{u}}^2 + \theta_v^2 B_v^2 + \theta_{\dot{v}}^2 B_{\dot{v}}^2 + \theta_r^2 B_r^2 + \theta_{\dot{r}}^2 B_{\dot{r}}^2 \tag{7.55}$$

In this expression the influence coefficients are found by applying (7.14) on (7.6)

$$\theta_{M_{Z\,measured}} = \frac{\partial N'}{\partial M_{Z_{measured}}} = \frac{2}{\rho(u^2+v^2) T_m L_{pp}^2} \tag{7.56}$$

$$\theta_{\rho} = \frac{\partial N'}{\partial \rho} = \frac{-2\left(M_{Z_{measured}} + I_Z \dot{r} + M(X_G(\dot{v}+ru) - Y_G(\dot{u}-rv))\right)}{\rho^2(u^2+v^2) T_m L_{pp}^2} \tag{7.57}$$

$$\theta_{T_m} = \frac{\partial N'}{\partial T_m} = \frac{-2\left(M_{Z_{measured}} + I_Z \dot{r} + M(X_G(\dot{v}+ru) - Y_G(\dot{u}-rv))\right)}{\rho(u^2+v^2) T_m^2 L_{pp}^2} \tag{7.58}$$

$$\theta_{L_{pp}} = \frac{\partial N'}{\partial T_m} = \frac{-4\left(M_{Z_{measured}} + I_Z \dot{r} + M(X_G(\dot{v}+ru) - Y_G(\dot{u}-rv))\right)}{\rho(u^2+v^2) T_m^2 L_{pp}^3} \tag{7.59}$$

$$\theta_{I_Z} = \frac{\partial N'}{\partial I_Z} = \frac{2\ \dot{r}}{\rho(u^2+v^2) T_m L_{pp}^2} \tag{7.60}$$

$$\theta_{X_G} = \frac{\partial N'}{\partial X_G} = \frac{2\ M(\dot{v}+ru)}{\rho(u^2+v^2) T_m L_{pp}^2} \tag{7.61}$$

$$\theta_{Y_G} = \frac{\partial N'}{\partial Y_G} = \frac{-2\,M(\dot{u} - rv)}{\rho(u^2 + v^2)T_m L_{pp}^2} \tag{7.62}$$

$$\theta_u = \frac{\partial N'}{\partial u} = \frac{2}{\rho(u^2 + v^2)T_m L_{pp}^2}\left[MX_G r - \frac{2u\left(M_{Z_{measured}} + I_Z\dot{r} + M(X_G(\dot{v} + ru) - Y_G(\dot{u} - rv))\right)}{(u^2 + v^2)}\right] \tag{7.63}$$

$$\theta_{\dot{u}} = \frac{\partial N'}{\partial \dot{u}} = \frac{-2\,MY_G}{\rho(u^2 + v^2)T_m L_{pp}^2} \tag{7.64}$$

$$\theta_v = \frac{\partial N'}{\partial v} = \frac{2}{\rho(u^2 + v^2)T_m L_{pp}^2}\left[MY_G r - \frac{2v\left(M_{Z_{measured}} + I_Z\dot{r} + M(X_G(\dot{v} + ru) - Y_G(\dot{u} - rv))\right)}{(u^2 + v^2)}\right] \tag{7.65}$$

$$\theta_{\dot{v}} = \frac{\partial N'}{\partial \dot{v}} = \frac{2\,MX_G}{\rho(u^2 + v^2)T_m L_{pp}^2} \tag{7.66}$$

$$\theta_r = \frac{\partial N'}{\partial r} = \frac{2\,M(X_G u + Y_G v)}{\rho(u^2 + v^2)T_m L_{pp}^2} \tag{7.67}$$

$$\theta_{\dot{r}} = \frac{\partial N'}{\partial \dot{r}} = \frac{2I_Z}{\rho(u^2 + v^2)T_m L_{pp}^2} \tag{7.68}$$

For the static tests the bias limit is defined as

$$B_{N'}^2 = \theta_{M_{Z\,maesured}}^2 B_{M_{Z\,maesured}}^2 + \theta_\rho^2 B_\rho^2 + \theta_{T_m}^2 B_{T_m}^2 + \theta_{L_{pp}}^2 B_{L_{pp}}^2 + \theta_{U_C}^2 B_{U_C}^2 \tag{7.69}$$

where the influence coefficients are found by applying (7.14) on (7.9).

$$\theta_{M_{Z\,measured}} = \frac{\partial N'}{\partial M_{Z_{measured}}} = \frac{2}{\rho U_C^2 T_m L_{pp}^2} \tag{7.70}$$

$$\theta_\rho = \frac{\partial N'}{\partial \rho} = \frac{-2\,M_{Z_{measured}}}{\rho^2 U_C^2 T_m L_{pp}^2} \tag{7.71}$$

$$\theta_{T_m} = \frac{\partial N'}{\partial T_m} = \frac{-2\,M_{Z_{measured}}}{\rho U_C^2 T_m^2 L_{pp}^2} \tag{7.72}$$

$$\theta_{L_{pp}} = \frac{\partial N'}{\partial L_{pp}} = \frac{-4\,M_{Z_{measured}}}{\rho U_C^2 T_m L_{pp}^3} \tag{7.73}$$

$$\theta_{U_C} = \frac{\partial N'}{\partial U_C} = \frac{-4\,M_{Z_{measured}}}{\rho U_C^3 T_m L_{pp}^2} \tag{7.74}$$

7.3 Estimation of individual bias limits

In the sections below, the bias limits for the quantities in the data reduction equations above are estimated.

7.3.1 Estimation of bias limit for water density, ρ

In the expressions for the bias limits above, one of the terms involves the bias limit, B_ρ for the water density. The bias limit of ρ is related to the uncertainty B_T of the temperature T_0 at which the test is conducted. For the thermometer applied, the uncertainty is $B_T = 0.15^\circ C$.

The relation between temperature and density adopted by the ITTC 1963 says that

$$\rho(T) = 999.784 + 0.0638 \cdot T - 0.00865 \cdot T^2 + 0.0000631 \cdot T^3 \tag{7.75}$$

With this expression the bias limit for ρ becomes

$$B_\rho = \frac{\partial \rho(T)}{\partial T} B_T \bigg|_{T=T_0} = (0.0638 - 0.173 \cdot T_0 + 0.0001893 \cdot T_0^2) \cdot 0.15 \tag{7.76}$$

T_0 [Deg.]	ρ [Kg/m^3]	B_ρ^2 [(Kg/m^3)^2]
15.7	998.9	0.15

Table 7.3.1.1. Bias limit for water density.

7.3.2 Estimation of bias limit for carriage speed, U_C

According to the ITTC guidelines for estimation of the bias limit for the carriage speed (ITTC 1999b) it can be determined end-to-end by calibrating against a known distance and a measured transit time. This means

$$U_{ref} = \frac{\Delta L}{\Delta T} \tag{7.77}$$

The bias limit includes two components: the calibration and the data acquisition, i.e.

$$B_{U_C} = \sqrt{B_{U_C\,calib}^2 + B_{U_C\,acquis}^2} \tag{7.78}$$

The calibration contribution is obtained from

$$B_{U_C\,calib,run} = \sqrt{\left(\frac{\partial U_{ref}}{\partial \Delta L} B_{\Delta L}\right)^2 + \left(\frac{\partial U_{ref}}{\partial \Delta T} B_{\Delta T}\right)^2} = \sqrt{\left(\frac{1}{\Delta T} B_{\Delta L}\right)^2 + \left(\frac{-\Delta L}{\Delta T^2} B_{\Delta T}\right)^2} \tag{7.79}$$

The distance ΔL is measured with a tape measure and the time with a stopwatch. The bias limits $B_{\Delta L}$ and $B_{\Delta T}$ for the measurements are assumed to equal 0.05 m and 0.05 sec, respectively. The results of the calibration measurements are given in Table 7.3.2.1 below.

Based on the data in Table 7.3.2.1, the bias limit from the calibration is calculated from

$$B_{U_C\,calib} = \sqrt{\sum_{i=1}^{6}(B_{U_C\,calib,run\,i})^2} \tag{7.80}$$

i	ΔL [m]	ΔT [s]	U_{ref} [m/s]	$U_{carriage}$ [m/s]	$B_{U_C\,calib,run}$ [m/s]
1	41.99	96.03	0.437	0.439	0.000568
2	41.99	95.93	0.438	0.439	0.000569
3	77.99	90.22	0.864	0.865	0.000733
4	77.99	90.22	0.864	0.865	0.000733
5	101.97	57.66	1.768	1.768	0.001762
6	101.97	57.65	1.769	1.769	0.001762

Table 7.3.2.1. Velocity calibration data.

According to the ITTC guidelines the bias limit for the data acquisition can, based on the U_{ref} and $U_{carriage}$ velocity pairs in the table, be calculated from

$$B_{U_C\,acquis} = 2 \cdot SEE \tag{7.81}$$

where

$$SEE = \sqrt{\sum_{i=1}^{6}\frac{(U_{carraige,i} - U_{ref,i})^2}{4}} \tag{7.82}$$

The bias limit for U_C is shown in Table 7.3.2.2.

$B_{U_C\,calib}$ [m/s]	$B_{U_C\,acquis}$ [m/s]	B_{U_C} [m/s]
0.0028	0.0024	0.0037

Table 7.3.2.2. Bias limit for carriage speed.

7.3.3 Estimation of bias limit for total model mass, M

The bias limit related to the total model mass originates from the uncertainties of the mass of the model inclusive gauges plus the weights used for ballasting the model. The uncertainties of the masses ε_{M_i} are set on the basis of the accuracy of the weights, which are used for weighing the ballast weights. Table 7.3.3.1 below shows the items included in the total model mass.

It should be noted that in the total weight, the weight of the gauges is included. In the PMM set-up this weight is balanced by counter weights (45.25 kg), so the resulting mass of the model including ballast, which is balanced by the buoyancy, is 190.65 kg. Compared to the displacement of 189.70 kg, the model weighs 0.95 kg too much, but the reason is that the model is ballasted to the marks and not to the displacement.

Item	Group no.	No of Weights n	Total Weight [kg] nM_i	Accuracy	
				Individual weights [kg] ε_{M_i}	Group weights [kg] $\sqrt{n\varepsilon_{M_i}^2}$
Model incl. gauges	1	1	96.3	0.1	0.1
Ballast 2kg	2	2	4	0.001	0.0014
Ballast 5kg	3	1	5	0.05	0.05
Ballast 10kg	4	9	90	0.05	0.15
Ballast 20kg	5	2	40	0.05	0.07
Calib. fitting	6	1	0.6	0.001	0.0010
Total weight			235.9		

Table 7.3.3.1. Model and ballast weights including uncertainties.

Finally, it should also be noted, that in spite of the 45.25 kg being lifted in the Z-direction, the total weight of M=235.9 kg is still the one used in the data reduction equations, since it is this weight, which is moved in surge, sway and yaw motions.
Based on the accuracy of the individual group weights in Table 7.3.3.1, the uncertainty in the total model mass can be expressed as

$$B_M = \sqrt{\sum_{i=1}^{N} (Accuracy\ of\ \ group\, weight_i)^2} \tag{7.83}$$

which gives the result in Table 7.3.3.2.

B_M [kg]
0.20

Table 7.3.3.2. Bias limit for model mass.

7.3.4 Estimation of bias limit for total moment of inertia, I_Z

The total moment of inertia of the model I_Z consists of a contribution from the ballast weights and from the model itself, including gauges. Each $I_{Z,i}$ of the individual ballast weights consists of two contributions. One is their own moment of inertia with respect to their own centers of gravity $I_{Z,own,i}$ and the other, $r_i^2 M_i$, is due to the distance between the mid-ship position and the center of gravity of the individual weights. With N ballast weights this can be expressed as

$$I_Z = \sum_{i=1}^{N} I_{Z,i} + I_{Z,model} = \sum_{i=1}^{N} (I_{Z,own,i} + r_i^2 M_i) + I_{Z,model} \tag{7.84}$$

The bias limit for the total moment of inertia can be expressed as

$$B_{I_Z} = \sqrt{B_{I_{Z,\text{model}}}^2 + \sum_{i=1}^{N} B_{I_{Z,i}}^2} \tag{7.85}$$

where $B_{I_{Z,model}}$ is the uncertainty of the models moment of inertia, $\varepsilon_{I_{Z,model}}$. $B_{I_{Z,i}}$ is the uncertainty of the moment of inertia of the individual components. $B_{I_{Z,i}}$ is found from

$$B_{I_{Z,i}} = \sqrt{\left(\frac{\partial I_{Z,i}}{\partial I_{Z,own,i}}\varepsilon_{I_{Z,own,i}}\right)^2 + \left(\frac{\partial I_{Z,i}}{\partial r_i}\varepsilon_{r_i}\right)^2 + \left(\frac{\partial I_{Z,i}}{\partial M_i}\varepsilon_{M_i}\right)^2} \tag{7.86}$$

which is equivalent to

$$B_{I_{Z,i}} = \sqrt{\varepsilon_{I_{Z,own,i}}^2 + \left(2r_i M_i \varepsilon_{r_i}\right)^2 + \left(r_i^2 \varepsilon_{M_i}\right)^2} \tag{7.87}$$

Item	No, i	$I_{Z,own,i}$	$\pm\varepsilon_{I_{Z,own,i}}$	M_i	$\pm\varepsilon_{M_i}$	r_i	ε_{r_i}	$B_{I_{Z,i}}$
Weight 1	1	0.0054	0.00005	2.0	0.001	1.136	0.005	0.0228
Weight 2	2	2.2772	0.04554	20.0	0.05	0.768	0.005	0.1629
Weight 3	3	2.2772	0.04554	20.0	0.05	0.768	0.005	0.1629
Weight 4	4	1.1272	0.02254	10.0	0.05	0.768	0.005	0.0853
Weight 5	5	1.1272	0.02254	10.0	0.05	0.313	0.005	0.0389
Weight 6	6	1.1272	0.02254	10.0	0.05	0.313	0.005	0.0389
Weight 7	7	1.1272	0.02254	10.0	0.05	0.313	0.005	0.0389
Weight 8	8	1.1272	0.02254	10.0	0.05	0.140	0.005	0.0266
Weight 9	9	1.1272	0.02254	10.0	0.05	0.247	0.005	0.0336
Weight 10	10	0.0054	0.00005	2.0	0.001	1.250	0.005	0.0250
Weight 11	11	0.0250	0.00025	5.0	0.05	0.770	0.005	0.0486
Weight 12	12	1.1272	0.02254	10.0	0.05	0.640	0.005	0.0709
Weight 13	13	1.1272	0.02254	10.0	0.05	0.640	0.005	0.0709
Weight 14	14	1.1272	0.02254	10.0	0.05	0.640	0.005	0.0709
Calib. fitt.	15	0.0060	0.00006	0.6	0.001	2.232	0.005	0.0143

Table 7.3.4.1. Moment of inertia of ballast weights including uncertainties.

In (7.87) M_i is the mass of the component and ε_{M_i} is the uncertainty of the mass. r_i is the distance from the mid-ship position to the center of gravity of the component and ε_{r_i} is the uncertainty of the distance. Finally, $\varepsilon_{I_{Z,own,i}}$ is the uncertainty of components own moment of inertia. Table 7.3.4.1 below summarizes the moment of inertia data for the ballast weights.

The moment of inertia of the model itself, including gauges, is determined by swinging the model in a steel rod with the torsion stiffness G, while measuring the swinging period. The procedure is as follows: The model and the yoke, which carries the model, are hung in the rod, which is located over mid-ship position. If the model is trimming, small additional balancing weights are put in the model to bring it back on even keel and

the distance $l_{balance,i}$ between the weights and the mid-ship position is measured. When this is done, the swinging is initiated and the time T_{swing} for N_{swing} cycles is measured in order to be able to calculate the mean period T_{mean} from

$$T_{mean} = \frac{T_{swing}}{N_{swing}} \tag{7.88}$$

Afterwards, the model is removed and the swinging is repeated for the yoke alone and the time $T_{swing,yoke}$ for $N_{swing,yoke}$ cycles is measured in order to be able to calculate the mean period $T_{mean,yoke}$ from

$$T_{mean,yoke} = \frac{T_{swing,yoke}}{N_{swing,yoke}} \tag{7.89}$$

The moment of inertia for the N balancing weights are calculated from

$$I_{balance} = \sum_{i=1}^{N} I_{balance,i} \tag{7.90}$$

where

$$I_{balance,i} = M_{balance,i}\, l_{balance,i}^2 \tag{7.91}$$

It should be noted, that the own moment of inertia of the balancing weights is neglected, since they are very small compared to the other quantities. Finally, the models moment of inertia can be found from

$$I_{Z,model} = Gg(T_{mean}^2 - T_{mean,yake}^2) - I_{balance} \tag{7.92}$$

where g is the gravitational constant.

The uncertainty of $I_{Z,model}$ is found from

$$B_{I_{Z,model}} = \sqrt{B_G^2 + B_{T_{mean}}^2 + B_{T_{mean\ yoke}}^2 + B_{I_{balance}}^2} \tag{7.93}$$

where

$$B_G = \frac{\partial I_{Z,model}}{\partial G} = g(T_{mean}^2 - T_{mean,yake}^2)\ \varepsilon_G \tag{7.94}$$

$$B_{T_{mean}} = \frac{\partial I_{Z,model}}{\partial T_{mean}} = 2GgT_{mean}\ \varepsilon_{T_{mena}} \tag{7.95}$$

$$B_{T_{mean,yoke}} = \frac{\partial I_{Z,model}}{\partial T_{mean,yoke}} = -2GgT_{mean,yoke}\ \varepsilon_{T_{mena,yoke}} \tag{7.96}$$

$$B_{I_{balance}} = \frac{\partial I_{Z,\,model}}{\partial I_{balance}} = -\,\varepsilon_{I_{balance}} \tag{7.97}$$

Here ε_G is the uncertainty of the torsion stiffness. $\varepsilon_{T_{mean}}$ is the uncertainty of the mean period for the model defined as

$$\varepsilon_{T_{mean}} = \sqrt{\left(\frac{\partial T_{mean}}{\partial T_{swing}}\varepsilon_{T_{swing}}\right)^2 + \left(\frac{\partial T_{mean}}{\partial N_{swing}}\varepsilon_{N_{swing}}\right)^2} = \sqrt{\left(\frac{1}{N_{swing}}\varepsilon_{T_{swing}}\right)^2 + \left(\frac{-T_{swing}}{N_{swing}^2}\varepsilon_{N_{swing}}\right)^2} \tag{7.98}$$

where $\varepsilon_{T_{swing}}$ and $\varepsilon_{N_{swing}}$ are the uncertainties of the measured time and number of periods.
$\varepsilon_{T_{mean,\,yoke}}$ is the uncertainty of the mean period for the yoke defined as

$$\varepsilon_{T_{mean,\,yoke}} = \sqrt{\left(\frac{\partial T_{mean,\,yoke}}{\partial T_{swing,\,yoke}}\varepsilon_{T_{swing,\,yoke}}\right)^2 + \left(\frac{\partial T_{mean,\,yoke}}{\partial N_{swing,\,yoke}}\varepsilon_{N_{swing,\,yoke}}\right)^2} = \sqrt{\left(\frac{1}{N_{swing,\,yoke}}\varepsilon_{T_{swing,\,yoke}}\right)^2 + \left(\frac{-T_{swing,\,yoke}}{N_{swing,\,yoke}^2}\varepsilon_{N_{swing,\,yoke}}\right)^2} \tag{7.99}$$

where $\varepsilon_{T_{swing,\,yoke}}$ and $\varepsilon_{N_{swing,\,yoke}}$ are the uncertainties of the measured time and number of periods.

Finally, $\varepsilon_{I_{balance}}$ is the uncertainty of the moment of inertia of applied balancing weights, which is calculated from

$$\varepsilon_{I_{balance}} = \sqrt{\sum_{i=1}^{N}(\varepsilon_{I_{balance,\,i}})^2} \tag{7.100}$$

where

$$\varepsilon_{I_{balance,\,i}} = \sqrt{\left(\frac{\partial I_{balance,\,i}}{\partial M_{balance,\,i}}\varepsilon_{M_{balance,\,i}}\right)^2 + \left(\frac{\partial I_{balance,\,i}}{\partial l_{balance,\,i}}\varepsilon_{l_{balance,\,i}}\right)^2} = \sqrt{(l_{balance,\,i}^2\ \varepsilon_{M_{balance,\,i}})^2 + (2M_i l_{balance,\,i}\ \varepsilon_{l_{balance,\,i}})^2} \tag{7.101}$$

ε_{M_i} and ε_{l_i} are the uncertainties of M_i and l_i, respectively.
The tables below summarize the quantities used for calculation of the moment of inertia.

Entity	Value	Uncertainty, ε
T_{swing}	251.18 s	0.01 s
N_{swing}	5	0.0025
T_{mean}	50.24 s	0.00224s

Table 7.3.4.2. Swinging of model.

Entity	Value	Uncertainty, ε
$T_{swing,\,yoke}$	172.39 s	0.01 s
$N_{swing,\,yoke}$	5	0.0025
$T_{mean,\,yoke}$	34.48 s	0.00212s

Table 7.3.4.3. Swinging of yoke.

Entity	Value	Uncertainty, ε
G	0.01511 kgm	0.00001 kgm

Table 7.3.4.4. Torsion stiffness.

Entity	Value	Uncertainty, ε
$M_{balance}$	8.4 kg	0.05 kg
$l_{balance}$	1.935 m	0.005 m
$I_{balance}$	31.45 kgm^2	0.2479 kgm^2

Table 7.3.4.5. Balancing weights.

B_G	$B_{T_{mean}}$	$B_{T_{mean,\,yoke}}$	$B_{I_{balance}}$
0.364	0.375	-0.177	-0.248

Table 7.3.4.6. Bias limit contributions to the models moment of inertia.

$I_{Z,\,model}$	$B_{I_{Z,\,model}}$
166.4 kgm^2	0.605 kgm^2

Table 7.3.4.7. Models moment of inertia.

I_Z	B_{I_Z}
225.3 kgm^2	0.666 kgm^2

Table 7.3.4.8. I_Z and its bias limit.

With all the quantities above known, it is possible to find the total moment of inertia of the model including the gauges and the ballast weights. Table 7.3.4.8 shows the result.

7.3.5 Estimation of bias limit for mean draft, T_m

The bias limit for the mean draft depends on whether the model is ballasted on the basis of 1) the displacement or 2) the marks.
If the displacement 1) is used, the error related to the tolerance in the manufacturing process may give an error on the hull form, which will influence the draft. If the model can be manufactured with an average tolerance of ± 1 mm in all directions, the model hull form may be slightly different from the CAD definition. Therefore, if the model is ballasted with a fixed weight corresponding to the displacement calculated from the CAD definition, the different hull form may result in a draft that is slightly different from the

one applied in the CAD model. It is difficult to calculate this effect, so in the present case, an ad hoc method is used. Due to the accuracy related to the manufacturing process the length and the beam of the ship can increase with 2 mm, while the draft can increase with 1 mm. If these new dimensions are considered, while keeping the block coefficient constant, it is possible to calculate the displacement corresponding to the new dimensions, $\nabla' = 0.506*4.0103*0.5402*0.1746 = 0.1914$ m^3. Compared to the original displacement of $\nabla = 0.1897$ m^3 the displacement has increased with $\Delta\nabla = 0.0017$ m^3. Since the model is loaded on displacement, the error in the hull form is partially compensated for by a smaller draft. With the above increase of the displacement and a water-plane area of 1.6661 m^2 the draft decreases with 1.02 mm, which is assumed to be uncertainty or bias limit of the mean draft,

$$B_{T_m 1,\, manufacturing} = 0.00102\, m \tag{7.102}$$

If the model is loaded to displacement, an additional error source to the mean draft is the uncertainty related to the weight of the model, i.e. the mass of the weights used for ballasting the model and the model itself. With $\rho = 1000$ kg/m^3 and a water plane area of 1.6661 m^2 a change in the model weight of 1 kg leads to a change in the draft of 0.0006 m. Therefore, if the model weight has an uncertainty of $B_M = 0.2\, kg$ (found earlier) the corresponding uncertainty of the mean draft becomes

$$B_{T_m 1,\, weight} = 0.2 \cdot 0.0006\, m = 0.00012\, m \tag{7.103}$$

The total bias limit for the draft is calculated by means of the root sum square of the two contributions above. The results are summarized in the table below

$B_{T_m 1,\, manufacturing}$ [m]	$B_{T_m 1,\, weight}$ [m]	$B_{T_m,\, on\ displacement}$ [m]
0.00102	0.00012	0.00103

Table 7.3.5.1. Bias limit for mean draft. Model loaded on displacement.

$B_{T_m 2,\, marking}$ [m]	$B_{T_m,\, on\ mark}$ [m]
0.001	0.001

Table 7.3.5.2. Bias limit for mean draft. Model loaded on marks.

If the marks 2) are used, which is the case for the present test, the model is ballasted so it ends up on the marks. In this case the model weight may be slightly different from the CAD based displacement. This is also seen for the present model, which weighs 0.95 kg too much, compared to the displacement. The uncertainty or bias limit of the draft in this approach is assumed to depend on how accurate it is possible to draw the marks on the model. With the present model this accuracy is assumed to be within $\pm$1mm. The bias limit can therefore be given as

$$B_{T_m 2,\, marking} = 0.001 m \tag{7.104}$$

7.3.6 Estimation of bias limit for the perpendicular length, L_{pp}

The error in the length between perpendiculars is assessed based on the tolerance related to the model manufacturing. The reason is that this dimension is a pure geometrical definition, which does not change with loading condition, as was the case

for the draft. As mentioned above the milling machine works with a tolerance of ± 1 mm I all directions. This means that L_{pp} can be in the range from $L_{pp} - 2mm$ to $L_{pp} + 2mm$, i.e. an uncertainty of 2 mm. Therefore, the bias limit for L_{pp} is assumed to be as shown in Table 7.3.6.1.

$B_{L_{pp}}$ [m]
0.002

Table 7.3.6.1. Bias limit for the ship length.

7.3.7 Estimation of bias limit for X_G

X_G is the longitudinal distance between the mid-ship position and the axial location of the center of gravity of the model. The bias limit related to X_G originates from two sources. One is the uncertainty, $\varepsilon_{X_G,1}$, related to how accurate the model can be mounted in PMM set-up. This means how well the longitudinal point of rotation coincides with the mid-ship position. The other is the uncertainty of the location of the center of gravity, $\varepsilon_{X_G,2}$. Therefore, the bias limit for X_G can be expressed as

$$B_{X_G} = \sqrt{\varepsilon_{X_G,1}^2 + \varepsilon_{X_G,2}^2} \tag{7.105}$$

The results are summarized in Table 7.3.7.1.

$\varepsilon_{X_G,1}$ [m]	$\varepsilon_{X_G,2}$ [m]	B_{X_G} [m]
0.002	0.005	0.0054

Table 7.3.7.1. Bias limit for X_G.

7.3.8 Estimation of bias limit for Y_G

Y_G is the transverse distance between the mid-ship position and the transverse location of the center of gravity of the model. The bias limit related to Y_G originates from two sources. One is the uncertainty, $\varepsilon_{Y_G,1}$, related to how accurate the model can be mounted in PMM set-up. This means how well the transverse point of rotation coincides with the mid-ship position. The other is the uncertainty of the location of the center of gravity, $\varepsilon_{Y_G,2}$. Therefore, the bias limit for Y_G can be expressed as

$$B_{Y_G} = \sqrt{\varepsilon_{Y_G,1}^2 + \varepsilon_{Y_G,2}^2} \tag{7.106}$$

The results are summarized in Table 7.3.8.1.

$\varepsilon_{Y_G,1}$ [m]	$\varepsilon_{Y_G,2}$ [m]	B_{Y_G} [m]
0.001	0.002	0.0022

Table 7.3.8.1. Bias limit for Y_G.

7.3.9 Estimation of bias limit for ψ in dynamic tests

The bias limit for the heading (6.1) of the model during the PMM test is required for some of the subsequent bias limit estimates. The cyclic yaw motion applied in the PMM test is generated by means of the Scotch yoke type mechanism mentioned in Section 6. Focus is here placed on the uncertainties introduced via the sway crank amplitude, S_{mm}, the yaw crank amplitude, Y_{mm}, the number of PMM rotations per minute, N, the projected length of the tangent generator fork, R, the time t and the drift angle, β. The bias limit, $B_{heading}$, of the heading (6.1) is found from

$$B_{heading} = \sqrt{B_R^2 + B_N^2 + B_{Y_{mm}}^2 + B_t^2 + B_\beta^2} \tag{7.107}$$

where

$$B_R = \frac{\partial \psi}{\partial R}\varepsilon_R = \frac{Y_{mm}\cos(\omega t)}{R^2(1+(a\cos(\omega t))^2)}\varepsilon_R \tag{7.108}$$

$$B_N = \frac{\partial \psi}{\partial N}\varepsilon_N = \frac{2\pi t a\sin(\omega t)}{60(1+(a\cos(\omega t))^2)}\varepsilon_N \tag{7.109}$$

$$B_{Y_{mm}} = \frac{\partial \psi}{\partial Y_{mm}}\varepsilon_{Y_{mm}} = \frac{-\cos(\omega t)}{R(1+(a\cos(\omega t))^2)}\varepsilon_{Y_{mm}} \tag{7.110}$$

$$B_t = \frac{\partial \psi}{\partial t}\varepsilon_t = \frac{2\pi N a\sin(\omega t)}{60(1+(a\cos(\omega t))^2)}\varepsilon_t \tag{7.111}$$

$$B_\beta = \frac{\partial \psi}{\partial \beta}\varepsilon_\beta = \varepsilon_\beta \tag{7.112}$$

Here ε_R, ε_N, $\varepsilon_{Y_{mm}}$, ε_t and ε_β are the uncertainties of R, N, Y_{mm}, t and β, respectively. As seen from the above expressions, the sway amplitude S_{mm} does not appear in any of them. However, for pure yaw it is still an input parameter, which has to set on the PMM. This means that it has to be accounted for in the bias limit estimate, but also that is difficult to include the uncertainty $\varepsilon_{S_{mm}}$ directly in the bias limit estimate. However, since the relation (6.7) must be satisfied during pure yaw, it is possible to express the uncertainty of the sway amplitude S_{mm} as an additional uncertainty, $\varepsilon_{Y_{mm}2}$ in Y_{mm}. This is done by means of the following expressions

$$Y_{mm} = \frac{2\omega R}{U}S_{mm} \tag{7.113}$$

$$\varepsilon_{Y_{mm}2} = \frac{\partial Y_{mm}}{\partial S_{mm}}\varepsilon_{S_{mm}} = \frac{2\omega R}{U}\varepsilon_{S_{mm}} \tag{7.114}$$

If the uncertainty contribution from the yaw amplitude Y_{mm} is named $\varepsilon_{Y_{mm}1}$, the two uncertainty contributions from S_{mm} and Y_{mm} for pure yaw can be expressed as

$$\varepsilon_{Y_{mm}} = \sqrt{(\varepsilon_{Y_{mm}1})^2 + (\varepsilon_{Y_{mm}2})^2} \tag{7.115}$$

For pure sway, the heading is zero, since $Y_{mm} = 0$. However, if Y_{mm} is not exactly zero, the heading may be slightly different from zero, so it still has to be included in the bias limit estimate.

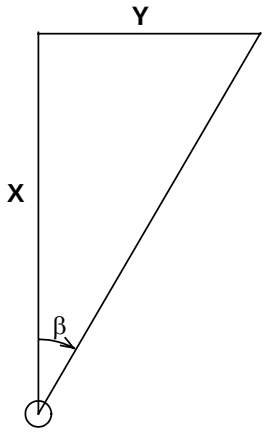

Figure 7.3.9.1. System used for checking the drift angle.

With respect to ε_β it consists of two contributions, one from the uncertainty of the drift angle setting $\varepsilon_{\beta,drift}$ and one from the alignment of the model $\varepsilon_{\beta,align}$, i.e.

$$\varepsilon_\beta = \sqrt{\varepsilon_{\beta,drift}^2 + \varepsilon_{\beta,align}^2} \tag{7.116}$$

$\varepsilon_{\beta,drift}$ is estimated end-to-end by calibrating against a known reference drift angle

$$\beta_{ref} = \text{Atan}\left(\frac{Y}{X}\right) \tag{7.117}$$

which is determined on the basis of the two known distances X and Y in Figure 7.3.9.1. When using this approach, $\varepsilon_{\beta,drift}$ includes two components, namely the uncertainty related to the applied reference angle and the uncertainty related to the difference between the reference angle and the acquired drift angle, i.e.

$$\varepsilon_{\beta,drift} = \sqrt{B_{\beta\,ref}^2 + B_{\beta\,acquis}^2} \tag{7.118}$$

The $B_{\beta\,ref}$ contribution for one set of (X_i, Y_i) values is obtained from

$$B_{\beta\,ref,i} = \sqrt{\left(\frac{\partial\beta_{ref,i}}{\partial X_i}\varepsilon_{X_i}\right)^2 + \left(\frac{\partial\beta_{ref,i}}{\partial Y_i}\varepsilon_{Y_i}\right)^2} \tag{7.119}$$

which based on the expression for β_{ref} gives

$$B_{\beta\,ref,i} = \sqrt{\left(\frac{-Y_i}{X_i^2(1+(Y_i/X_i)^2)}\varepsilon_X\right)^2 + \left(\frac{1}{X_i(1+(Y_i/X_i)^2)}\varepsilon_Y\right)^2} \tag{7.120}$$

The distances X and Y are measured with a ruler and the accuracies ε_X and ε_Y of the measurements are assumed to equal 0.001m. The results of the measurements are given in Table 7.3.9.1 below and based on the data in the table, the bias limit for the reference drift angle can be calculated from

$$B_{\beta\,ref} = \sqrt{\sum_{i=1}^{12}(B_{\beta\,ref,i})^2} \tag{7.121}$$

i	X [m]	Y [m]	$\beta_{ref,i}$ [deg.]	β_i [deg.]	$B_{\beta\,ref,i}$ [deg.]
1	3.296	0.114	1.98	2.00	0.00030
2	3.296	0.229	3.97	4.00	0.00031
3	3.296	0.345	5.97	6.00	0.00031
4	3.296	0.462	7.97	8.00	0.00031
5	3.296	0.580	9.97	10.00	0.00032
6	3.296	0.699	11.97	12.00	0.00032
7	3.296	-0.115	-2.00	-2.00	0.00030
8	3.296	-0.229	-3.97	-4.00	0.00031
9	3.296	-0.345	-5.98	-6.00	0.00031
10	3.296	-0.462	-7.97	-8.00	0.00031
11	3.296	-0.579	-9.96	-10.00	0.00032
12	3.296	-0.699	-11.97	-12.00	0.00032

Table 7.3.9.1. Drift angle data.

The $B_{\beta\,acquic}$ contribution is obtained on the basis of the β_{ref} and β pairs in Table 7.3.9.1 together with the following expressions

$$B_{\beta\,acquis} = 2 \cdot SEE \tag{7.122}$$

where

$$SEE = \sqrt{\sum_{i=1}^{12}\frac{(\beta_i - \beta_{ref,i})^2}{10}} \tag{7.123}$$

Table 7.3.9.2. summarizes the drift angle related bias limits.

$B_{\beta\,ref}$ [deg]	$B_{\beta\,acquic}$ [deg]	$\varepsilon_{\beta,drift}$ [deg]
0.062	0.064	0.09

Table 7.3.9.2. Bias limits for drift angle.

With respect to $\varepsilon_{\beta,align}$, it is assumed that the model can be aligned with an accuracy of 0.03 degree. Table 7.3.9.3 shows a summary of all the applied uncertainties.

Pure sway	
Uncertainty	Magnitude
ε_R	0.0001 m
ε_N	0.00786 rpm
ε_t	0.0022 s
$\varepsilon_{\beta,drift}$	0.0016 rad
$\varepsilon_{\beta,align}$	0.0005 rad
ε_β	0.0017 rad
$\varepsilon_{Y_{mm}} = \varepsilon_{Y_{mm}1}$	0.0001 m

(a)

Pure yaw	
Uncertainty	Magnitude
ε_R	0.0001 m
ε_N	0.00786 rpm
ε_t	0.0022 s
$\varepsilon_{\beta,drift}$	0.0016 rad
$\varepsilon_{\beta,align}$	0.0005 rad
ε_β	0.0017 rad
$\varepsilon_{Y_{mm}1}$	0.0001 m
$\varepsilon_{S_{mm}}$	0.0001 m
$\varepsilon_{Y_{mm}2}$	0.000041 m
$\varepsilon_{Y_{mm}}$	0.000108 m

(b)

Table 7.3.9.3. Uncertainties applied in connection with the estimate of $B_{heading}$. (a) Pure sway and (b) pure yaw and yaw and drift.

Finally, in sections C.1.1, C.2.1 and C.3.1 in Appendix C it is possible to see examples on time series for the bias limits related to the heading in pure yaw, pure sway and yaw and drift, respectively.

7.3.10 Estimation of bias limit for v in dynamic tests

Based on the expression for the transverse PMM velocity v_{PMM} in Section 6 the sway velocity v of the model can be expressed as function of v_{PMM}, the heading ψ and the carriage speed U_C. Figure 7.3.10.1.

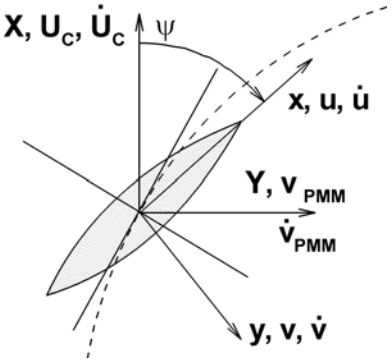

Figure 7.3.10.1. Definition of velocities and accelerations.

$$v = v_{PMM}\cos(\psi) - U_C\sin(\psi) \tag{7.124}$$

Based on this expression the bias limit for the models sway velocity is found as

$$B_v = \sqrt{(B_{U_C}^{sway})^2 + (B_\psi^{sway})^2 + (B_{v_{PMM}}^{sway})^2} \tag{7.125}$$

where

$$B_{U_C}^{sway} = \frac{\partial v}{\partial U_C}\varepsilon_{U_C} = -\sin(\psi)\varepsilon_{U_C} \tag{7.126}$$

$$B_{\psi}^{sway} = \frac{\partial v}{\partial \psi}\varepsilon_{\psi} = -\left(v_{PMM}\sin(\psi) + U_C\cos(\psi)\right)\varepsilon_{\psi} \tag{7.127}$$

$$B_{v_{PMM}}^{sway} = \frac{\partial v}{\partial v_{PMM}}\varepsilon_{v_{PMM}} = \cos(\psi)\varepsilon_{v_{PMM}} \tag{7.128}$$

ε_{U_C} is the uncertainty of the carriage speed and it was found in 7.3.2, where $\varepsilon_{U_C} = B_{U_C}$. ε_{ψ} is the uncertainty of the heading, which was found in 7.3.9, where $\varepsilon_{\psi} = B_{heading}$. Note, when using the data from 7.3.9 it is necessary to take the value corresponding to the considered type of test, i.e. pure sway ($\psi = 0$) or pure yaw and yaw and drift ($\psi \neq 0$).

The last uncertainty $\varepsilon_{v_{PMM}}$ is the one related to the transverse PMM velocity v_{PMM}, which is defined in Section 6. The expression for v_{PMM} shows that the uncertainty can be introduced via the number of PMM revolutions N, the sway amplitude S_{mm} and the time, at which the sway velocity is calculated. Therefore, $\varepsilon_{v_{PMM}}$ can be expressed as

$$\varepsilon_{v_{PMM}} = \sqrt{(B_N)^2 + (B_{S_{mm}})^2 + (B_t)^2} \tag{7.129}$$

where

$$B_N = \frac{\partial v_{PMM}}{\partial N}\varepsilon_N = -\frac{4\pi S_{mm}}{60}\left[\cos(\omega t) - \omega t\sin(\omega t)\right]\varepsilon_N \tag{7.130}$$

$$B_{S_{mm}} = \frac{\partial v_{PMM}}{\partial S_{mm}}\varepsilon_{S_{mm}} = -2\omega\cos(\omega t)\varepsilon_{S_{mm}} \tag{7.131}$$

$$B_t = \frac{\partial v_{PMM}}{\partial t}\varepsilon_t = 2\omega^2 S_{mm}\sin(\omega t)\varepsilon_t \tag{7.132}$$

In these expressions ε_N and ε_t are the uncertainties related to N and t, respectively. The values are the same as used in connection with the heading in 7.3.9.
With respect to $\varepsilon_{S_{mm}}$ it is estimated differently depending on the type motion considered, but basically there are two contributions to $\varepsilon_{S_{mm}}$ namely one from the sway setting $\varepsilon_{S_{mm}1}$ and one from the yaw setting $\varepsilon_{S_{mm}2}$.
For pure sway, S_{mm} is the only amplitude input parameter, so the uncertainty is only related to how accurate it is possible to set S_{mm} on the PMM, i.e. $\varepsilon_{S_{mm}} = \varepsilon_{S_{mm}1}$.

Pure sway	
Uncertainty	Magnitude
ε_N	0.00786 rpm
ε_t	0.0022 s
ε_{U_C}	0.0037 m/s
$\varepsilon_{S_{mm}} = \varepsilon_{S_{mm}1}$	0.0001 m

(a)

Pure yaw	
Uncertainty	Magnitude
ε_N	0.00786 rpm
ε_t	0.0022 s
ε_{U_C}	0.0037 m/s
$\varepsilon_{S_{mm}1}$	0.0001 m
$\varepsilon_{Y_{mm}}$	0.0001 m
$\varepsilon_{S_{mm}2}$	0.00024 m
$\varepsilon_{S_{mm}}$	0.00026 m

(b)

Table 7.3.10.1. Uncertainties applied in connection with the estimate of B_v. (a) pure sway and (b) pure yaw and yaw and drift.

For pure yaw the situation is a little different, because even though the expression for the sway velocity does not include the yaw amplitude Y_{mm} directly it still has to be set on the PMM in order to satisfy the relation (6.7). Therefore, both S_{mm} and Y_{mm} are necessary input parameters. As mentioned, Y_{mm} does not appear in the expression for v_{PMM}, so the uncertainty of Y_{mm} cannot be included directly in the bias limit estimate. However, based on the relation above it is possible to express the uncertainty $\varepsilon_{Y_{mm}}$ in Y_{mm} as an additional uncertainty $\varepsilon_{S_{mm}2}$ in S_{mm}. On the basis of (6.7) the following expression is applied

$$\varepsilon_{S_{mm}2} = \frac{\partial S_{mm}}{\partial Y_{mm}} \varepsilon_{Y_{mm}} = \frac{U}{2\omega R} \varepsilon_{Y_{mm}} \tag{7.133}$$

If the two uncertainty contributions from S_{mm} and Y_{mm} are combined, $\varepsilon_{S_{mm}}$ for pure yaw can finally be expressed as

$$\varepsilon_{S_{mm}} = \sqrt{(\varepsilon_{S_{mm}1})^2 + (\varepsilon_{S_{mm}2})^2} \tag{7.134}$$

Table 7.3.10.1 shows the data applied for the bias limit estimates and sections C.1.1, C.2.1 and C.3.1 in Appendix C show examples on time series for the bias limits related to v and v_{PMM} in pure yaw, pure sway and yaw and drift, respectively.

7.3.11 Estimation of bias limit for $\dot{v}$ in dynamic tests

The sway acceleration $\dot{v}$ of the model can be expressed as function of the transverse PMM acceleration $\dot{v}_{PMM}$ (6.6), the heading ψ (6.1), the transverse PMM velocity (6.5) and the carriage acceleration $\dot{U}_C$

$$\dot{v} = \dot{v}_{PMM}\cos(\psi) - \dot{U}_C \sin(\psi) - r(U_C \cos(\psi) + v_{PMM}\sin(\psi)) \tag{7.135}$$

The carriage acceleration is assumed to be zero, i.e. $\dot{U}_C = 0$, so the sway acceleration becomes

$$\dot{v} = \dot{v}_{PMM}\cos(\psi) - r(U_C\cos(\psi) + v_{PMM}\sin(\psi)) \tag{7.136}$$

Based on this expression the bias limit for the models sway acceleration is found from

$$B_{\dot{v}} = \sqrt{(B_{\psi}^{sway})^2 + (B_{\dot{v}_{PMM}}^{sway})^2 + (B_{v_{PMM}}^{sway})^2 + (B_r^{sway})^2} \tag{7.137}$$

where

$$B_{\psi}^{sway} = \frac{\partial \dot{v}}{\partial \psi}\varepsilon_{\psi} = (-\dot{v}_{PMM}\sin(\psi) - r(-U_C\sin(\psi) + v_{PMM}\cos(\psi)))\varepsilon_{\psi} \tag{7.138}$$

$$B_{\dot{v}_{PMM}}^{sway} = \frac{\partial \dot{v}}{\partial \dot{v}_{PMM}}\varepsilon_{\dot{v}_{PMM}} = \cos(\psi)\varepsilon_{\dot{v}_{PMM}} \tag{7.139}$$

$$B_{v_{PMM}}^{sway} = \frac{\partial \dot{v}}{\partial v_{PMM}}\varepsilon_{v_{PMM}} = r\sin(\psi)\varepsilon_{v_{PMM}} \tag{7.140}$$

$$B_r^{sway} = \frac{\partial \dot{v}}{\partial r}\varepsilon_r = -(U_C\cos(\psi) + v_{PMM}\sin(\psi))\varepsilon_r \tag{7.141}$$

ε_{ψ} is the uncertainty of the heading, which was found in 7.3.9, where $\varepsilon_{\psi} = B_{heading}$. Note, when using the data from 7.3.9 it is necessary to take the value corresponding to the considered type of test, i.e. pure sway ($\psi = 0$) or yaw. $\varepsilon_{v_{PMM}}$ is the uncertainty of the transverse PMM velocity v_{PMM}, which was found in 7.3.10. ε_r is the uncertainty of the yaw rate, which is found in 7.3.12, where $\varepsilon_r = B_r$.
The last uncertainty $\varepsilon_{\dot{v}_{PMM}}$ is the one related to the transverse PMM acceleration $\dot{v}_{PMM}$, which is defined in Section 6. The expression for $\dot{v}_{PMM}$ shows that the uncertainty can be introduced via the number of PMM revolutions N, the sway amplitude S_{mm} and the time, at which the sway velocity is calculated. Therefore, $\varepsilon_{\dot{v}_{PMM}}$ can be expressed as

$$\varepsilon_{\dot{v}_{PMM}} = \sqrt{(B_N)^2 + (B_{S_{mm}})^2 + (B_t)^2} \tag{7.142}$$

Based on the expression for the PMM acceleration in Section 6 the three terms under the square root above are given by

$$B_N = \frac{\partial \dot{v}_{PMM}}{\partial N}\varepsilon_N = \frac{\pi S_{mm}\omega}{15}\left[2\sin(\omega t) + \omega t\cos(\omega t)\right]\varepsilon_N \tag{7.143}$$

$$B_{S_{mm}} = \frac{\partial \dot{v}_{PMM}}{\partial S_{mm}}\varepsilon_{S_{mm}} = 2\omega^2\sin(\omega t)\varepsilon_{S_{mm}} \tag{7.144}$$

$$B_t = \frac{\partial \dot{v}_{PMM}}{\partial t}\varepsilon_t = 2\omega^3 S_{mm}\cos(\omega t)\varepsilon_t \tag{7.145}$$

With respect to the estimates of the uncertainties ε_N, ε_t and $\varepsilon_{S_{mm}}$ they are made on the basis of the same procedure as was used for the sway velocity. Therefore, $\varepsilon_{S_{mm}}$ has to be treated differently between the pure sway and pure yaw conditions.

Pure sway	
Uncertainty	Magnitude
ε_N	0.00786 rpm
ε_t	0.0022 s
$\varepsilon_{S_{mm}} = \varepsilon_{S_{mm}1}$	0.0001 m

(a)

Pure yaw	
Uncertainty	Magnitude
ε_N	0.00786 rpm
ε_t	0.0022 s
$\varepsilon_{S_{mm}1}$	0.0001 m
$\varepsilon_{Y_{mm}}$	0.0001 m
$\varepsilon_{S_{mm}2}$	0.00024 m
$\varepsilon_{S_{mm}}$	0.00026 m

(b)

Table 7.3.11.1. Uncertainties applied in connection with the estimate of B_v. (a) Pure sway and (b) pure yaw and yaw and drift.

Table 7.3.11.1 shows the data applied for the bias limit estimates. Sections C.1.1, C.2.1 and C.3.1 in Appendix C show examples on time series for the bias limits related to v and v_{PMM} in pure yaw, pure sway and yaw and drift, respectively.

7.3.12 Estimation of bias limit for r in dynamic tests

The expression for the PMM yaw rate r_{PMM} is given by (6.2) in Section 6. Since $r = r_{PMM}$, it is seen that the uncertainties in r can be introduced through R, N, t and Y_{mm}. Considering these four contributions the bias limit for r is given by

$$B_r = \sqrt{B_R^2 + B_N^2 + B_{Y_{mm}}^2 + B_t^2} \tag{7.146}$$

where the terms under the square root are defined by

$$B_R = \frac{\partial r}{\partial R}\varepsilon_R = -\frac{\omega Y_{mm}}{R^2}\sin(\omega t)\left(\frac{(a\cos(\omega t))^2 - 1}{(1+(a\cos(\omega t))^2)^2}\right)\varepsilon_R \tag{7.147}$$

$$B_N = \frac{\partial r}{\partial N}\varepsilon_N = \frac{2\pi a}{60}\left(\frac{(1+a^2)\left[\omega t\cos(\omega t)+\sin(\omega t)\right] + a^2\sin^2(\omega t)\left[\omega t\cos(\omega t)-\sin(\omega t)\right]}{(1+(a\cos(\omega t))^2)^2}\right)\varepsilon_N \tag{7.148}$$

$$B_{Y_{mm}} = \frac{\partial r}{\partial Y_{mm}}\varepsilon_{Y_{mm}} = -\frac{\omega}{R}\sin(\omega t)\left(\frac{(a\cos(\omega t))^2 - 1}{(1+(a\cos(\omega t))^2)^2}\right)\varepsilon_{Y_{mm}} \tag{7.149}$$

$$B_t = \frac{\partial r}{\partial t}\varepsilon_t = a\omega^2\cos(\omega t)\left(\frac{1+a^2(1+\sin^2(\omega t))}{(1+(a\cos(\omega t))^2)^2}\right)\varepsilon_t \tag{7.150}$$

where ε_R, ε_N and ε_t are the uncertainties related to R, N and t, respectively. $\varepsilon_{Y_{mm}}$ is the uncertainty originating from the combination of S_{mm} and Y_{mm} calculated by means of

the same approach as was used in connection with the heading. Table 7.3.12.1 summarizes the applied uncertainties.

Pure sway	
Uncertainty	Magnitude
ε_R	0.0001 m
ε_N	0.00786 rpm
ε_t	0.0022 s
$\varepsilon_{Y_{mm}} = \varepsilon_{Y_{mm}1}$	0.0001 m

(a)

Pure yaw	
Uncertainty	Magnitude
ε_R	0.0001 m
ε_N	0.00786 rpm
ε_t	0.0022 s
$\varepsilon_{Y_{mm}1}$	0.0001 m
$\varepsilon_{S_{mm}}$	0.0001 m
$\varepsilon_{Y_{mm}2}$	0.000041 m
$\varepsilon_{Y_{mm}}$	0.000108 m

(b)

Table 7.3.12.1. Uncertainties applied in connection with the estimate of B_r. (a) Pure sway and (b) pure yaw and yaw and drift.

Sections C.1.1, C.2.1 and C.3.1 in Appendix C show examples on time series for the bias limits related to r in pure yaw, pure sway and yaw and drift, respectively.

7.3.13 Estimation of bias limit for $\dot{r}$ in dynamic tests

Based on the expression for the PMM yaw acceleration (6.3) in Section 6 and the fact that $\dot{r} = \dot{r}_{PMM}$, the uncertainty in $\dot{r}$ is introduced via R, N, t and Y_{mm}. Therefore, the bias limit $B_{\dot{r}}$ can be expressed as

$$B_{\dot{r}} = \sqrt{B_R^2 + B_N^2 + B_{Y_{mm}}^2 + B_t^2} \tag{7.151}$$

The four terms under the square root above are given by

$$B_R = \frac{\partial \dot{r}}{\partial R}\varepsilon_R = -\frac{Y_{mm}\,\omega^2\cos(\omega t)}{R^2(1+(a\cos(\omega t))^2)^3}\left[1 - a^4\cos^2(\omega t) + a^2\sin^2(\omega t)(6 - a^2\cos^2(\omega t))\right]\varepsilon_R \tag{7.152}$$

$$B_N = \frac{\partial \dot{r}}{\partial N}\varepsilon_N = -\left[\frac{2\pi a\omega}{60}\left(1 + a^2(1+\sin^2(\omega t))\right)\left[\frac{\omega t\sin(\omega t)(3(a\cos(\omega t))^2 - 1)}{(1+(a\cos(\omega t))^2)^3} + \frac{2\cos(\omega t)}{(1+(a\cos(\omega t))^2)^2}\right] - \frac{2\pi a^3\omega^2 t\cos^2(\omega t)\sin(\omega t)}{60(1+(a\cos(\omega t))^2)^2}\right]\varepsilon_N \tag{7.153}$$

$$B_{Y_{mm}} = \frac{\partial \dot{r}}{\partial Y_{mm}}\varepsilon_{Y_{mm}} = \frac{-\omega^2\cos(\omega t)}{R(1+(a\cos(\omega t))^2)^3}\left[3(a\cos(\omega t))^2 - 1 + (1+\sin^2(\omega t))((a\cos(\omega t))^2 - 3)a^2\right]\varepsilon_{Y_{mm}} \tag{7.154}$$

$$B_t = \frac{\partial \dot{r}}{\partial t}\varepsilon_t = \frac{-a\omega^2\sin(\omega t)}{(1+(a\cos(\omega t))^2)^2}\left[\frac{\omega\left[3a^2\cos^2(\omega t) - 1\right]\left[1 + a^2(1+\sin^2(\omega t))\right]}{1+(a\cos(\omega t))^2} - 2a^2\cos^2(\omega t)\right]\varepsilon_t \tag{7.155}$$

Pure sway	
Uncertainty	Magnitude
ε_R	0.0001 m
ε_N	0.00786 rpm
ε_t	0.0022 s
$\varepsilon_{Y_{mm}} = \varepsilon_{Y_{mm}1}$	0.0001 m

(a)

Pure yaw	
Uncertainty	Magnitude
ε_R	0.0001 m
ε_N	0.00786 rpm
ε_t	0.0022 s
$\varepsilon_{Y_{mm}1}$	0.0001 m
$\varepsilon_{S_{mm}}$	0.0001 m
$\varepsilon_{Y_{mm}2}$	0.000041 m
$\varepsilon_{Y_{mm}}$	0.000108 m

(b)

Table 7.3.13.1. Uncertainties applied in connection with the estimate of $B_{\dot{r}}$. (a) Pure sway and (b) pure yaw and yaw and drift.

ε_R, ε_N and ε_t are the uncertainties related to R, N and t, respectively. $\varepsilon_{Y_{mm}}$ is the uncertainty originating from the combination of S_{mm} and Y_{mm} calculated by means of the same approach as was used in connection with the heading. The applied uncertainty input to the estimates is shown in Table 7.3.13.1.
Sections C.1.1, C.2.1 and C.3.1 in Appendix C show examples on time series for the bias limits related to $\dot{r}$ in pure yaw, pure sway and yaw and drift, respectively.

7.3.14 Estimation of bias limit for u in dynamic tests

In connection with the data reduction equations of the forces and moments, the surge velocity u is used. u is the sum of the projections of the carriage speed U_C and the transverse PMM velocity v_{PMM} onto the models heading direction. So based on the model heading ψ it is possible to express u as

$$u = U_C \cos(\psi) + v_{PMM} \sin(\psi) \tag{7.156}$$

Based on this expression the bias limit of u is given by

$$B_u = \sqrt{B_{U_C}^2 + B_{v_{PMM}}^2 + B_\psi^2} \tag{7.157}$$

where

$$B_{U_C} = \frac{\partial u}{\partial U_C}\varepsilon_{U_C} = \cos(\psi)\varepsilon_{U_C} \tag{7.158}$$

$$B_{v_{PMM}} = \frac{\partial u}{\partial v_{PMM}}\varepsilon_{v_{PMM}} = \sin(\psi)\varepsilon_{v_{PMM}} \tag{7.159}$$

$$B_\psi = \frac{\partial u}{\partial \psi}\varepsilon_\psi = \left(-U_C \sin(\psi) + v_{PMM}\cos(\psi)\right)\varepsilon_\psi \tag{7.160}$$

ε_{U_C} is the uncertainty of the carriage speed, which is estimated in 7.3.2. $\varepsilon_{v_{PMM}}$ is the uncertainty of the transverse PMM velocity, which is estimated in 7.3.10. ε_ψ is the

uncertainty of the heading, which is estimated in 7.3.9. Note that for pure sway $\psi = 0$, so $B_{v_{PMM}} = 0$.

Sections C.1.1, C.2.1 and C.3.1 in Appendix C show examples on time series for the bias limits related to u in pure yaw, pure sway and yaw and drift, respectively.

7.3.15 Estimation of bias limit for $\dot{u}$ in dynamic tests

The surge acceleration $\dot{u}$ is the sum of the projections of the carriage acceleration, $\dot{U}_C$ and the transverse PMM acceleration $\dot{v}_{PMM}$ onto the models heading direction plus a cross coupling term. Therefore, it is possible to express $\dot{u}$ as

$$\dot{u} = \dot{U}_C \cos(\psi) + \dot{v}_{PMM} \sin(\psi) + r(v_{PMM} \cos(\psi) - U_C \sin(\psi)) \tag{7.161}$$

The carriage speed is assumed to be constant, $\dot{U}_C = 0$, i.e.

$$\dot{u} = \dot{v}_{PMM} \sin(\psi) + r(v_{PMM} \cos(\psi) - U_C \sin(\psi)) \tag{7.162}$$

Based on this expression the bias limit of $\dot{u}$ is given by

$$B_{\dot{u}} = \sqrt{B_{\dot{v}_{PMM}}^2 + B_{v_{PMM}}^2 + B_r^2 + B_\psi^2} \tag{7.163}$$

where

$$B_{\dot{v}_{PMM}} = \frac{\partial \dot{u}}{\partial \dot{v}_{PMM}} \varepsilon_{\dot{v}_{PMM}} = \sin(\psi) \varepsilon_{\dot{v}_{PMM}} \tag{7.164}$$

$$B_{v_{PMM}} = \frac{\partial \dot{u}}{\partial v_{PMM}} \varepsilon_{v_{PMM}} = r \cos(\psi) \varepsilon_{v_{PMM}} \tag{7.165}$$

$$B_r = \frac{\partial \dot{u}}{\partial r} \varepsilon_r = (v_{PMM} \cos(\psi) - U_C \sin(\psi)) \varepsilon_r \tag{7.166}$$

$$B_\psi = \frac{\partial \dot{u}}{\partial \psi} \varepsilon_\psi = (\dot{v}_{PMM} \cos(\psi) + r(-v_{PMM} \sin(\psi) - U_C \cos(\psi))) \varepsilon_\psi \tag{7.167}$$

$\varepsilon_{\dot{v}_{PMM}}$ is the uncertainty of the transverse PMM acceleration, which is estimated from (7.142) in 7.3.11. $\varepsilon_{v_{PMM}}$ is the uncertainty of the transverse PMM velocity, which is estimated from (7.129) in 7.3.10. ε_r is the uncertainty of the yaw rate, which is estimated from (7.146) in 7.3.12. ε_ψ is the uncertainty of the heading, which is estimated in 7.3.9. Note that for pure sway $\psi = 0$, so $B_{\dot{v}_{PMM}} = 0$.

Sections C.1.1, C.2.1 and C.3.1 in Appendix C show examples on time series for the bias limits related to $\dot{u}$ in pure yaw, pure sway and yaw and drift, respectively.

7.3.16 Estimation of bias limit for the measured *X*-force, F_X

The bias limit of the *X*-force measured at the gauges is assumed to consist of eleven components, which cover

- The error in the drift angle setting in the PMM
- The error in the alignment of the model when mounted in the PMM
- The error introduced in the calibration of the force gauges due to uncertainties in the applied weights
- The error introduced through the volt-force conversion during data acquisition
- The error introduced through the uncertainties in the surge velocities during the dynamic test.
- This error introduced through the uncertainties in the sway velocities during the dynamic test.
- The error introduced due to uncertainty in the obtained yaw rate during dynamic tests
- The error introduced through the uncertainties in the surge acceleration during the dynamic test.
- The error introduced through the uncertainties in the sway acceleration during the dynamic test.
- The error introduced through the uncertainties in the yaw acceleration during the dynamic test.
- The error introduced through the uncertainty in time.

These error contributions can be collected in following expression for the bias limit

$$B_{Fx} = \sqrt{B^2_{\beta,F_X} + B^2_{align,F_X} + B^2_{calib,F_X} + B^2_{acquis,F_X} + B^2_{u,F_X} + B^2_{v,F_X} + B^2_{r,F_X} + B^2_{\dot{u},F_X} + B^2_{\dot{v},F_X} + B^2_{\dot{r},F_X} + B^2_{t,F_X}} \tag{7.168}$$

Term	Static	Dynamic
B^2_{β,F_X}	X	
B^2_{align,F_X}	X	
B^2_{calib,F_X}	X	X
B^2_{acquis,F_X}	X	X
B^2_{u,F_X}		X
B^2_{v,F_X}		X
B^2_{r,F_X}		X
$B^2_{\dot{u},F_X}$		X
$B^2_{\dot{v},F_X}$		X
$B^2_{\dot{r},F_X}$		X
B^2_{t,F_X}		X

Table 7.3.16.1. Considered terms.

Depending of the type of test considered, different terms will be included in the uncertainty assessment. The table above shows the terms, which are included in the static and dynamic tests. The individual terms are described and estimated below.

Drift angle setting

B_{β,F_X} is the force bias limit related to how accurate the drift angle can be set in the PMM. It is estimated from

$$B_{\beta,F_X} = \frac{dF_X}{d\beta}\varepsilon_\beta \tag{7.169}$$

where the influence coefficient $\frac{dF_X}{d\beta}$ is the derivative of the measured F_X with respect to β and ε_β is the uncertainty related to the accuracy of the drift angle setting. With respect to the uncertainty, ε_β related to the drift angle setting in the test, it is estimated to be 0.09 degree.

Fn	$dF_X/d\beta$ [N/rad]	ε_β [rad]	B_{β,F_X} [N]
0.138	-4.89	$1.571\ 10^{-3}$	-0.008
0.280	-27.31	$1.571\ 10^{-3}$	-0.043
0.410	-58.47	$1.571\ 10^{-3}$	-0.092

Table 7.3.16.2. Bias limit data related to drift angle setting, $\beta = 10^\circ$ in static tests.

Concerning the influence coefficient, it is taken from the static drift test results, but it is taken around a specific β value in order to match the considered test type. Therefore, since the static test uncertainty analysis is conducted for $\beta = 10^\circ$, the slopes are evaluated around this drift angle. Table 7.3.16.2 shows the applied slopes.
For the dynamic test uncertainty assessment, the drift angle uncertainty is included via the heading uncertainty, which again is included in the uncertainties related to the surge and sway velocities and accelerations, see later subsections. Therefore, in order not to include the drift angle uncertainty twice $B_{\beta,F_X} = 0$ in all dynamic tests.

Alignment of model

B_{align,F_X} is the bias limit related to the alignment of the model when it is mounted in the PMM. It is estimated from

$$B_{align,F_X} = \frac{dF_X}{d\beta}\varepsilon_{alignment\ angle} \tag{7.170}$$

Again the influence coefficient is taken from the measurement as the slope of the measured F_X versus β. The uncertainty, $\varepsilon_{alignment\ angle}$, which is related to how well the model can be aligned with the towing direction, is assumed to be 0.03 degree.
Again the influence coefficient is taken around a specific β value in order to match the considered test types. In the static test the slopes in Table 7.3.16.3 are used. In the dynamic test, $B_{align,F_X} = 0$. The reason is the same as described above in connection with B_{β,F_X}.

Fr	$dF_X / d\beta$ [N/rad] from static drift	$\varepsilon_{alignment\ angle}$ [rad]	B_{align,F_X} [N]
0.138	-4.89	$0.524\ 10^{-3}$	-0.003
0.280	-27.31	$0.524\ 10^{-3}$	-0.014
0.410	-58.47	$0.524\ 10^{-3}$	-0.031

Table 7.3.16.3. Bias limit data related to drift angle setting, $\beta = 10^\circ$ in static tests.

Calibration of force gauges

B_{calib,F_X} is the bias limit related to the uncertainties of the weights used in the check calibration of the applied force gauges. The calibration is conducted with three weights each weighing 5 kilos. The uncertainty of each weight is $\varepsilon_m = \pm 0.005$ kg.

Weight [kg]	Uncertainty [kg]
5	$\varepsilon_{m1} = \varepsilon_m = \pm 0.005$
10	$\varepsilon_{m2} = \sqrt{2\varepsilon_m^2} = \pm 0.007$
15	$\varepsilon_{m3} = \sqrt{3\varepsilon_m^2} = \pm 0.009$

Table 7.3.16.4. Uncertainty of weights.

Based on Table 7.3.16.4, the bias limit can be calculated from

$$B_{calib,F_X} = \sqrt{\varepsilon_{m1}^2 + \varepsilon_{m2}^2 + \varepsilon_{m3}^2} \cdot 9.81 m/s^2 \tag{7.171}$$

B_{calib,F_X} [N]
0.120

Table 7.3.16.5. Weight related bias limit.

Data acquisition

B_{acquis,F_X} is the bias limit related to the errors introduced in connection with the voltage-to-force conversion with both of the applied force gauges, when they are mounted in the PMM setup. It should be noted, that the calibration used to determine the calibration constants are performed on a bench, whereas the present approach only is applied to check the difference between known and measured forces, when the gauges are mounted in the PMM. The check is conducted by means of three known weights: 5, 10 and 15 kilos and with the gravitational acceleration equal to $g = 9.81 m/s^2$, the three weights correspond to: 49.05 N, 98.10 N and 147.15 N.

It must be noted, that the measured *X*-force is obtained as the sum of the forces from the two gauges. However, in spite of the fact, that the system is designed in a way, where most of the load is taken by one of the gauges, it is not possible to determine how much weight each gauge takes. Because of this it is not possible to check the gauges individually in the PMM set-up, so the calibration is carried out for the total force, i.e. the sum of the two *X*-forces.

According to the ITTC guidelines (ITTC 1999b) the bias limit for the data acquisition can, based on the force pairs in the table, be calculated from

$$B_{acquis,F_X} = 2 \cdot SEE \tag{7.172}$$

where

$$SEE = \sqrt{\sum_{i=1}^{15} \frac{(F_{applied,i} - F_{measured,i})^2}{13}} \tag{7.173}$$

Weight [kg]	Applied Force [N]	Measured force [N]
-5	-49.05	-48.91
-10	-98.10	-97.67
-15	-147.15	-146.55
5	49.05	48.87
10	98.10	97.86
15	147.15	146.84
-5	-49.05	-48.57
-10	-98.10	-97.28
-15	-147.15	-146.29
5	49.05	49.00
10	98.10	98.04
15	147.15	147.04
-5	-49.05	-48.39
-10	-98.10	-97.38
-15	-147.15	-146.15

Table 7.3.16.6. Theoretical and measured calibration forces.

Based on the results Table 7.3.16.6, this leads to the bias limit shown in Table 7.3.16.7.

B_{acquis,F_X} [N]
1.16

Table 7.3.16.7. Acquisition related bias limit.

If the ITTC approach is applied, the error is smeared out over the whole measurement range. This means, that the error is assumed to be the same whether the gauge measure 10 N or 150 N. However, a study of the errors in the present case shows that the error is proportional to the load on the gauges, Figure 7.3.16.1. Therefore, instead of using the constant error from the ITTC procedure, the error is expressed as function of the applied load on the gauges. The approach is as follows. First, the absolute values of the corresponding error (applied force minus measured force) and force data are calculated, which leads to the results in Figure 7.3.16.1. Next the data obtained for a fixed applied force is considered in order to calculate the mean error based on

$$\overline{|\Delta Fx|} = \frac{1}{M}\sum_{k=1}^{M}|\Delta Fx| \tag{7.174}$$

where M is the number of observed errors.

When this is done, the standard deviation $S_{\overline{|\Delta Fx|}}$ is calculated by means of

$$S_{\overline{|\Delta Fx|}} = \left[\sum_{k=1}^{M} \frac{(|\Delta Fx|_k - \overline{|\Delta Fx|})^2}{M-1} \right]^{½} \tag{7.175}$$

The standard deviation is then used to calculate the precision limit for the error by means of

$$P_{\overline{|\Delta Fx|}} = \frac{2S_{\overline{|\Delta Fx|}}}{\sqrt{M}} \tag{7.176}$$

By applying the factor of 2 in the expression above and using $M \geq 10$, the error should be within a band of $\pm S_{\overline{|\Delta Fx|}}$ around the mean value in 95 out of 100 cases. Therefore, in order to come up with an upper limit for the error, the following expression is applied

$$\overline{|\Delta Fx|}_{\max} = \overline{|\Delta Fx|} + P_{\overline{|\Delta Fx|}} \tag{7.177}$$

If this procedure is used on the data for the three applied forces in Figure 7.3.16.1, the data in Table 7.3.16.8 occurs.

Applied absolute force [N]	M	$\overline{\lvert\Delta Fx\rvert}_{\max}$
49.05	12	0.7350
98.10	12	1.0533
147.15	5	1.3094

Table 7.3.16.8. Error as function of applied force.

It should be noted, that the present error assessment approach was developed after the test was conducted, so unfortunately it was not possible to obtain data enough to satisfy $M \geq 10$ for all the conditions. It was possible to find some additional data for the low and medium forces from another test, where the same gauge system was applied, but unfortunately no data was available for the highest load. However, in future applications the check program should be designed, so more data is available.

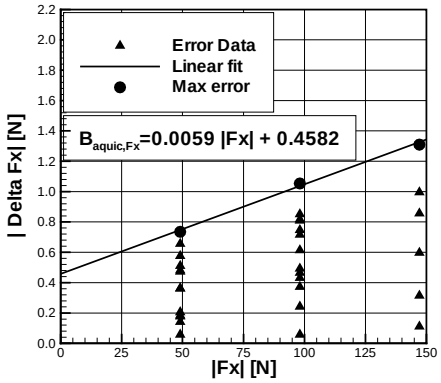

Figure 7.3.16.1. Error in X-force as function of the applied force.

Finally, in order to come up with an expression for the error as function of the force applied at the gauges, a linear curve is fitted through the three maximum errors in Figure 7.3.16.1. In the following analysis B_{acquis,F_X} is approximated by the resulting linear expression for the error, i.e.

$$B_{acquis,F_X} = 0.0059\left|F_X\right| + 0.4582 \tag{7.178}$$

where F_X is the measured X-force.

Surge velocity of model

B_{u,F_X} is the bias limit of the *X*-force related to the surge velocity of the model. The bias limit is defined as

$$B_{u,F_X} = \frac{\partial F_X}{\partial u}\varepsilon_{surge} \tag{7.179}$$

The influence coefficient in this expression is the partial derivative of the measured F_X with respect to u and ε_{surge} is the uncertainty of surge velocity, which equals B_u, which was found in 7.3.14. In order to determine the influence coefficient, the time series for F_X is transformed into a function, $\tilde{F}_X$, of the velocities and accelerations by means of a polynomial approximation, which is faired through the data points and which can be differentiated with respect to u. With $\tilde{F}_X$ known it is possible to estimate B_{u,F_X} by means of the approximation

$$B_{u,F_X} \approx \frac{\partial \tilde{F}_X}{\partial u}\varepsilon_{surge} \tag{7.180}$$

Concerning $\tilde{F}_X$ different polynomials are applied, in order to match the considered type of test, i.e.

Pure yaw:

$$\tilde{F}_X = X_0 + X_u\,u + X_r\,r + X_{rr}\,r^2 + X_{\dot{u}}\,\dot{u} + X_{\dot{r}}\,\dot{r} + X_v\,v + X_{\dot{v}}\,\dot{v} \tag{7.181}$$

Pure sway:

$$\tilde{F}_X = X_0 + X_u\,u + X_r\,r + X_{\dot{u}}\,\dot{u} + X_{\dot{r}}\,\dot{r} + X_v\,v + X_{\dot{v}}\,\dot{v} + X_{vv}\,v^2 \tag{7.182}$$

Yaw and drift:

$$\tilde{F}_X = X_0 + X_u\,u + X_r\,r + X_{rr}\,r^2 + X_{\dot{u}}\,\dot{u} + X_{\dot{r}}\,\dot{r} + X_v\,v + X_{\dot{v}}\,\dot{v} + X_{uu}\,u^2 + X_{vv}\,v^2 + X_{vr}\,vr \tag{7.183}$$

The coefficients for the three polynomials are shown in Tables 7.3.16.9 to 7.3.16.11.

Fr	0.138	0.280	0.410
X_0	9.67	24.23	16.82
X_u	-16.45	-25.35	-29.40
X_r	-0.80	-2.88	-5.23
X_{rr}	-8.01	19.39	-49.45
$X_{\dot{u}}$	-261.92	-267.06	-269.57
$X_{\dot{r}}$	-9.20	-4.53	-0.78
X_v	18.21	-18.13	204.66
$X_{\dot{v}}$	34.68	88.15	-42.15

Table 7.3.16.9. Coefficients for polynomial fairing in pure yaw. (Dimensional).

Fr	0.280
X_0	23.99
X_u	-25.50
X_r	0.00
$X_{\dot{u}}$	0.00
$X_{\dot{r}}$	0.00
X_v	-1.35
$X_{\dot{v}}$	-0.68
X_{vv}	-23.13

Table 7.3.16.10. Coefficients for polynomial fairing in pure sway. (Dimensional).

Fr	0.280
X_0	24.2
X_u	-25.35
X_r	-2.88
X_{rr}	19.39
$X_{\dot{u}}$	-267.06
$X_{\dot{r}}$	-4.53
X_v	-1.35
$X_{\dot{v}}$	-0.68
X_{uu}	-42.13
X_{vv}	1312
X_{vr}	254.4

Table 7.3.16.11. Coefficients for polynomial fairing in yaw and drift. (Dimensional).

Finally, it must be noted, that the error related to the polynomial fairing is not included in the analysis.

Sway velocity of model

B_{v,F_X} is the bias limit of the *X*-force related to the sway velocity of the model. The bias limit is defined as

$$B_{v,F_X} = \frac{\partial F_X}{\partial v}\varepsilon_{sway} \approx \frac{\partial \tilde{F}_X}{\partial v}\varepsilon_{sway} \tag{7.184}$$

As was the case for B_{u,F_X} the polynomial approximation is applied in order to estimate the influence coefficient. $\tilde{F}_X$ is given by expressions (7.181) to (7.183). ε_{sway} is the uncertainty of the yaw rate, which equals B_v found in 7.3.10.

Yaw rate of model

B_{r,F_X} is the bias limit of the *X*-force related to the uncertainty in the applied yaw rate of the model. The bias limit is defined as

$$B_{r,F_X} = \frac{\partial F_X}{\partial r}\varepsilon_{yaw\,rate} \approx \frac{\partial \tilde{F}_X}{\partial r}\varepsilon_{yaw\,rate} \tag{7.185}$$

The influence coefficient in this expression is approximated by the derivative of $\tilde{F}_X$ with respect to r. $\varepsilon_{yaw\,rate}$ is the uncertainty of the yaw rate, which equals B_r found in 7.3.12.

Surge acceleration of model

$B_{\dot{u},F_X}$ is the bias limit of the *X*-force related to the uncertainty in the surge acceleration of the model. The bias limit is defined as

$$B_{\dot{u},F_X} = \frac{\partial F_X}{\partial \dot{u}}\varepsilon_{surge\,acc.} \approx \frac{\partial \tilde{F}_X}{\partial \dot{u}}\varepsilon_{surge\,acc.} \tag{7.186}$$

The influence coefficient in this expression is calculated on the basis of expressions (7.181) to (7.183). $\varepsilon_{surge\,acc.}$ is the uncertainty of the surge acceleration, which equals $B_{\dot{u}}$ found in 7.3.15.

Sway acceleration of model

$B_{\dot{v},F_X}$ is the bias limit of the *X*-force related to the uncertainty in the applied sway acceleration of the model. It is given by

$$B_{\dot{v},F_X} = \frac{\partial F_X}{\partial \dot{v}}\varepsilon_{sway\,acc.} \approx \frac{\partial \tilde{F}_X}{\partial \dot{v}}\varepsilon_{sway\,acc.} \tag{7.187}$$

where $\tilde{F}_X$ is given by (7.181) to (7.183). $\varepsilon_{sway\,acc.}$ is the uncertainty of the sway acceleration, which equals $B_{\dot{v}}$ found in 7.3.11.

Yaw acceleration of model

$B_{\dot{r},F_X}$ is the bias limit of the *X*-force related to the uncertainty in the applied yaw acceleration of the model. It is given by

$$B_{\dot{r},F_X} = \frac{\partial F_X}{\partial \dot{r}}\varepsilon_{yaw\,acc.} \approx \frac{\partial \tilde{F}_X}{\partial \dot{r}}\varepsilon_{yaw\,acc.} \tag{7.188}$$

where $\widetilde{F}_X$ is given by (7.181) to (7.183). $\varepsilon_{yaw\,acc.}$ is the uncertainty of the sway acceleration, which equals $B_{\dot{r}}$ found in 7.3.13.

Time

B_{t,F_X} is the bias limit of the *X*-force related to an uncertainty of the time at which the data is measured. B_{t,F_X} is obtained by means of the following expression

$$B_{t,F_X} = \frac{\partial F_X}{\partial t}\varepsilon_t \tag{7.189}$$

The influence coefficient is determined by means of differentiation of the time series for F_X with respect to time. $\varepsilon_t = 0.0022$ second is the uncertainty related to time.

Examples on the numerical values of the bias limits described above can be found in sections C.1.2, C.2.2 and C.3.2 in Appendix C for pure yaw, pure sway and yaw and drift, respectively.

7.3.17 Estimation of bias limit for *Y*-force, F_Y

In connection with estimation of the bias limit for F_Y the same error sources as for F_X are considered. It must be mentioned that the total *Y*-force is considered for most of the bias limits. The only exceptions are in connection with the calibration and acquisition contributions, where the fore and aft *Y*-forces are considered individually in order to include the effect of the two forces being measured by different gauges.

$$B_{F_Y} = \sqrt{B^2_{\beta,F_Y} + B^2_{align,F_Y} + B^2_{calib,F_Y} + B^2_{acquis,F_Y} + B^2_{u,F_Y} + B^2_{v,F_Y} + B^2_{r,F_Y} + B^2_{\dot{u},F_Y} + B^2_{\dot{v},F_Y} + B^2_{\dot{r},F_Y} + B^2_{t,F_Y}} \tag{7.190}$$

Term	Static	Dynamic
B^2_{β,F_Y}	X	
B^2_{align,F_Y}	X	
B^2_{calib,F_Y}	X	X
B^2_{acquis,F_Y}	X	X
B^2_{u,F_Y}		X
B^2_{v,F_Y}		X
B^2_{r,F_Y}		X
$B^2_{\dot{u},F_Y}$		X
$B^2_{\dot{v},F_Y}$		X
$B^2_{\dot{r},F_Y}$		X
B^2_{t,F_Y}		X

Table 7.3.17.1. Considered terms.

Table 7.3.17.1 shows which of the terms that are included in the static and dynamic tests. The individual terms are described and estimated below.

Drift angle setting

B_{β,F_Y} is the force bias limit of the Y-force related to how accurate the drift angle can be set in the PMM. It is estimated from

$$B_{\beta,F_Y} = \frac{dF_Y}{d\beta}\varepsilon_\beta \tag{7.191}$$

where the influence coefficient $\frac{dF_Y}{d\beta}$ is the derivative of the measured F_Y with respect to β and ε_β is the uncertainty related to the accuracy of the drift angle setting. With respect to the uncertainty, ε_β related to the drift angle setting in the test, it is estimated to be 0.09 degree. As was the case in connection with B_{β,F_X} the influence coefficient is taken from the static drift test results around a specific β value in order to match the considered test. For the static drift test the slopes in Table 7.3.17.2 are used. For the dynamic tests, $B_{\beta,F_Y} = 0$.

Fr	$dF_Y/d\beta$ [N/rad]	ε_β [rad]	B_{β,F_Y} [N]
0.138	114.78	$1.571\ 10^{-3}$	0.180
0.280	539.32	$1.571\ 10^{-3}$	0.847
0.410	1154.48	$1.571\ 10^{-3}$	1.813

Table 7.3.17.2. Bias limit data related to drift angle setting, $\beta = 10^\circ$ in static test.

Alignment of model

B_{align,F_Y} is the bias limit related to the alignment of the model when it is mounted in the PMM. It is estimated from

$$B_{align,F_Y} = \frac{dF_Y}{d\beta}\varepsilon_{alignment\ angle} \tag{7.192}$$

Again the influence coefficient is taken from the measurement as the slope of the measured F_Y versus β. The uncertainty, $\varepsilon_{alignment\ angle}$, which is related to how well the model can be aligned with the towing direction, is assumed to be 0.03 degree. The influence coefficient is taken around $\beta = 10^\circ$ in order to match the considered test. The static test uses the slopes in Table 7.3.17.3, while $B_{align,F_Y} = 0$ for the dynamic tests.

Fr	$dF_Y/d\beta$ [N/rad] from static drift	$\varepsilon_{alignment\ angle}$ [rad]	B_{align,F_Y} [N]
0.138	114.78	$0.524\ 10^{-3}$	0.060
0.280	539.32	$0.524\ 10^{-3}$	0.282
0.410	1154.48	$0.524\ 10^{-3}$	0.604

Table 7.3.17.3. Bias limit data related to drift angle setting, $\beta = 10^\circ$ in static test.

Calibration of force gauges

B_{calib,F_Y} is the bias limit of the *Y*-force related to the uncertainties of the weights used in the calibration of the applied force gauges, the moment arms and a possible off-set of the model away from the centerline. The latter component is included, because if the model is not mounted exactly at the centerline, the *X*-force will contribute to the moment, which can be felt by the *Y*-forces.

In opposition to the *X*-force it is now possible to consider the two force gauges individually. In order to calibrate each force gauge it is necessary to consider the system shown in Figure 7.3.17.1. The figure shows the calibration configuration, where the known forces $F_{calib,x}$ and $F_{calib,y}$ are applied to the model.

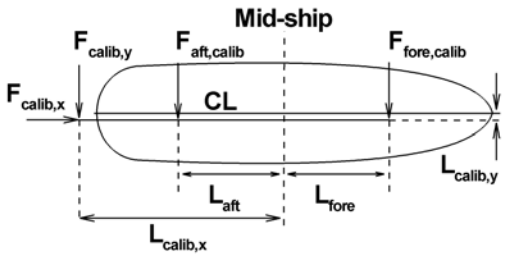

Figure 7.3.17.1. Definition of calibration forces and moment arms.

Based on moment equilibrium the local forces $F_{fore,calib}$ and $F_{aft,calib}$ corresponding to $F_{calib,x}$ and $F_{calib,y}$ are given by

$$F_{fore,calib} = -F_{calib,y}\frac{L_{calib,x} - L_{aft}}{L_{aft} + L_{fore}} - F_{calib,x}\frac{L_{calib,y}}{L_{aft} + L_{fore}} \tag{7.193}$$

and

$$F_{aft,calib} = F_{calib,y}\frac{L_{calib,x} + L_{fore}}{L_{aft} + L_{fore}} + F_{calib,x}\frac{L_{calib,y}}{L_{aft} + L_{fore}} \tag{7.194}$$

From these two equations, it is seen that the calibration force applied locally at the two gauges may be influenced by errors from the applied weight and the four arms. Starting with $F_{fore,calib}$ the uncertainty related to the local calibration force can therefore be expressed as

$$B_{F_{fore,calib,i}} = \sqrt{B^2_{L_{calib,x,f}} + B^2_{L_{calib,y,f}} + B^2_{L_{fore,f}} + B^2_{L_{aft,f}} + B^2_{F_{calib,x,f}} + B^2_{F_{calib,y,f}}} \tag{7.195}$$

where *i* is the index of the individual calibration weight and

$$B_{L_{calib,x,f}} = \frac{\partial F_{fore,calib}}{\partial L_{calib,x}}\varepsilon_{L_{calib,x}} = \frac{-F_{calib,y}}{L_{aft} + L_{fore}}\varepsilon_{L_{calib,x}} \tag{7.196}$$

$$B_{L_{calib,y,f}} = \frac{\partial F_{fore,calib}}{\partial L_{calib,y}} \varepsilon_{L_{calib,y}} = \frac{-F_{calib,x}}{L_{aft} + L_{fore}} \varepsilon_{L_{calib,y}} \tag{7.197}$$

$$B_{L_{fore,f}} = \frac{\partial F_{fore,calib}}{\partial L_{fore}} \varepsilon_{L_{fore}} = \left(F_{calib,y} \frac{L_{calib,x} - L_{aft}}{(L_{aft} + L_{fore})^2} + F_{calib,x} \frac{L_{calib,y}}{(L_{aft} + L_{fore})^2} \right) \varepsilon_{L_{fore}} \tag{7.198}$$

$$B_{L_{aft,f}} = \frac{\partial F_{fore,calib}}{\partial L_{aft}} \varepsilon_{L_{aft}} = \left(F_{calib,y} \frac{(L_{fore} + L_{calib,x})}{(L_{aft} + L_{fore})^2} + F_{calib,x} \frac{L_{calib,y}}{(L_{aft} + L_{fore})^2} \right) \varepsilon_{L_{aft}} \tag{7.199}$$

$$B_{F_{calib,x,f}} = \frac{\partial F_{fore,calib}}{\partial F_{calib,x}} \varepsilon_{F_{calib,x}} = -\frac{L_{calib,y}}{L_{aft} + L_{fore}} \varepsilon_{F_{calib,x}} \tag{7.200}$$

$$B_{F_{calib,y,f}} = \frac{\partial F_{fore,calib}}{\partial F_{calib,y}} \varepsilon_{F_{calib,y}} = -\frac{L_{calib,x} - L_{aft}}{L_{aft} + L_{fore}} \varepsilon_{F_{calib,y}} \tag{7.201}$$

Similar, the uncertainty related to the $F_{aft,calib}$ can be expressed by

$$B_{F_{aft,calib,i}} = \sqrt{B^2_{L_{calib,x,a}} + B^2_{L_{calib,y,a}} + B^2_{L_{fore,a}} + B^2_{L_{aft,a}} + B^2_{F_{calib,x,a}} + B^2_{F_{calib,y,a}}} \tag{7.202}$$

where

$$B_{L_{calib,x,a}} = \frac{\partial F_{aft,calib}}{\partial L_{calib,x}} \varepsilon_{L_{calib,x}} = \frac{F_{calib,y}}{L_{aft} + L_{fore}} \varepsilon_{L_{calib,x}} \tag{7.203}$$

$$B_{L_{calib,y,a}} = \frac{\partial F_{aft,calib}}{\partial L_{calib,y}} \varepsilon_{L_{calib,y}} = \frac{F_{calib,x}}{L_{aft} + L_{fore}} \varepsilon_{L_{calib,y}} \tag{7.204}$$

$$B_{L_{fore,a}} = \frac{\partial F_{aft,calib}}{\partial L_{fore}} \varepsilon_{L_{fore}} = \left(F_{calib,y} \frac{(L_{aft} - L_{calib,x})}{(L_{aft} + L_{fore})^2} - F_{calib,x} \frac{L_{calib,y}}{(L_{aft} + L_{fore})^2} \right) \varepsilon_{L_{fore}} \tag{7.205}$$

$$B_{L_{aft,a}} = \frac{\partial F_{aft,calib}}{\partial L_{aft}} \varepsilon_{L_{aft}} = \left(-F_{calib,y} \frac{L_{calib,x} + L_{fore}}{(L_{aft} + L_{fore})^2} - F_{calib,x} \frac{L_{calib,y}}{(L_{aft} + L_{fore})^2} \right) \varepsilon_{L_{aft}} \tag{7.206}$$

$$B_{F_{calib,x},a} = \frac{\partial F_{aft,calib}}{\partial F_{calib,x}} \varepsilon_{F_{calib,x}} = \frac{L_{calib,y}}{L_{aft} + L_{fore}} \varepsilon_{F_{calib,x}} \tag{7.207}$$

$$B_{F_{calib,y},a} = \frac{\partial F_{aft,calib}}{\partial F_{calib,y}} \varepsilon_{F_{calib,y}} = \frac{L_{calib,x} + L_{fore}}{L_{aft} + L_{fore}} \varepsilon_{F_{calib,y}} \tag{7.208}$$

In the expressions above $\varepsilon_{L_{calib,x}}$, $\varepsilon_{L_{calib,y}}$, $\varepsilon_{L_{fore}}$ and $\varepsilon_{L_{aft}}$ are the uncertainties of the lengths $L_{calib,x}$, $L_{calib,y}$, L_{fore} and L_{aft}, respectively. Tables 7.3.17.4 and 7.3.17.5. $\varepsilon_{F_{calib,x}}$

and $\varepsilon_{F_{calib,y}}$ are the uncertainties related to the applied calibration forces and they are assumed to consist of the uncertainties of the individual weights. Table 7.3.17.6.
Based on the uncertainties above and the three pairs of calibration forces, $F_{calib,x} = F_{calib,y} = F_{calib}$ (i =1,2,3 in the table above), the results shown in Table 7.3.17.7 are obtained for the fore gauge.

Arm	Length [m]
$L_{calib,x}$	2.215
$L_{calib,y}$	0.000
L_{fore}	1.4960
L_{aft}	1.4945

Table 7.3.17.4. Length of arms.

Uncertainty	Magnitude [m]
$\varepsilon_{L_{calib,x}}$	0.001
$\varepsilon_{L_{calib,y}}$	0.001
$\varepsilon_{L_{fore}}$	0.0005
$\varepsilon_{L_{aft}}$	0.0005

Table 7.3.17.5. Uncertainties of arms.

i	Weight [kg] m_i	Uncertainty [kg]	Force [N] $F_{calib} = m_i \cdot 9.81 m/S^2$	Uncertainty [N] $\varepsilon_{m\,i} \cdot 9.81 m/S^2$
1	5	$\varepsilon_{m1} = \varepsilon_m = \pm 0.005$	49.05	± 0.049
2	10	$\varepsilon_{m2} = \sqrt{2\varepsilon_m^2} = \pm 0.007$	98.10	± 0.069
3	15	$\varepsilon_{m3} = \sqrt{3\varepsilon_m^2} = \pm 0.009$	147.15	± 0.085

Table 7.3.17.6. Uncertainties of the calibration weights.

Fore							
i	$B_{L_{calib,x,\,f}}$ [N]	$B_{L_{calib,y,\,f}}$ [N]	$B_{L_{fore,\,f}}$ [N]	$B_{L_{aft,\,f}}$ [N]	$B_{F_{calib,x,\,f}}$ [N]	$B_{F_{calib,y,\,f}}$ [N]	$B_{F_{fore,calib,\,i}}$ [N]
1	-0.016	-0.016	0.002	0.010	0.000	-0.012	0.028
2	-0.033	-0.033	0.004	0.020	0.000	-0.017	0.054
3	-0.049	-0.049	0.006	0.031	0.000	-0.021	0.079

Table 7.3.17.7. Individual bias limit contributions for the fore gauge.

Aft							
i	$B_{L_{calib,x,\,f}}$ [N]	$B_{L_{calib,y,\,f}}$ [N]	$B_{L_{fore,\,f}}$ [N]	$B_{L_{aft,\,f}}$ [N]	$B_{F_{calib,x,\,f}}$ [N]	$B_{F_{calib,y,\,f}}$ [N]	$B_{F_{fore,calib,\,i}}$ [N]
1	0.016	0.016	-0.002	-0.010	0.000	0.061	0.066
2	0.033	0.033	-0.004	-0.020	0.000	0.086	0.100
3	0.049	0.049	-0.006	-0.031	0.000	0.106	0.130

Table 7.3.17.8. Individual bias limit contributions for the aft gauge.

The total bias limit for the calibration force applied to the fore gauge is

$$B_{F_{fore,calib}} = \sqrt{\sum_{i=1}^{3} B_{F_{fore,\,calib,\,i}}^2} \tag{7.209}$$

With respect to the aft gauge the results in Table 7.3.17.8 are found. The total bias limit for the calibration force applied to the aft gauge is

$$B_{F_{aft,calib}} = \sqrt{\sum_{i=1}^{3} B_{F_{aft,\,calib,\,i}}^2} \tag{7.210}$$

By evaluating the expressions for $B_{F_{fore,calib}}$ and $B_{F_{aft,calib}}$ above, the two local calibration force bias limits in Table 7.3.17.9 are found.

$B_{F_{fore,calib}}$ [N]	$B_{F_{aft,calib}}$ [N]
0.099	0.177

Table 7.3.17.9. Bias limit aft and fore.

Finally, it is possible to find the total bias limit for the *Y*-force

$$B_{calib,F_Y} = \sqrt{B_{F_{fore,calib}}^2 + B_{F_{aft,calib}}^2} \tag{7.211}$$

B_{calib,F_Y} [N]
0.203

Table 7.3.17.10. Total calibration bias limit for the Y-force.

Data acquisition

B_{acquis,F_Y} is the bias limit related to the uncertainties in connection with volt-to-force conversion with both of the applied force gauges. The theoretical values for the applied forces $F_{Y_{fore}}$ and $F_{Y_{aft}}$ are calculated by means of the expressions for $F_{fore,calib}$ and $F_{aft,calib}$ given in the calibration section above with $L_{calib,y} = 0$. B_{acquis,F_Y} is calculated by means of the same approach as was used for B_{acquis,F_X}, i.e. the absolute values of the errors are used for calculation of the maximum error corresponding to each of the applied loads. If the approach is applied on the errors plotted in Figure 7.3.17.2, the maximum errors in Table 7.3.17.11 occur.

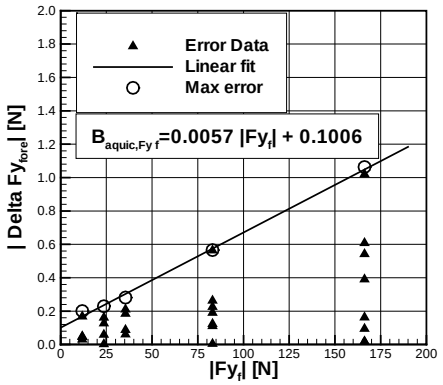

Figure 7.3.17.2. Errors at the fore gauge.

Applied absolute force [N]	M	$\overline{\lvert \Delta Fy, fore \rvert}_{\max}$
11.82	4	0.2005
23.64	4	0.2291
35.45	4	0.2814
83.07	7	0.5659
166.15	8	1.0636

Table 7.3.17.11. Error as function of applied force at the fore gauge.

If a linear curve is faired through the $\overline{\lvert \Delta Fy, fore \rvert}_{\max}$ values in Table 7.3.17.11, the results in Figure 7.3.17.2 occur, and it turns out that the bias limit related to the acquisition with the fore gauge can be expressed as

$$B_{acquis,F_Y,fore} = 0.0057 \left| F_{Y,fore} \right| + 0.1006 \tag{7.212}$$

If the same procedure is applied to the aft gauge, the results in Table 7.3.17.12. and Figure 7.3.17.3 are found.

Applied absolute force [N]	M	$\overline{\lvert \Delta Fy, aft \rvert}_{\max}$
34.02	7	0.4165
60.87	4	0.7715
68.05	8	0.6269
121.74	4	1.0837
182.60	4	1.5268

Table 7.3.17.12. Error as function of applied force at aft gauge.

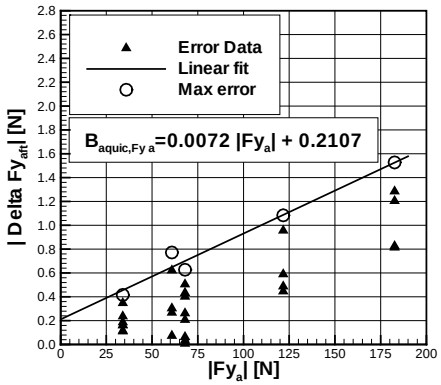

Figure 7.3.17.3. Errors at aft gauge.

If a linear curve again is faired through the $\overline{|\Delta Fy, aft|}_{\max}$ values in Table 7.3.17.12, the results in Figure 7.3.17.3 occur, and it turns out that the bias limit related to the acquisition with the aft gauge can be expressed as

$$B_{acquis,F_Y,aft} = 0.0072\left|F_{Y,aft}\right| + 0.2107 \tag{7.213}$$

Finally, it is possible to find the total acquisition bias limit for the Y-force by means of

$$B_{acquis,F_Y} = \sqrt{B^2_{acquis,F_Y,fore} + B^2_{acquis,F_Y,aft}} \tag{7.214}$$

Surge velocity of model

B_{u,F_Y} is the bias limit of the *Y*-force related to the surge velocity of the model. The bias limit is defined as

$$B_{u,F_Y} = \frac{\partial F_Y}{\partial u}\varepsilon_{surge} \tag{7.215}$$

The influence coefficient in this expression is the partial derivative of the measured F_Y with respect to u and ε_{surge} is the uncertainty of the surge velocity, which equals B_u found in 7.3.14.

With respect to the method for determination of the influence coefficient, it is similar to the polynomial approximation used in connection with B_{u,F_X} in section 7.3.16, so it will not be described here. The following approximation for B_{u,F_Y} is applied

$$B_{u,F_Y} \approx \frac{\partial \tilde{F}_Y}{\partial u}\varepsilon_{surge} \tag{7.216}$$

where $\tilde{F}_Y$ is represented by different polynomials in order to match the considered type of test, i.e.

Pure yaw:

$$\tilde{F}_Y = Y_0 + Y_u\, u + Y_r\, r + Y_{rrr}\, r^3 + Y_{\dot{u}}\, \dot{u} + Y_{\dot{r}}\, \dot{r} + Y_v\, v + Y_{\dot{v}}\, \dot{v} \tag{7.217}$$

Pure sway:

$$\tilde{F}_Y = Y_0 + Y_u\, u + Y_r\, r + Y_{\dot{u}}\, \dot{u} + Y_{\dot{r}}\, \dot{r} + Y_v\, v + Y_{\dot{v}}\, \dot{v} + Y_{v|v|}\, v|v| \tag{7.218}$$

Yaw and drift:

$$\tilde{F}_Y = Y_0 + Y_u\, u + Y_r\, r + Y_{\dot{r}}\, \dot{r} + X_{rrr}\, r^3 + Y_{\dot{u}}\, \dot{u} + Y_v\, v + Y_{\dot{v}}\, \dot{v} + Y_{vu}\, vu + Y_{v|v|}\, v|v| + Y_{v|r|}\, v|r| + Y_{r|v|}\, r|v| + Y_{rvv}\, rv^2 + Y_{vrr}\, vr^2 \tag{7.219}$$

The coefficients for the three polynomials are shown in Tables 7.3.17.13 to 7.3.17.15.

Fr	0.138	0.280	0.410
Y_0	5.92	18.22	73
Y_u	-6.98	-10.31	-28.03
Y_r	-254.57	-564.73	-817.73
$Y_{\dot{r}}$	-82.36	-49.46	-92.14
Y_{rrr}	1288.75	424.38	69.9
$Y_{\dot{u}}$	-2.54	-6.68	-11.69
Y_v	-149.7	-242.64	-134.43
$Y_{\dot{v}}$	-203.17	-58.73	10.35

Table 7.3.17.13. Coefficients for polynomial fairing in pure yaw. (Dimensional).

Fr	0.280
Y_0	51.51
Y_u	-29.09
Y_r	0
$Y_{\dot{r}}$	0
$Y_{\dot{u}}$	0
Y_v	-143.26
$Y_{\dot{v}}$	-394.25
$Y_{v\|v\|}$	-204.65

Table 7.3.17.14. Coefficients for polynomial fairing in pure sway. (Dimensional).

Fr	0.280
Y_0	18.22
Y_u	-10.31
Y_r	-564.73
$Y_{\dot{r}}$	-49.46
Y_{rrr}	424.38
$Y_{\dot{u}}$	-6.68
Y_v	-143.26
$Y_{\dot{v}}$	-394.25
Y_{vu}	-7.09
$Y_{v\|v\|}$	-204.65
$Y_{v\|r\|}$	47.99
$Y_{r\|v\|}$	2383.73
Y_{rvv}	-8823.34
Y_{vrr}	-2999.15

Table 7.3.17.15. Coefficients for polynomial fairing in yaw and drift. (Dimensional).

Sway velocity of model

B_{v,F_Y} is the bias limit of the *Y*-force related to the sway velocity of the model. The bias limit is defined as

$$B_{v,F_Y} = \frac{\partial F_Y}{\partial v}\varepsilon_{sway} \approx \frac{\partial \tilde{F}_Y}{\partial v}\varepsilon_{sway} \tag{7.220}$$

As was the case for B_{u,F_Y} the polynomial approximation is applied in order to estimate the influence coefficient. $\tilde{F}_Y$ is given by expressions (7.217) to (7.219). ε_{sway} is the uncertainty of the yaw rate, which equals B_v found in 7.3.10.

Yaw rate of model

B_{r,F_Y} is the bias limit of the *Y*-force related to the uncertainty in the applied yaw rate of the model. The bias limit is defined as

$$B_{r,F_Y} = \frac{\partial F_Y}{\partial r}\varepsilon_{yaw\,rate} \approx \frac{\partial \tilde{F}_Y}{\partial r}\varepsilon_{yaw\,rate} \tag{7.221}$$

The influence coefficient in this expression is approximated by the derivative of $\tilde{F}_Y$ with respect to r. $\varepsilon_{yaw\,rate}$ is the uncertainty of the yaw rate, which equals B_r found in 7.3.12.

Surge acceleration of model

$B_{\dot{u},F_Y}$ is the bias limit of the *Y*-force related to the uncertainty in the applied surge acceleration of the model. The bias limit is defined as

$$B_{\dot{u},F_Y} = \frac{\partial F_Y}{\partial \dot{u}}\varepsilon_{surge\,acc.} \approx \frac{\partial \tilde{F}_Y}{\partial \dot{u}}\varepsilon_{surge\,acc.} \tag{7.222}$$

The influence coefficient in this expression is calculated on the basis of expressions (7.217) to (7.219). $\varepsilon_{surge\,acc.}$ is the uncertainty of the surge acceleration, which equals $B_{\dot{u}}$ found in 7.3.15.

Sway acceleration of model

$B_{\dot{v},F_Y}$ is the bias limit of the *Y*-force related to the uncertainty in the applied sway acceleration of the model. The bias limit is defined as

$$B_{\dot{v},F_Y} = \frac{\partial F_Y}{\partial \dot{v}} \varepsilon_{sway\,acc.} \approx \frac{\partial \tilde{F}_Y}{\partial \dot{v}} \varepsilon_{sway\,acc.} \tag{7.223}$$

where $\tilde{F}_Y$ is given by (7.217) to (7.219). $\varepsilon_{sway\,acc.}$ is the uncertainty of the sway acceleration, which equals $B_{\dot{v}}$ found in 7.3.11.

Yaw acceleration of model

$B_{\dot{r},F_Y}$ is the bias limit of the *Y*-force related to the uncertainty in the applied yaw acceleration of the model. It is given by

$$B_{\dot{r},F_Y} = \frac{\partial F_Y}{\partial \dot{r}} \varepsilon_{yaw\,acc.} \approx \frac{\partial \tilde{F}_Y}{\partial \dot{r}} \varepsilon_{yaw\,acc.} \tag{7.224}$$

where $\tilde{F}_Y$ is given by (7.217) to (7.219). $\varepsilon_{yaw\,acc.}$ is the uncertainty of the sway acceleration, which equals $B_{\dot{r}}$ found in 7.3.13.

Time

B_{t,F_Y} is the bias limit of the *Y*-force related to an uncertainty of the time at which the data is measured. B_{t,F_Y} is obtained by means of the following expression

$$B_{t,F_Y} = \frac{\partial F_Y}{\partial t} \varepsilon_t \tag{7.225}$$

The influence coefficient is determined by means of differentiation of the time series for F_Y with respect to time. $\varepsilon_t = 0.0022$ second is the uncertainty related to time.

Examples on the numerical values of the bias limits described above can be found in sections C.1.3, C.2.3 and C.3.3 in Appendix C for pure yaw, pure sway and yaw and drift, respectively.

7.3.18 Estimation of bias limit for yaw moment, M_Z

In connection with estimation of the bias limit, B_{M_Z} for the yaw moment, the same error sources as for the *X*- and *Y*-forces are considered.

Term	Static	Dynamic
B^2_{β,M_Z}	X	
B^2_{align,M_Z}	X	
B^2_{calib,M_Z}	X	X
B^2_{acquis,M_Z}	X	X
B^2_{u,M_Z}		X
B^2_{v,M_Z}		X
B^2_{r,M_Z}		X
$B^2_{\dot{u},M_Z}$		X
$B^2_{\dot{v},M_Z}$		X
$B^2_{\dot{r},M_Z}$		X
B^2_{t,M_Z}		X

Table 7.3.18.1. Considered terms.

It must be mentioned that the yaw moment, which is taken around the mid-ship position, is calculated on the basis of the two *Y*-forces and the distance between the gauges and the mid-ship position, i.e.

$$M_Z = M_{Z,fore} + M_{Z,aft} = L_{fore}F_{Y,fore} + L_{aft}F_{Y,aft} \tag{7.226}$$

However, for most of the bias limits for M_Z the total moment is considered. The only exceptions are in connection with the calibration and acquisition contributions, where the moment contributions from the fore and aft *Y*-forces are considered individually. The expression for the total bias limit is

$$B_{M_Z} = \sqrt{B^2_{\beta,M_Z} + B^2_{align,M_Z} + B^2_{calib,M_Z} + B^2_{acquis,M_Z} + B^2_{u,M_Z} + B^2_{v,M_Z} + B^2_{r,M_Z} + B^2_{\dot{u},M_Z} + B^2_{\dot{v},M_Z} + B^2_{\dot{r},M_Z} + B^2_{t,M_Z}} \tag{7.227}$$

Table 7.3.18.1 above shows which of the terms that are included in the static and dynamic tests. The individual terms are described and estimated below.

Drift angle setting

B_{β,M_Z} is the bias limit related to how accurate the drift angle can be set in the PMM. It is estimated from

$$B_{\beta,M_Z} = \frac{dM_Z}{d\beta}\varepsilon_\beta \tag{7.228}$$

where the influence coefficient $\frac{dM_Z}{d\beta}$ is the derivative of the measured M_Z with respect to β and ε_β is the uncertainty related to the accuracy of the drift angle setting. With respect to the uncertainty, ε_β related to the drift angle setting in the test, it is estimated to be 0.09 degree.

As was the case in connection with B_{β,F_X} the influence coefficient is taken from the static drift test results around $\beta = 10^\circ$ in order to match the considered test. For the static pure drift tests the slopes in Table 7.3.18.2 are used. Finally, $B_{\beta,M_Z} = 0$ for the dynamic tests.

Fn	$dM_Z/d\beta$ [Nm/rad]	ε_β [rad]	B_{β,M_Z} [Nm]
0.138	190.43	$1.571\ 10^{-3}$	0.299
0.280	942.22	$1.571\ 10^{-3}$	1.480
0.410	2016.94	$1.571\ 10^{-3}$	3.168

Table 7.3.18.2. Bias limit data related to drift angle setting, $\beta = 10^\circ$ in static test.

Alignment of model

B_{align,M_Z} is the bias limit related to the alignment of the model when it is mounted in PMM. It is estimated from

$$B_{align,M_Z} = \frac{dM_Z}{d\beta}\varepsilon_{alignment\ angle} \tag{7.229}$$

Again the influence coefficient is taken from the measurement as the slope of the measured M_Z versus β. The uncertainty, $\varepsilon_{alignment\ angle}$, which is related to how well the model can be aligned with the towing direction, is assumed to be 0.03 degree. The influence coefficient is taken around $\beta = 10^\circ$. The static test uses the slopes in Table 7.3.18.3, while $B_{align,M_Z} = 0$ in the dynamic tests.

Fn	$dM_Z/d\beta$ [Nm/rad] from static drift	$\varepsilon_{alignment\ angle}$ [rad]	B_{β,M_Z} [Nm]
0.138	190.43	$0.524\ 10^{-3}$	0.100
0.280	942.22	$0.524\ 10^{-3}$	0.493
0.410	2016.94	$0.524\ 10^{-3}$	1.056

Table 7.3.18.3. Bias limit data related to drift angle setting, $\beta = 10^\circ$

Calibration

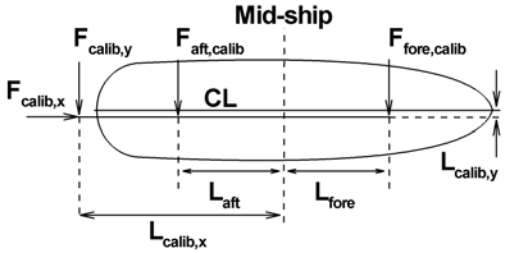

Figure 7.3.18.1. Definition of calibration forces and moment arms.

B_{calib,M_Z} is the bias limit of the yaw moment related to the uncertainties of the weights used in the calibration of the applied force gauges, the moment arms and a possible off-set of the model from the centerline. The latter component is included, because if the

model is not mounted exactly at the centerline, the *X*-force will contribute to the moment. As was the case with the *Y*-forces it is necessary to consider two components, since the moment is based on a contribution from the force measured with the aft gauge and a contribution from the gauge in the fore body. The same force and arm definitions, as was used in connection with the *Y*-force in section 7.3.17, is used below.

Figure 7.3.18.1 shows the configuration for the calibration condition. The two forces $F_{fore,calib}$ and $F_{aft,calib}$ are known, since they can be expressed by $F_{calib,x}$ and $F_{calib,y}$ according to the section about calibration of the *Y*-forces. With $L_{calib,y} = 0$ the yaw moment taken with respect to the mid-ship position can be expressed by known quantities

$$M_{Z,calib} = M_{Z,fore,calib} - M_{Z,aft,calib} = L_{fore}F_{fore,calib} - L_{aft}F_{aft,calib} \tag{7.230}$$

Based on this expression the bias limit B_{calib,M_Z} for M_Z can be expressed as

$$B_{calib,M_Z} = \sqrt{B_{M_Z,fore,calib}^2 + M_{M_Z,aft,calib}^2} \tag{7.231}$$

where

$$B_{M_{Z,fore,calib}} = \sqrt{\sum_{i=1}^{N} B_{M_{Z,fore,calib,i}}^2} \tag{7.232}$$

$$B_{M_{Z,aft,calib}} = \sqrt{\sum_{i=1}^{N} B_{M_{Z,aft,calib,i}}^2} \tag{7.233}$$

where

$$B_{M_{Z,fore,calib,i}} = \sqrt{B_{F_{fore,calib,Mz}}{}^2 + B_{L_{fore,Mz}}{}^2} \tag{7.234}$$

$$B_{M_{Z,aft,calib,i}} = \sqrt{B_{F_{aft,calib,Mz}}{}^2 + B_{L_{aft,Mz}}{}^2} \tag{7.235}$$

Here the four bias limits are

$$B_{F_{fore,calib,Mz}} = \frac{\partial M_Z}{\partial F_{fore,calib}} \varepsilon_{F_{fore,calib}} = L_{fore}\ \varepsilon_{F_{fore,calib}} \tag{7.236}$$

$$B_{L_{fore,Mz}} = \frac{\partial M_Z}{\partial L_{fore}} \varepsilon_{L_{fore}} = F_{fore,calib}\ \varepsilon_{L_{fore}} \tag{7.237}$$

$$B_{F_{aft,calib,Mz}} = \frac{\partial M_Z}{\partial F_{aft,calib}} \varepsilon_{F_{aft,calib}} = -L_{aft}\ \varepsilon_{F_{aft,calib}} \tag{7.238}$$

$$B_{L_{aft,Mz}} = \frac{\partial M_Z}{\partial L_{aft}} \varepsilon_{L_{aft}} = -F_{aft,calib}\ \varepsilon_{L_{aft}} \tag{7.239}$$

In these expressions $\varepsilon_{L_{fore}}$ and $\varepsilon_{L_{aft}}$ are the uncertainties of the two lengths L_{fore} and L_{aft}, respectively. The uncertainties, $\varepsilon_{F_{fore,calib}}$ and $\varepsilon_{F_{aft,calib}}$ of the local calibration forces, $F_{fore,calib}$ and $F_{aft,calib}$ due to uncertainties in the calibration weights, the arms and a possible off-set of the model of the centerline, are found in the previous section about estimation of the calibration related bias limit of the *Y*-force, so $\varepsilon_{F_{fore,calib}} = B_{F_{fore,calib,i}}$ and $\varepsilon_{F_{aft,calib}} = B_{F_{aft,calib,i}}$.

Arm	Length [m]
L_{fore}	1.4960
L_{aft}	1.4945

Table 7.3.18.4. Length of PMM arms.

Uncertainty	Magnitude [m]
$\varepsilon_{L_{fore}}$	0.0005
$\varepsilon_{L_{aft}}$	0.0005

Table 7.3.18.5. Uncertainties of PMM arms.

i	m	$F_{fore,calib}$ [N]	$\varepsilon_{F_{fore,calib}}$ [N]	$F_{aft,calib}$ [N]	$\varepsilon_{F_{aft,calib}}$ [N]
1	5	-11.82	0.028	60.87	0.066
2	10	-23.64	0.054	121.74	0.100
3	15	-35.45	0.079	182.60	0.130

Table 7.3.18.6. Uncertainties of calibration forces.

With all the quantities in Tables 7.3.18.4 to 7.3.18.5 known, it is possible to calculate the local bias limits for the moments obtained with data from the fore and aft gauges.

Fore			
i	$B_{F_{fore,calib,Mz}}$ [Nm]	$B_{L_{fore,Mz}}$ [Nm]	$B_{M_{Z,fore,calib,i}}$ [Nm]
1	0.042	-0.006	0.042
2	0.080	-0.012	0.081
3	0.118	-0.018	0.119

Table 7.3.18.7. Bias limits for the yaw moment at the fore gauge.

Aft			
i	$B_{F_{aft,calib,Mz}}$ [Nm]	$B_{L_{aft,Mz}}$ [Nm]	$B_{M_{Z,aft,calib,i}}$ [Nm]
1	-0.099	-0.030	0.103
2	-0.149	-0.061	0.161
3	-0.194	-0.091	0.215

Table 7.3.18.8. Bias limits for the yaw moment at the aft gauge.

The total bias limits for the fore and aft calibration moments are found from (7.232) and (7.233) with $N = 3$.

The total bias limit, based on (7.231), is shown in Table 7.3.18.9.

B_{calib,M_Z} [Nm]
0.325

Table 7.3.18.9. Total bias limit for calibration moment.

Data acquisition

B_{acquis,M_Z} is the bias limit related to the uncertainty of the yaw moment, which originates from the error in the volt-to-force conversion during the measurement of the *Y*-forces, which are used for calculation of the moment. The theoretical values $M_{Z_{fore}}$ and $M_{Z_{aft}}$ are calculated by means of

$$M_{Z,fore} = L_{fore} F_{Y_{fore}} \tag{7.240}$$

$$M_{Z,aft} = L_{aft} F_{Yaft} \tag{7.241}$$

where $F_{Y_{fore}}$ and $F_{Y_{aft}}$ are the theoretically derived transverse local forces corresponding to the applied weights. $F_{Y_{fore}}$ and $F_{Y_{aft}}$ are the same as used in section 7.3.17. B_{acquis,M_Z} is calculated by means of the same approach as was used for B_{acquis,F_X} and B_{acquis,F_Y}, i.e. the absolute values of the errors are used for calculation of the maximum error corresponding to each of the applied loads. For the moments originating from the force at the fore gauge the errors in Figure 7.3.18.2 and the maximum errors in Table 7.3.18.10 are found.

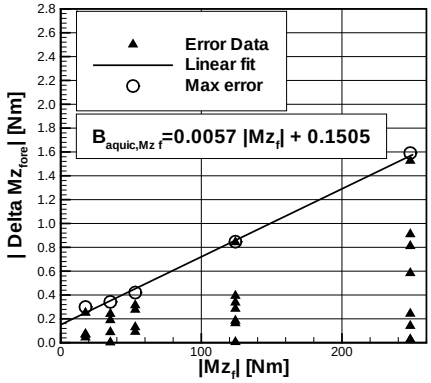

Figure 7.3.18.2. Errors at the fore gauge.

Applied absolute moment [Nm]	M	$\overline{\lvert \Delta Mz, fore \rvert}_{\max}$ [Nm]
17.68	4	0.3000
35.36	4	0.3427
53.04	4	0.4209
124.28	7	0.8466
248.56	8	1.5911

Table 7.3.18.10. Error as function of applied moment at the fore gauge.

If a linear curve is faired through the $\overline{\lvert \Delta Mz, fore \rvert}_{\max}$ values in Table 7.3.18.10, the results in Figure 7.3.18.2 occur, and it turns out that the bias limit related to the acquisition with the fore gauge can be expressed as

$$B_{acquis,M_z,fore} = 0.0057 \left| M_{Z,fore} \right| + 0.1505 \tag{7.242}$$

Applied absolute moment [N]	M	$\overline{\lvert \Delta Mz, aft \rvert}_{\max}$ [Nm]
50.85	7	0.5277
90.97	4	1.1530
101.70	8	1.3152
181.93	4	1.6196
272.90	4	2.2818

Table 7.3.18.11. Error as function of applied moment at aft gauge.

If the same procedure is applied to the aft gauge, the results in Table 7.3.18.11. and Figure 7.3.18.3 are found.

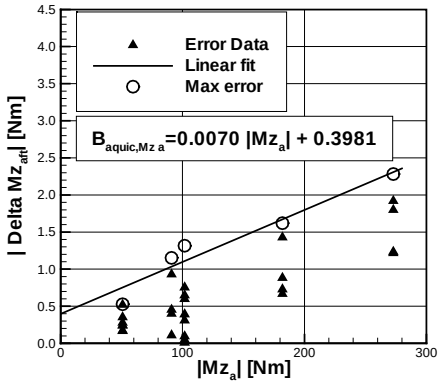

Figure 7.3.18.3. Errors at aft gauge.

If a linear curve again is faired through the $\overline{\lvert \Delta Mz, aft \rvert}_{\max}$ values in Table 7.3.18.11, the results in Figure 7.2.18.3 occur, and it turns out that the bias limit related to the acquisition with the aft gauge can be expressed as

$$B_{acquis,M_Z,aft} = 0.0070 \left| M_{Z,aft} \right| + 0.3981 \tag{7.243}$$

Finally, it is possible to find the total acquisition bias limit for the yaw moment by means of

$$B_{acquis,M_Z} = \sqrt{B^2_{acquis,fore,M_Z} + B^2_{acquis,aft,M_Z}} \tag{7.244}$$

Surge velocity of model

B_{u,M_Z} is the bias limit of the yaw moment related to the surge velocity of the model. The bias limit is defined as

$$B_{u,M_Z} = \frac{\partial M_Z}{\partial u}\varepsilon_{surge} \tag{7.245}$$

The influence coefficient in this expression is the partial derivative of the measured M_Z with respect to u and ε_{surge} is the uncertainty of the surge velocity, which equals B_u found in 7.3.14.

With respect to the method for determination of the influence coefficient, it is similar to the polynomial approximation used in connection with B_{u,F_X} in section 7.3.16, so it will not be described here. The following approximation for B_{u,M_Z} is applied

$$B_{u,M_Z} \approx \frac{\partial \tilde{M}_Z}{\partial u}\varepsilon_{surge} \tag{7.246}$$

where $\tilde{M}_Z$ is represented by different polynomials to match the considered type of test.

Pure yaw:

$$\tilde{M}_Z = M_0 + M_u\,u + M_r\,r + M_{rrr}\,r^3 + M_{\dot{u}}\,\dot{u} + M_{\dot{r}}\,\dot{r} + M_v\,v + M_{\dot{v}}\,\dot{v} \tag{7.247}$$

Pure sway:

$$\tilde{M}_Z = M_0 + M_u\,u + M_r\,r + M_{\dot{u}}\,\dot{u} + M_{\dot{r}}\,\dot{r} + M_v\,v + M_{\dot{v}}\,\dot{v} + M_{v|v|}\,v|v| \tag{7.248}$$

Yaw and drift:

$$\begin{aligned}\tilde{M}_Z = {} & M_0 + M_u\,u + M_r\,r + M_{\dot{r}}\,\dot{r} + M_{rrr}\,r^3 + M_{\dot{u}}\,\dot{u} + M_v\,v + M_{\dot{v}}\,\dot{v} + M_{vu}\,vu + M_{v|v|}\,v|v| + \\ & M_{v|r|}\,v|r| + M_{r|v|}\,r|v| + M_{rvv}\,rv^2 + M_{vrr}\,vr^2\end{aligned} \tag{7.249}$$

Fr	0.138	0.280	0.410
M_0	-12.24	18.49	-6.94
M_u	15.12	-9.42	4.85
M_r	-173.95	-437.71	-870.11
$M_{\dot{r}}$	-411.8	-445.19	-456.17
M_{rrr}	435.5	-152.82	-96.22
$M_{\dot{u}}$	-1.97	-0.45	0.36
M_v	-281.1	-483.93	-174.62
$M_{\dot{v}}$	86.28	-115.75	-14.74

Table 7.3.18.12. Coefficients for polynomial fairing in pure yaw. (Dimensional).

Fr	0.280
M_0	266.39
M_u	-150.83
M_r	0
$M_{\dot{r}}$	0
$M_{\dot{u}}$	0
M_v	-354.67
$M_{\dot{v}}$	-69.05
$Y_{v\|v\|}$	-204.65

Table 7.3.18.13. Coefficients for polynomial fairing in pure sway. (Dimensional).

Fr	0.280
M_0	18.49
M_u	-9.42
M_r	-437.71
$M_{\dot{r}}$	-445.19
M_{rrr}	-152.82
$M_{\dot{u}}$	-0.45
M_v	-354.67
$M_{\dot{v}}$	-69.05
M_{vu}	1.09
$M_{v\|v\|}$	-296.11
$M_{v\|r\|}$	139.6
$M_{r\|v\|}$	-4693.14
M_{rvv}	13062.26
M_{vrr}	-2726.29

Table 7.3.18.14. Coefficients for polynomial fairing in yaw and drift. (Dimensional).

The coefficients for the three polynomials in (7.247) to (7.249) are shown in Tables 7.3.18.12 to 7.3.18.14.

Sway velocity of model

B_{v,M_Z} is the bias limit of the yaw moment related to the sway velocity of the model. The bias limit is defined as

$$B_{v,M_Z} = \frac{\partial M_Z}{\partial v}\varepsilon_{sway} \approx \frac{\partial \tilde{M}_Z}{\partial v}\varepsilon_{sway} \tag{7.250}$$

Again the polynomial approximation is applied in order to estimate the influence coefficient. $\tilde{M}_Z$ is given by expressions (7.247) to (7.249). ε_{sway} is the uncertainty of the yaw rate, which equals B_v found in 7.3.10.

Yaw rate of model

B_{r,M_Z} is the bias limit of the yaw moment related to the uncertainty in the applied yaw rate of the model. The bias limit is defined as

$$B_{r,M_Z} = \frac{\partial M_Z}{\partial r}\varepsilon_{yaw\,rate} \approx \frac{\partial \tilde{M}_Z}{\partial r}\varepsilon_{yaw\,rate} \tag{7.251}$$

The influence coefficient in this expression is approximated by the derivative of $\tilde{M}_Z$ in (7.247) to (7.249) with respect to r. $\varepsilon_{yaw\,rate}$ is the uncertainty of the yaw rate, which equals B_r found in 7.3.12.

Surge acceleration of model

$B_{\dot{u},M_Z}$ is the bias limit of the yaw moment related to the uncertainty in the applied surge acceleration of the model. The bias limit is defined as

$$B_{\dot{u},M_Z} = \frac{\partial M_Z}{\partial \dot{u}}\varepsilon_{surge\,acc.} \approx \frac{\partial \tilde{M}_Z}{\partial \dot{u}}\varepsilon_{surge\,acc.} \tag{7.252}$$

The influence coefficient in this expression is calculated on the basis of expressions (7.247) to (7.249). $\varepsilon_{surge\,acc.}$ is the uncertainty of the surge acceleration, which equals $B_{\dot{u}}$ found in 7.3.15.

Sway acceleration of model

$B_{\dot{v},M_Z}$ is the bias limit of the yaw moment related to the uncertainty in the applied sway acceleration of the model. The bias limit is defined as

$$B_{\dot{v},M_Z} = \frac{\partial M_Z}{\partial \dot{v}}\varepsilon_{sway\,acc.} \approx \frac{\partial \tilde{M}_Z}{\partial \dot{v}}\varepsilon_{sway\,acc.} \tag{7.253}$$

where $\tilde{M}_Z$ is given by (7.247) to (7.249). $\varepsilon_{sway\,acc.}$ is the uncertainty of the sway acceleration, which equals $B_{\dot{v}}$ found in 7.3.11.

Yaw acceleration of model

$B_{\dot{r},M_Z}$ is the bias limit of the yaw moment related to the uncertainty in the applied yaw acceleration of the model. It is given by

$$B_{\dot{r},M_Z} = \frac{\partial M_Z}{\partial \dot{r}} \varepsilon_{yaw\,acc.} \approx \frac{\partial \tilde{M}_Z}{\partial \dot{r}} \varepsilon_{yaw\,acc.} \tag{7.254}$$

where $\tilde{M}_Z$ is given by (7.247) to (7.249). $\varepsilon_{yaw\,acc.}$ is the uncertainty of the sway acceleration, which equals $B_{\dot{r}}$ found in 7.3.13.

Time

B_{t,M_Z} is the bias limit of the yaw moment related to an uncertainty of the time at which the data is measured. B_{t,M_Z} is obtained by means of the following expression

$$B_{t,M_Z} = \frac{\partial Z_Z}{\partial t} \varepsilon_t \tag{7.255}$$

The influence coefficient is determined by means of differentiation of the time series for M_Z with respect to time. $\varepsilon_t = 0.0022$ second is the uncertainty related to time.

Examples on the numerical values of the bias limits described above can be found in sections C.1.4, C.2.4 and C.3.4 in Appendix C for pure yaw, pure sway and yaw and drift, respectively.

7.4 Precision limits

The precision limits are assessed through repeated tests, which are built into the test program. The model has not been dismounted from the carriage during the test, so in order to "disturb" the system the repeat tests has been mixed with the other test configurations. According to (ITTC 1999a) the precision limit is estimated from

$$P_{\bar{r}} = \frac{2S_{\bar{r}}}{\sqrt{M}} \tag{7.256}$$

where M is the number of repeats and the factor of 2 is applied for $M \geq 10$. $S_{\bar{r}}$ is the standard deviation defined as

$$S_{\bar{r}} = \left[\sum_{k=1}^{M} \frac{(r_k - \bar{r})^2}{M-1} \right]^{½} \tag{7.257}$$

Here r_k is the value from each repeat test and $\bar{r}$ is the mean value of all the quantities from the repeat tests. $\bar{r}$ is defined as

$$\bar{r} = \frac{1}{M} \sum_{k=1}^{M} r_k \tag{7.258}$$

For the present application focus is placed on the non-dimensional forces and moments X', Y' and N' defined in equations (7.4) to (7.6). With $M = 12$ the equations shown below can be used for the three quantities.

7.3.1 Longitudinal force, X'

$$P_{\overline{X}'} = \frac{2S_{\overline{X}'}}{\sqrt{12}} \tag{7.259}$$

$$S_{\overline{X}'} = \left[\sum_{k=1}^{12} \frac{(X_k' - \overline{X}')^2}{11}\right]^{½} \tag{7.260}$$

$$\overline{X}' = \frac{1}{12}\sum_{k=1}^{12} X_k' \tag{7.261}$$

7.3.2 Transverse force, Y'

$$P_{\overline{Y}'} = \frac{2S_{\overline{Y}'}}{\sqrt{12}} \tag{7.262}$$

$$S_{\overline{Y}'} = \left[\sum_{k=1}^{12} \frac{(Y_k' - \overline{Y}')^2}{11}\right]^{½} \tag{7.263}$$

$$\overline{Y}' = \frac{1}{12}\sum_{k=1}^{12} Y_k' \tag{7.264}$$

7.3.3 Yaw moment, N'

$$P_{\overline{N}'} = \frac{2S_{\overline{N}'}}{\sqrt{12}} \tag{7.265}$$

$$S_{\overline{N}'} = \left[\sum_{k=1}^{12} \frac{(N_k' - \overline{N}')^2}{11}\right]^{½} \tag{7.266}$$

$$\overline{N}' = \frac{1}{12}\sum_{k=1}^{12} N_k' \tag{7.267}$$

It should be noted that for the static test all the quantities in the expressions above are time averaged and as such constant. But, in the dynamic tests, they are all varying in time. This means that the expressions are being applied on sets of data from the time series, which are taken at fixed times throughout the PMM cycle, i.e. at $t = 0, t_1, t_2, ..., t_{period}$. The time step applied in the present work is 0.0222 second.

8. Discussion of test results

The results from the PMM test are discussed below. The results related to the static tests are shown in Appendix B, while the results from the part of the dynamic tests, which is considered for uncertainty analysis, are shown in Appendix C. The remaining dynamic results are shown in Appendix D.

8.1 Static tests

The static tests, which are pure drift tests, are conducted for Froude numbers equal to 0.138, 0.280 and 0.410. The test program in Appendix A shows the considered drift angles. For the two lowest Froude numbers the drift angles range from –20 to 20 degrees, but for the highest Froude number, it was only possible to cover –12 to 12 degrees.

With respect to the precision limit part of the uncertainty analysis described earlier, the $\beta = 10^\circ$ condition is repeated 12 times at each speed in order to estimate the precision limits. Concerning the bias limits, Tables 8.1.1 to 8.1.3 below show the bias limits related to the measured dimensional forces and moments. According to sections 7.3.16 to 7.3.18 the bias limit are composed of four components: one from the accuracy of the drift angle setting, B_β, one from the accuracy of the alignment of the model in the PMM, B_{align}, one from accuracy of the weights used for the check calibration of the gauge system, B_{calib} and finally, one from the acquisition of the measured quantities, B_{acquis}, i.e. one which quantify how well the measured values compare with the known weights applied for the calibration.

Term	Fr=0.138	Fr=0.280	Fr=0.410
B_{β,F_X} [N]	0.008	0.043	0.092
B_{align,F_X} [N]	0.003	0.014	0.031
B_{calib,F_X} [N]	0.120	0.120	0.120
B_{acquis,F_X} [N]	0.485	0.581	0.833
$B_{F_{X\,measured}} = B_{F_X}$ [N]	0.499	0.595	0.847

Table 8.1.1. Summary of bias limits for the measured F_X at 10 degrees drift.

Term	Fr=0.138	Fr=0.280	Fr=0.410
B_{β,F_Y} [N]	0.180	0.847	1.813
B_{align,F_Y} [N]	0.060	0.282	0.604
B_{calib,F_Y} [N]	0.203	0.203	0.203
B_{acquis,F_Y} [N]	0.296	0.610	1.284
$B_{F_{Y\,measured}} = B_{F_Y}$ [N]	0.406	1.100	2.312

Table 8.1.2. Summary of bias limits for the measured F_Y at 10 degrees drift.

Term	Fr=0.138	Fr=0.280	Fr=0.410
B_{β,M_Z} [Nm]	0.299	1.480	3.168
B_{align,M_Z} [Nm]	0.100	0.493	1.056
B_{calib,M_Z} [Nm]	0.325	0.325	0.325
B_{acquis,M_Z} [Nm]	0.508	0.952	1.946
$B_{M_{Z\,measured}} = B_{M_Z}$ [Nm]	0.680	1.856	3.879

Table 8.1.3. Summary of bias limits for the measured M_Z at $\beta = 10^\circ$.

Term	Fr=0.138	Fr=0.280	Fr=0.410
$\theta^2_{F_{X_{measured}}} B^2_{F_{X_{measured}}}$	3.735 10^{-6}	3.111 10^{-7}	1.376 10^{-7}
$\theta^2_\rho B^2_\rho$	4.543 10^{-11}	5.697 10^{-11}	1.160 10^{-10}
$\theta^2_{T_m} B^2_{T_m}$	1.004 10^{-8}	1.259 10^{-8}	2.563 10^{-8}
$\theta^2_{L_{pp}} B^2_{L_{pp}}$	7.558 10^{-11}	9.478 10^{-11}	1.930 10^{-10}
$\theta^2_{U_C} B^2_{U_C}$	2.226 10^{-8}	6.765 10^{-9}	6.434 10^{-9}
$B_{X'}$	0.00194	0.00058	0.00041
$P_{X'}$	0.00033	0.00031	0.00014
$U_{X'}$	0.00197	0.00065	0.00043
X'	0.0174	0.0195	0.0278
$U_{X'}$ in % X'	11.3	3.4	1.6

Table 8.1.4. Summary of uncertainties for X' from the static drift test, $\beta = 10^\circ$.

Term	Fr=0.138	Fr=0.280	Fr=0.410
$\theta^2_{F_{Y_{measured}}} B^2_{F_{Y_{measured}}}$	2.466 10^{-6}	1.064 10^{-6}	1.026 10^{-6}
$\theta^2_\rho B^2_\rho$	4.414 10^{-10}	5.723 10^{-10}	7.985 10^{-10}
$\theta^2_{T_m} B^2_{T_m}$	9.756 10^{-8}	1.265 10^{-7}	1.765 10^{-7}
$\theta^2_{L_{pp}} B^2_{L_{pp}}$	7.343 10^{-10}	9.522 10^{-10}	1.328 10^{-9}
$\theta^2_{U_C} B^2_{U_C}$	2.163 10^{-7}	6.796 10^{-8}	4.429 10^{-8}
$B_{Y'}$	0.00167	0.00112	0.00112
$P_{Y'}$	0.00086	0.00066	0.00074
$U_{Y'}$	0.00188	0.00130	0.00134
Y'	0.0542	0.0617	0.0729
$U_{Y'}$ in % Y'	3.5	2.1	1.8

Table 8.1.5. Summary of uncertainties for Y' from the static drift test, $\beta = 10^\circ$.

Based on the bias limits in the Tables 8.1.1 to 8.1.3 it is seen that the acquisition component is the dominating term for the *X*-force. An increase of the speed increases the bias limits, but it has only minor influence on the composition of the error sources within each condition. For the *Y*-force and the yaw moment the bias errors also increase with increased speed, but the composition does also change. The acquisition component

is largest at the low speed, but when the speed is increased, the drift angle component starts to become the dominating error.

Moving to the non-dimensional quantities, Tables 8.1.4 to 8.1.6 show the results of the uncertainty analysis for the non-dimensional forces and moments obtained for the considered speeds. In the Tables 8.1.4 to 8.1.6 the first 5 rows show the bias related error sources. The next three rows show the total bias limit, the precision limit (based on the expressions in sections 7.3.1 to 7.3.3.) and finally, the total uncertainty. Finally, the last two rows show the force or moment coefficients and the uncertainty in percent of the coefficients, respectively. A study of the different error sources reveals the following: For X' the total uncertainty is relatively high for the low speed, but it decays rapidly when the speed goes up. If the uncertainty is divided into precision and bias contributions, it appears that the precision limits are relatively small for all the considered speeds, which indicates a fair repeatability of the measured *X*-forces. With respect to the bias limit, it tends to be larger than the precision limit. For the low speed it dominates the uncertainty, but as the speed is increased it gets smaller and smaller. A study of the bias limit contributions in the tables shows that the term originating from the measured *X*-force $\theta^2_{F_{X_{measured}}} B^2_{F_{X_{measured}}}$ is the largest, even though it decreases with speed due to the influence coefficient. Recalling the previously described bias limit related to the measured *X*-force, it was found that it increased with the speed. Though, the increase with speed is not as strong as the one for the resistance. Therefore, the error will seem large relative to the measured force at the low speed where the measured force is small, but as the speed is increased the measured force increases and the bias limit will be relatively smaller. To give an example, the measured *X*-force is around 4 N at the low speed, i.e. the bias limit constitutes around 11% of the measured value. But, at the highest speed the force is around 64 N, so the bias limit is around 1.5%. 11% may seem a little high, but it should be noted, that the present model is quite small compared to the models, which are normally used in the PMM tests. Combined with the relative low speed at the lowest Froude number the small model results in forces, which are in the lower range of what normally is measured.

Uncertainty	Fr=0.138	Fr=0.280	Fr=0.410
$\theta^2_{M_{Z_{measured}}} B^2_{M_{Z_{measured}}}$	$1.540\ 10^{-7}$	$6.645\ 10^{-8}$	$6.404\ 10^{-8}$
$\theta^2_\rho B^2_\rho$	$1.013\ 10^{-10}$	$1.407\ 10^{-10}$	$2.023\ 10^{-10}$
$\theta^2_{T_m} B^2_{T_m}$	$2.239\ 10^{-8}$	$3.109\ 10^{-8}$	$4.470\ 10^{-8}$
$\theta^2_{L_{pp}} B^2_{L_{pp}}$	$6.742\ 10^{-10}$	$9.360\ 10^{-10}$	$1.346\ 10^{-9}$
$\theta^2_{U_C} B^2_{U_C}$	$4.964\ 10^{-8}$	$1.670\ 10^{-8}$	$1.122\ 10^{-8}$
$B_{N'}$	0.00048	0.00034	0.00035
$P_{N'}$	0.00032	0.00066	0.00040
$U_{N'}$	0.00058	0.00074	0.00053
N'	0.0260	0.0306	0.0367
$U_{N'}$ in % N'	2.2	2.4	1.4

Table 8.1.6. Summary of uncertainties for N' from the static drift test, $\beta = 10^\circ$.

For Y' the total uncertainty is highest at the lowest speed, but at the medium and high speeds the magnitudes are basically the same. When related to the force coefficient, the uncertainty becomes smaller relative to the coefficient as speed is increased. The

precision limits are again smaller than the bias limits, even though the difference between the bias and precision contributions is relatively smaller than was the case for X'. Again the term $\theta^2_{F_{Y_{measured}}} B^2_{F_{Y_{measured}}}$, which is related to the measured force, is largest, even though it decreases when the speed is increased. This behavior is the opposite of the one observed for $B_{F_{Y_{measured}}}$, since this quantity increases with speed. However, the nature of the influence coefficient counteracts this effect.

For N' the bias limit has approximately the same order of magnitude as the precision limit, which is different from X' and Y'. With respect to the individual bias limit contributions, their behavior is similar to the one for Y'. Finally, it can also be noted, that the clear trend with decreasing error percentage, which was observed for both X' and Y', is not seen for N'.

Uncertainty	Fr=0.138	Fr=0.280	Fr=0.410
S_{FP} [m]	0.00042	0.01474	0.02056
$P_{S_{FP}}$	0.00016	0.00056	0.00066
$P_{S_{FP}}$ in % of S_{FP}	38.1	3.8	3.2

Table 8.1.7. Sinkage at FP.

Before discussing all the results from the static tests, a final remark should be given to the sinkage of the model, which also was measured during the test. The present uncertainty analysis focuses on the forces, so no bias limit estimates has been made for the sinkage. However, since sinkage results are available from the repeat tests, the precision limits have been estimated for three cases above. The results are shown in Tables 8.1.7 and 8.1.8, where positive sinkage means that the draft increases.

Uncertainty	Fr=0.138	Fr=0.280	Fr=0.410
S_{AP} [m]	0.00237	0.00614	0.03523
$P_{S_{AP}}$	0.00045	0.00046	0.00061
$P_{S_{AP}}$ in % of S_{AP}	19.0	7.5	1.7

Table 8.1.8. Sinkage at AP.

Finally, the results from the entire static drift test are shown in Figures B.1 and B.2 in Appendix B together with the error bands from the three conditions described above. Starting with X' in Figures B.1 (a) to (c) there appear to be an asymmetry with respect to the drift angle. It is most clearly seen for the low speed. With the width of the uncertainty band it is difficult to say if the asymmetry is caused by the uncertainty components mentioned above, or if it is caused by an asymmetry in the model geometry, which is not accounted for in the uncertainty analysis. One could argue, that if the uncertainty bands for X' are overlapping for $\pm\beta$, it is not possible to detect the reason without reducing the individual uncertainty components so that the uncertainty bands are no longer overlapping. If the uncertainty band for $\beta = 10^\circ$ is assumed to be representative for $\beta = -10^\circ$ as well, the uncertainty bands will overlap for $\beta = \pm 10^\circ$, so the asymmetry may just be a part of the uncertainty. For the medium speed, the asymmetry is still present even though it is less pronounced. But, again the $\beta = \pm 10^\circ$ uncertainties are overlapping. However, at the highest speed, the error band is so narrow, that no overlap is possible, so this could indicate, that there is a slight

asymmetry somewhere in the model. Moving to Y' and N' the curves in Figures B.1 (d)-(f) and B.2 (a)-(c) show a behavior, which is normal for this kind of results, i.e. they are linear in the region around $\beta = 0^\circ$ and then they become non-linear as β increases. Further, the asymmetry, which was seen for X', is less pronounced for Y' and N'. Finally, the last results in Figure (d)-(f) show the sinkage at FP an AP. For the low speed, the sinkage is relatively small at both FP an AP. At the medium speed the FP sinkage increases strongly with the drift angle, while the AP sinkage still is relatively small. This is not changed until the speed is increased to the highest speed level. The FP sinkage shows the same behavior as for the medium speed, but at AP it increases strongly.

8.2 Dynamic test (Pure yaw)

According to the test program in Appendix A, the PMM test covers a number of pure yaw conditions. But, only one condition, $r' = 0.3$, at each of the Froude numbers 0.138, 0.280 and 0.410 are considered for uncertainty assessment. The three cases are marked with "*" in the test program. In this context focus is placed on the uncertainty assessment, so the discussion of the results will cover the three conditions, which are presented in sections C.1, C.4 and C.5 in appendix C. The time series for the remaining conditions are plotted in Appendix D. A relatively detailed discussion will be given for the Fr=0.280 condition and afterwards the findings will briefly be related to the results from the two other Froude numbers.

Starting with the results in C.1, the section is subdivided into five subsections. Section C.1.1 shows the time series over one period for all the motion parameters, i.e. the heading, the velocities and the accelerations plus the uncertainty components related to these quantities. Section C.1.2 shows the measured and the non-dimensionalized *X*-force plus the uncertainty contributions from the error sources described earlier in the report. Sections C.1.3 and C.1.4 do the same, but instead of the *X*-force they show the *Y*-force and the yaw moment, respectively. Finally, C.1.5 shows the sinkage at AP and FP together with the precision limit. In connection with the presented data two things should be noted: 1) When the term "measured" is used for the forces and moments it means the quantity as measured at the gauge, i.e. it is the quantity, which goes into the data reduction equations, which again means that it consists of both hydrodynamic and inertial contributions. 2) The heading, the velocities, the accelerations and the sinkage values are all mean values based on the average of the 12 repeat tests. This means that the plotted value at some time t_0 is obtained as the average of 12 values, which are taken out of the time series at t_0.

With respect to the bias limit contributions described in sections 7.3.9 to 7.3.15 the following can be observed for the motion parameters.

The heading ψ is shown in Figure C.1.1.1 (a) together with the uncertainty band representing $B_{heading}$. If the error composition is studied closer, Figure C.1.1.1 (b) shows that the dominating source originates from the uncertainty B_{beta} in the drift angle, i.e. the errors related to the setting of the drift angle on the PMM and the alignment of the model.

The transverse PMM velocity v_{PMM} is shown in Figure C.1.1.2 (a) together with the total uncertainty band $Epsilon_{vPMM}$. Figure C.1.1.2 (b) shows that there is no dominating error source since the errors are of approximately the same size. Though, it should be noted,

that the contribution from the PMM revolutions B_N tend to become stronger throughout the period.

The sway velocity v is shown in Figure C.1.1.3 (a) together with the total uncertainty band B_v. Ideally, v should be zero for pure yaw during the whole PMM cycle. However, due to the way the PMM is designed, the $v = 0$ condition can only be obtained in the point where $r = r_{\max}$. In the other points v is different from zero but also very small. However, with the observed magnitude of the uncertainty, the v deviation from zero is so small, that it disappears in the "noise" band of the system. It should be noted that v is included in the data reduction equations, so inertial forces caused by v being different from zero are accounted for in the results. With respect to the uncertainty Figure C.1.1.3 (b) shows that the heading error $B_{psi\ sway}$ dominates B_v. Recalling the drift angle dominated results for ψ it therefore turns out that v to a certain degree is dominated by the uncertainty related to the drift angle.

The transverse PMM acceleration $\dot{v}_{PMM}$ is shown in Figure C.1.1.4 (a) together with the total uncertainty $Epsilon_{vdotPMM}$. Figure C.1.1.4 (b) shows that there is no dominating error source since the errors are of approximately the same size. Though, as was the case for v_{PMM} the contribution from the PMM revolutions B_N tends to become larger throughout the period.

The sway acceleration $\dot{v}$ is shown in Figure C.1.1.5 (a) together with the total uncertainty band representing $B_{\dot{v}}$. Ideally, $\dot{v}$ should be zero for pure yaw, but due to variations in v described above, this cannot be obtained. Concerning the uncertainty Figure C.1.1.5 (b) shows that the uncertainties related to the PMM acceleration $B_{vdotPMM\ sway}$ and the yaw rate $B_{r\ sway}$ dominate. Both of these uncertainties are to a certain degree governed by the PMM revolutions, which again influences $\dot{v}$. It should also here be noted that $\dot{v}$ is included in the data reduction equations, so inertial forces caused by $\dot{v}$ being different from zero are accounted for in the results.

The yaw rate r is shown in Figure C.1.1.6 (a) together with the total uncertainty B_r. Figure C.1.1.6 (b) shows that there is no dominating error source since the errors are of approximately the same size. Though, as was the case for v_{PMM} the contribution from the PMM revolutions B_N tends to become larger throughout the period.

The yaw acceleration $\dot{r}$ is shown in Figure C.1.1.7 (a) together with the total uncertainty $B_{\dot{r}}$. Figure C.1.1.7 (b) shows that the errors are of approximately the same size and that the contribution from the PMM revolutions B_N tends to become larger throughout the period.

The surge velocity u is shown in Figure C.1.1.8 (a) together with the total uncertainty B_u. As seen u varies with time, but this is the consequence of running the dynamic pure yaw test with fixed carriage speed. With respect to the uncertainties Figure C.1.1.8 (b) does not surprisingly show that the uncertainty mainly is related to the uncertainty of the carriage speed.

Finally, the surge acceleration $\dot{u}$ is shown in Figure C.1.1.9 (a) together with $B_{\dot{u}}$. From Figure C.1.1.9 (b) it appears that $B_{\dot{u}}$ mainly is governed by the uncertainty related to the transverse PMM velocity and acceleration. It should be noted that any uncertainty originating from acceleration of the carriage is not included in the analysis.

The next quantity is the longitudinal force, for which the bias limit contributions related to the measured force F_X and to the non-dimensional force coefficient X' are described in sections 7.3.16 and 7.2.1, respectively.
Figures C.1.2.1 (a) and (b) shows the total uncertainty of F_X plus all the individual bias limit contributions. Based on the figures it is seen that it mainly consists of the contribution from the acquisition $B_{acquis,FX}$, which originates from the check calibration of the gauges in the *X*-direction. It appears that $B_{acquis,FX}$ is approximately three times larger than the next largest contribution $B_{vdot,FX}$. Finally, Figure C.1.2.3 (a) shows F_X together with the uncertainty band given by B_{F_X}.

With respect to the non-dimensional *X*-force X', Figures 1.2.2 (a) and (b) shows all the individual contributions to the uncertainty $U_{X'}$ of X'. From the figures it is seen that two contributions dominates the uncertainty. The two originates from the measured *X*-force F_X and from the surge velocity u. Based on earlier findings these two contributions are dominated by uncertainties from the acquisition in the calibration and the carriage speed. Finally, Figure C.1.2.3 (b) summarizes the results. It shows X' together with the bias and precision limits and the total uncertainty. The precision limit is quite small, which indicates a good repeatability of the measurement. The result is that the total uncertainty mainly consists of bias errors.

Concerning the transverse *Y*-force the bias limit contributions related to the measured force F_Y and to the non-dimensional force coefficient Y' are described in sections 7.3.17 and 7.2.2, respectively. Figures C.1.3.1 (a) and (b) show the total uncertainty B_{F_Y} of F_Y plus all the individual bias limit contributions. Based on the figures it is seen that it mainly consists of the contributions from 1) the sway velocity, $B_{v,FY}$ and 2) the acquisition, $B_{acquis,FY}$, which originates from the calibration of the gauges in the *Y*-direction. Recalling the results for v the uncertainty related to this quantity was drift angle dominated, so indirectly, the drift angle uncertainty has a relatively strong influence on the *Y*-force via v. Finally, Figure C.1.3.3 (a) summarizes the results by showing F_Y together with the uncertainty band given by B_{F_Y}.

With respect to Y', Figures 1.3.2 (a) and (b) show all the individual contributions to the uncertainty $U_{Y'}$ of Y'. Based on the figures it is seen that the contribution originating from the measured *Y*-force F_Y dominates. By tracing the error sources through the previous findings it turns out that the significant sources to B_{F_Y} basically originate from the uncertainties in F_Y related to the drift angle and the acquisition. Finally, Figure C.1.3.3 (b) shows Y' together with the bias and precision limits and the total uncertainty $U_{Y'}$. Again the precision limit is quite small, which indicates a good repeatability of the measurement and the outcome is that the total uncertainty mainly consists of pure bias errors.

The final quantities to be discussed, covers the yaw moment. However, based on Figures C.1.4.1 (a) and (b) it turns out that the behavior of the bias limits related to the measured yaw moment M_Z is similar to the behavior of B_{F_Y}. The same is the case for the bias limits related to N' in Figures C.1.4.2 (a) and (b), since it turns out that they behave as the bias limits for Y'. This may not be surprising since the moment is

determined on the basis of the *Y*-force. Finally, Figures C.1.4.2 (a) and (b) show M_Z and N' together with their uncertainties.

As mentioned above two additional pure yaw cases have been considered, namely one at a lower speed, $Fr = 0.138$ and one at higher speed $Fr = 0.410$ than the case discussed above. The results for $Fr = 0.138$ are shown in sections C.2.1 to C.2.4, while the $Fr = 0.410$ results are shown in sections C.3.1 to C.3.4. The variation in the individual bias limits in the figures will not be described in detail here, so the reader should check the figures for details. Instead the overall features will briefly be summarized. First of all the trend where the bias limit dominates over the precision limit is observed for both the high and the low Froude number. With respect to how the error sources contribute to the uncertainties of the forces and moment for the high and low speed, they are basically the same as for the medium speed. This means that F_X is dominated by acquisition and X' by acquisition and carriage speed. F_X, M_Z, Y' and N' are dominated by drift angle and acquisition.

In connection with the static test results the uncertainties were expressed as percentages of the considered force or moment, but with the time varying and zero crossing forces this will lead to percentages, which vary from a finite value to infinity throughout the period. Therefore, in order to take out some values, which can be used for a quantitative comparison between the three conditions, the values at the maximum yaw rate, which is a kind of target yaw rate for the individual test, will be used.
Table 8.2.1 shows the data for the *X*-force and the related uncertainties. Starting with the measured *X*-force F_X it is seen that the bias limit is highest at the low speed and that it decreases when the speed is increased. If the bias limit is related to the magnitude of the force, the percentage is relatively high at the low speed, where the measured force naturally is small. However, as speed is increased, the bias limit starts to play a less important role so the percentage decreases. The composition of error contributions in the bias limit is discussed above. With respect to the non-dimensional *X*-force, the table shows, that the bias errors dominates the uncertainty. Further, the uncertainty is high at the lowest speed, but it decreases as the speed is increased. As was mentioned in connection with the static drift results, the small model size combined with the low speed at $Fr = 0.138$ results in small forces, so the uncertainty appears relatively high.

	Fr=0.138	Fr=0.280	Fr=0.410
$r_{\max}$ [rad/s]	0.065	0.132	0.193
B_{F_X} [N]	0.504	0.604	1.255
F_X [N]	-4.569	-20.229	-61.660
B_{F_X} in % of F_X [%]	11.0	3.0	2.0
$B_{X'}$ [--]	0.00197	0.00063	0.00077
$P_{X'}$ [--]	0.00031	0.00007	0.00011
$U_{X'}$ [--]	0.00199	0.00064	0.00078
X' [--]	-0.01761	-0.01882	-0.02688
$U_{X'}$ in % of X' [%]	11.3	3.4	2.9

Table 8.2.1. Uncertainties and bias limits related to the X-force, where $r = r_{\max}$.

	Fr=0.138	Fr=0.280	Fr=0.410
$r_{\max}$ [rad/s]	0.065	0.132	0.193
B_{F_Y} [N]	0.433	0.954	1.175
F_Y [N]	-16.200	-73.236	-155.433
B_{F_Y} in % of F_Y [%]	2.7	1.3	0.8
$B_{Y'}$ [--]	0.00174	0.00094	0.00056
$P_{Y'}$ [--]	0.00057	0.00025	0.00018
$U_{Y'}$ [--]	0.00183	0.00097	0.00059
Y' [--]	-0.01155	-0.01759	-0.01704
$U_{Y'}$ in % of Y' [%]	15.8	5.5	3.5

Table 8.2.2. Uncertainties and bias limits related to the Y-force, where $r = r_{\max}$.

Table 8.2.2 shows the data for the *Y*-force together with its uncertainties. For the measured *Y*-force F_Y, it is found that the bias limit increases with the speed. However, so does the measured force, so the uncertainty is generally small relative to the force. The composition of error contributions in the bias limit is discussed above. With respect to Y', the table shows that the bias limits dominate the uncertainty compared to the precision limits and that the uncertainty relative to the force coefficient decreases with the speed.
If the behavior of the uncertainties for the *Y*-force is compared with the one for the *X*-force, one notices that B_{F_X} in percent of F_X is of the same order of magnitude as $U_{X'}$ in percent of X'. But, this is not the case for the *Y*-force. If $U_{Y'}$ for the low Froude number in Table 8.2.2 is compared with $U_{Y'}$ for static drift in Table 8.1.5, they are basically the same, which indicates that the magnitude of the uncertainty has not changed dramatically. Therefore, the percentage of 15.8% is related to the magnitude of Y', which represents the hydrodynamic part of the *Y*-force. It turns out that the measured *Y*-force is around 16 N. Out of this force the hydrodynamic part only constitutes 3 N, while the rest is inertial forces. Therefore, the uncertainty becomes relatively large compared to the hydrodynamic force. For the *X*-force the measured force approximately equals the hydrodynamic part, so the percentage does not change much.

Table 8.2.3 shows the yaw moment and the related uncertainties. As was the case for the *Y*-force both the bias limit and the measured moment increase with speed. However, the moment increase is larger than the bias limit increase, so relatively the bias limits constitute a smaller and smaller part of the measured moment when speed is increased. The composition of error contributions in the bias limit is discussed above. With respect to N', the table shows, that the bias errors dominates the uncertainty. Further, the uncertainty is highest at the lowest speed, but it decreases with increased speed.

	Fr=0.138	Fr=0.280	Fr=0.410
$r_{\max}$ [rad/s]	0.065	0.132	0.193
B_{M_Z} [Nm]	0.750	1.762	1.771
M_Z [Nm]	-10.217	-56.129	-162.448
B_{M_Z} in % of M_Z [%]	7.3	3.1	1.1
$B_{N'}$ [--]	0.00074	0.00043	0.00024
$P_{N'}$ [--]	0.00008	0.00011	0.00009
$U_{N'}$ [--]	0.00075	0.00045	0.00026
N' [--]	-0.01025	-0.01348	-0.01821
$U_{N'}$ in % of N' [%]	7.3	3.3	1.4

Table 8.2.3. Uncertainties and bias limits related to the yaw moment, where $r = r_{\max}$.

The final quantity to be mentioned is the sinkage of the model at AP and FP. As mentioned earlier, no bias limit estimates has been made for these quantities. But, since data is available from the twelve repeat tests, is has been possible to estimate the precision limits. Figures C.1.5.1 (a) and (b) in section C.1.5 show the results at FP and AP, respectively for pure yaw at $Fr = 0.280$. It appears that the sinkage varies through the period. Though, the variations are small and they are clearly taking place around specific vales. This means that the sinkage is oscillating around 0.0081m at FP and around 0.0026m at AP. The results for the remaining two conditions $Fr = 0.138$ and $Fr = 0.410$ are found in Figures C.4.5.1 (a) and (b) in section C.4.5 and in Figures C.5.5.1 (a) and (b) in section C.5.5, respectively.

8.3 Dynamic test (Pure sway)

According to Appendix A, the PMM test covers three pure sway conditions at the Froude number 0.280. One of them is considered for uncertainty assessment, which means that it is repeated twelve times in order to be able to estimate the precision limits. The condition is marked with "*" in the test program. The discussion of the results will be focused on the uncertainty assessment case, which is presented in section C.2 in appendix C. The time series for the remaining conditions are plotted in Appendix D.

Concerning the bias limit contributions described in sections 7.3.9 to 7.3.15 the following can be observed for the motion parameters in pure sway.
The heading ψ, which equals zero for pure sway, is shown in Figure C.2.1.1 (a) together with the uncertainty band representing $B_{heading}$. As was the case for pure yaw, Figure C.2.1.1 (b) shows that the dominating error source originates from the uncertainty B_{beta} in the drift angle, i.e. errors related to the setting of the drift angle on the PMM and the alignment of the model.
The transverse PMM velocity v_{PMM} is shown in Figure C.2.1.2 (a) together with the total uncertainty band $Epsilon_{vPMM}$. Figure C.2.1.2 (b) shows that there is no dominating error source since the errors are of approximately the same size. However, it should be noted, that the contribution from the PMM revolutions B_N tends to become stronger throughout the period. Since the PMM rpms and sway setting are the same as for pure yaw, the uncertainties are the same.

The sway velocity v is shown in Figure C.2.1.3 (a) together with the total uncertainty band B_v. In opposition to pure yaw, v is different from zero in the pure sway condition. With respect to the uncertainty Figure C.2.1.3 (b) shows that the heading error $B_{psi\ sway}$ dominates B_v. Recalling the drift angle dominated results for ψ it therefore turns out that v to a certain degree is dominated by the uncertainty related to the drift angle.

The transverse PMM acceleration $\dot{v}_{PMM}$ is shown in Figure C.2.1.4 (a) together with the total uncertainty $Epsilon_{vdotPMM}$ and Figure C.2.1.4 (b) shows the individual contributions to the total uncertainty. $\dot{v}_{PMM}$ is the same as for pure yaw, so it will not be discussed further here.

The sway acceleration $\dot{v}$ is shown in Figure C.2.1.5 (a) together with the total uncertainty band representing $B_{\dot{v}}$. In opposition to pure yaw, $\dot{v}$ is no longer zero. Concerning the uncertainty Figure C.2.1.5 (b) shows that the PMM acceleration error $B_{vdotPMM\ sway}$ and the yaw rate error $B_{r\ sway}$ are the only contributions to the uncertainties. Both of these uncertainties are to a certain degree governed by the PMM revolutions, which again influences $\dot{v}$.

The yaw rate r, which is zero for pure sway, is shown in Figure C.2.1.6 (a) together with the total uncertainty B_r. Figure C.2.1.6 (b) shows that the only contribution to the uncertainty is the one originating from the setting of the yaw amplitude.

The yaw acceleration $\dot{r}$, which also is zero, is shown in Figure C.2.1.7 (a) together with the total uncertainty $B_{\dot{r}}$. Further, Figure C.2.1.7 (b) shows that uncertainty only originates from yaw amplitude setting, as was the case for the yaw rate.

The surge velocity u, which for pure sway equals the carriage speed, is shown in Figure C.2.1.8 (a) together with the total uncertainty B_u. In the analysis it is assumed that the carriage speed is constant, but it appears that u varies slightly through the run. With respect to the uncertainties Figure C.2.1.8 (b) shows that the uncertainty mainly is related to the uncertainty of the carriage speed.

Finally, the surge acceleration $\dot{u}$, which is assumed to be zero, is shown in Figure C.2.1.9 (a) together with $B_{\dot{u}}$. From Figure C.2.1.9 (b) it appears that $B_{\dot{u}}$ is governed by the uncertainty related to the heading. However, it should be noted that any uncertainty originating from acceleration of the carriage is not included in the analysis. But, based on the variation of the velocity, which was observed in Figure C.2.1.8, there is a small acceleration of the carriage. In future applications, this acceleration could be accounted for by including the observed acceleration as an extra uncertainty in $B_{\dot{u}}$.

The next quantity is the longitudinal force, for which the bias limit contributions related to the measured force F_X and to the non-dimensional force coefficient X' are described in sections 7.3.16 and 7.2.1, respectively.

Figures C.2.2.1 (a) and (b) shows the total uncertainty of F_X plus all the individual bias limit contributions. From the figures it is seen that the uncertainty mainly consists of the contribution from the acquisition $B_{acquis,FX}$, which originates from the check calibration of the gauges in the *X*-direction. Since $B_{acquis,FX}$ dominates, the bias limit related to F_X in sway is approximately the same as for pure yaw. Finally, Figure C.2.2.3 (a) shows F_X together with the uncertainty band given by B_{F_X}.

With respect to the non-dimensional *X*-force X', Figures 2.2.2 (a) and (b) shows all the individual contributions to the uncertainty $U_{X'}$ of X'. As was the case for pure yaw, it is

seen that two contributions dominates the uncertainty. The two originates from the measured *X*-force F_X and from the surge velocity u. Based on earlier findings these two contributions are dominated by uncertainties from the acquisition in the calibration and the carriage speed. Finally, Figure C.2.2.3 (b) summarizes the results. It shows X' together with the bias and precision limits and the total uncertainty. As was the case for pure yaw, the precision limit is quite small, which indicates a good repeatability of the measurement. The result is that the total uncertainty almost is pure bias limit.

For the transverse *Y*-force the bias limit contributions related to the measured force F_Y and to the non-dimensional force coefficient Y' are described in sections 7.3.17 and 7.2.2, respectively. Figures C.2.3.1 (a) and (b) show the total uncertainty of F_Y plus all the individual bias limit contributions. Based on the figures it is seen that it mainly consists of the contributions from 1) the acquisition, $B_{acquis,FY}$, which originates from the calibration of the gauges in the *Y*-direction and 2) the sway velocity, $B_{v,FY}$. Recalling the results for v the uncertainty related to this quantity was drift angle dominated, so indirectly, the drift angle uncertainty has a strong influence on the *Y*-force via v. This was also observed for pure yaw. Finally, Figure C.2.3.3 (a) summarizes the results by showing F_Y together with the uncertainty band given by B_{F_Y}.

With respect to Y', Figures 2.3.2 (a) and (b) show all the individual contributions to the uncertainty $U_{Y'}$ of Y'. Based on the figures it is seen that the contribution originating from the measured *Y*-force F_Y dominates. By tracing the error sources through the previous findings it turns out that the significant sources to B_{F_Y} basically originate from the uncertainties in F_Y related to the acquisition and the drift angle. Finally, Figure C.2.3.3 (b) shows Y' together with the bias and precision limits and the total uncertainty $U_{Y'}$. Again the precision limit is quite small, which indicates a good repeatability of the measurement and the outcome is that the total uncertainty is mainly pure bias errors.

The final quantities to be discussed concern the yaw moment. However, based on Figures C.2.4.1 (a) and (b) it turns out that the behavior of the bias limits related to the measured yaw moment M_Z is similar to the behavior of B_{F_Y}. The same is the case for the bias limits related to N' in Figures C.2.4.2 (a) and (b), since it turns out that they behave as the bias limits for Y'. This may not be surprising since the moment is determined on the basis of the *Y*-force. Finally, M_Z and N' are shown in Figures C.2.4.2 (a) and (b) together with their uncertainties.

In connection with the pure yaw results above data was extracted at characteristic conditions in order to find data, which could be used for a quantitative study. In the pure yaw case the characteristic condition was chosen as the one where the maximum yaw rate occurs. A similar characteristic condition for pure sway is the condition where $v = v_{\max}$, i.e. where the sway velocity has its maximum.

	Fr=0.280
$v_{\max}$ [m/s]	0.304
B_{F_X} [N]	0.616
F_X [N]	-23.336
B_{F_X} in % of F_X [%]	2.6
$B_{X'}$ [--]	0.00064
$P_{X'}$ [--]	0.00009
$U_{X'}$ [--]	0.00065
X' [--]	-0.02128
$U_{X'}$ in % of X' [%]	3.1

Table 8.3.1. Uncertainties and bias limits related to the X-force, where $v = v_{\max}$.

	Fr=0.280
$v_{\max}$ [m/s]	0.304
B_{F_Y} [N]	0.965
F_Y [N]	-61.348
B_{F_Y} in % of F_Y [%]	1.6
$B_{Y'}$ [--]	0.00099
$P_{Y'}$ [--]	0.00013
$U_{Y'}$ [--]	0.00100
Y' [--]	-0.05658
$U_{Y'}$ in % of Y' [%]	1.8

Table 8.3.2. Uncertainties and bias limits related to the Y-force, where $v = v_{\max}$.

	Fr=0.280
$v_{\max}$ [m/s]	0.304
B_{M_Z} [Nm]	1.751
M_Z [Nm]	-133.538
B_{M_Z} in % of M_Z [%]	1.3
$B_{N'}$ [--]	0.00046
$P_{N'}$ [--]	0.00013
$U_{N'}$ [--]	0.00047
N' [--]	-0.03043
$U_{N'}$ in % of N' [%]	1.5

Table 8.3.3. Uncertainties and bias limits related to the yaw moment, where $v = v_{\max}$.

Tables 8.3.1 to 8.3.3 show the data for the *X*-force, the *Y*-force and the yaw moment. It can be noted that for all the data the bias limits are somewhat larger than the precision limits. If the magnitudes of the bias limits are compared with the pure yaw case at the corresponding Froude number in Tables 8.2.1 to 8.2.3, it turns out that the bias limits for pure sway has approximately the same size as in pure yaw. If the uncertainties are

expressed as percentage of the measured forces and moments the results in the tables below occur and it is seen, that they are smaller than in pure yaw. The reason is that the hydrodynamic transverse forces and yaw moments are much more pronounced in pure sway than in pure yaw. Actually, the flow in the pure sway condition is more like pure drift.

With respect to sinkage at AP and FP Figures C.2.5.1 (a) and (b) in section C.2.5 show the sinkage and the corresponding precision limits.

8.4 Dynamic test (Yaw and drift)

The final test type covers the yaw and drift test shown in the test program in Appendix A. Three yaw and drift tests are conducted at the Froude number 0.280 and one of them are considered for uncertainty assessment, i.e. it is repeated twelve times in order to estimate the precision limits. The condition is marked with "*" in the test program. The discussion of the results will be focused on the uncertainty assessment case, which is presented in section C.3 in appendix C. The time series for the remaining conditions are plotted in Appendix D.

With respect to the bias limit contributions of the motion parameters in sections 7.3.9 to 7.3.15, they are basically the same as for pure yaw, since the PMM setting and motion are the same. The only difference is the preset drift angle set on the PMM. In pure yaw the drift angle is zero, while $\beta \neq 0^\circ$ in yaw and drift. This leads to sway velocities and accelerations, which are different from zero, see Figures C.3.1.3 and C.3.1.5. Due to the similarity with pure yaw the motion parameters will not be discussed again. Instead the discussion can be found in section 8.2.

Concerning the longitudinal force, Figures C.3.2.1 (a) and (b) show the total uncertainty of F_X plus all the individual bias limit contributions. Based on the figures it is seen that the dominating contribution originates from the sway velocity $B_{v,FX}$. Compared to pure yaw this situation is different, since B_{F_X} is twice as big in yaw and drift due to the larger influence from the sway velocity. Finally, Figure C.3.2.3 (a) shows F_X together with the uncertainty band given by B_{F_X}.

With respect to the non-dimensional *X*-force X', Figures C.3.2.2 (a) and (b) shows all the individual contributions to the uncertainty $U_{X'}$ of X'. Based on a comparison with the pure yaw condition, it is found that all the contributions except for one are almost the same. The one, which is different, is the one occurring from the measured force bias limit, which according to the above discussion is twice the size in yaw and drift. Since B_{F_X} is v dominated and $B_{v,FX}$ to a large degree is heading dominated, which again is drift angle dominated, the results indicate, that the accuracy of the drift angle setting is more important in yaw and drift than in pure yaw. Finally, Figure C.3.2.3 (b) summarizes the results. It shows X' together with the bias and precision limits and the total uncertainty. The precision limit is quite small, which indicates a good repeatability of the measurement. The result is that the total uncertainty mainly consists of pure bias errors.

For the transverse *Y*-force the bias limit contributions related to the measured force F_Y and to the non-dimensional force coefficient Y' are described in sections 7.3.17 and 7.2.2, respectively. Figures C.3.3.1 (a) and (b) show the total uncertainty of F_Y plus all

the individual bias limit contributions. As was the case for pure yaw, the figures show that the uncertainty mainly consists of the contributions from 1) the acquisition, $B_{acquis,FY}$, which originates from the calibration of the gauges in the *Y*-direction and 2) the sway velocity, $B_{v,FY}$. Recalling the results for v the uncertainty related to this quantity was drift angle dominated, so indirectly, the drift angle uncertainty has a strong influence on the *Y*-force via v. Finally, Figure C.3.3.3 (a) summarizes the results by showing F_Y together with the uncertainty band given by B_{F_Y}.

With respect to Y', Figures C.3.3.2 (a) and (b) show all the individual contributions to the uncertainty $U_{Y'}$ of Y'. Based on the figures it is seen that the contribution originating from the measured *Y*-force F_Y dominates. By tracing the error sources through the previous findings it turns out that the significant sources to B_{F_Y} basically originate from the uncertainties in F_Y related to the acquisition and the drift angle. Finally, Figure C.3.3.3 (b) shows Y' together with the bias and precision limits and the total uncertainty $U_{Y'}$. Again the precision limit is quite small, which indicates a good repeatability of the measurement and the outcome is that the total uncertainty mainly consists of bias errors.

The final quantity is the yaw moment. Based on Figures C.3.4.1 (a) and (b) it turns out that the behavior of the bias limits related to the measured yaw moment M_Z is similar to the behavior of B_{F_Y}. The same is the case for the bias limits related to N' in Figures C.3.4.2 (a) and (b), since it turns out that they behave as the bias limits for Y'. Finally, Figures C.3.4.2 (a) and (b) show M_Z and N' together with their uncertainties.

The characteristic condition chosen for yaw and drift in order to find data, which can be used for a quantitative study, is the same as for pure yaw, i.e. at the maximum yaw rate, $r = r_{\max}$. During the PMM cycle, there are to positions, where the yaw rate has a maximum, but due to the preset drift angle, they are different. At $r = r_{\max}$ the model points into the turn and at $r = -r_{\max}$ it points out of the turn. The situation where the model points into the turn is the most realistic seen from a maneuvering point of view, so the condition $r = r_{\max}$ is used.

	Fr=0.280
$r_{\max}$ [rad/s]	0.132
B_{F_X} [N]	1.373
F_X [N]	-34.456
B_{F_X} in % of F_X [%]	4.0
$B_{X'}$ [--]	0.00133
$P_{X'}$ [--]	0.00012
$U_{X'}$ [--]	0.00134
X' [--]	-0.02325
$U_{X'}$ in % of X' [%]	5.8

Table 8.4.1. Uncertainties and bias limits related to the *X*-force, where $r = r_{\max}$.

	Fr=0.280
$r_{\max}$ [rad/s]	0.132
B_{F_Y} [N]	0.892
F_Y [N]	-4.888
B_{F_Y} in % of F_Y [%]	18.2
$B_{Y'}$ [--]	0.00091
$P_{Y'}$ [--]	0.00032
$U_{Y'}$ [--]	0.00096
Y' [--]	0.04588
$U_{Y'}$ in % of Y' [%]	2.1

Table 8.4.2. Uncertainties and bias limits related to the *Y*-force, where $r = r_{\max}$.

The Tables 8.4.1 to 8.4.3 show the data for the *X*-force, the *Y*-force and the yaw moment. For all the data it appears that the bias limits are larger than the precision limits. If the magnitudes of the bias limits are compared with the pure yaw case at the corresponding Froude number in Tables 8.2.1 to 8.2.3, it turns out that the bias limits for the measured *X*-force in yaw and drift is almost twice the size of the value in pure yaw. For the *Y*-force and the yaw moment they are approximately the same. When it comes to the total uncertainties of the non-dimensional forces, they follow same trend as the bias limit, which is natural since the bias limit dominates the uncertainties. If the uncertainties are expressed as percentage of the force coefficients a comparison with the pure yaw condition reveals that $U_{X'}$ is bigger in yaw and drift, while $U_{Y'}$ and $U_{N'}$ are smaller than in pure yaw.

	Fr=0.280
$r_{\max}$ [rad/s]	0.132
B_{M_Z} [Nm]	1.416
M_Z [Nm]	59.150
B_{M_Z} in % of M_Z [%]	2.4
$B_{N'}$ [--]	0.00035
$P_{N'}$ [--]	0.00005
$U_{N'}$ [--]	0.00036
N' [--]	0.01354
$U_{N'}$ in % of N' [%]	2.7

Table 8.4.3. Uncertainties and bias limits related to the yaw moment, where $r = r_{\max}$.

With respect to sinkage at AP and FP Figures C.3.5.1 (a) and (b) in section C.3.5 show the sinkage and the corresponding precision limits.

9. Conclusion

The present report covers the work related to the development of a procedure for uncertainty assessment in connection with the Planar Motion Mechanism (PMM) test plus

application of the procedure on three static and five dynamic test cases, which are conducted with a model of the DDG51 Frigate. The static test cases cover pure drift at three different Froude numbers: $Fr = 0.138$, $Fr = 0.280$ and $Fr = 0.410$, while the dynamic test cases cover pure yaw at three conditions: $Fr = 0.138$, $Fr = 0.280$ and $Fr = 0.410$ plus one pure sway and one yaw and drift condition at $Fr = 0.280$.
The uncertainty assessment procedure focuses on the *X*- and *Y*-forces and the yaw moment in model scale and it is based on a set of data reduction equations adopted from the maneuvering community. The procedure covers estimates of 1) bias limits, i.e. the systematic errors in the system and 2) precision limits, i.e. the random errors. The bias limits are found on the basis of a number of error sources, which have been identified in a study of the PMM test system, while the precision limits are found on the basis of repeat tests.
With respect to the results of the application of the uncertainty assessment procedure, the following can be concluded:

I) For all the tests, i.e. static as well as dynamic, the repeatability is fairly good. Therefore, the results show an overall trend in the composition of the errors, where the bias errors dominate compared to the precision errors.

II) For the non-dimensional force coefficients from the static tests, the errors related to the measured forces themselves dominate compared to the errors introduced via the water density, the draft, the ship length and the carriage speed. With respect to the composition of the errors related to the measured forces, the acquisition or calibration error dominates the *X*-force for all speeds. For the *Y*-force and the yaw moment, the acquisition error dominates at low speed, but as speed is increased the error related to the applied drift angle setting on the PMM becomes more important. When all the error sources are combined into the final total uncertainty of the force and moment coefficients, and the individual uncertainties are related to the magnitude of the coefficients, it turns out that the uncertainty is highest at the low speed and that it decreases as speed is increased. Based on these findings two final remarks should be given for the static test: 1) One should be aware that when tests are conducted at low speeds the measured forces are small and consequently the bias dominated uncertainty of the measurement constitutes a relatively larger part of the measured force and 2) if it is desired to decrease the uncertainties, focus should be placed on the check calibration of the force gauges and the accuracy of the drift angle setting.

III) For the non-dimensional force coefficients from the dynamic pure yaw tests, the errors related to the measured forces themselves and to the surge and sway velocities dominate compared to the errors introduced via the water density, the draft, the ship length, the other motion parameters (velocities and accelerations), the model mass, the moment of inertia and the position of the center of gravity. Concerning the composition of the errors related to the measured forces, the *X*-force mainly consists of the acquisition errors at low speed, while both acquisition and surge velocity errors appear at the higher speeds. For the *Y*-force and the yaw moment, the acquisition error is present at all speeds, but as the speed is increased, the sway velocity also starts to play a role. When tracing the errors through the system, it turns out that the errors related to surge velocity originates from the uncertainty in the carriage speed, while error related to the sway velocity is governed by the uncertainty of the model heading, which is introduced via the uncertainty of the drift angle.
If the magnitudes of the total uncertainties of the non-dimensionalized force and moment coefficients are compared with the static drift results, the two sets of

uncertainties are of approximately the same size. However, if the uncertainties are related to the magnitude of the coefficients themselves at characteristic conditions (at maximum yaw rate), the fraction, which the uncertainty constitutes of the force, is in some cases higher in pure yaw, particularly at the low speed. The reason for this is that the force and moment coefficients represent the hydrodynamic forces and moments, which means that the inertial components have been removed. This means that in some cases the force experienced by the gauge may seem large, but if the force mainly is due to inertia the hydrodynamic part is small, so the uncertainty may seem higher when put in relation to the hydrodynamic force.
Based on these findings three final remarks should be given for the pure yaw test: 1) As for the static test, one should be aware that when tests are conducted at low speeds the measured forces are small and consequently the bias dominated uncertainty of the measurement constitutes a larger part of the measured force, 2) the uncertainty may seem small compared to the measured signal, but compared to the hydrodynamic force it may be somewhat higher and 3) if it is desired to decrease the uncertainties, focus should be placed on the check calibration of the force gauges, the accuracy of the drift angle setting and the uncertainty of the carriage speed.

IV) In the dynamic pure sway tests, the errors related to the measured forces themselves and to the surge and sway velocities dominate, as was the case in the pure yaw test. Concerning the composition of the errors related to the measured forces, the *X*-force mainly consists of the acquisition error. However, when the force is non-dimensionalized, the surge velocity also becomes important. For the *Y*-force and the yaw moment, both the acquisition and sway velocity errors influences the uncertainty related to the measured quantities, so they become dominant when the non-dimensional coefficients are calculated. Tracing the errors through the system shows that the errors related to the sway velocity is governed by the uncertainty of the drift angle, while the surge velocity is governed by the carriage speed.
The magnitude of the total uncertainties of the non-dimensionalized force and moment coefficients are approximately the same as for the pure yaw results. But, if the uncertainties are related to the magnitude of the coefficients themselves at characteristic conditions (at maximum sway velocity), the fraction, which the uncertainty constitutes of the force, is lower than in pure yaw, but similar to the static drift case.
Based on these findings it should be noted, that if it is desired to decrease the uncertainties, focus should be placed on the check calibration of the force gauges, the accuracy of the drift angle setting and the uncertainty of the carriage speed.

V) In the yaw and drift test, the errors related to the measured forces themselves and to the surge and sway velocities dominate, as was the case in the pure yaw test. Concerning the composition of the errors related to the measured *X*-force, the acquisition and the sway velocity errors are the most important ones. Actually, the sway velocity contribution is two times stronger than in pure yaw. When the force is non-dimensionalized, the surge velocity also becomes important, but this was also the case in pure yaw. For the *Y*-forces and the yaw moments, both the acquisition and sway velocity errors cause the measured quantities to be dominant when the non-dimensional coefficients are calculated. Tracing the errors through the system shows that the errors related to the sway velocity are governed by the uncertainty of the drift angle, while the surge velocity is governed by the carriage speed.
The magnitude of the total uncertainties of the *Y*-force and the moment are approximately the same as for the pure yaw results. But, the *X*-force is an exception, since it is larger. If the uncertainties are related to the magnitude of the coefficients

themselves at characteristic conditions (at maximum yaw rate), the fraction, which the uncertainty constitutes of the force, is slightly different from the pure yaw condition.
Based on these findings it should be noted, that if it is desired to decrease the uncertainties, focus should be placed on the check calibration of the force gauges, the accuracy of the drift angle setting and the uncertainty of the carriage speed.

In order to summarize and give a final comment on the results, it can be said that the present study reveals an acceptable level of the uncertainties related to the non-dimesionalized hydrodynamic forces, which are obtained on the basis of the data measured with the PMM equipment. Though, at low speed testing with small models, one must be aware of the fact that the uncertainties, relatively, constitute a larger part of the force or moment coefficients. As mentioned in the introduction the present model is quite small compared to the models, which are normally used for PMM testing. Therefore, the combination of the relatively low speed at the lowest Froude number and the small model results in forces, which are in the lower range of what normally, is measured. Therefore, the level of the uncertainties is expected to be higher at the lowest speed. Finally, it should be noted that with the present uncertainties, which are dominated by the drift angle setting, the carriage speed and the calibration, the uncertainty contributions from the PMM settings like the sway and yaw amplitudes are negligible. This is also the case for other quantities, which are related to things like masses, moments of inertia and geometry.

10. Recommendations for future work

In connection with future work on uncertainty assessment in connection with the PMM test, the following issues are of interest in future.

I) The effect of roll is not considered, so the model is fixed with zero heel angle, $\varphi = 0$. In the future the method should be extended in order to account for roll and heel by redoing parts of the presented analysis based on the equations of motion including roll and heel. If this were done it would also be possible to account for the errors in the up-right position of the model in 3-DOF tests of the same type as presented in this report.

II) In the present method it is assumed that the forced motion of the model is based on pure harmonic motions. However, the uncertainty analysis should be extended in order to investigate how deviations from the pure harmonic motions influence the results.

III) The carriage acceleration is assumed to be zero in the present work. Therefore, uncertainties related to acceleration of the carriage, which is introduced via variations in the carriage speed during the run, are not accounted for. In future work, this effect should be included, in order to determine the importance of this uncertainty contribution.

IV) No bias estimates were made for the sinkage of the model, so a method for assessment of this quantity should be developed.

V) Finally, it must be noted that the present work focuses on the force level only. This means that the uncertainties are estimated only for the coefficients defined above and that the uncertainties related to the traditional hydrodynamic derivatives and their

influence on later full scale maneuvering simulations are not considered. Investigation of these features could also be of interest in the future.

11. Acknowledgement

FORCE Technology and the US Office of Naval Research grant N00014-03-1-0347 under the Naval International Cooperative Opportunities in Science and Technology Program (NICOP) sponsored the present work.

References

Chislett, M. S. and Wagner Smitt, L.
"A Brief Description of the HyA Large Amplitude PMM System",
Hydro- and Aerodynamic Laboratory, Report No. Hy-16, Lyngby, Denmark, 1973.

Chislett, M. S.
"The Addition of a Heel-roll Servo Mechanism to the DMI Horizontal Planar Motion Mechanism",
Preprint of paper to be presented for discussion at MARSIM & ICSM '90, Tokyo, June 1990.

ITTC, 1999a
"Uncertainty Analysis in EFD, Uncertainty Assessment Methodology, 4.9-03-01-01",
22nd International Towing Tank Conference, Seoul, Korea/Beijing, China.

ITTC, 1999b
"Uncertainty Analysis, Example for Resistance Test, 4.9-03-01-01",
22nd International Towing Tank Conference, Seoul, Korea/Beijing, China.

Appendix A. Test programs

In the current appendix the applied test programs are listed in tables. The nomenclature, which is used in the tables are the same as used in the report. Though, there are two exceptions. The maximum yaw and sway velocities and accelerations are given in non-dimensional form. In order to bring them back to the dimensional form used in the report, the following relations can be used: $r'_{\max} = r_{\max} L_{pp}/U$, $v'_{\max} = v_{\max}/U$, $\dot{r}'_{\max} = \dot{r}_{\max}(L_{pp}/U)^2$ and $\dot{v}'_{\max} = \dot{v}_{\max} L_{pp}/U^2$.

Finally, a number "Run ID" is given for all the dynamic conditions, which are not considered in the uncertainty analysis. This number corresponds to the time series number, which is printed on the result pages in Appendix D.

A.1 Approach speed, Fr=0.138

Froude number, Fr [-]	Carriage speed, U_C [m/s]	Drift angle, β [deg.]
0.138	0.865	-20, -16, -12, -11, -10, -9, -6, -2, 0, 20, 16, 12, 11, 10*, 9, 6, 2

Table A.1.1. Test program for the static tests. "*" Indicates conditions, for which 12 repeat tests are conducted.

Fr [-]	U_C [m/s]	β [deg.]	$N-PMM$ [rpm]	S_{mm} [m]	Y_{mm} [m]	$r'_{\max}$ [--]	$\dot{r}'_{\max}$ [--]	No. of repeat.	Run ID
0.138	0.865	0	4.0	0.0266	0.0129	0.05	0.10	1	1066
0.138	0.865	0	4.0	0.0799	0.0387	0.15	0.29	1	1067
0.138*	0.865	0	4.0	0.1598	0.0774	0.30	0.57	12	---
0.138	0.865	0	4.0	0.2397	0.1161	0.45	0.83	1	1068
0.138	0.865	0	4.0	0.3196	0.1548	0.60	1.06	1	1069
0.138	0.865	0	5.0	0.2557	0.1548	0.75	1.66	1	1070

Table A.1.2. Test program for the dynamic pure yaw test. "*" Indicates the condition, for which uncertainty the analysis is conducted.

A.2 Approach speed, Fr=0.280

Froude number, Fr [-]	Carriage speed, U_C [m/s]	Drift angle, β [deg.]
0.280	1.755	-20, -16, -12, -11, -10, -9, -6, -2, 0, 20, 16, 12, 11, 10*, 9, 6, 2

Table A.2.1. Test program for the static tests. "*" Indicates conditions, for which 12 repeat tests are conducted.

Fr [-]	U_C [m/s]	Corresp. β [deg.]	$N-PMM$ [rpm]	S_{mm} [m]	Y_{mm} [m]	$v'_{\max}$ [--]	$\dot{v}'_{\max}$ [--]	No. of repeat.	Run ID
0.280	1.755	2	7.0	0.0418	0.0	0.03	0.06	1	1157
0.280	1.755	4	7.0	0.0835	0.0	0.07	0.12	1	1158
0.280*	1.755	10	7.0	0.2079	0.0	0.17	0.29	12	---

Table A.2.2. Test program for the dynamic pure sway test. "*" Indicates the condition, for which uncertainty the analysis is conducted. Note that the β setting on the PMM is 0 for pure sway.

Fr [-]	U_C [m/s]	β [deg.]	$N-PMM$ [rpm]	S_{mm} [m]	Y_{mm} [m]	$r'_{\max}$ [--]	$\dot{r}'_{\max}$ [--]	No. of repeat.	Run ID
0.280	1.755	0	7.0	0.0358	0.0150	0.05	0.08	1	1071
0.280	1.755	0	7.0	0.1074	0.0449	0.15	0.25	1	1072
0.280*	1.755	0	7.0	0.2148	0.0897	0.30	0.49	12	---
0.280	1.755	0	7.0	0.3222	0.1346	0.45	0.70	1	1126
0.280	1.755	0	9.0	0.2599	0.1396	0.60	1.20	1	1127
0.280	1.755	0	9.0	0.3249	0.1745	0.75	1.44	1	1128

Table A.2.3. Test program for the dynamic pure yaw test. "*" Indicates the condition, for which uncertainty the analysis is conducted.

Fr [-]	U_C [m/s]	β [deg.]	$N-PMM$ [rpm]	S_{mm} [m]	Y_{mm} [m]	$r'_{\max}$ [--]	$\dot{r}'_{\max}$ [--]	No. of repeat.	Run ID
0.280	1.755	9	7.0	0.2148	0.0897	0.30	0.49	1	1159
0.280	1.755	11	7.0	0.2148	0.0897	0.30	0.49	1	1160
0.280*	1.755	10	7.0	0.2148	0.0897	0.30	0.49	12	---

Table A.2.4. Test program for the dynamic yaw and drift test. "*" Indicates the condition, for which uncertainty the analysis is conducted.

A.3 Approach speed, Fr=0.410

Froude number, Fr [-]	Carriage speed, U_C [m/s]	Drift angle, β [deg.]
0.410	2.570	-12, -11, -10, -9, -6, -2, 0, 12, 11, 10*, 9, 6, 2

Table A.3.1. Test program for the static tests. "*" Indicates conditions, for which 12 repeat tests are conducted.

Fr [-]	U_C [m/s]	β [deg.]	$N-PMM$ [rpm]	S_{mm} [m]	Y_{mm} [m]	$r'_{\max}$ [--]	$\dot{r}'_{\max}$ [--]	No. of repeat.	Run ID
0.410	2.570	0	7.0	0.0768	0.0219	0.05	0.06	1	1129
0. 410	2.570	0	7.0	0.2303	0.0657	0.15	0.17	1	1130
0. 410*	2.570	0	12.5	0.1444	0.0736	0.30	0.60	12	---
0. 410	2.570	0	12.5	0.2167	0.1104	0.45	0.87	1	1131

Table A.3.2. Test program for the dynamic pure yaw test. "*" Indicates the condition, for which uncertainty the analysis is conducted.

Appendix B. Results from static tests

The current appendix shows the forces and moments measured in the static drift tests.

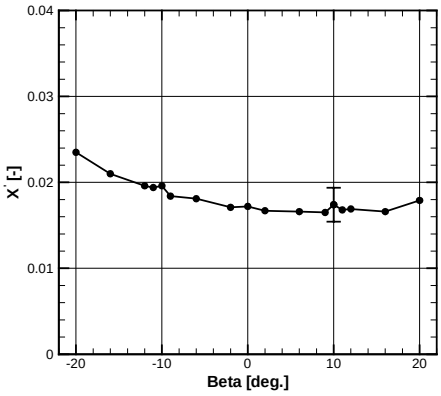

(a) X-force, $Fr = 0.138$

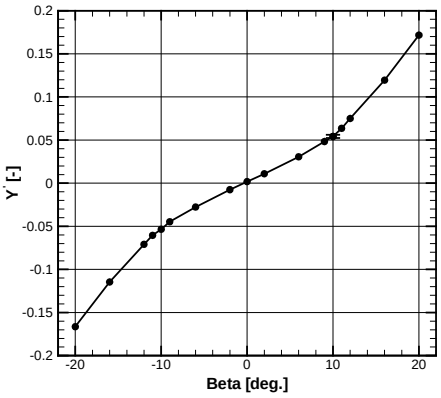

(d) Y-force, $Fr = 0.138$

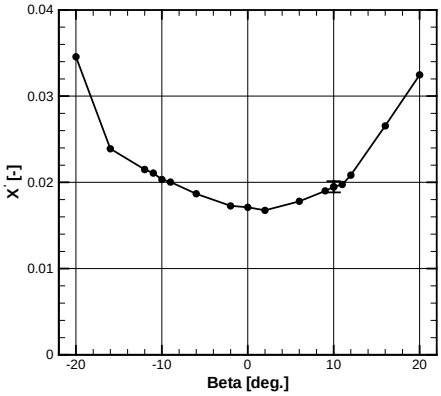

(b) X-force, $Fr = 0.280$

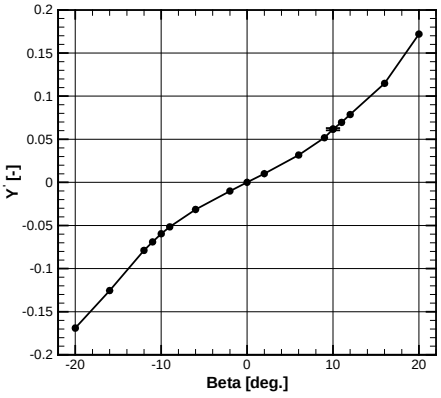

(e) Y-force, $Fr = 0.280$

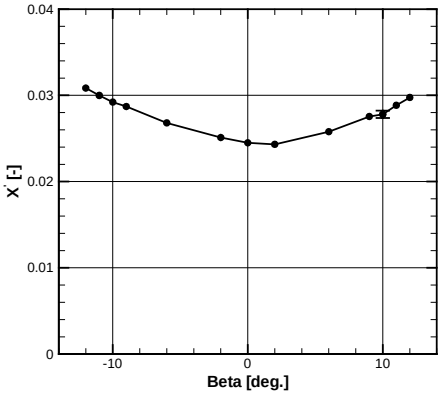

(c) X-force, $Fr = 0.410$

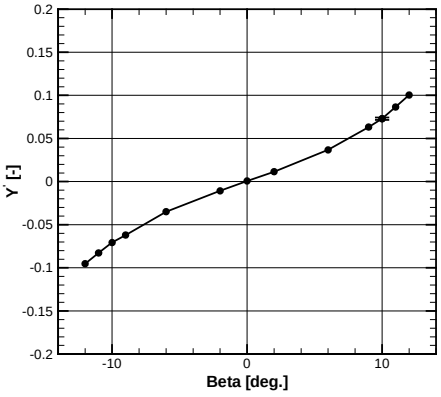

(f) Y-force, $Fr = 0.410$

Figure B.1. X- and Y-forces measured in pure drift at three different Froude numbers.

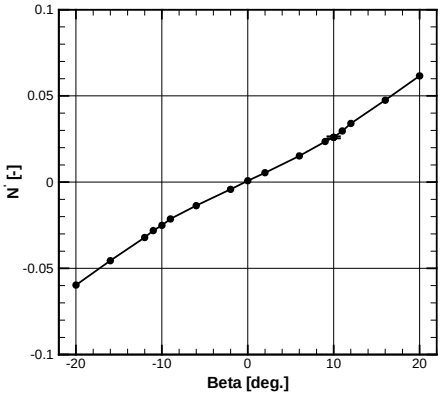

(a) Yaw moment, $Fr = 0.138$

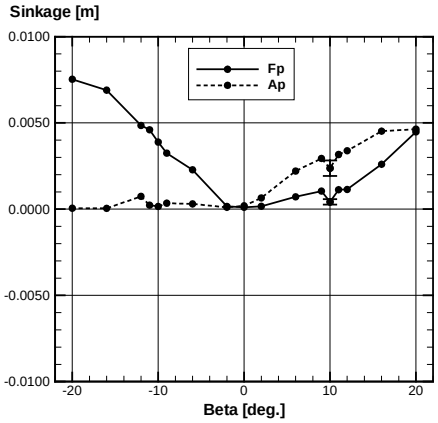

(d) Sinkage at AP and FP, $Fr = 0.138$

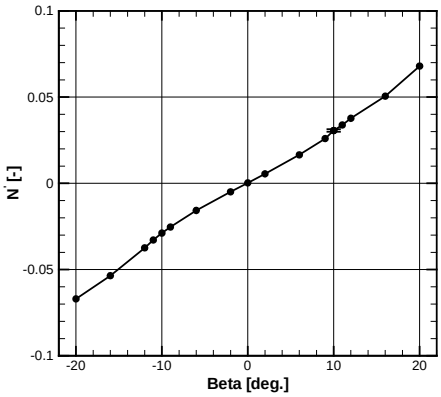

(b) Yaw moment, $Fr = 0.280$

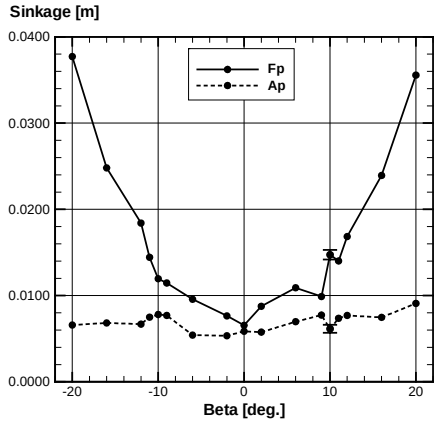

(e) Sinkage at AP and FP, $Fr = 0.280$

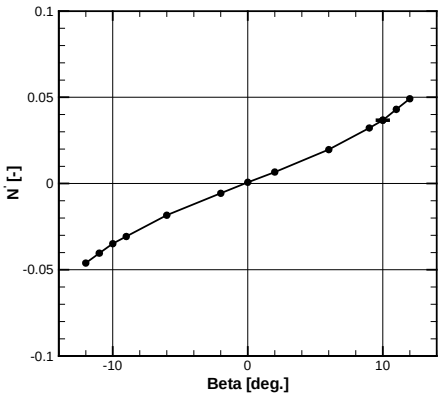

(c) Yaw moment, $Fr = 0.410$

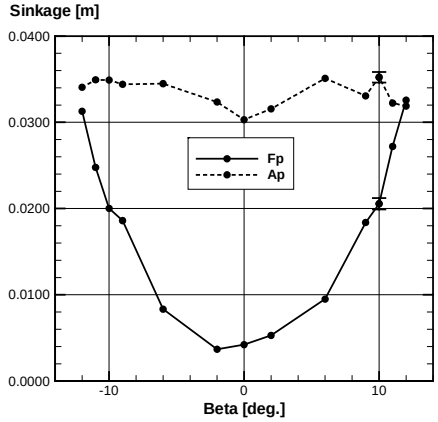

(f) Sinkage at AP and FP, $Fr = 0.410$

Figure B.2. Yaw moment and sinkage measured in pure drift at three different Froude numbers.

Appendix C. Results from uncertainty analysis on dynamic test cases

The present appendix shows the time series for the dynamic test cases, which are dealt with in the uncertainty analysis. The shown quantities cover motion parameters, forces and moments and the uncertainties related to these quantities.

C.1 Dynamic test (Pure yaw), Fr=0.280

C.1.1 Motion parameters

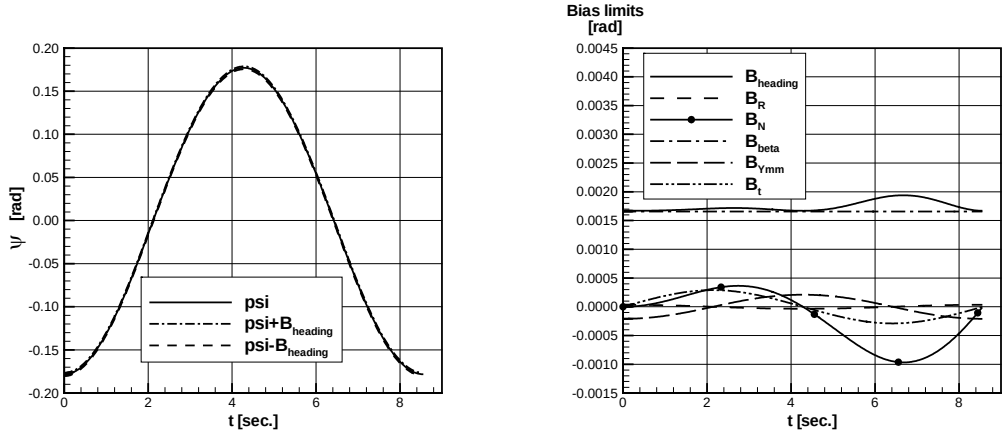

(a) (b)

Figure C.1.1.1. (a) Heading angle and (b) bias limits.

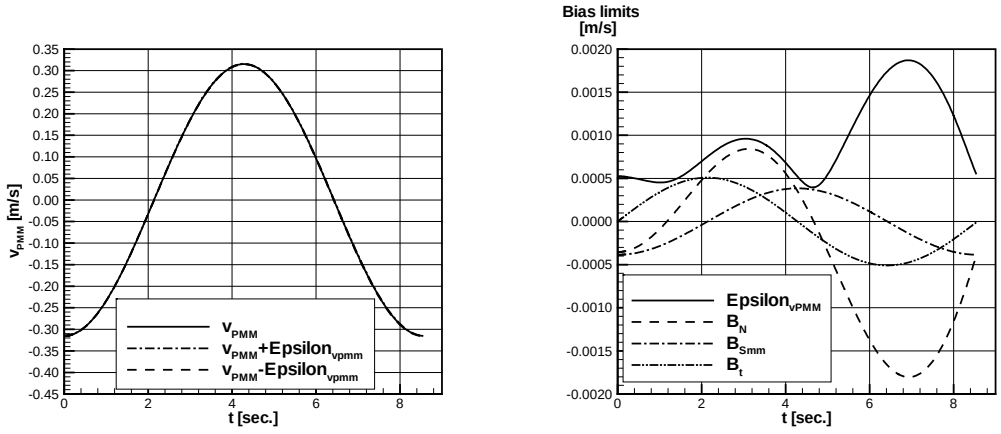

(a) (b)

Figure C.1.1.2. (a) Transverse PMM velocity and (b) bias limits.

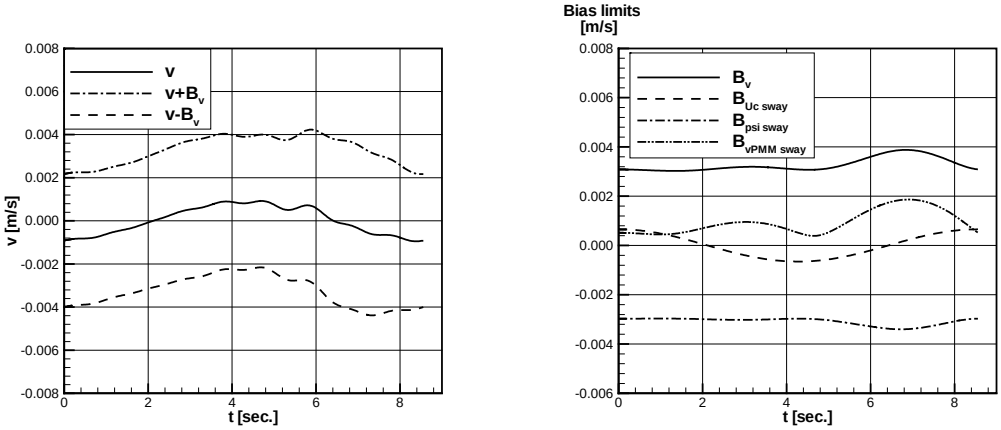

(a) (b)

Figure C.1.1.3. (a) Sway velocity and (b) bias limits.

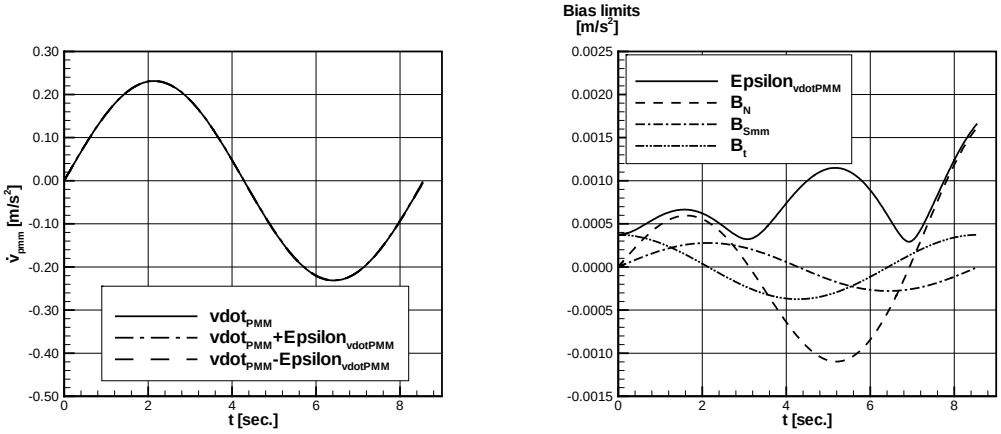

(a) (b)

Figure C.1.1.4. (a) Transverse PMM acceleration and (b) bias limits.

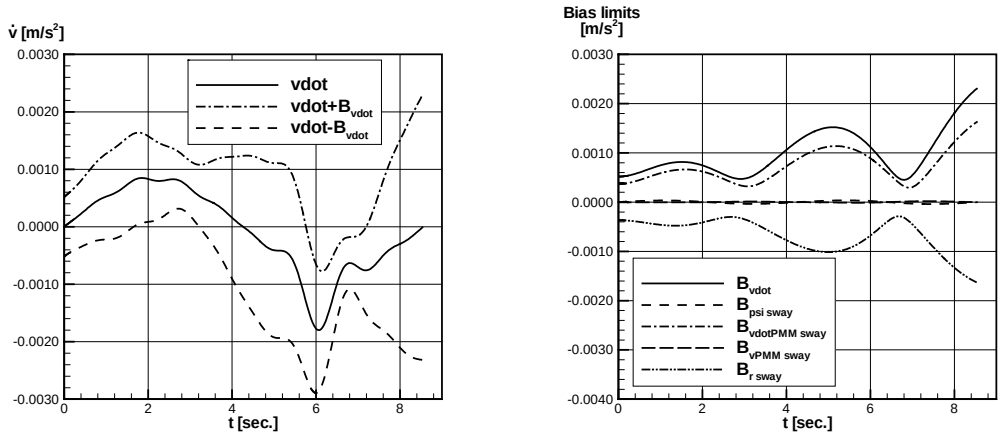

(a) (b)

Figure C.1.1.5. (a) Sway acceleration and (b) bias limits.

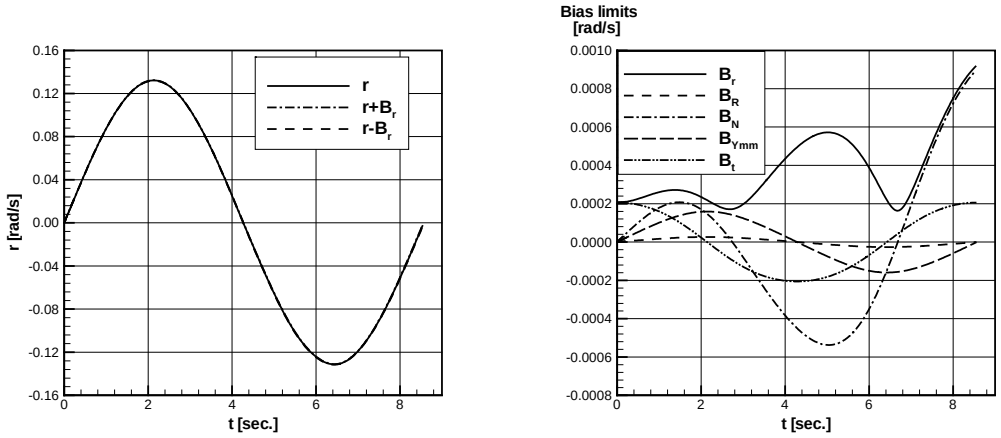

(a) (b)

Figure C.1.1.6. (a) Yaw rate and (b) bias limits.

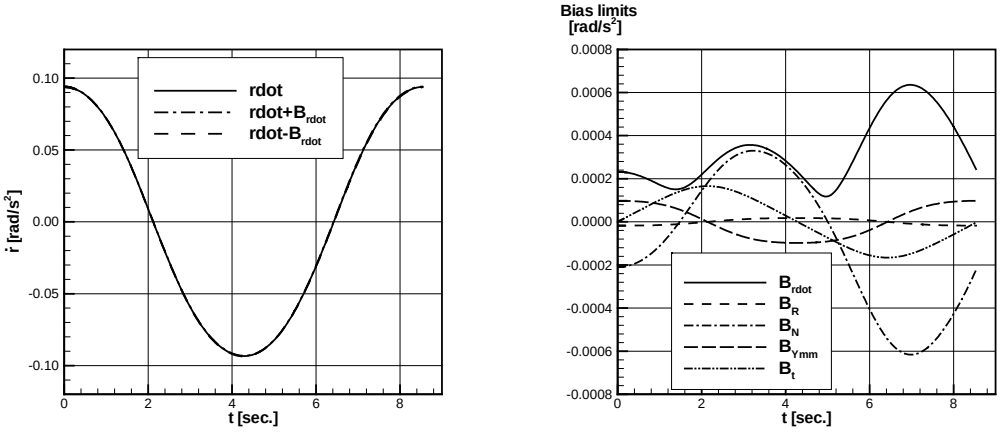

(a) (b)

Figure C.1.1.7. (a) Yaw acceleration and (b) bias limits.

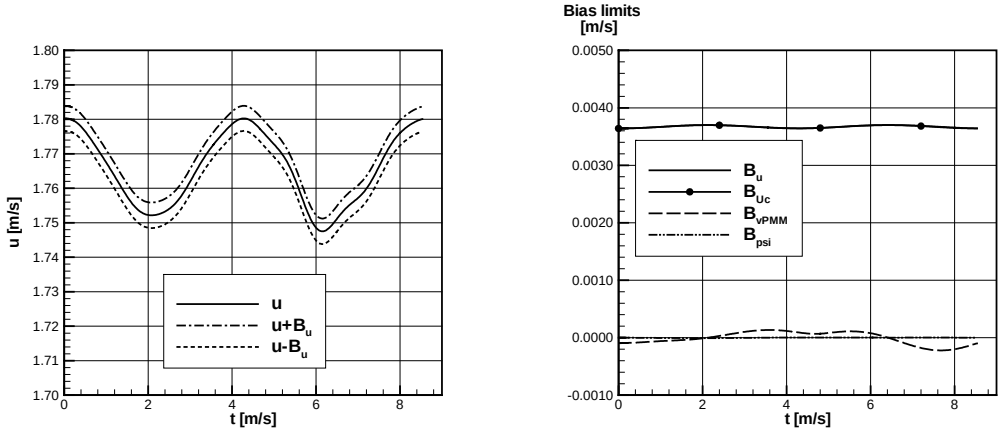

(a) (b)

Figure C.1.1.8. (a) Surge velocity and (b) bias limits.

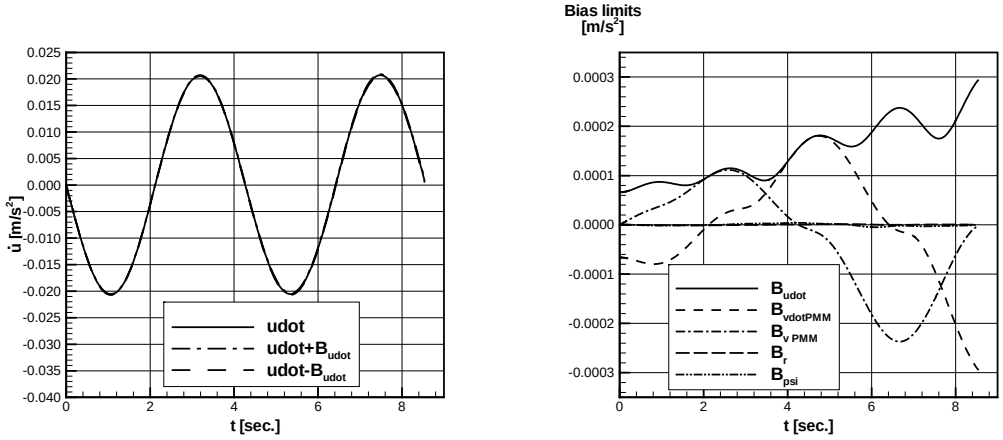

(a) (b)

Figure C.1.1.9. (a) Surge acceleration and (b) bias limits.

C.1.2 Longitudinal force

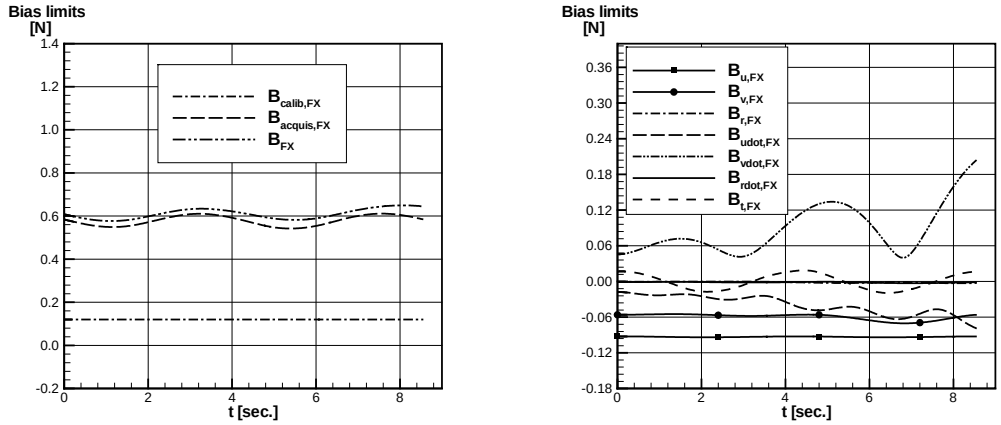

(a) (b)

Figure C.1.2.1. (a) and (b) bias limits for measured X-force.

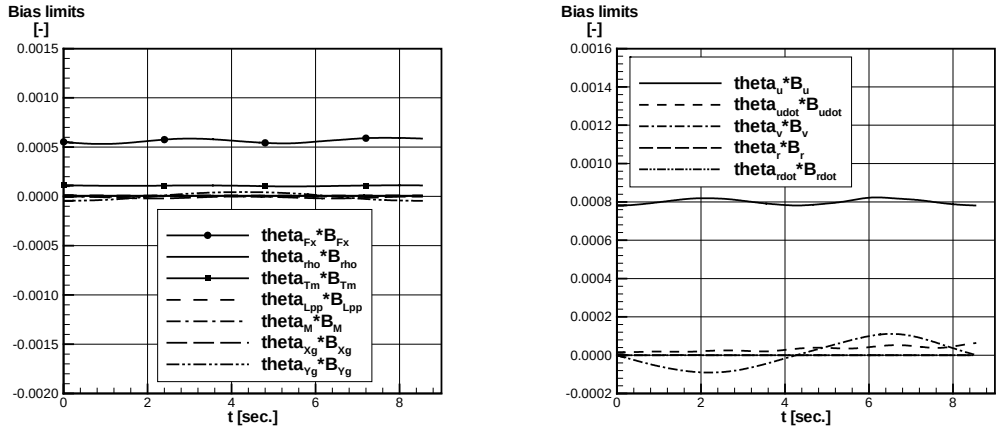

(a) (b)

Figure C.1.2.2. (a) and (b) bias limits for X'.

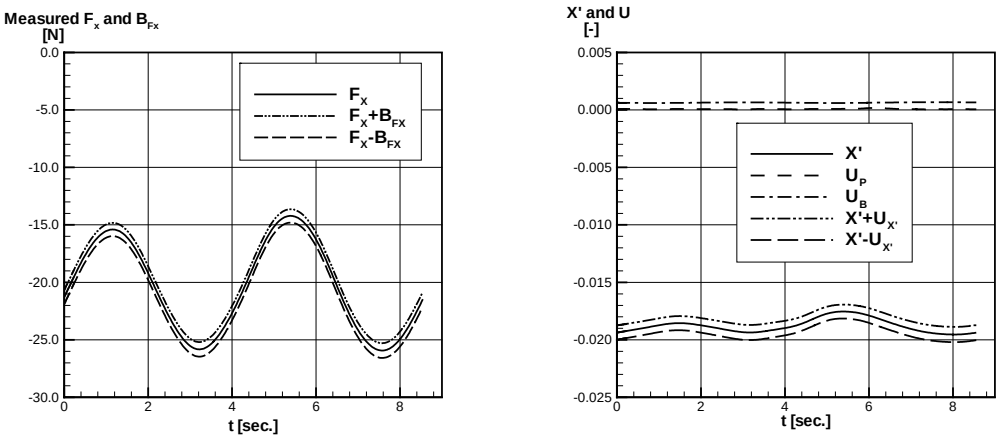

(a) (b)

Figure C.1.2.3. (a) Measured F_X and its bias limit. (b) X' including uncertainty.

C.1.3 Transverse force

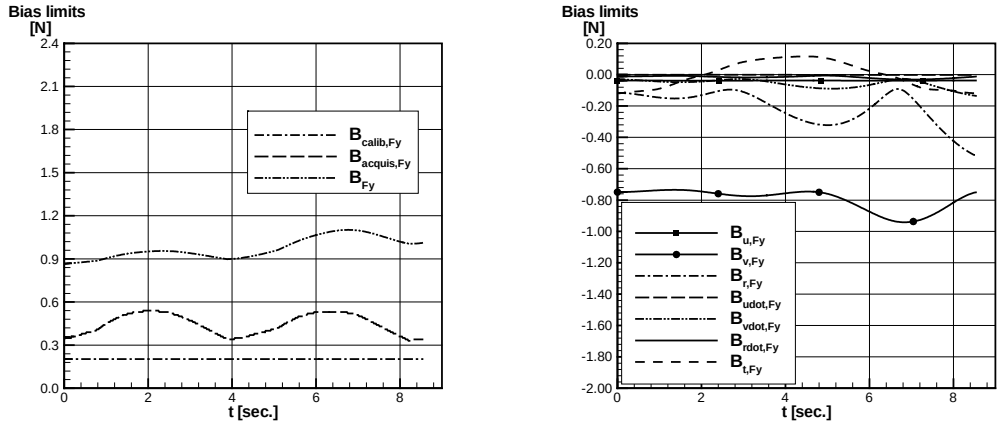

(a) (b)

Figure C.1.3.1. (a) and (b) bias limits for measured Y-force.

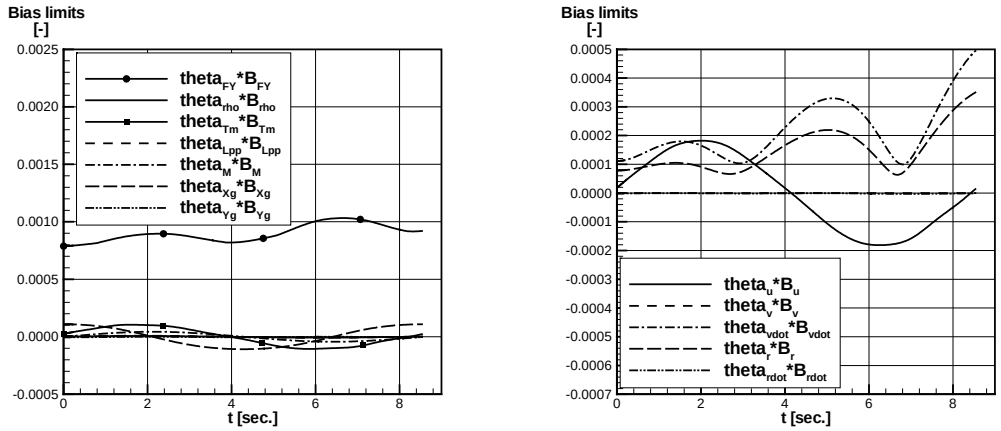

(a) (b)

Figure C.1.3.2. (a) and (b) bias limits for Y'.

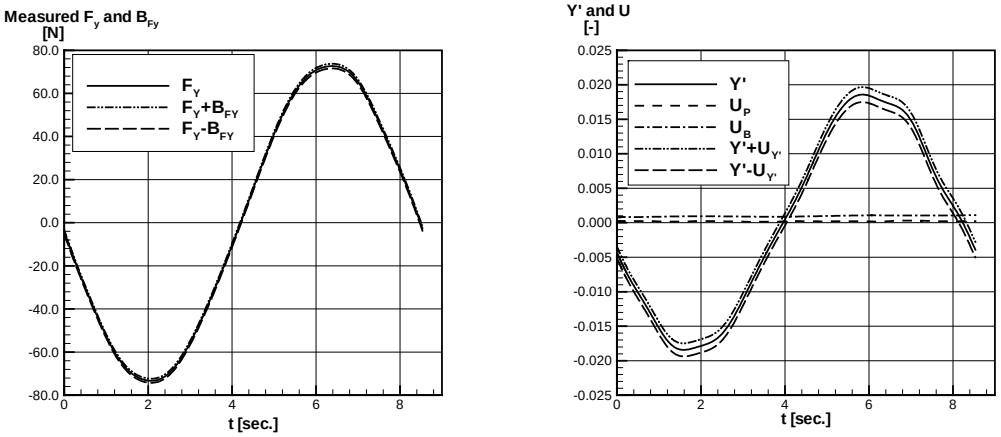

(a) (b)

Figure C.1.3.3. (a) Measured F_Y and its bias limit. (b) Y' including uncertainty.

C.1.4 Yaw moment

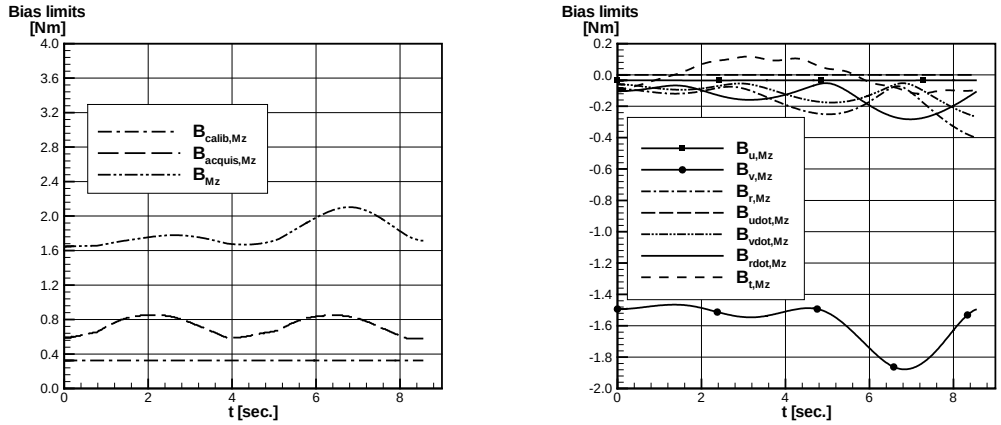

(a) (b)

Figure C.1.4.1. (a) and (b) bias limits for measured yaw moment M_Z.

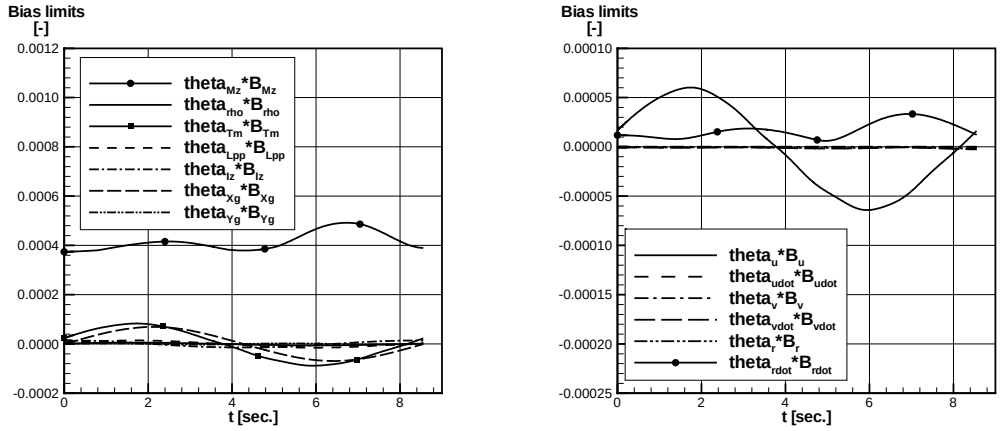

(a) (b)

Figure C.1.4.2. (a) and (b) bias limits for N'.

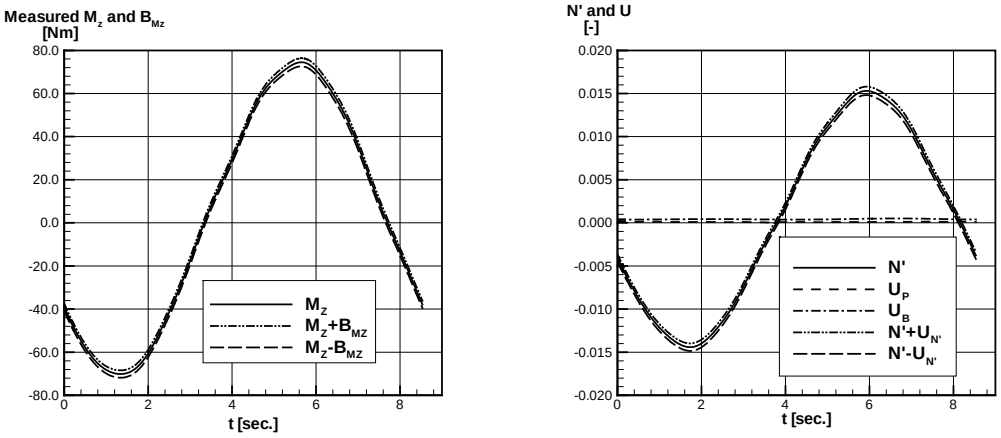

(a) (b)

Figure C.1.4.3. (a) Measured M_Z and its bias limit. (b) N' including uncertainty.

C.1.5 Sinkage at FP and AP

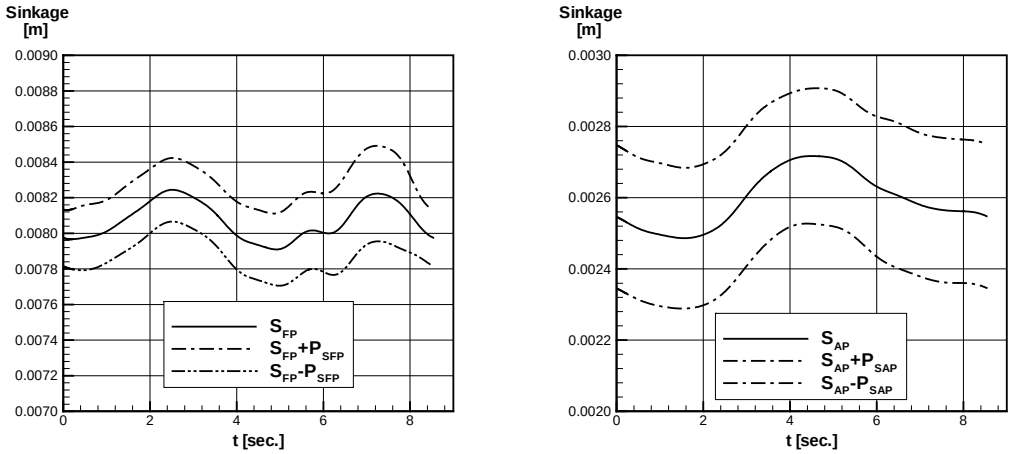

(a) (b)

Figure C.1.5.1. Sinkage, (a) at FP and (b) at AP.

C.2 Dynamic test (Pure sway), Fr=0.280

C.2.1 Motion parameters

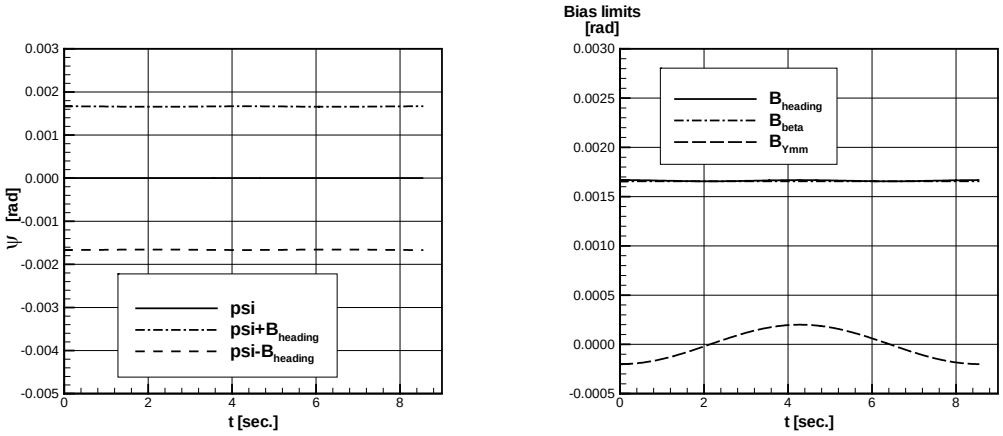

(a) (b)

Figure C.2.1.1. (a) Heading angle and (b) bias limits.

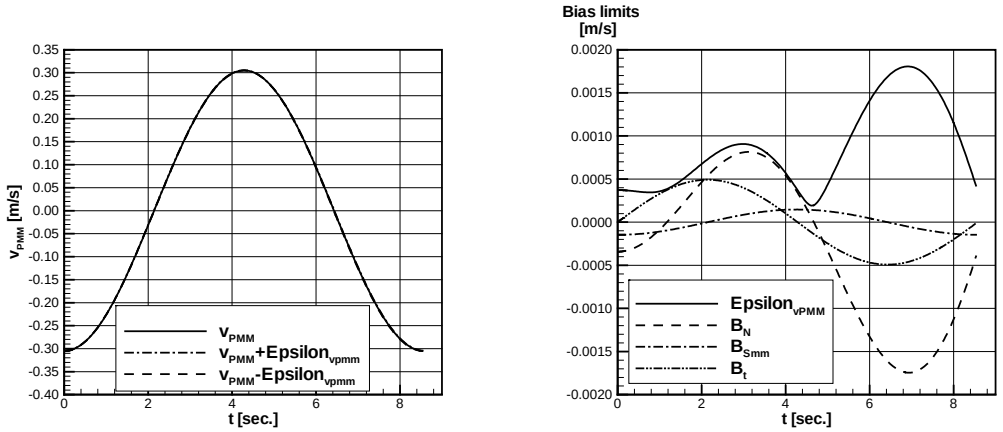

(a) (b)

Figure C.2.1.2. (a) Transverse PMM velocity and (b) bias limits.

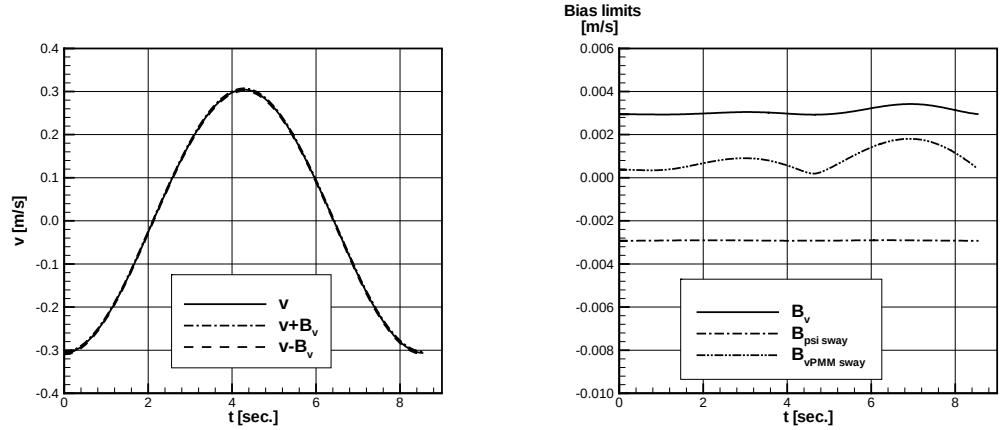

(a) (b)

Figure C.2.1.3. (a) Sway velocity and (b) bias limits.

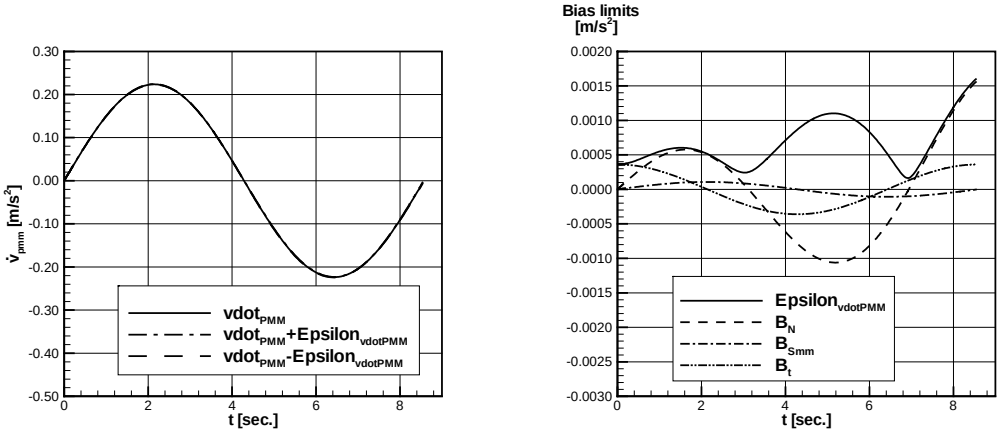

(a) (b)

Figure C.2.1.4. (a) Transverse PMM acceleration and (b) bias limits.

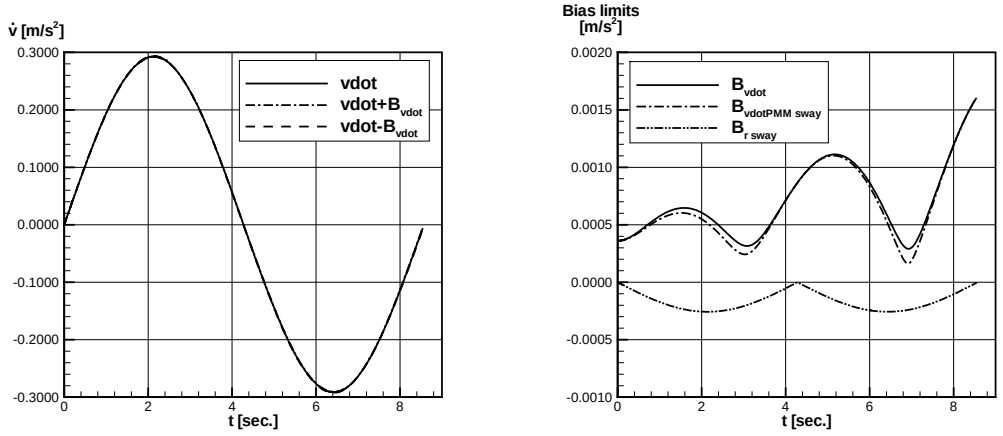

(a) (b)

Figure C.2.1.5. (a) Sway acceleration and (b) bias limits.

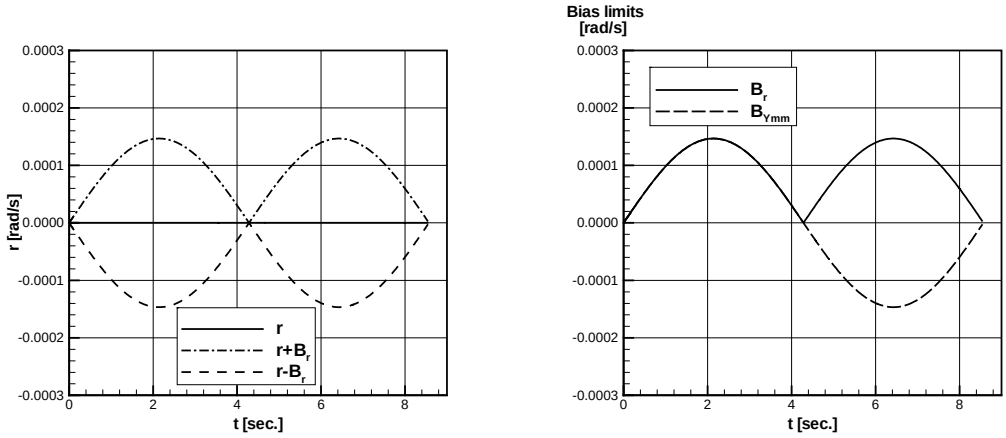

(a) (b)

Figure C.2.1.6. (a) Yaw rate and (b) bias limits.

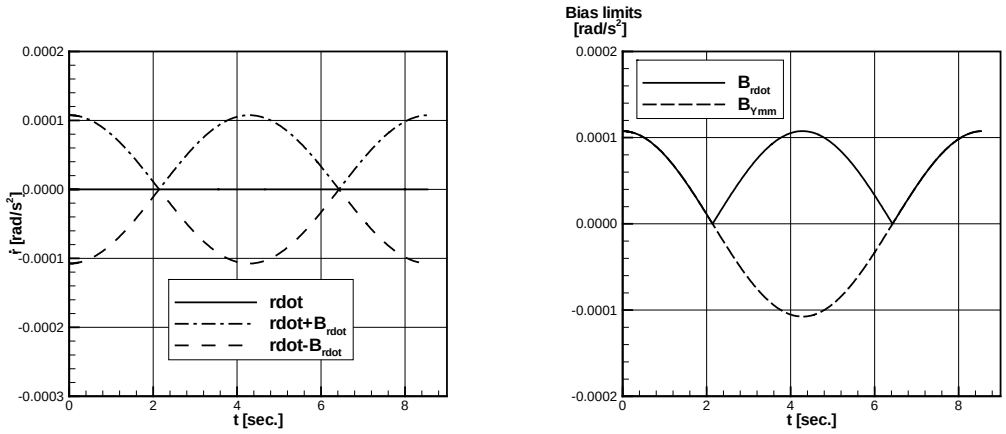

(a) (b)

Figure C.2.1.7. (a) Yaw acceleration and (b) bias limits.

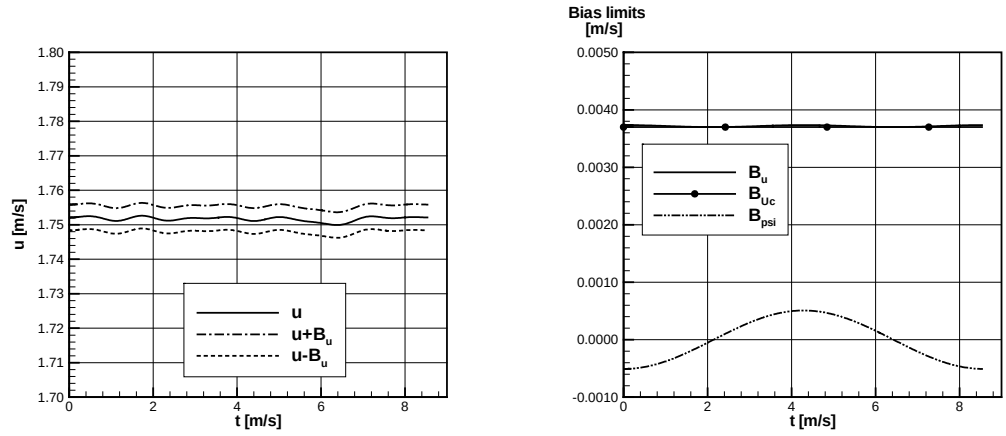

(a) (b)

Figure C.2.1.8. (a) Surge velocity and (b) bias limits.

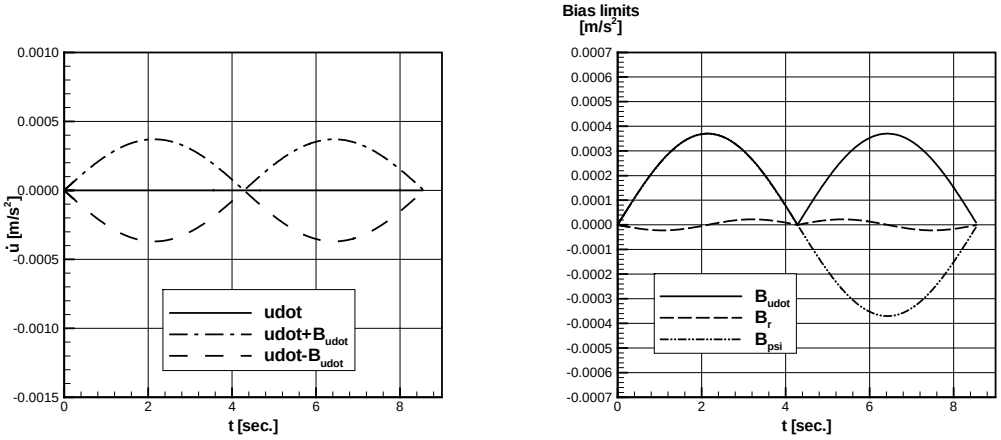

(a) (b)

Figure C.2.1.9. (a) Surge acceleration and (b) bias limits.

C.2.2 Longitudinal force

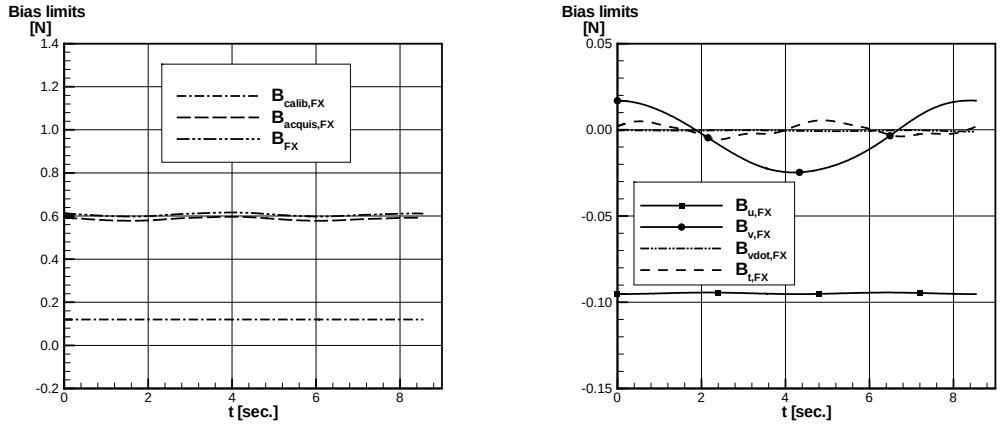

(a) (b)

Figure C.2.2.1. (a) and (b) bias limits for measured X-force.

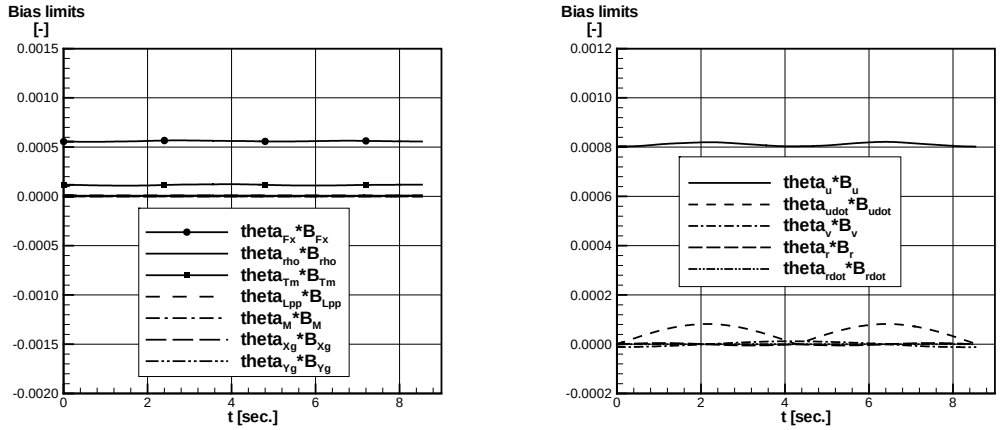

(a) (b)

Figure C.2.2.2. (a) and (b) bias limits for X'.

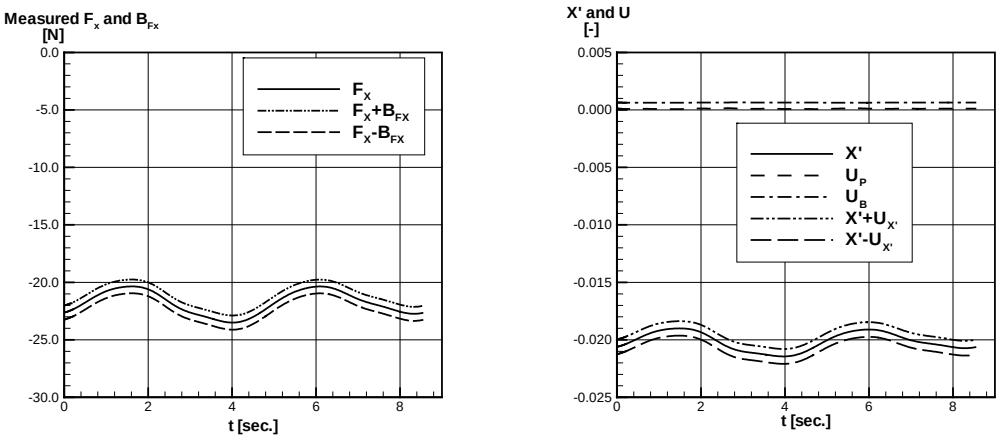

(a) (b)

Figure C.2.2.3. (a) Measured F_X and its bias limit. (b) X' including uncertainty.

C.2.3 Transverse force

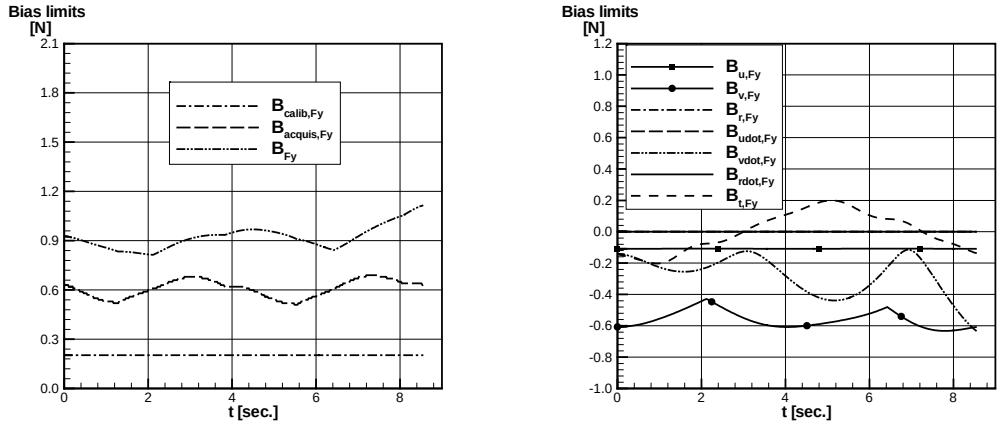

(a) (b)

Figure C.2.3.1. (a) and (b) bias limits for measured Y-force.

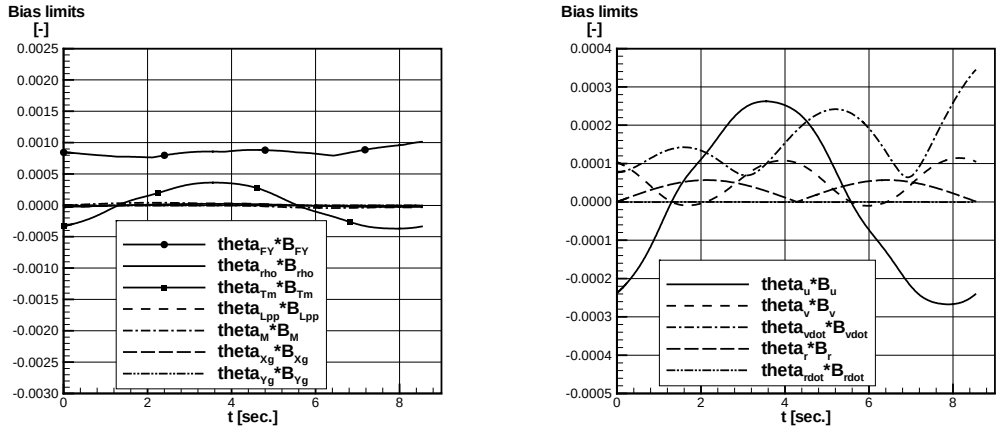

(a) (b)

Figure C.2.3.2. (a) and (b) bias limits for Y'.

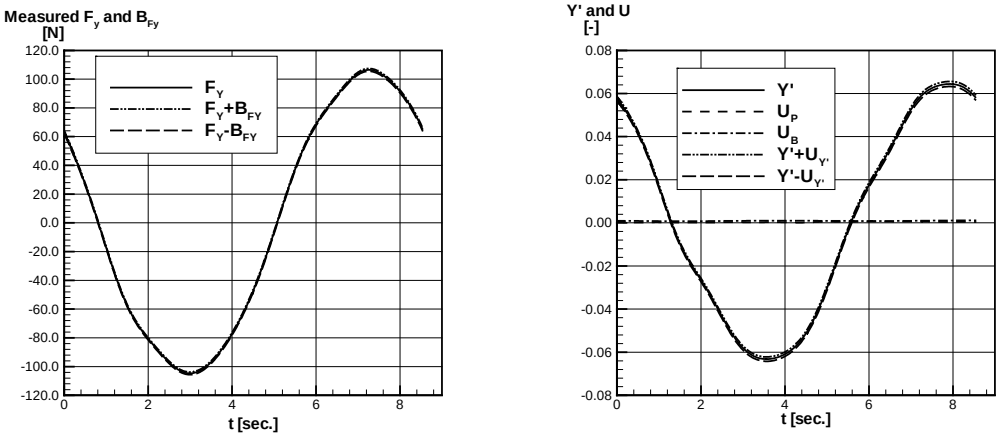

(a) (b)

Figure C.2.3.3. (a) Measured F_Y and its bias limit. (b) Y' including uncertainty.

C.2.4 Yaw moment

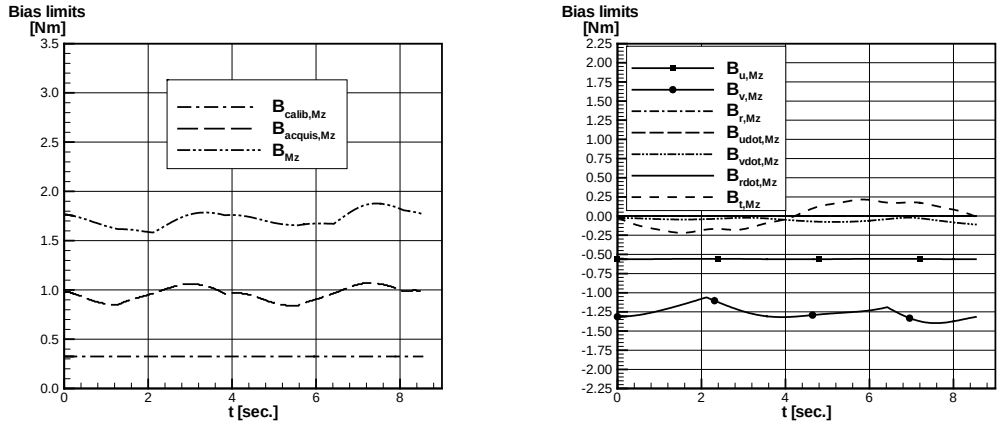

(a) (b)

Figure C.2.4.1. (a) and (b) bias limits for measured yaw moment M_Z.

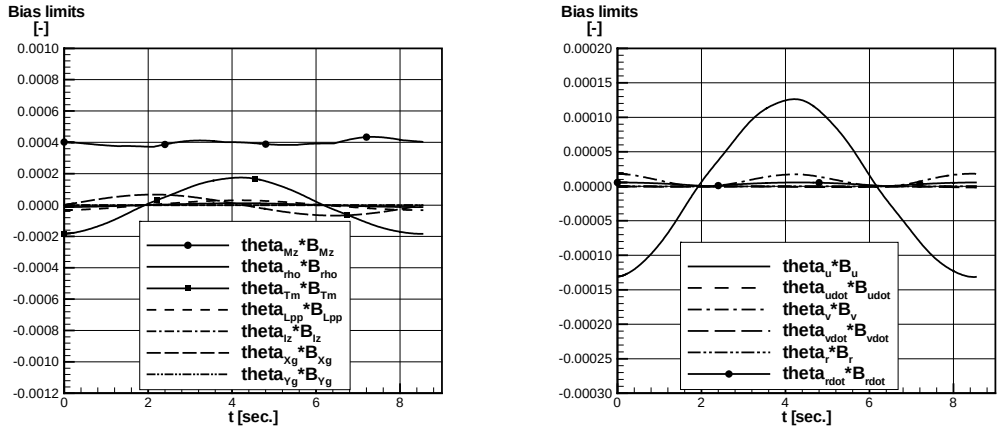

(a) (b)

Figure C.2.4.2. (a) and (b) bias limits for N'.

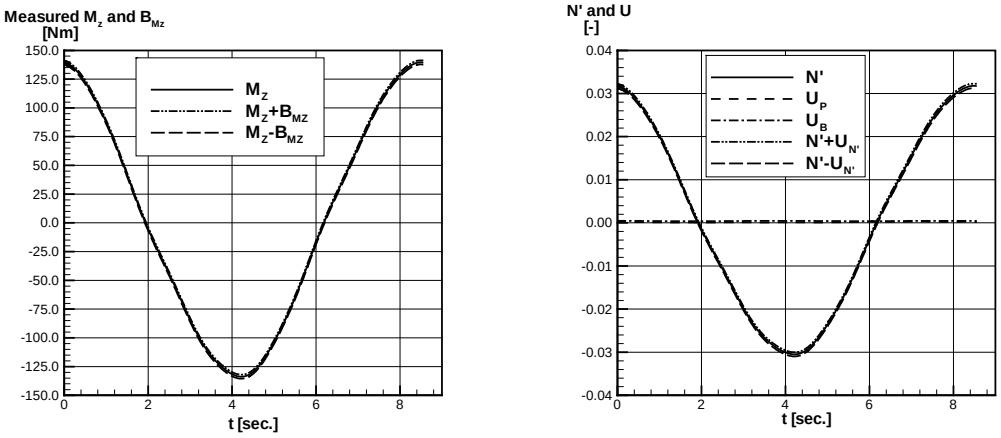

(a) (b)

Figure C.2.4.3. (a) Measured M_Z and its bias limit. (b) N' including uncertainty.

C.2.5 Sinkage at FP and AP

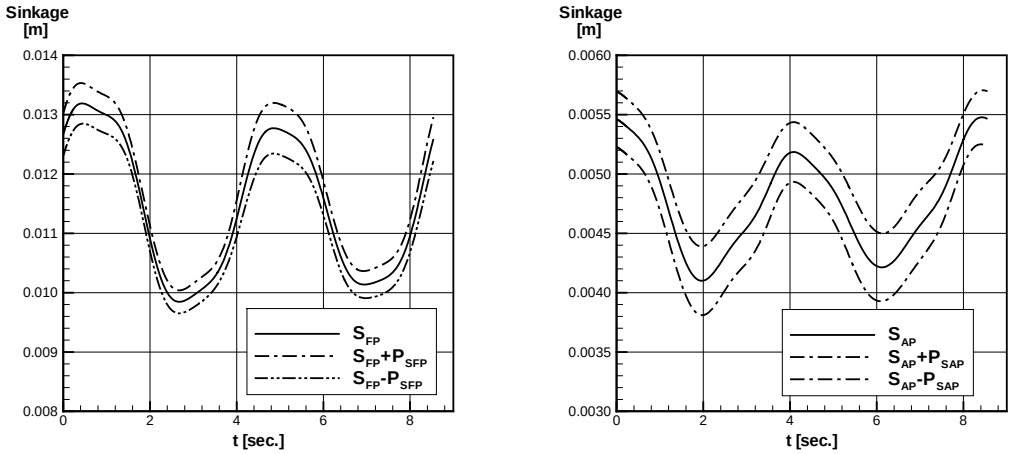

(a) (b)

Figure C.2.5.1. Sinkage, (a) at FP and (b) at AP.

C.3 Dynamic test (Yaw and drift), Fr=0.280

C.3.1 Motion parameters

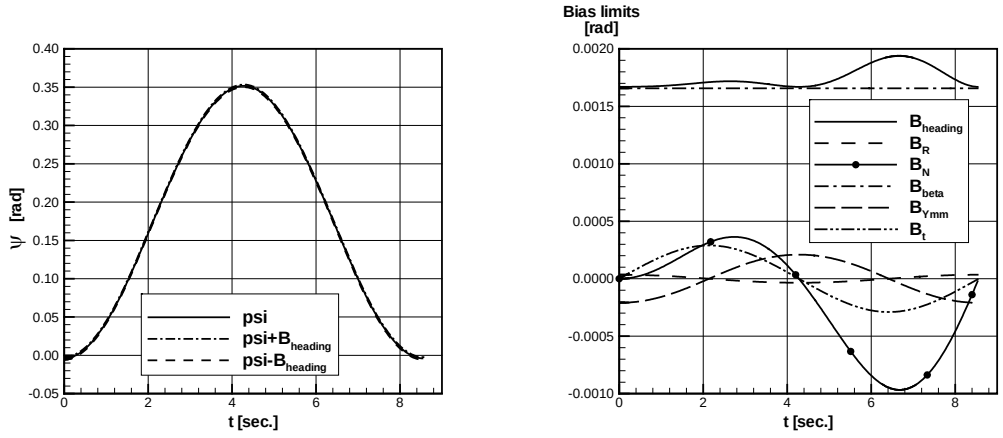

(a) (b)

Figure C.3.1.1. (a) Heading angle and (b) bias limits.

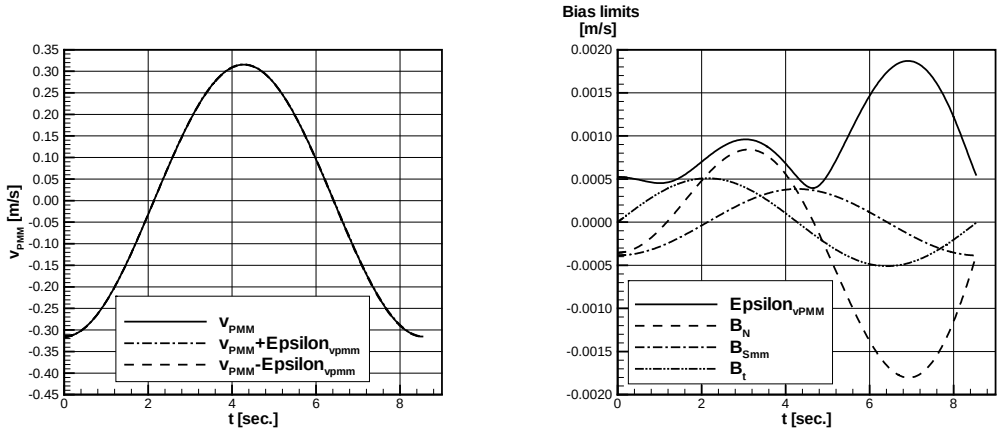

(a) (b)

Figure C.3.1.2. (a) Transverse PMM velocity and (b) bias limits.

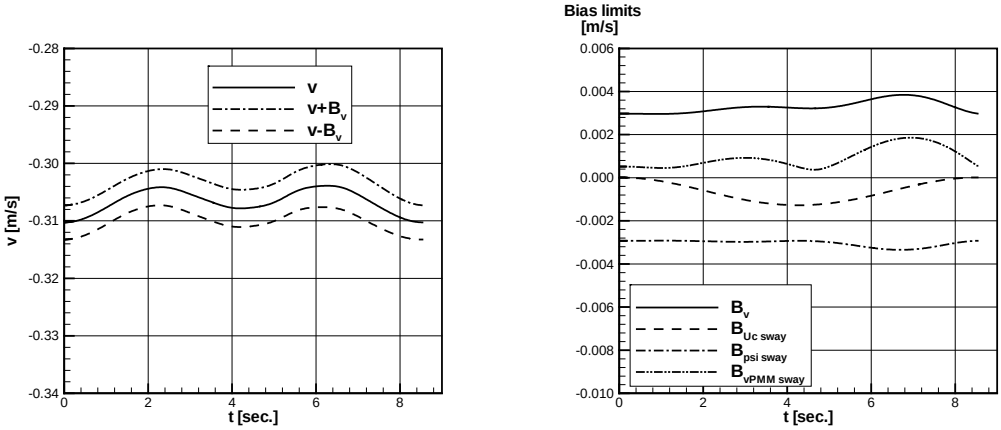

(a) (b)

Figure C.3.1.3. (a) Sway velocity and (b) bias limits.

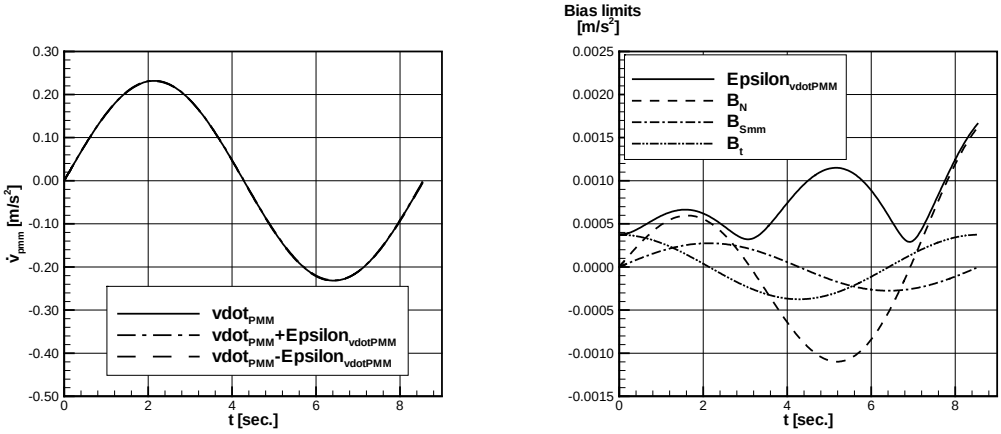

(a) (b)

Figure C.3.1.4. (a) Transverse PMM acceleration and (b) bias limits.

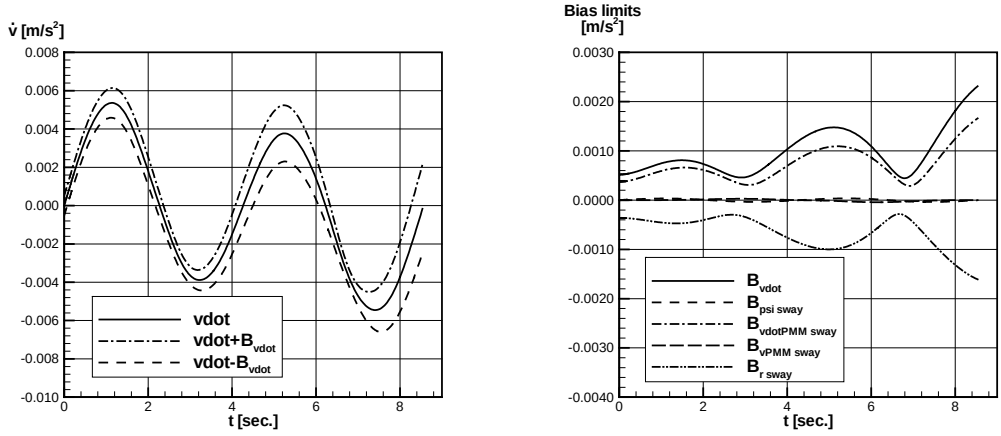

(a) (b)

Figure C.3.1.5. (a) Sway acceleration and (b) bias limits.

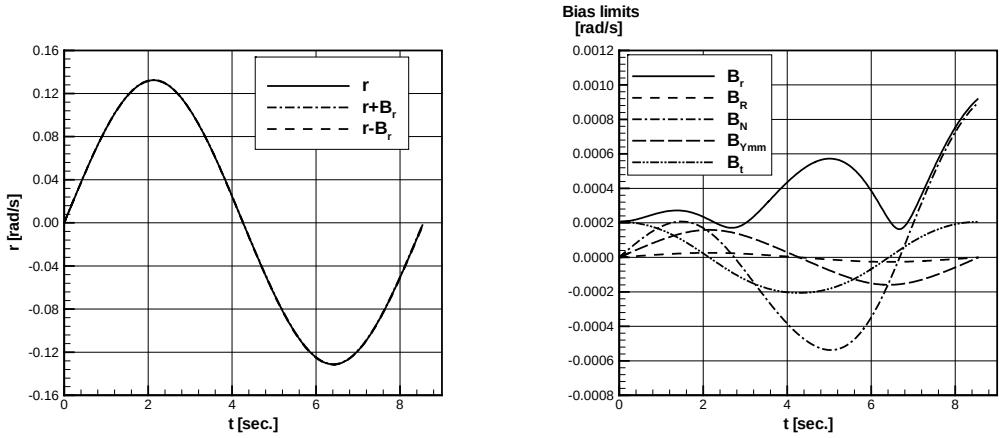

(a) (b)

Figure C.3.1.6. (a) Yaw rate and (b) bias limits.

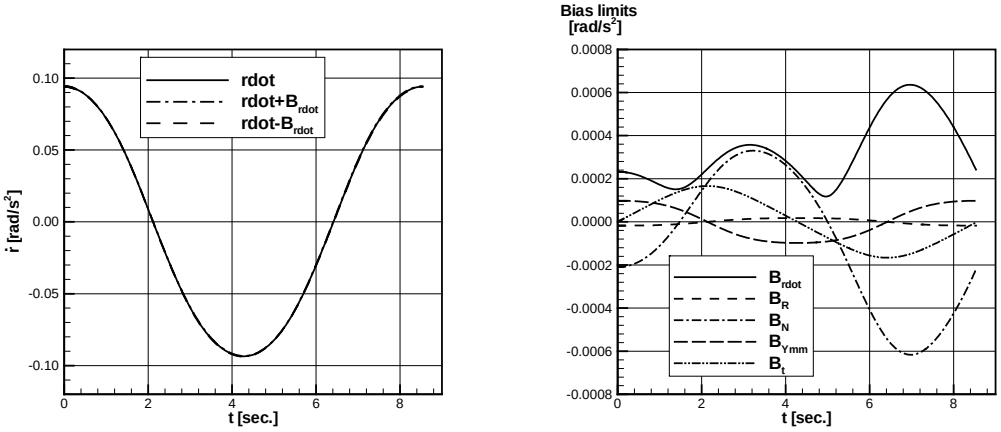

(a) (b)

Figure C.3.1.7. (a) Yaw acceleration and (b) bias limits.

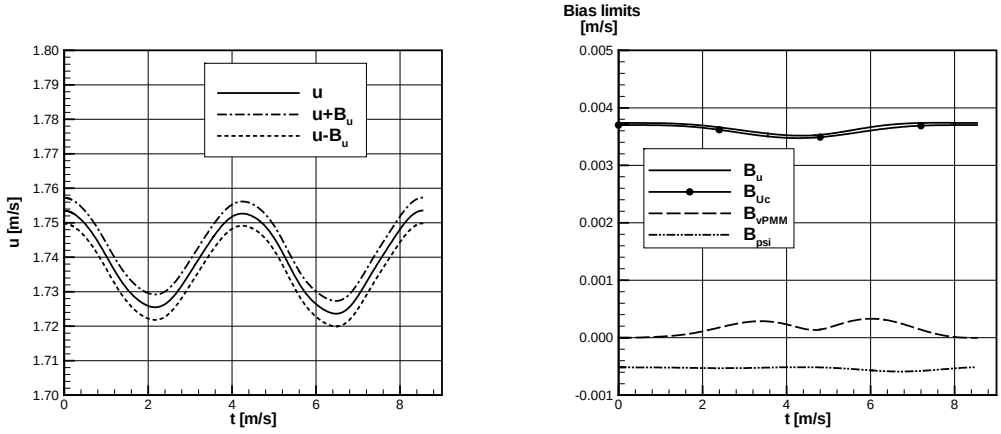

(a) (b)

Figure C.3.1.8. (a) Surge velocity and (b) bias limits.

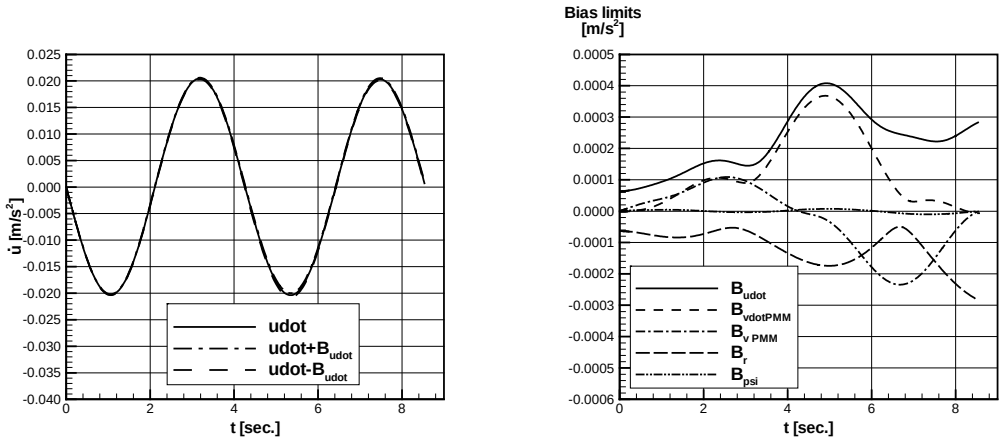

(a) (b)

Figure C.3.1.9. (a) Surge acceleration and (b) bias limits.

C.3.2 Longitudinal force

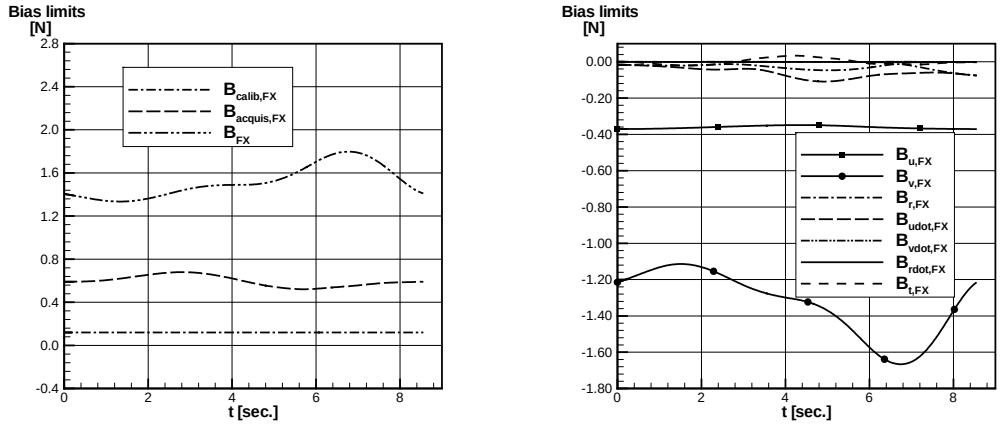

(a) (b)

Figure C.3.2.1. (a) and (b) bias limits for measured X-force.

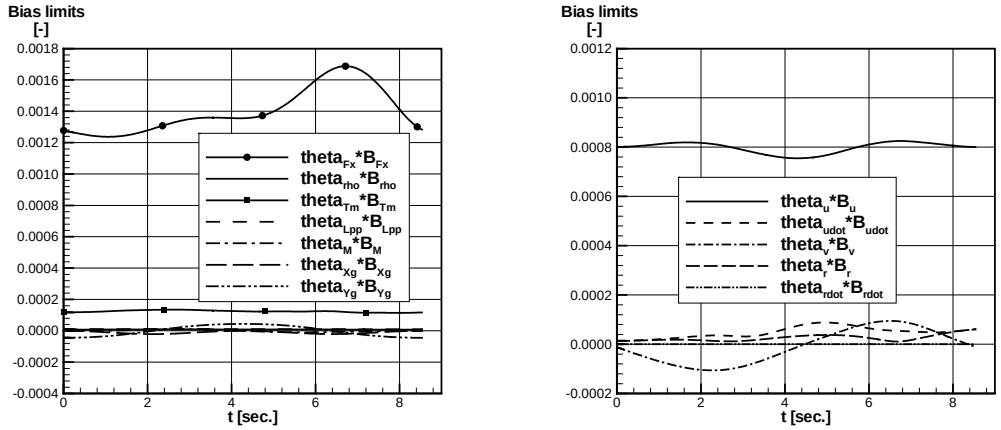

(a) (b)

Figure C.3.2.2. (a) and (b) bias limits for X'.

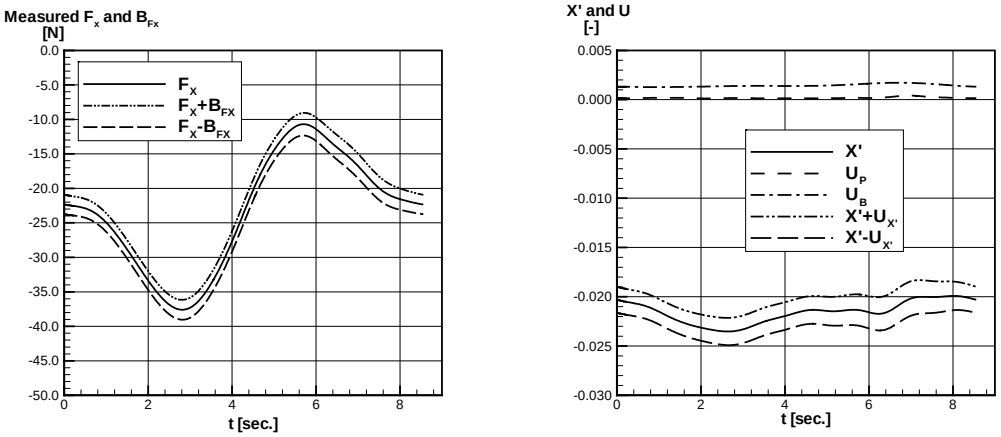

(a) (b)

Figure C.3.2.3. (a) Measured F_X and its bias limit. (b) X' including uncertainty.

C.3.3 Transverse force

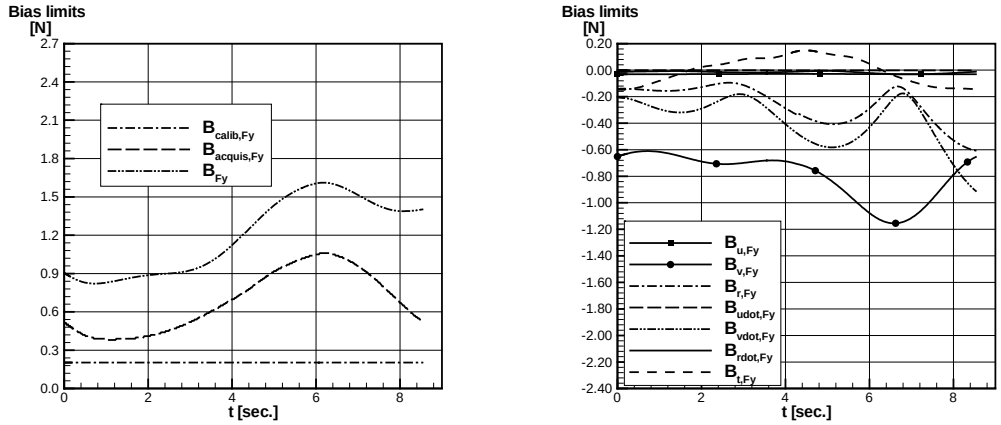

(a) (b)

Figure C.3.3.1. (a) and (b) bias limits for measured Y-force.

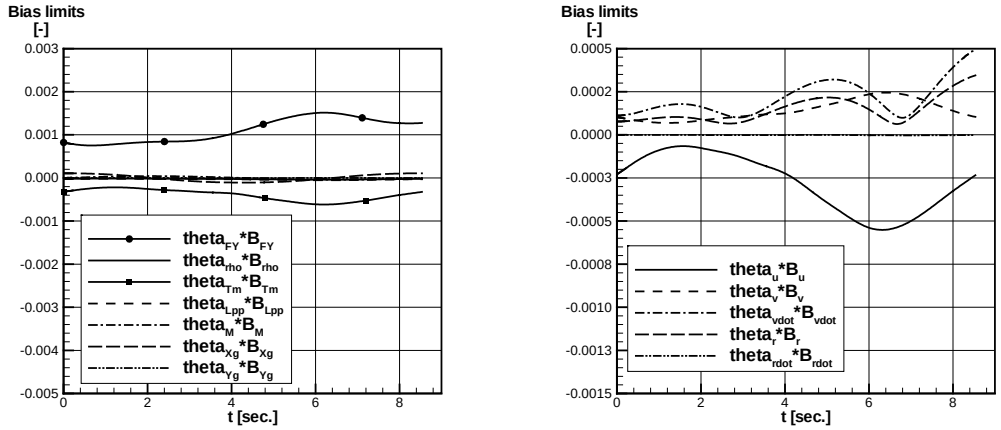

(a) (b)

Figure C.3.3.2. (a) and (b) bias limits for Y'.

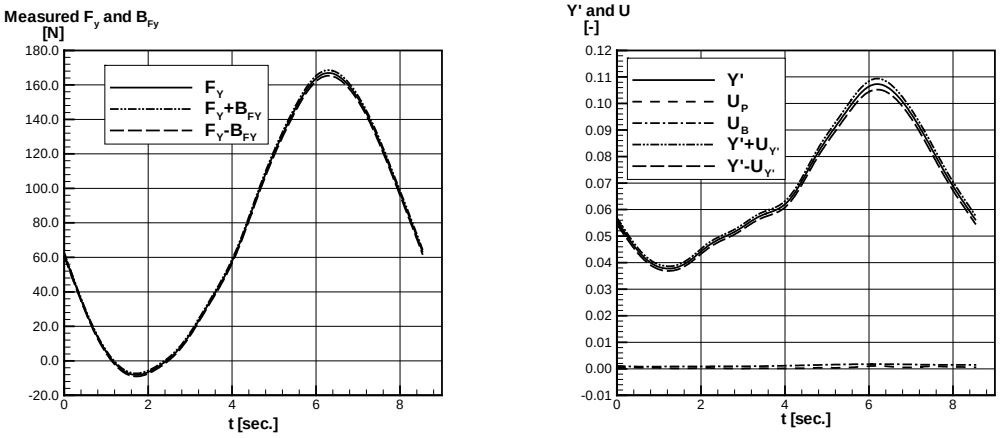

(a) (b)

Figure C.3.3.3. (a) Measured F_Y and its bias limit. (b) Y' including uncertainty.

C.3.4 Yaw moment

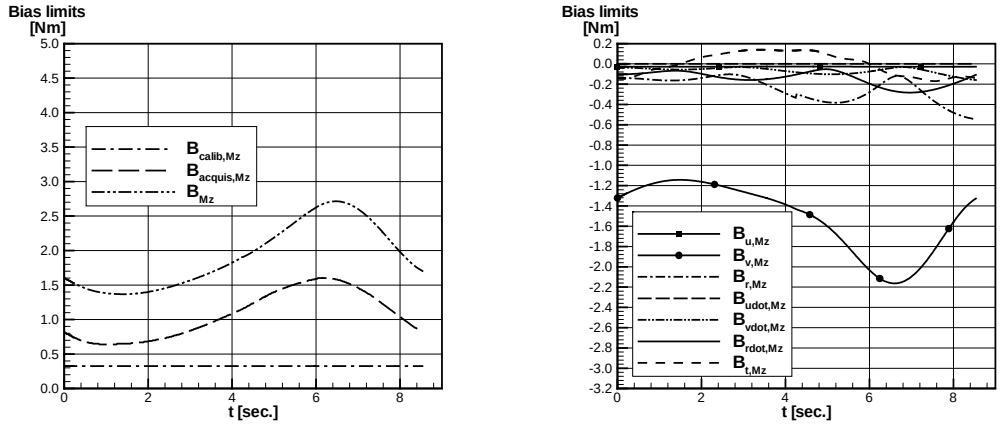

(a) (b)

Figure C.3.4.1. (a) and (b) bias limits for measured yaw moment M_Z.

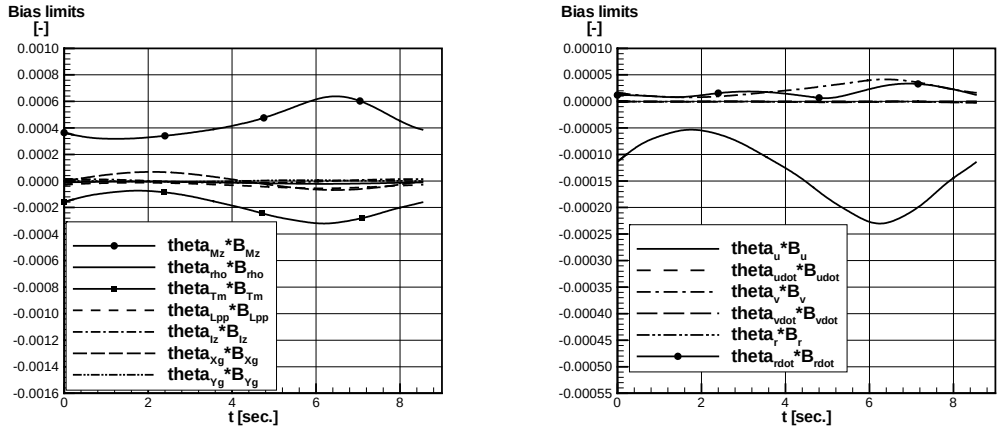

(a) (b)

Figure C.3.4.2. (a) and (b) bias limits for N'.

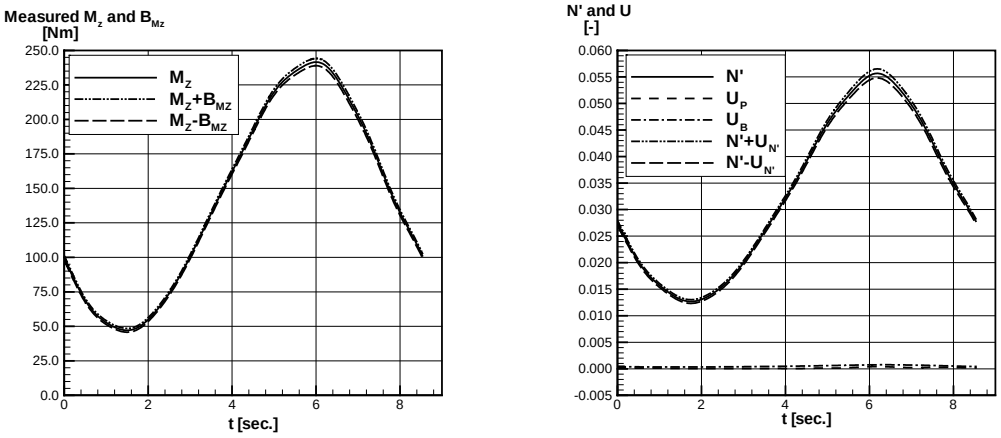

(a) (b)

Figure C.3.4.3. (a) Measured M_Z and its bias limit. (b) N' including uncertainty.

C.3.5 Sinkage at FP and AP

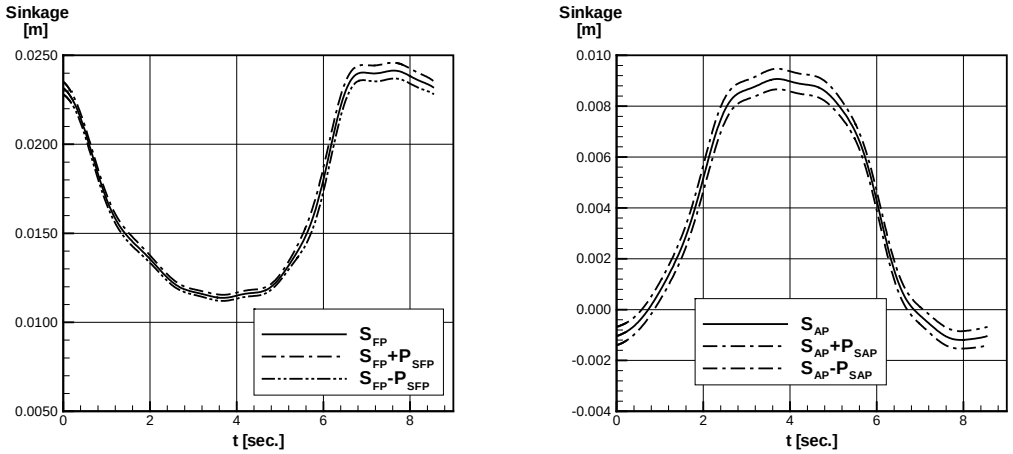

(a) (b)

Figure C.3.5.1. Sinkage, (a) at FP and (b) at AP.

C.4 Dynamic test (Pure yaw), Fr=0.138

C.4.1 Motion parameters

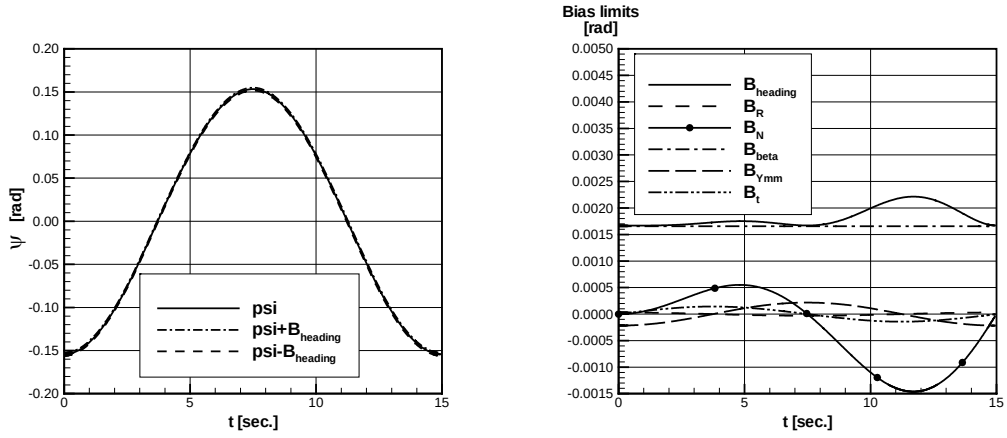

(a) (b)

Figure C.4.1.1. (a) Heading angle and (b) bias limits.

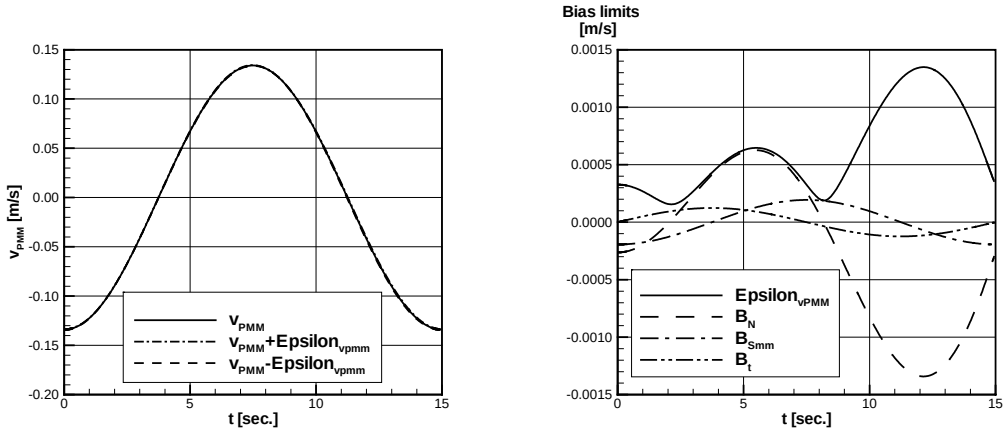

(a) (b)

Figure C.4.1.2. (a) Transverse PMM velocity and (b) bias limits.

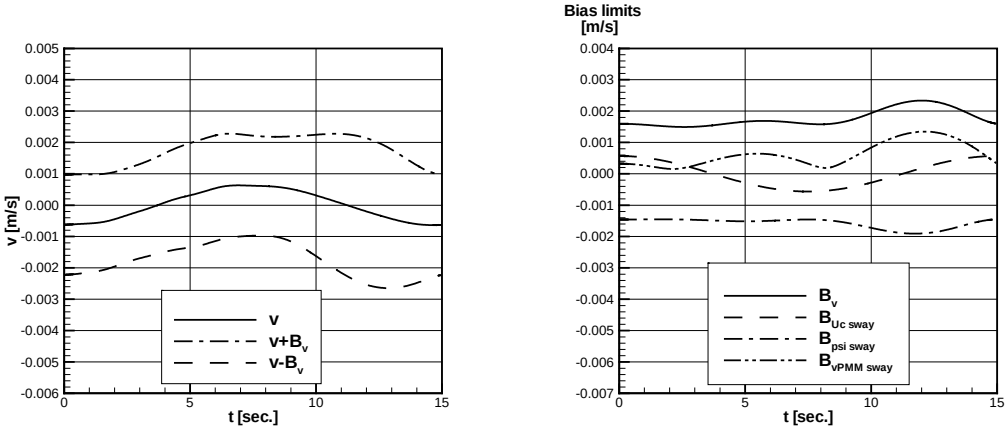

(a) (b)

Figure C.4.1.3. (a) Sway velocity and (b) bias limits.

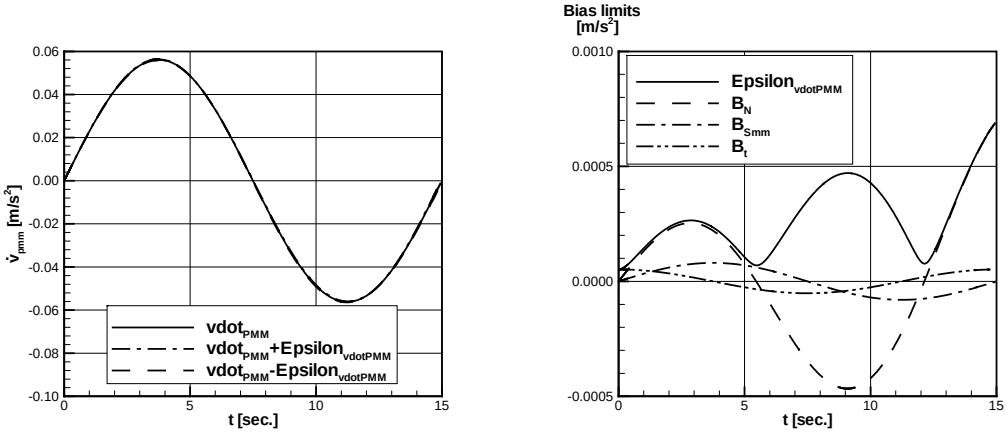

(a) (b)

Figure C.4.1.4. (a) Transverse PMM acceleration and (b) bias limits.

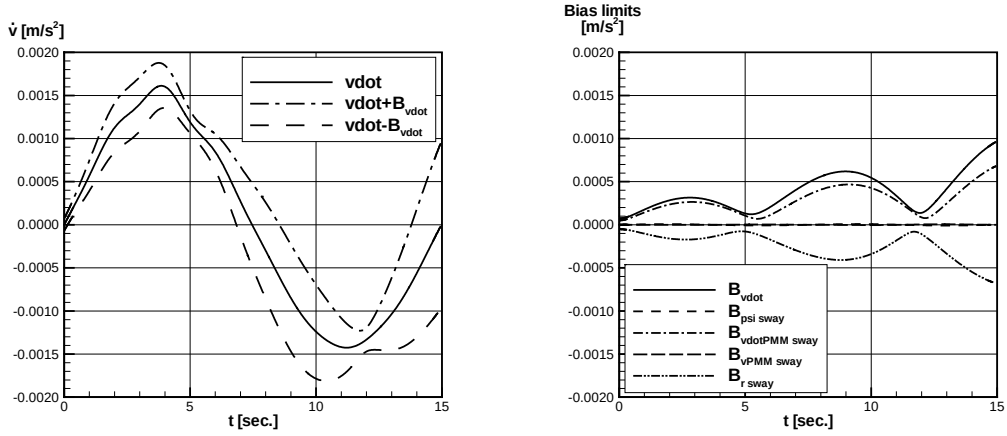

(a) (b)

Figure C.4.1.5. (a) Sway acceleration and (b) bias limits.

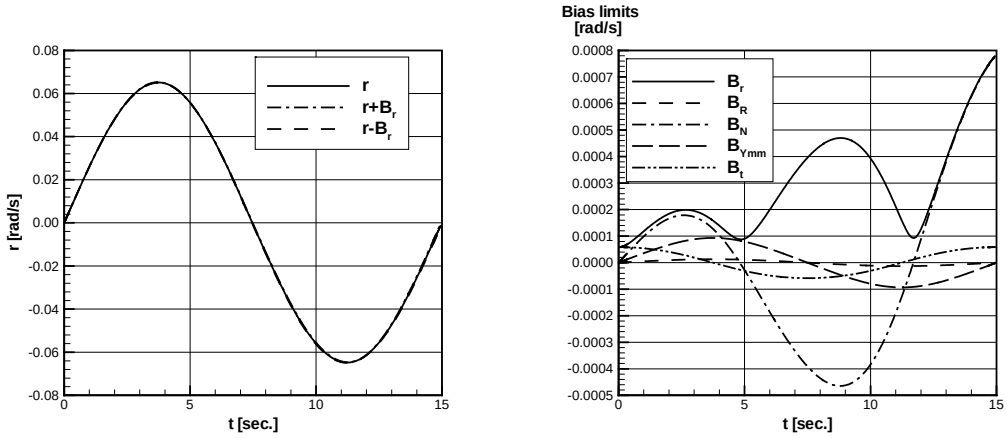

(a) (b)

Figure C.4.1.6. (a) Yaw rate and (b) bias limits.

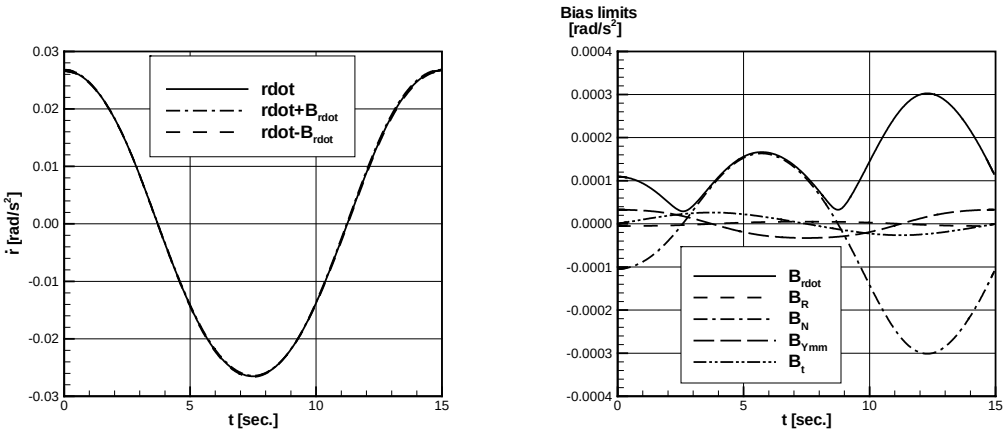

(a) (b)

Figure C.4.1.7. (a) Yaw acceleration and (b) bias limits.

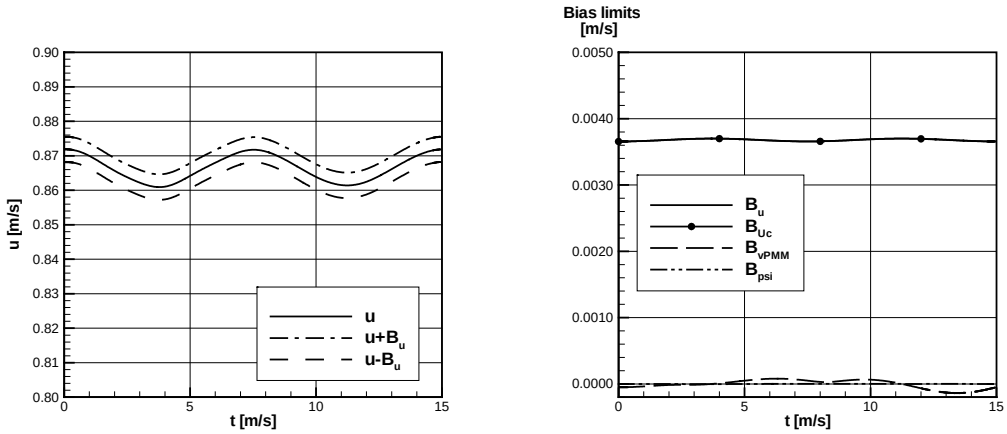

(a) (b)

Figure C.4.1.8. (a) Surge velocity and (b) bias limits.

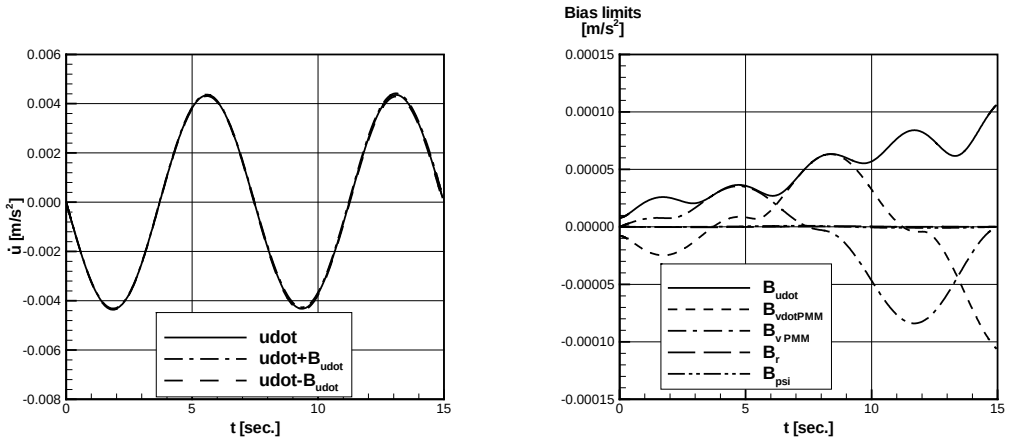

(a) (b)

Figure C.4.1.9. (a) Surge acceleration and (b) bias limits.

C.4.2 Longitudinal force

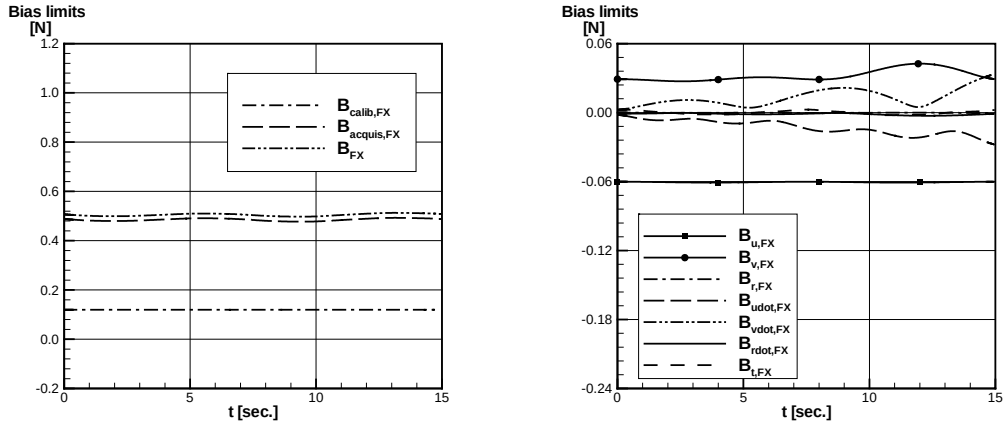

(a) (b)

Figure C.4.2.1. (a) and (b) bias limits for measured X-force.

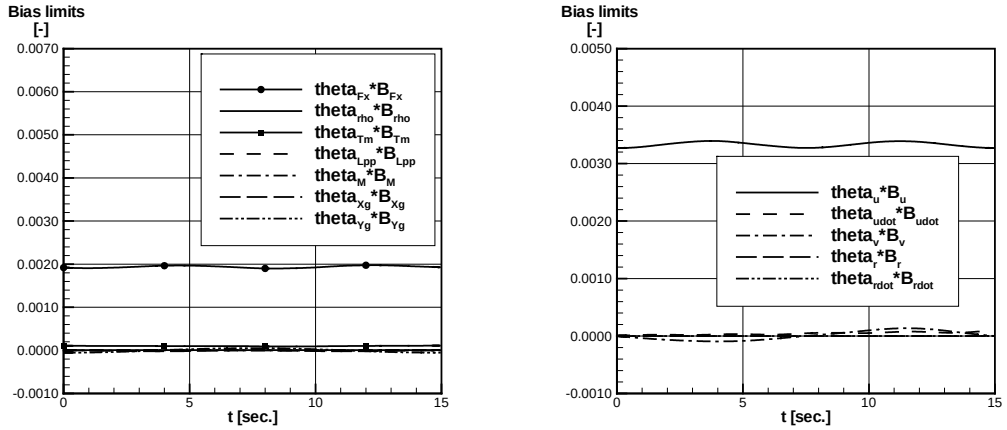

(a) (b)

Figure C.4.2.2. (a) and (b) bias limits for X'.

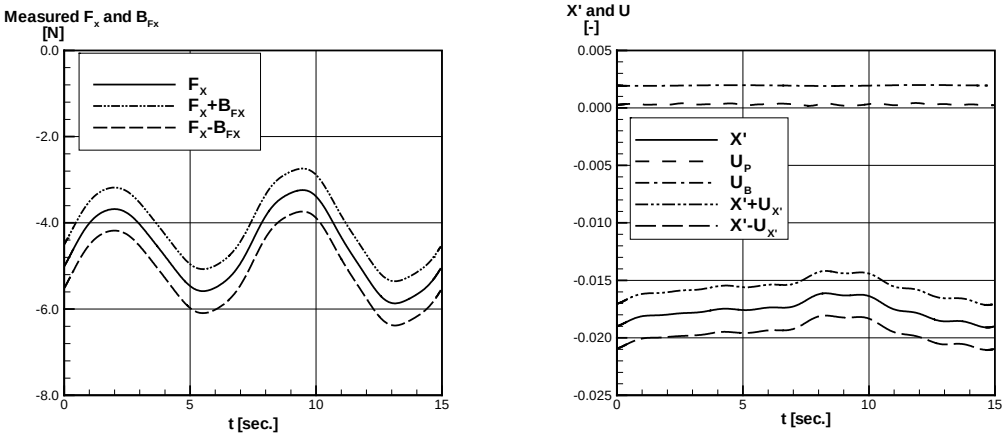

(a) (b)

Figure C.4.2.3. (a) Measured F_X and its bias limit. (b) $X^{'}$ including uncertainty.

C.4.3 Transverse force

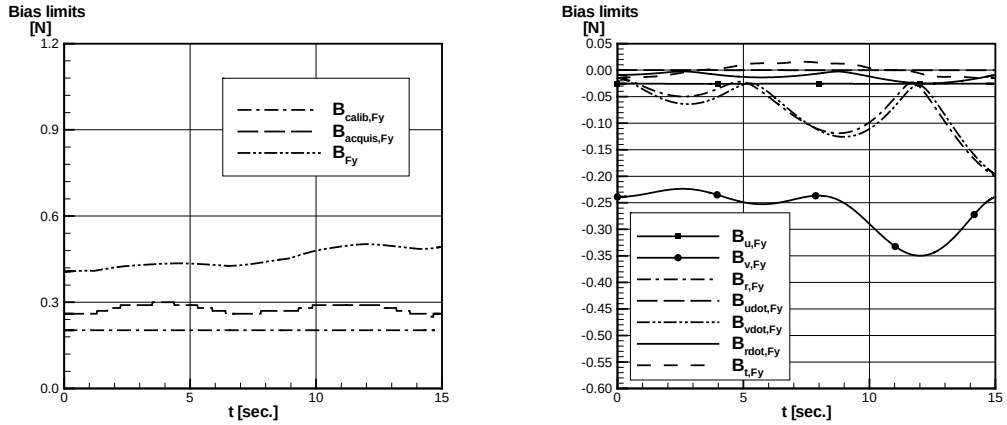

(a) (b)

Figure C.4.3.1. (a) and (b) bias limits for measured Y-force.

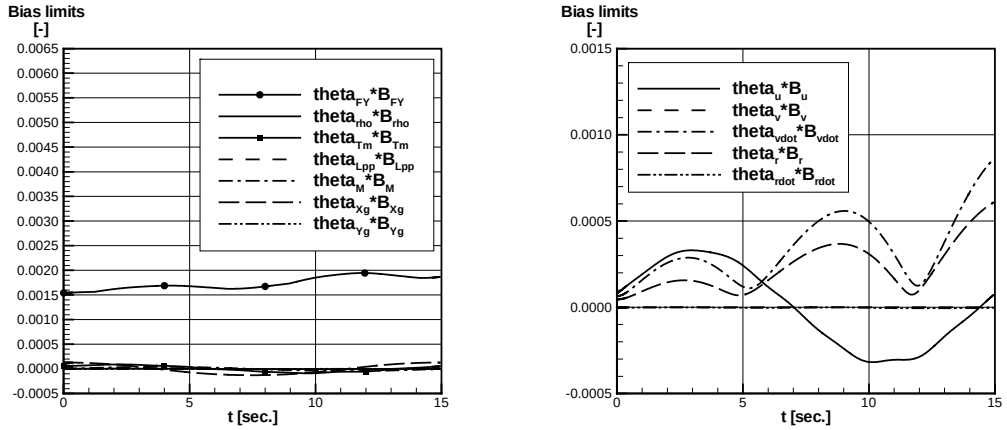

(a) (b)

Figure C.4.3.2. (a) and (b) bias limits for Y'.

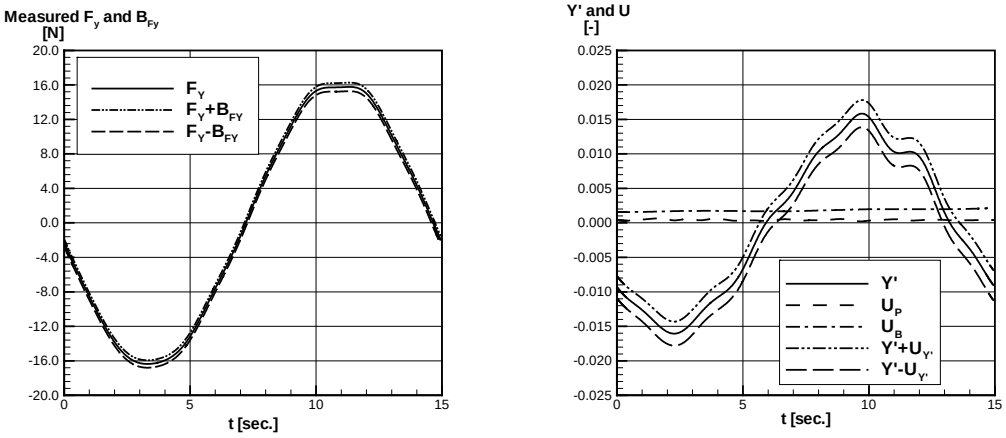

(a) (b)

Figure C.4.3.3. (a) Measured F_Y and its bias limit. (b) Y' including uncertainty.

C.4.4 Yaw moment

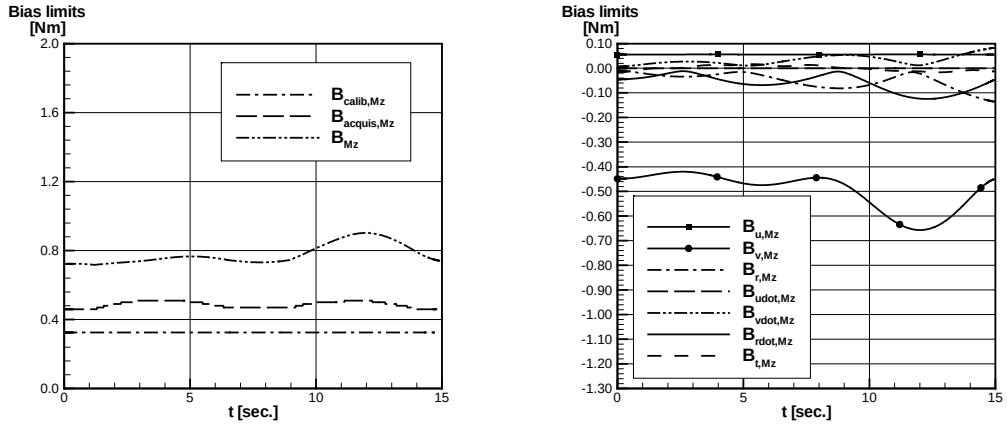

(a) (b)

Figure C.4.4.1. (a) and (b) bias limits for measured yaw moment M_Z.

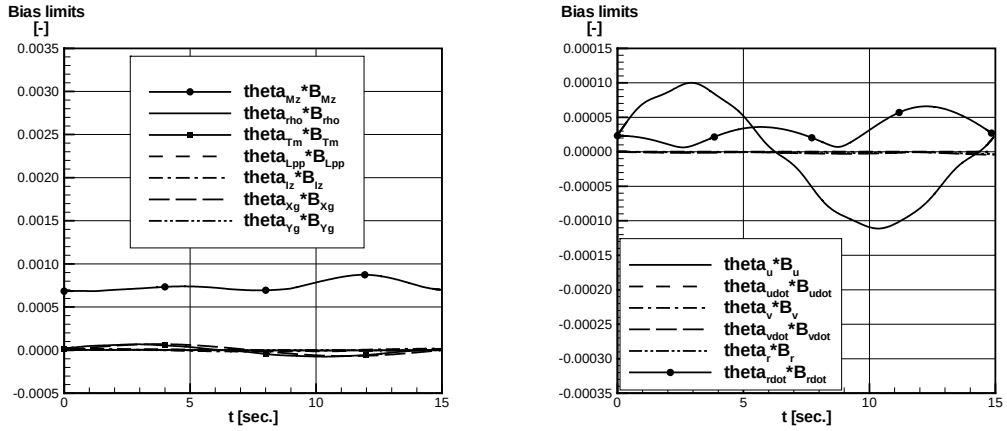

(a) (b)

Figure C.4.4.2. (a) and (b) bias limits for N'.

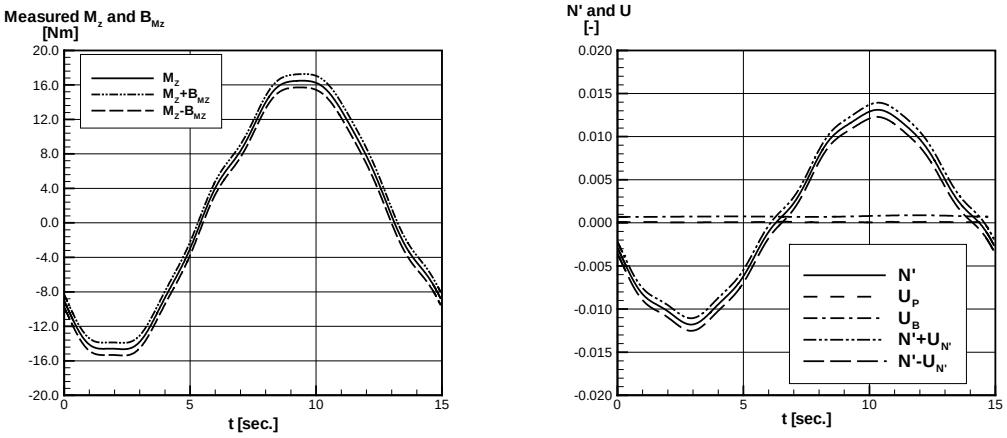

(a) (b)

Figure C.4.4.3. (a) Measured M_Z and its bias limit. (b) N' including uncertainty.

C.4.5 Sinkage at FP and AP

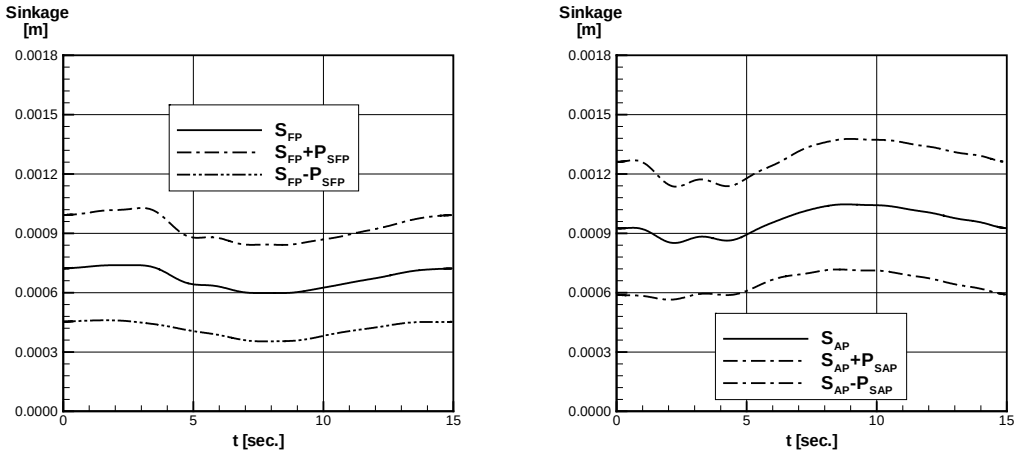

(a) (b)

Figure C.4.5.1. Sinkage, (a) at FP and (b) at AP.

C.5 Dynamic test (Pure yaw), Fr=0.410

C.5.1 Motion parameters

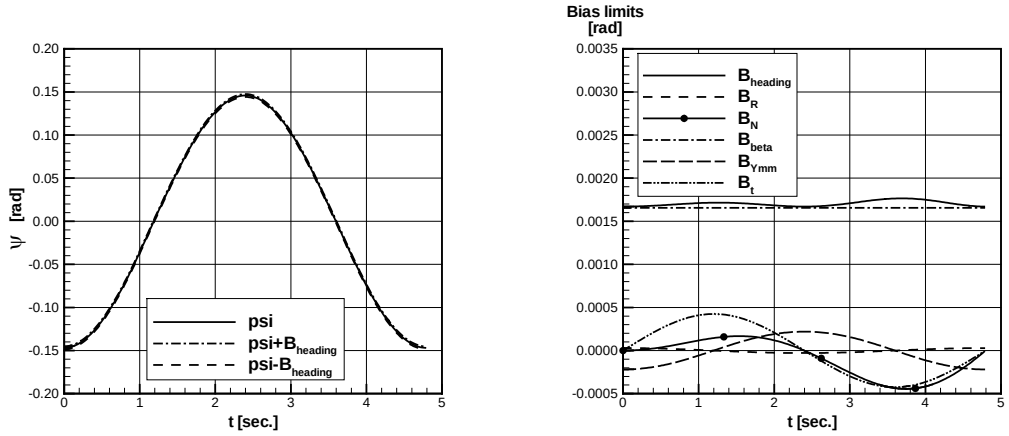

(a) (b)

Figure C.5.1.1. (a) Heading angle and (b) bias limits.

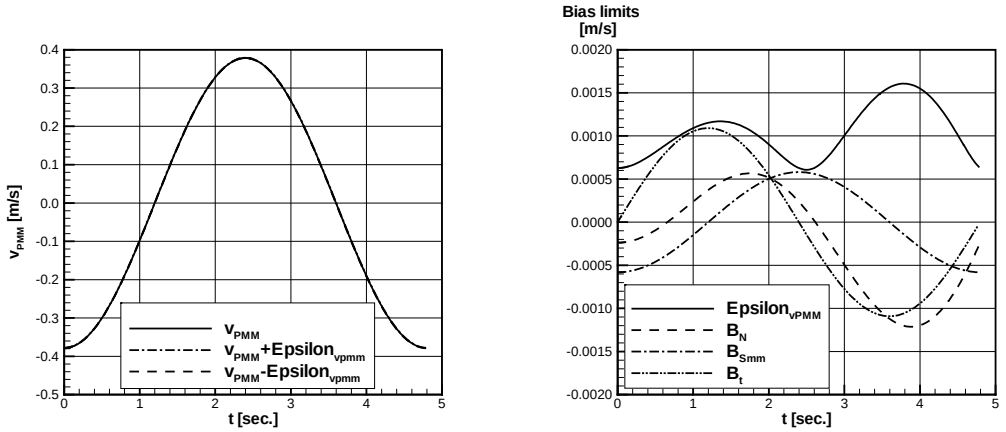

(a) (b)

Figure C.5.1.2. (a) Transverse PMM velocity and (b) bias limits.

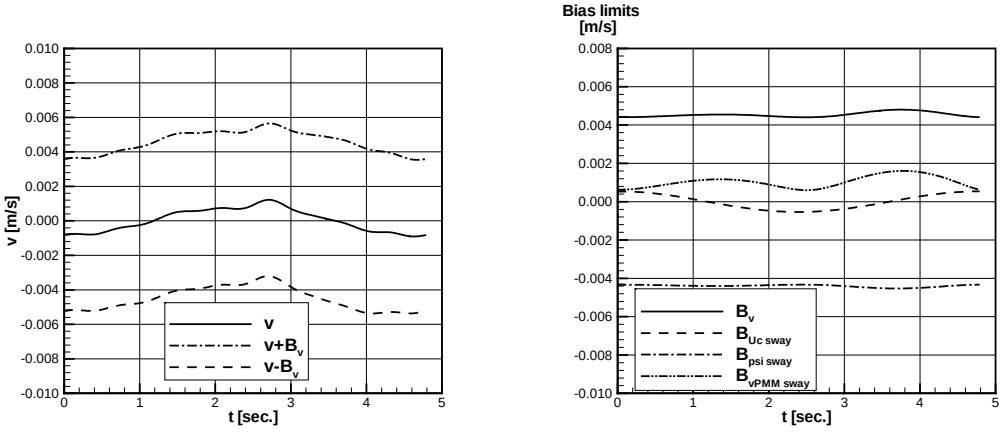

(a) (b)

Figure C.5.1.3. (a) Sway velocity and (b) bias limits.

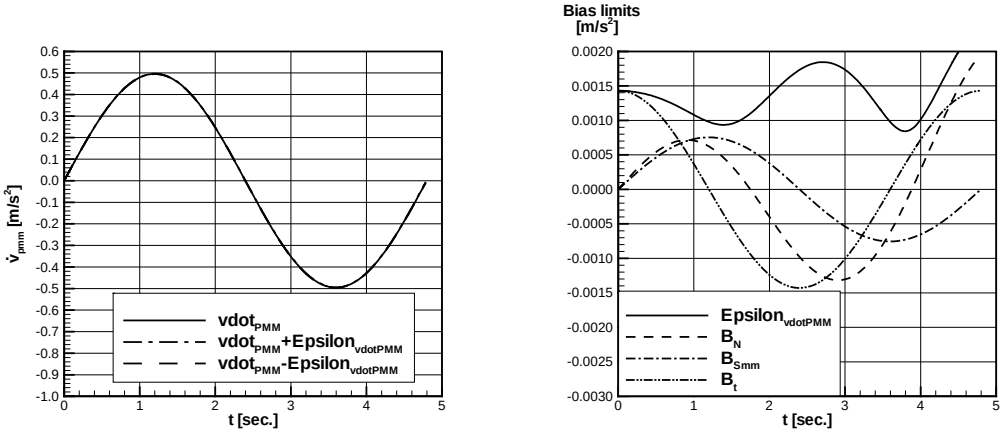

(a) (b)

Figure C.5.1.4. (a) Transverse PMM acceleration and (b) bias limits.

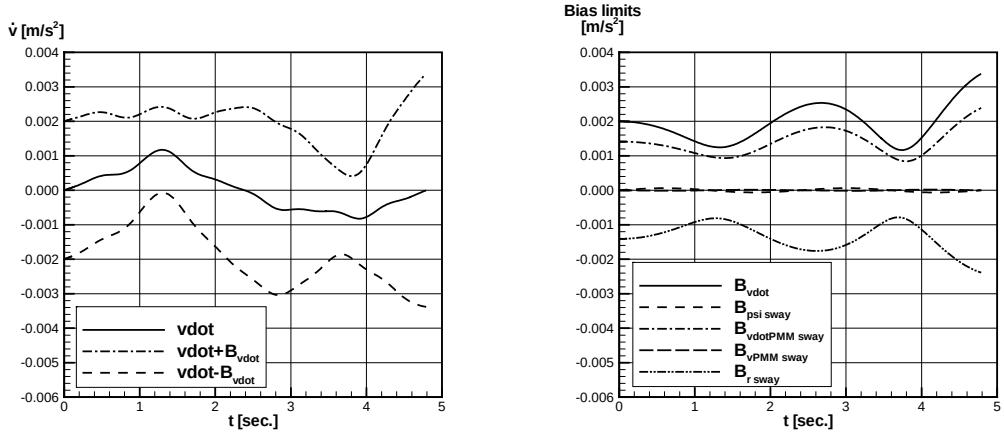

(a) (b)

Figure C.5.1.5. (a) Sway acceleration and (b) bias limits.

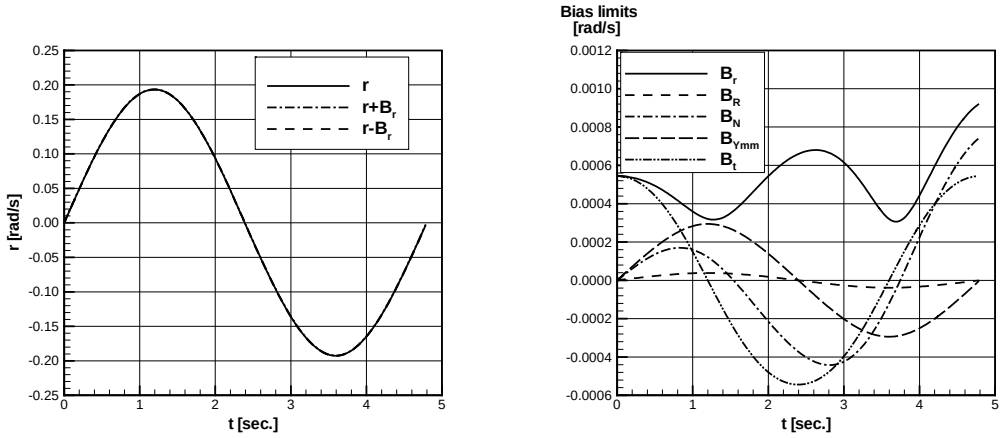

(a) (b)

Figure C.5.1.6. (a) Yaw rate and (b) bias limits.

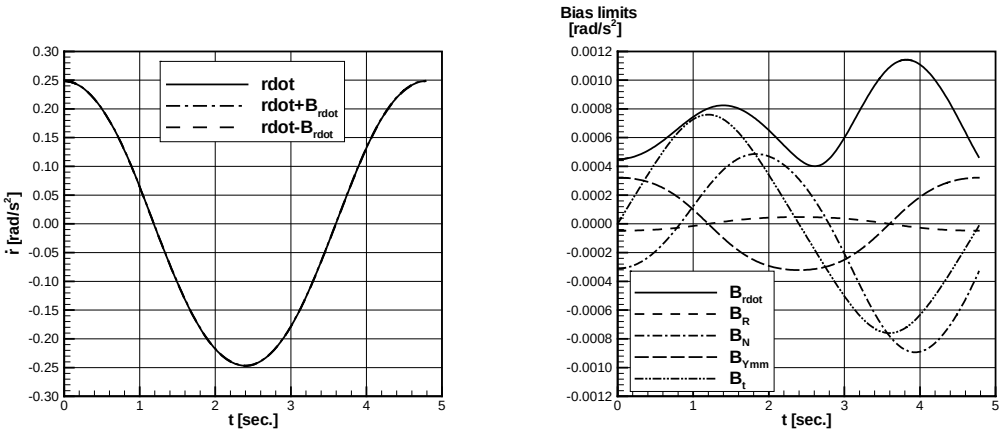

(a) (b)

Figure C.5.1.7. (a) Yaw acceleration and (b) bias limits.

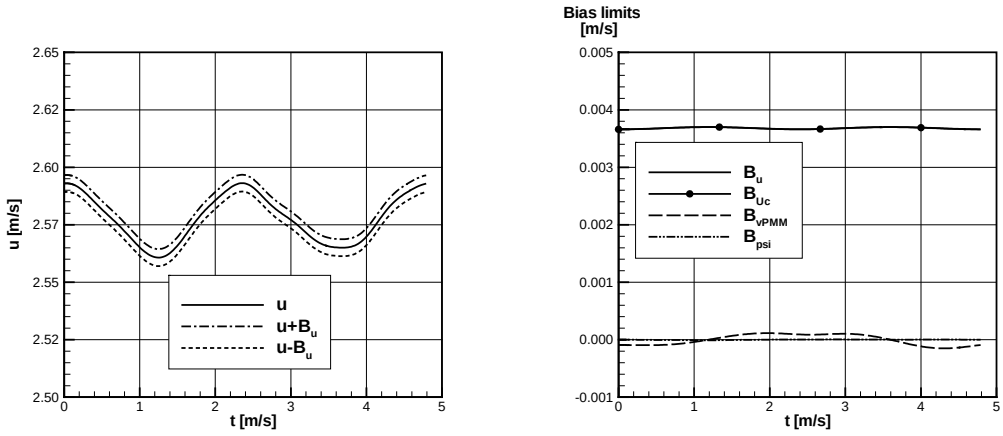

(a) (b)

Figure C.5.1.8. (a) Surge velocity and (b) bias limits.

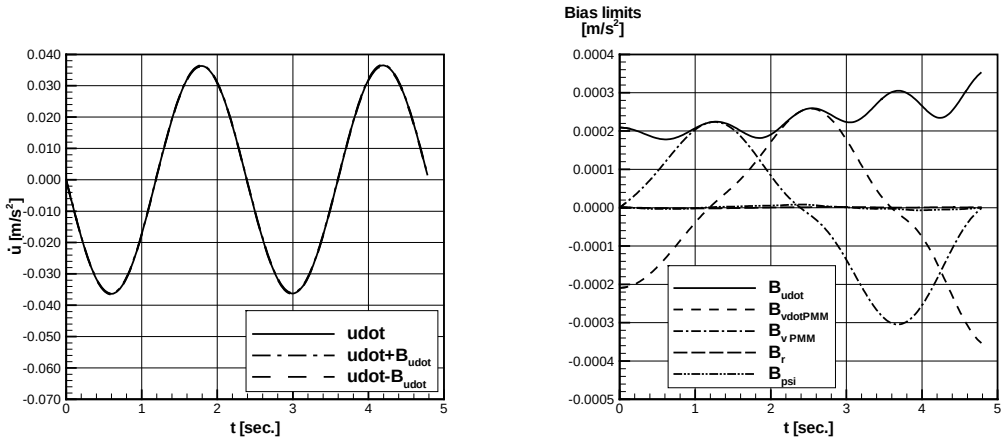

(a) (b)

Figure C.5.1.9. (a) Surge acceleration and (b) bias limits.

C.5.2 Longitudinal force

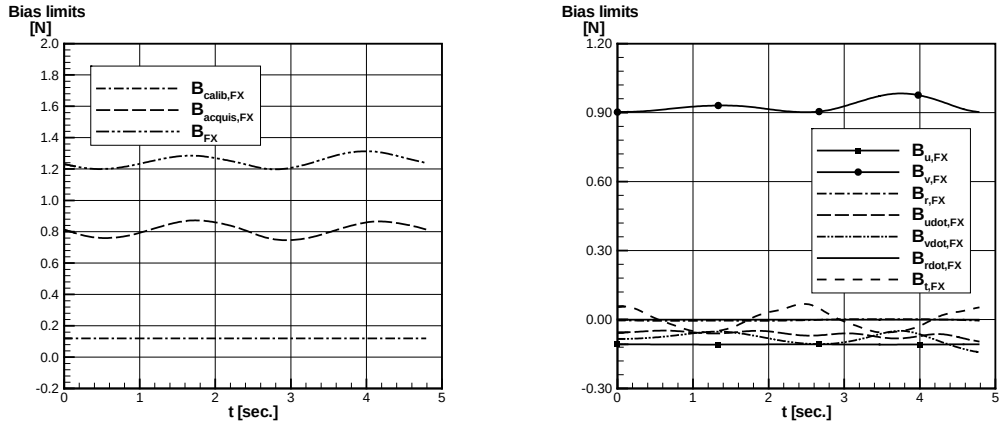

(a) (b)

Figure C.5.2.1. (a) and (b) bias limits for measured X-force.

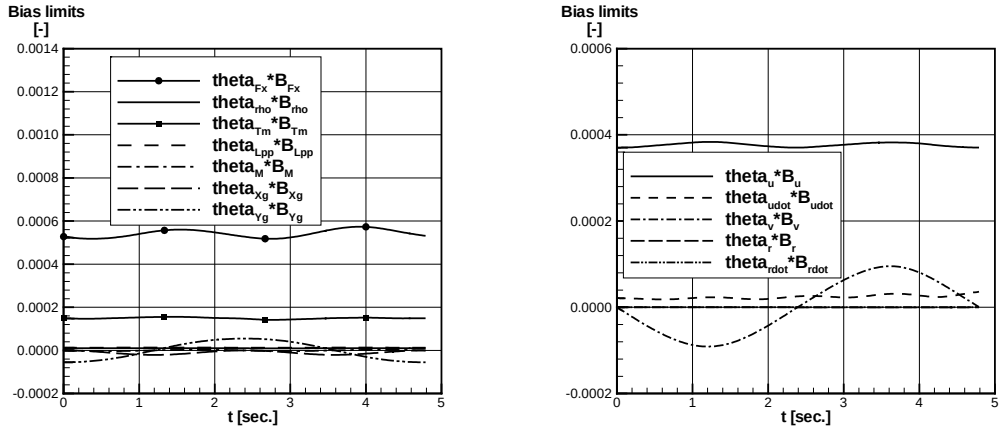

(a) (b)

Figure C.5.2.2. (a) and (b) bias limits for X'.

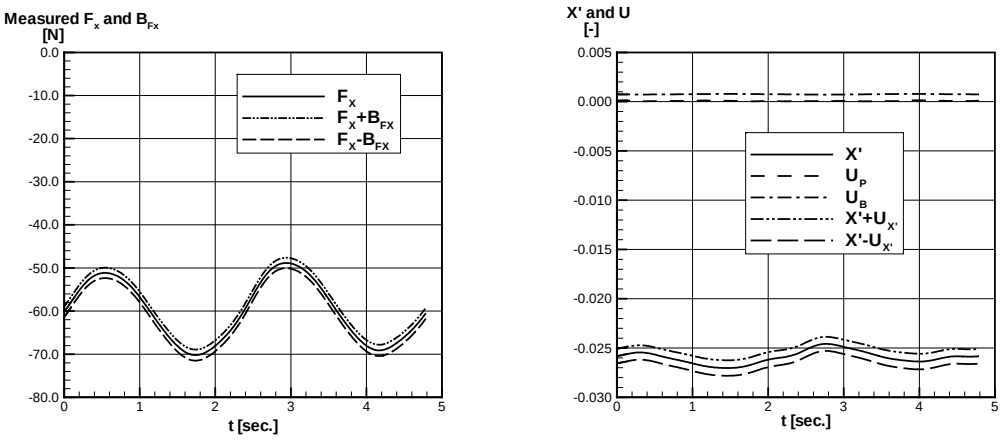

(a) (b)

Figure C.5.2.3. (a) Measured F_X and its bias limit. (b) X' including uncertainty.

C.5.3 Transverse force

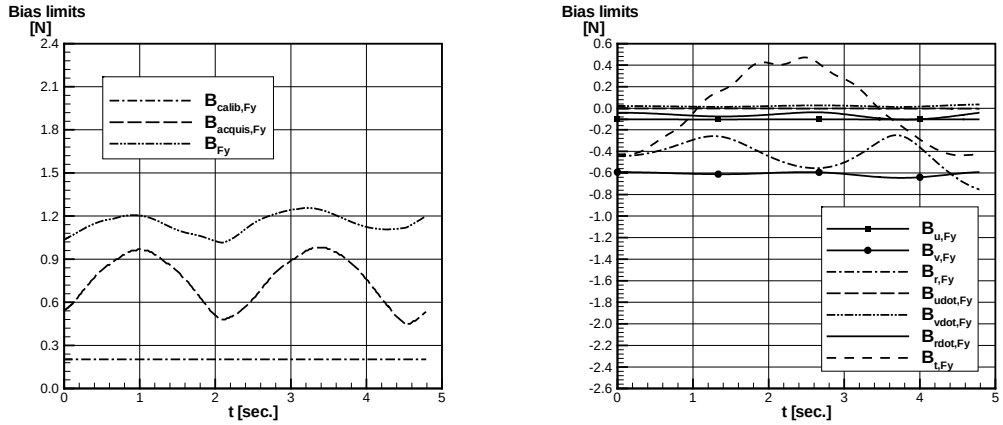

(a) (b)

Figure C.5.3.1. (a) and (b) bias limits for measured Y-force.

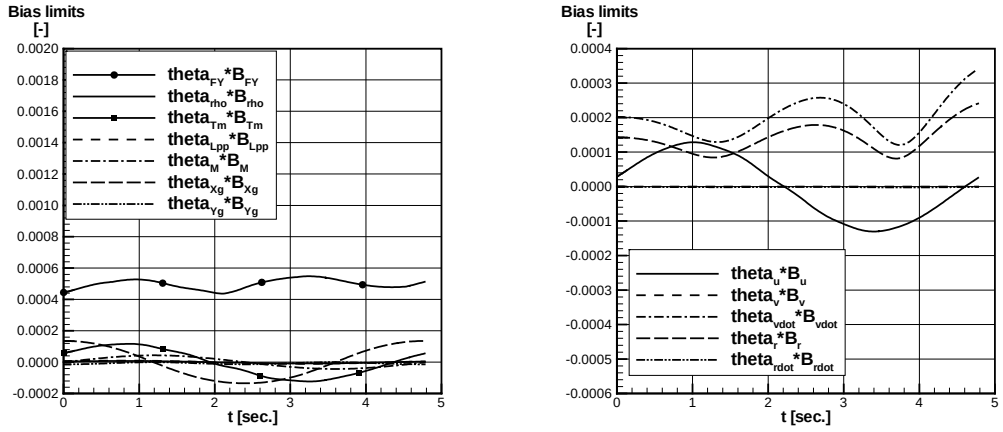

(a) (b)

Figure C.5.3.2. (a) and (b) bias limits for Y'.

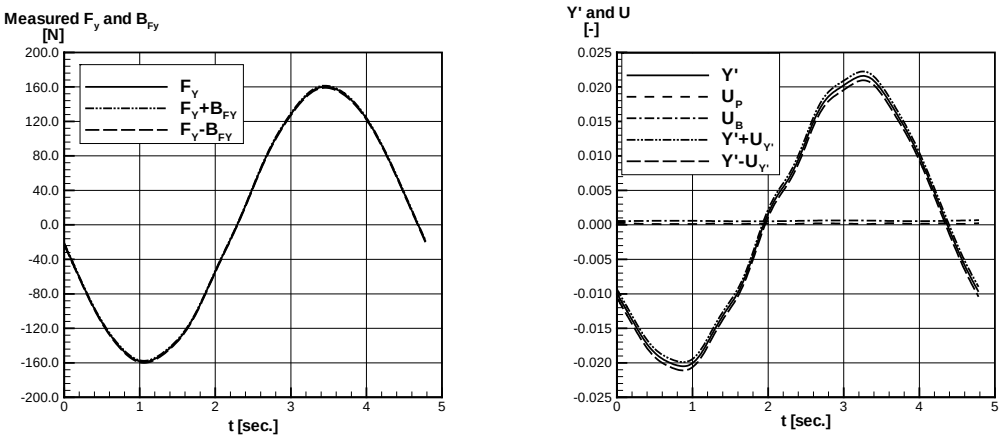

(a) (b)

Figure C.5.3.3. (a) Measured F_Y and its bias limit. (b) Y' including uncertainty.

C.5.4 Yaw moment

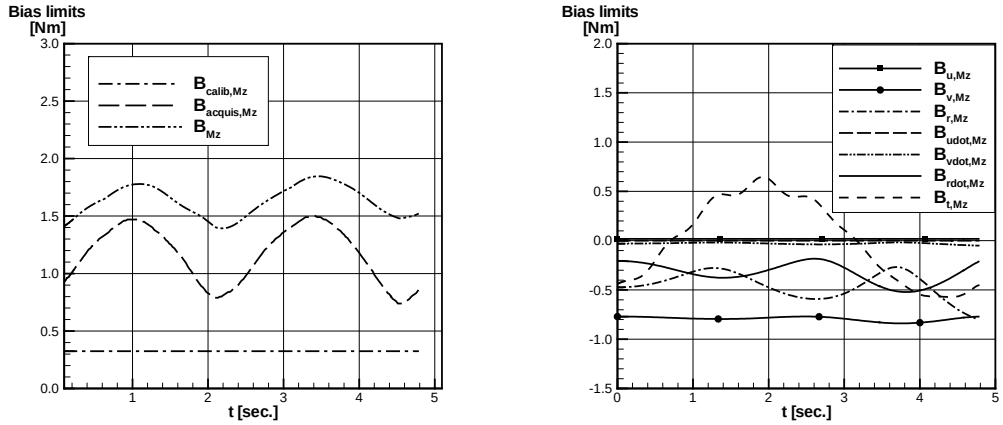

(a) (b)

Figure C.5.4.1. (a) and (b) bias limits for measured yaw moment M_Z.

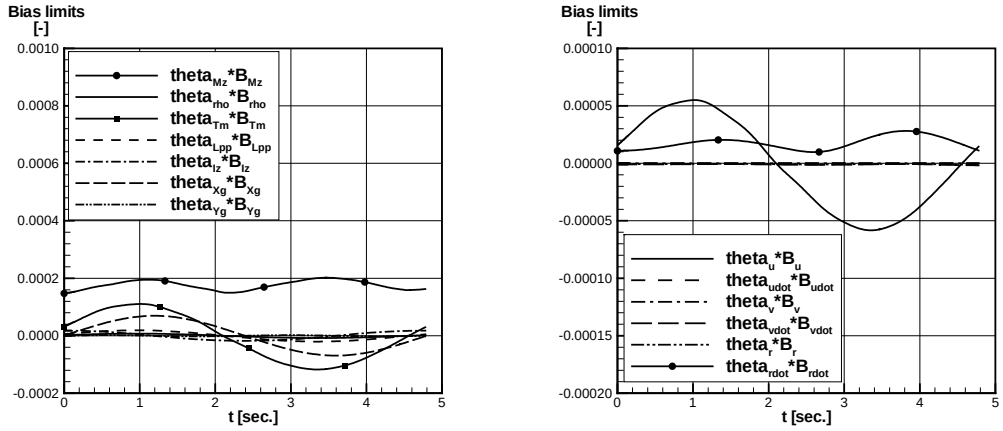

(a) (b)

Figure C.5.4.2. (a) and (b) bias limits for N'.

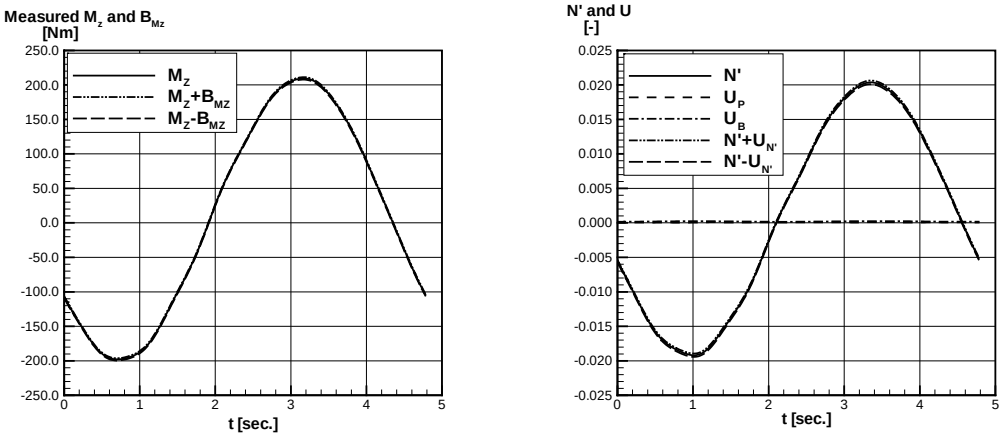

(a) (b)

Figure C.5.4.3. (a) Measured M_Z and its bias limit. (b) N' including uncertainty.

C.5.5 Sinkage at FP and AP

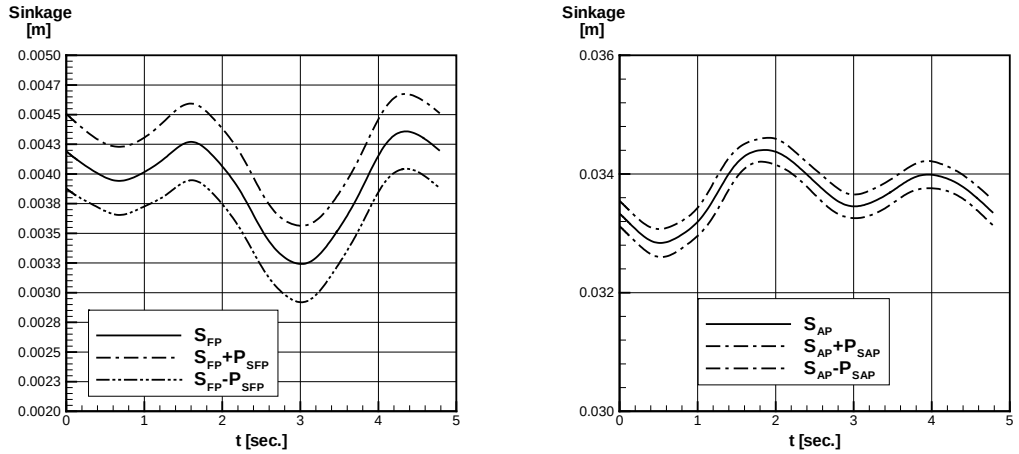

(a) (b)

Figure C.5.5.1. Sinkage, (a) at FP and (b) at AP.

Appendix D. Results from dynamic tests without uncertainty assessment

Appendix D shows the time series for all the dynamic test cases, which are not dealt with in the uncertainty analysis. Each condition is marked with a time series number printed at the bottom of each page. This number is the Run ID shown in the test program in Appendix A.

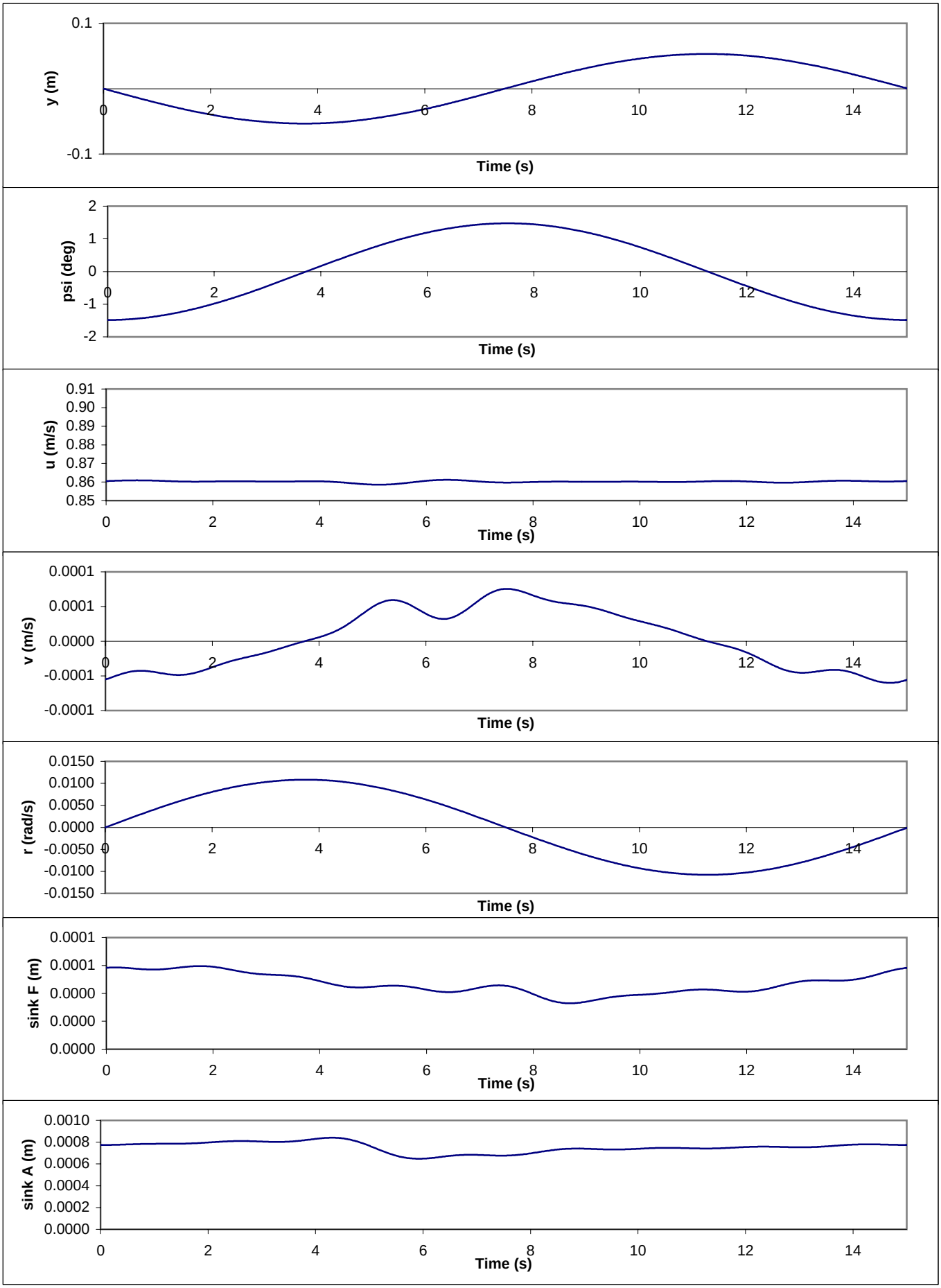
y (m)
0.1
-0.1
0
2
4
6
8
10
12
14
Time (s)
psi (deg)
2
1
0
-1
-2
Time (s)
u (m/s)
0.91
0.90
0.89
0.88
0.87
0.86
0.85
Time (s)
v (m/s)
0.0001
0.0001
0.0000
-0.0001
-0.0001
Time (s)
r (rad/s)
0.0150
0.0100
0.0050
0.0000
-0.0050
-0.0100
-0.0150
Time (s)
sink F (m)
0.0001
0.0001
0.0000
0.0000
0.0000
Time (s)
sink A (m)
0.0010
0.0008
0.0006
0.0004
0.0002
0.0000
Time (s)

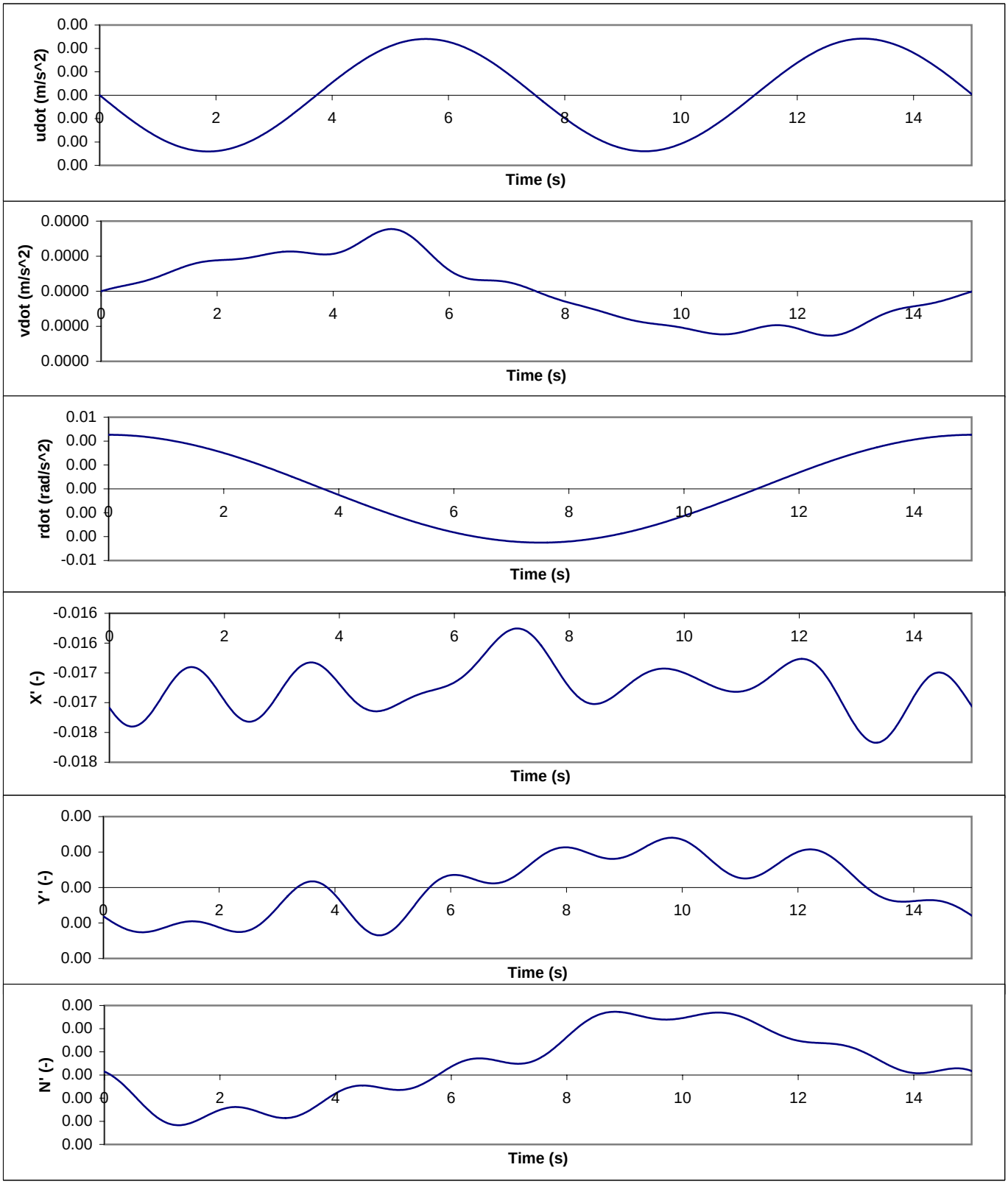
udot (m/s^2)
0.00
0.00
0.00
0.00
0.00
0.00
0.00
0 2 4 6 8 10 12 14
Time (s)
vdot (m/s^2)
0.0000
0.0000
0.0000
0.0000
0.0000
0 2 4 6 8 10 12 14
Time (s)
rdot (rad/s^2)
0.01
0.00
0.00
0.00
0.00
0.00
-0.01
0 2 4 6 8 10 12 14
Time (s)
X' (-)
-0.016
-0.016
-0.017
-0.017
-0.018
-0.018
0 2 4 6 8 10 12 14
Time (s)
Y' (-)
0.00
0.00
0.00
0.00
0.00
0 2 4 6 8 10 12 14
Time (s)
N' (-)
0.00
0.00
0.00
0.00
0.00
0.00
0.00
0 2 4 6 8 10 12 14
Time (s)

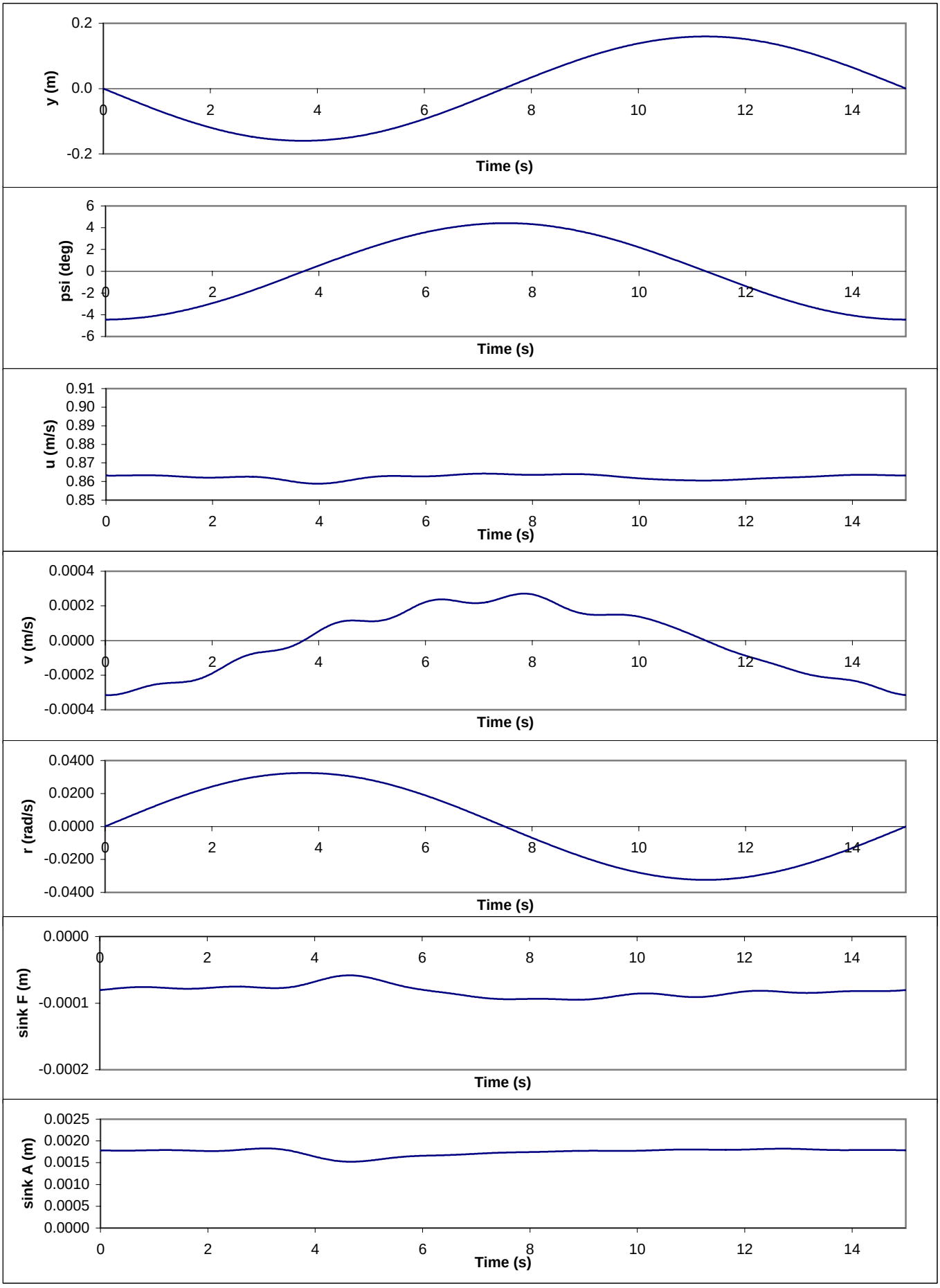
y (m)
0.2
0.0
-0.2
0
2
4
6
8
10
12
14
Time (s)
psi (deg)
6
4
2
0
-2
-4
-6
Time (s)
u (m/s)
0.91
0.90
0.89
0.88
0.87
0.86
0.85
Time (s)
v (m/s)
0.0004
0.0002
0.0000
-0.0002
-0.0004
Time (s)
r (rad/s)
0.0400
0.0200
0.0000
-0.0200
-0.0400
Time (s)
sink F (m)
0.0000
-0.0001
-0.0002
Time (s)
sink A (m)
0.0025
0.0020
0.0015
0.0010
0.0005
0.0000
Time (s)

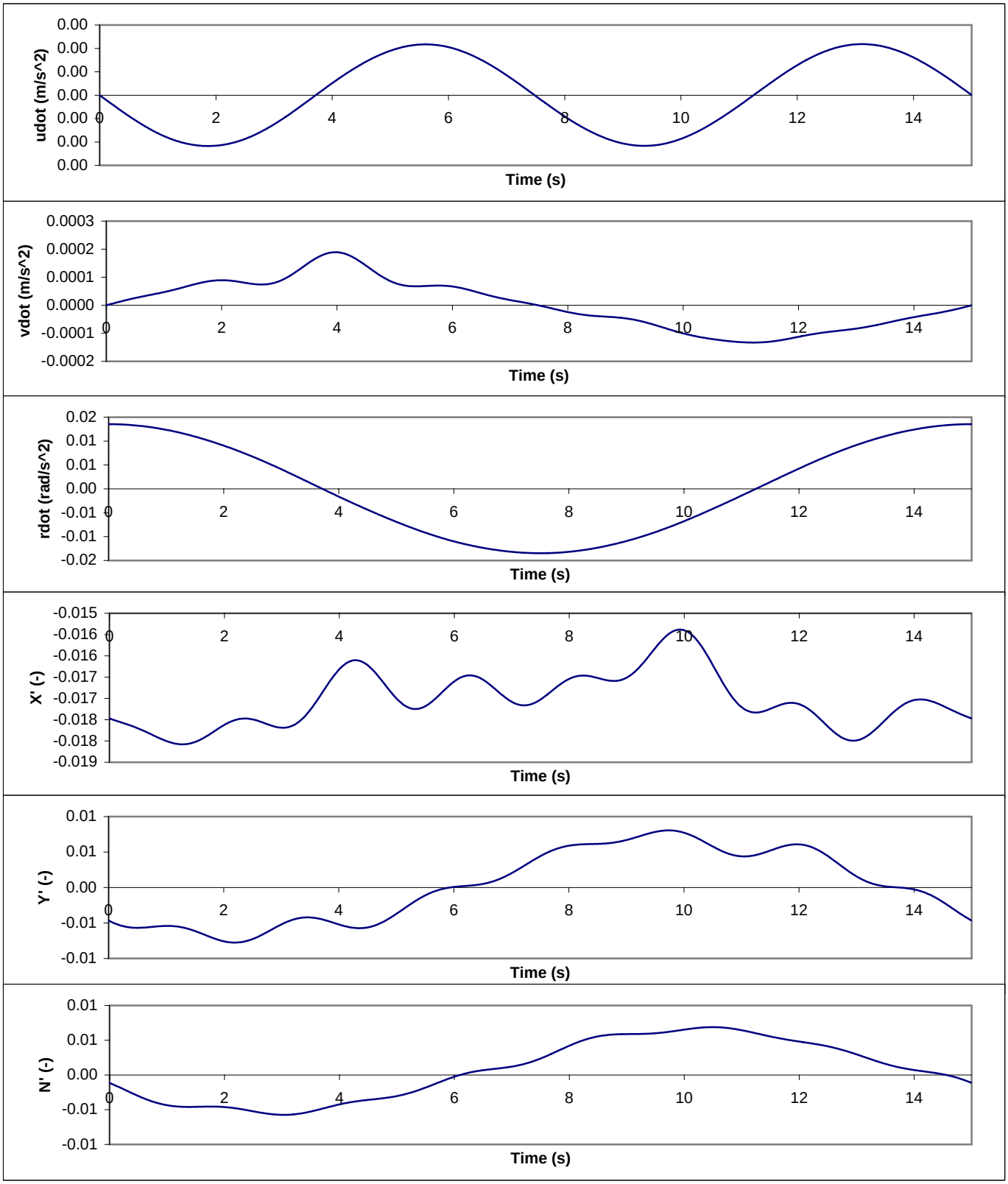
udot (m/s^2)
0.00
0.00
0.00
0.00
0.00
0.00
0.00
0 2 4 6 8 10 12 14
Time (s)
vdot (m/s^2)
0.0003
0.0002
0.0001
0.0000
-0.0001
-0.0002
0 2 4 6 8 10 12 14
Time (s)
rdot (rad/s^2)
0.02
0.01
0.01
0.00
-0.01
-0.01
-0.02
0 2 4 6 8 10 12 14
Time (s)
X' (-)
-0.015
-0.016
-0.016
-0.017
-0.017
-0.018
-0.018
-0.019
0 2 4 6 8 10 12 14
Time (s)
Y' (-)
0.01
0.01
0.00
-0.01
-0.01
0 2 4 6 8 10 12 14
Time (s)
N' (-)
0.01
0.01
0.00
-0.01
-0.01
0 2 4 6 8 10 12 14
Time (s)

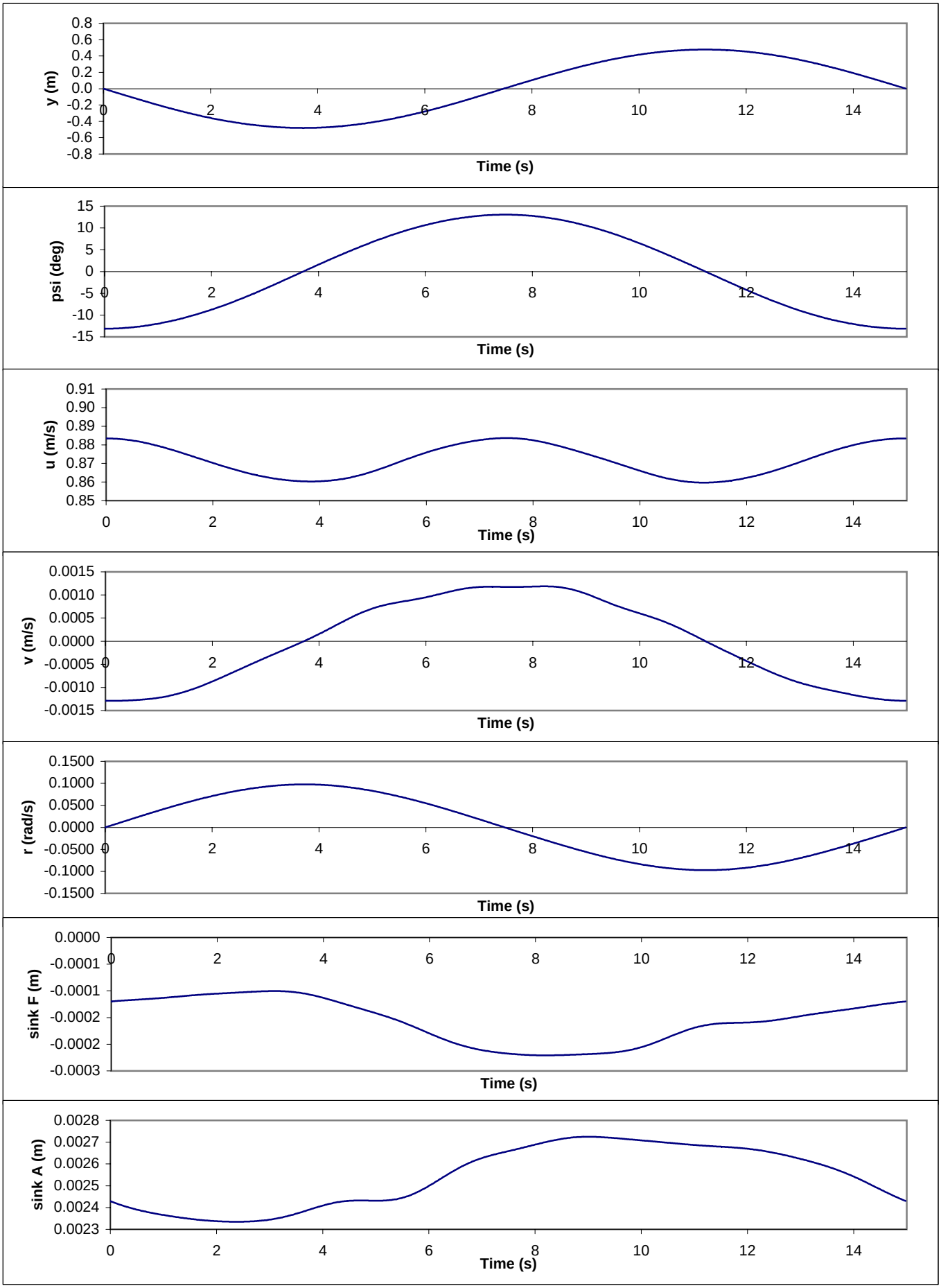
y (m)
0.8
0.6
0.4
0.2
0.0
-0.2
-0.4
-0.6
-0.8
0 2 4 6 8 10 12 14
Time (s)
psi (deg)
15
10
5
0
-5
-10
-15
0 2 4 6 8 10 12 14
Time (s)
u (m/s)
0.91
0.90
0.89
0.88
0.87
0.86
0.85
0 2 4 6 8 10 12 14
Time (s)
v (m/s)
0.0015
0.0010
0.0005
0.0000
-0.0005
-0.0010
-0.0015
0 2 4 6 8 10 12 14
Time (s)
r (rad/s)
0.1500
0.1000
0.0500
0.0000
-0.0500
-0.1000
-0.1500
0 2 4 6 8 10 12 14
Time (s)
sink F (m)
0.0000
-0.0001
-0.0001
-0.0002
-0.0002
-0.0003
0 2 4 6 8 10 12 14
Time (s)
sink A (m)
0.0028
0.0027
0.0026
0.0025
0.0024
0.0023
0 2 4 6 8 10 12 14
Time (s)

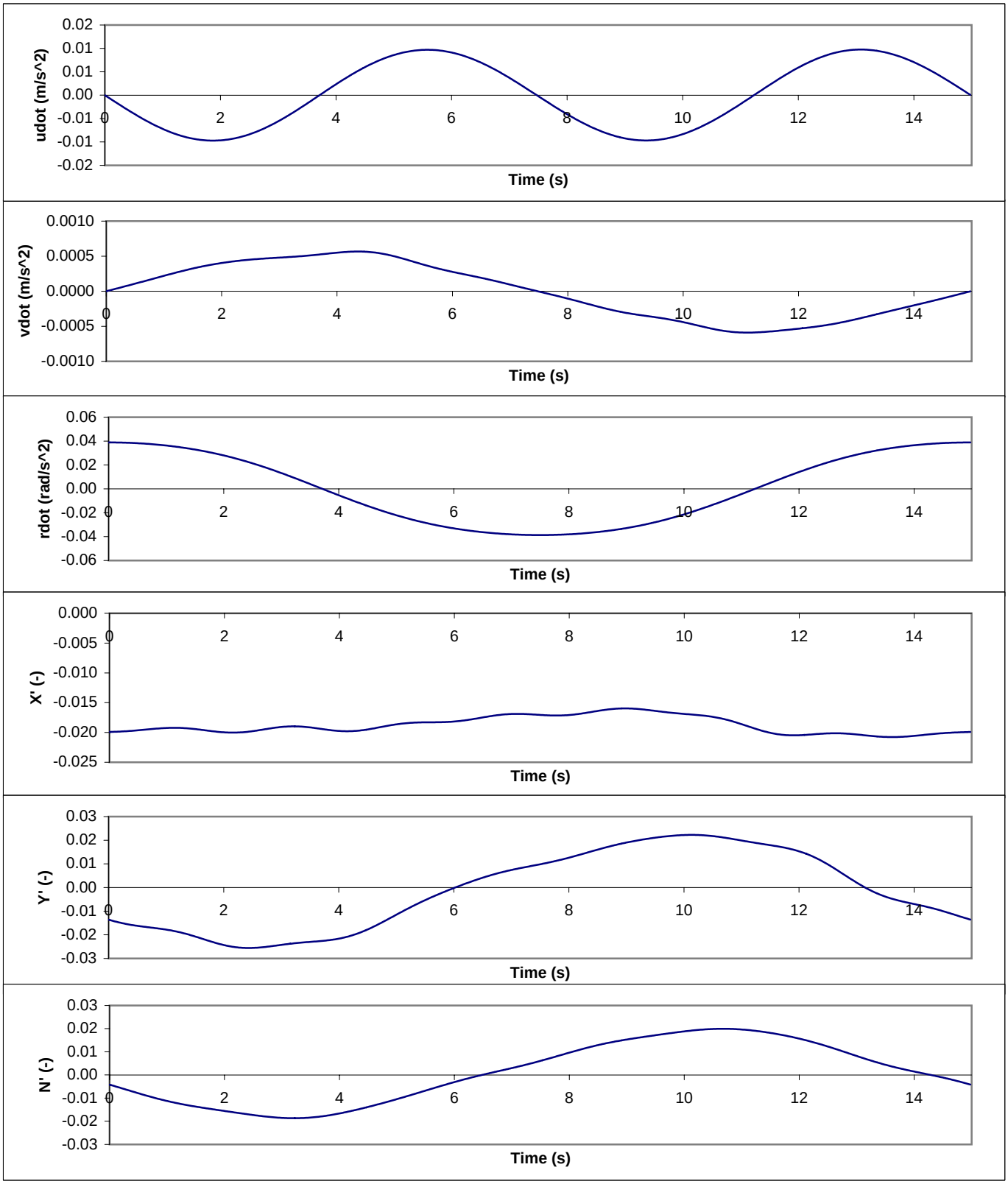
udot (m/s^2)
0.02
0.01
0.01
0.00
-0.01
-0.01
-0.02
0
2
4
6
8
10
12
14
Time (s)
vdot (m/s^2)
0.0010
0.0005
0.0000
-0.0005
-0.0010
Time (s)
rdot (rad/s^2)
0.06
0.04
0.02
0.00
-0.02
-0.04
-0.06
Time (s)
X' (-)
0.000
-0.005
-0.010
-0.015
-0.020
-0.025
Time (s)
Y' (-)
0.03
0.02
0.01
0.00
-0.01
-0.02
-0.03
Time (s)
N' (-)
0.03
0.02
0.01
0.00
-0.01
-0.02
-0.03
Time (s)

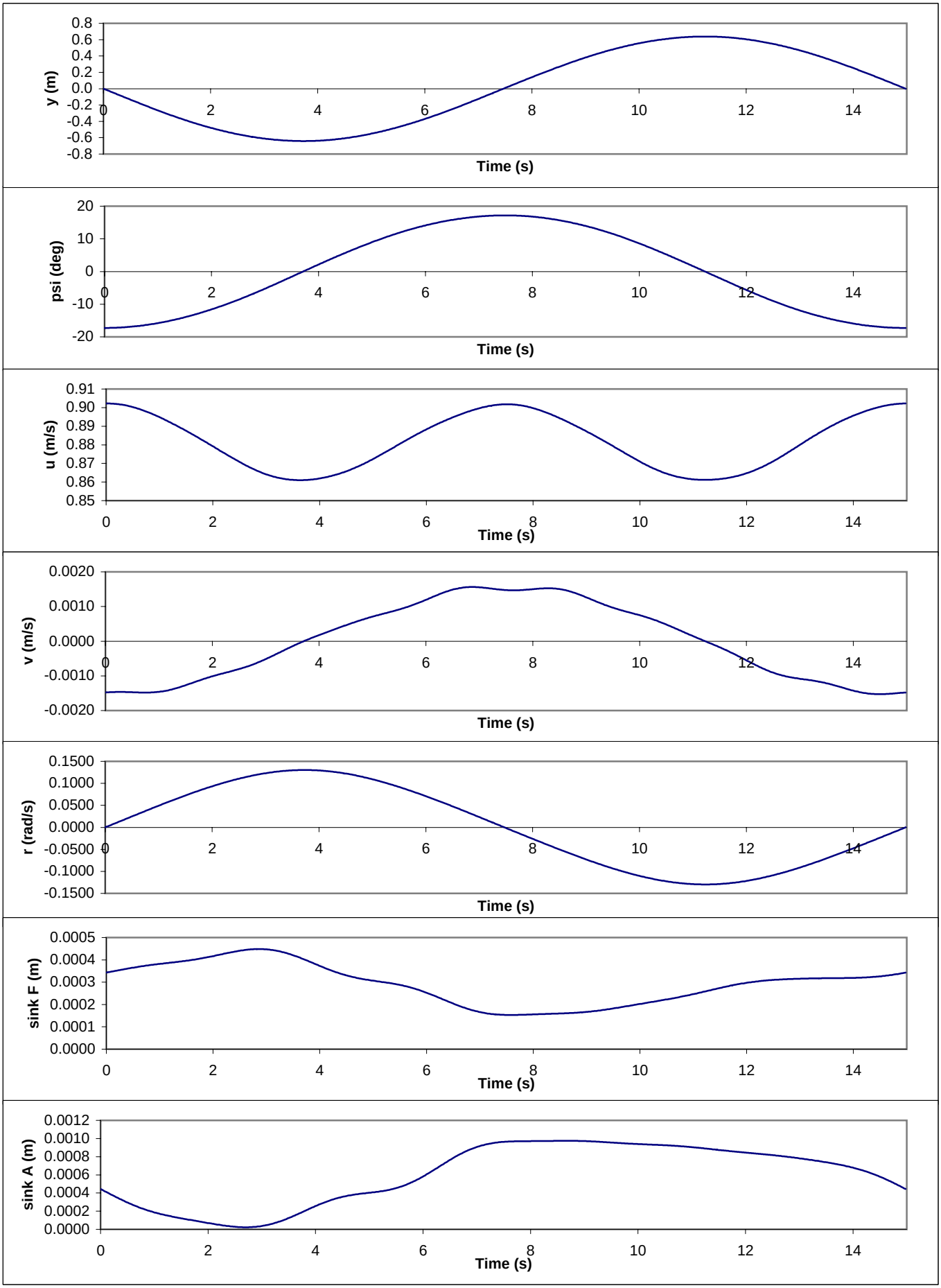
y (m)
0.8
0.6
0.4
0.2
0.0
-0.2
-0.4
-0.6
-0.8
0
2
4
6
8
10
12
14
Time (s)
psi (deg)
20
10
0
-10
-20
Time (s)
u (m/s)
0.91
0.90
0.89
0.88
0.87
0.86
0.85
Time (s)
v (m/s)
0.0020
0.0010
0.0000
-0.0010
-0.0020
Time (s)
r (rad/s)
0.1500
0.1000
0.0500
0.0000
-0.0500
-0.1000
-0.1500
Time (s)
sink F (m)
0.0005
0.0004
0.0003
0.0002
0.0001
0.0000
Time (s)
sink A (m)
0.0012
0.0010
0.0008
0.0006
0.0004
0.0002
0.0000
Time (s)

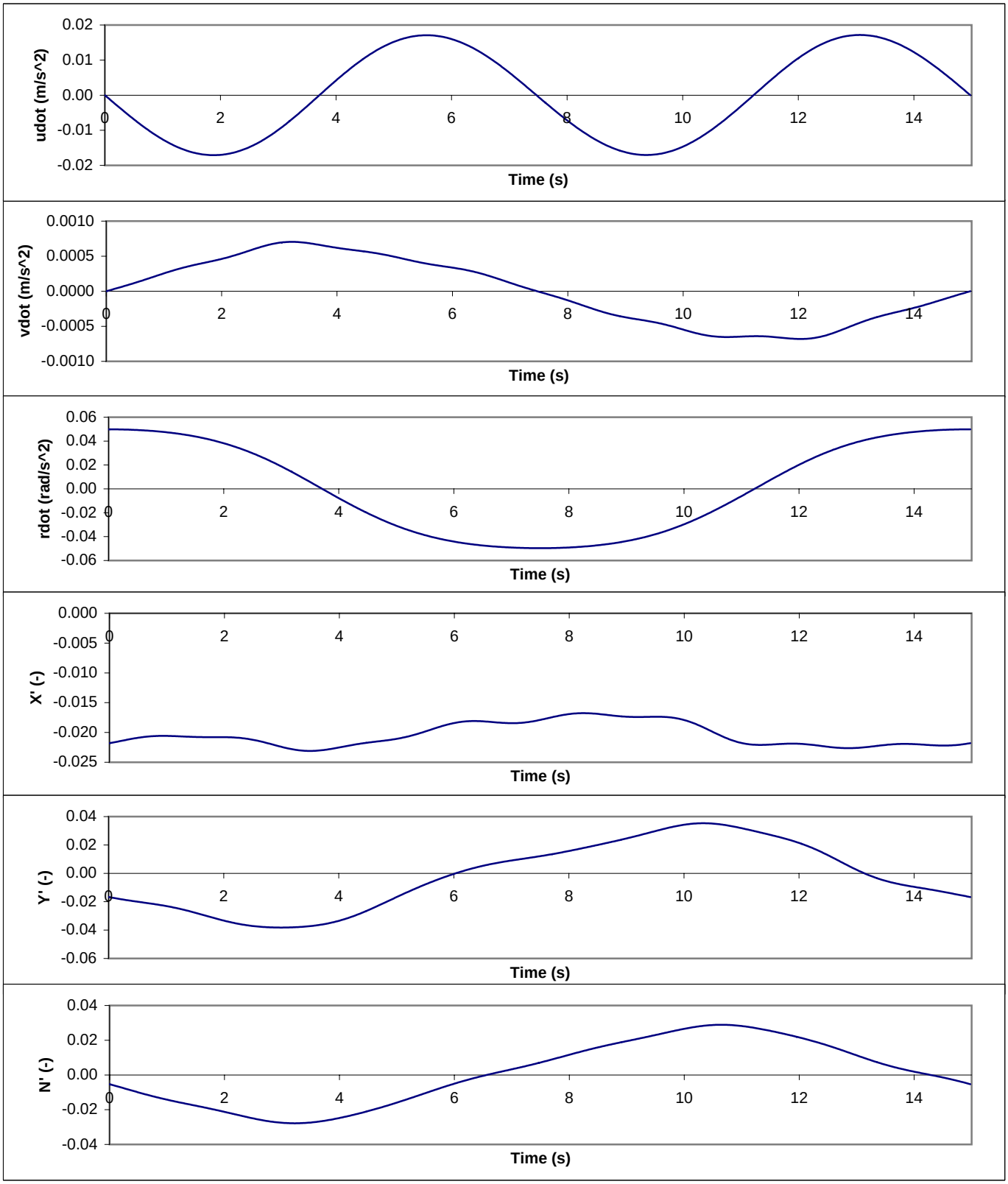
udot (m/s^2)
0.02
0.01
0.00
-0.01
-0.02
0
2
4
6
8
10
12
14
Time (s)
vdot (m/s^2)
0.0010
0.0005
0.0000
-0.0005
-0.0010
Time (s)
rdot (rad/s^2)
0.06
0.04
0.02
0.00
-0.02
-0.04
-0.06
Time (s)
X' (-)
0.000
-0.005
-0.010
-0.015
-0.020
-0.025
Time (s)
Y' (-)
0.04
0.02
0.00
-0.02
-0.04
-0.06
Time (s)
N' (-)
0.04
0.02
0.00
-0.02
-0.04
Time (s)

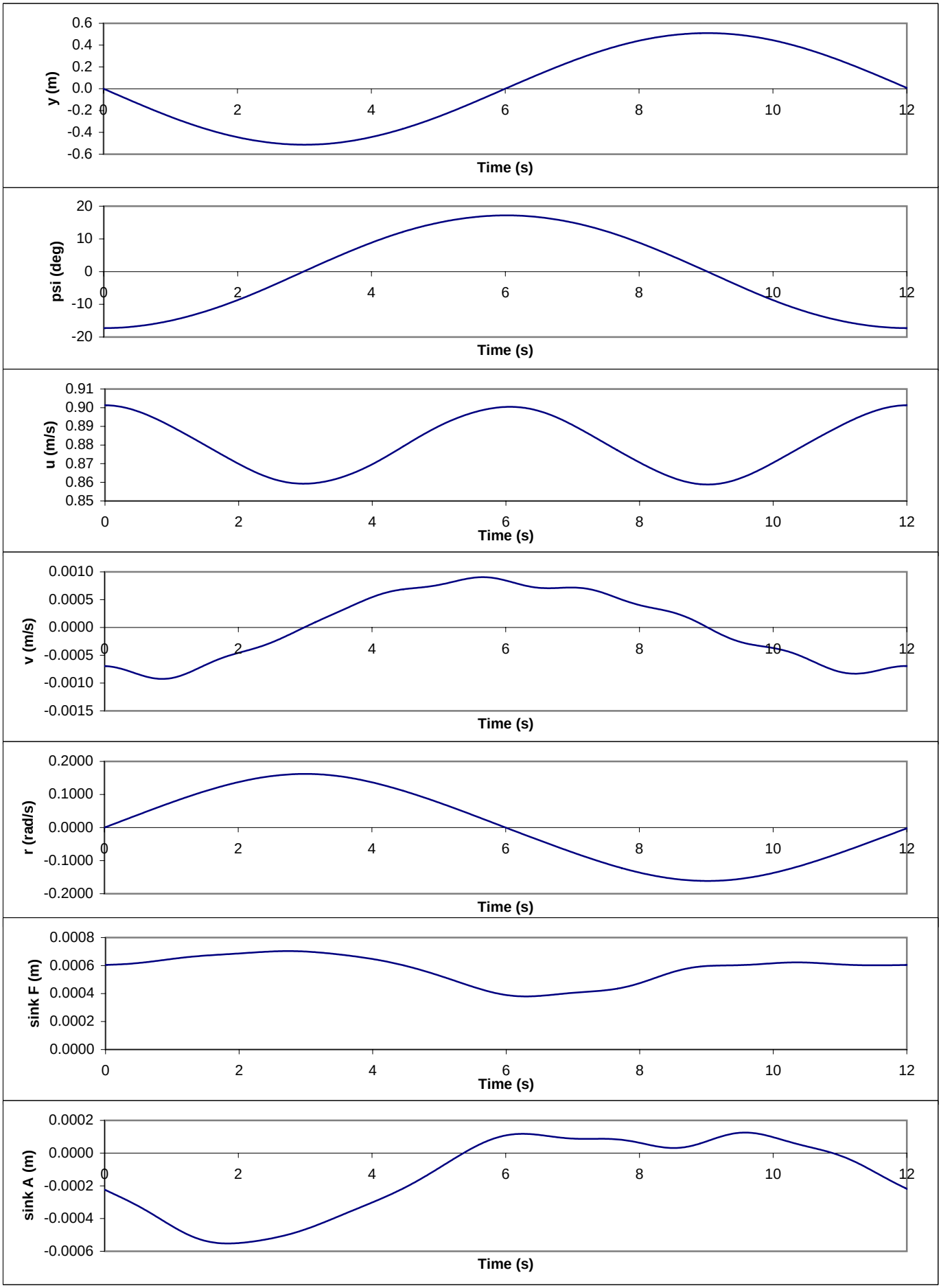
y (m)
0.6
0.4
0.2
0.0
-0.2
-0.4
-0.6
0
2
4
6
8
10
12
Time (s)
psi (deg)
20
10
0
-10
-20
0
2
4
6
8
10
12
Time (s)
u (m/s)
0.91
0.90
0.89
0.88
0.87
0.86
0.85
0
2
4
6
8
10
12
Time (s)
v (m/s)
0.0010
0.0005
0.0000
-0.0005
-0.0010
-0.0015
0
2
4
6
8
10
12
Time (s)
r (rad/s)
0.2000
0.1000
0.0000
-0.1000
-0.2000
0
2
4
6
8
10
12
Time (s)
sink F (m)
0.0008
0.0006
0.0004
0.0002
0.0000
0
2
4
6
8
10
12
Time (s)
sink A (m)
0.0002
0.0000
-0.0002
-0.0004
-0.0006
0
2
4
6
8
10
12
Time (s)

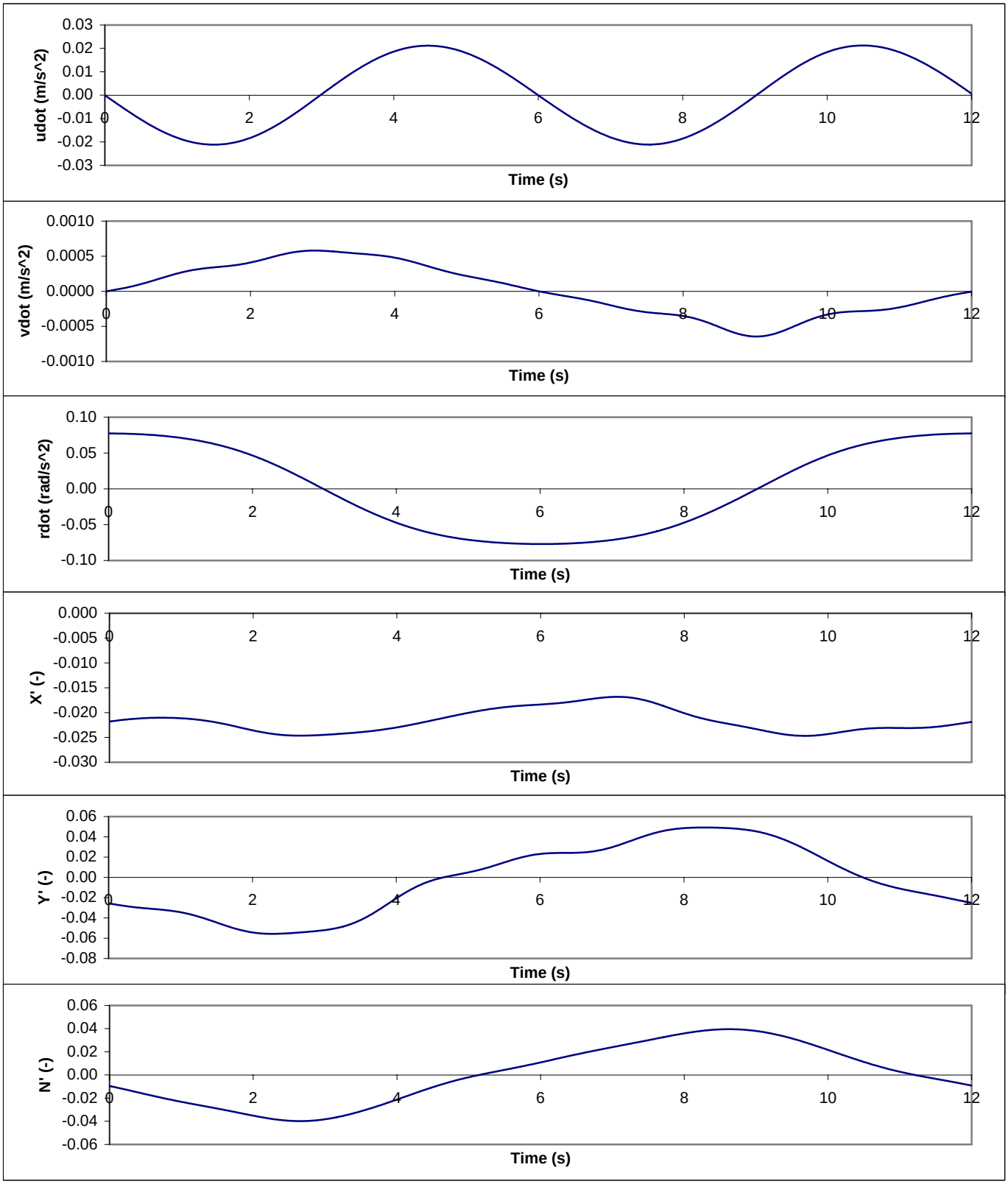
udot (m/s^2)
0.03
0.02
0.01
0.00
-0.01
-0.02
-0.03
0
2
4
6
8
10
12
Time (s)
vdot (m/s^2)
0.0010
0.0005
0.0000
-0.0005
-0.0010
Time (s)
rdot (rad/s^2)
0.10
0.05
0.00
-0.05
-0.10
Time (s)
X' (-)
0.000
-0.005
-0.010
-0.015
-0.020
-0.025
-0.030
Time (s)
Y' (-)
0.06
0.04
0.02
0.00
-0.02
-0.04
-0.06
-0.08
Time (s)
N' (-)
0.06
0.04
0.02
0.00
-0.02
-0.04
-0.06
Time (s)

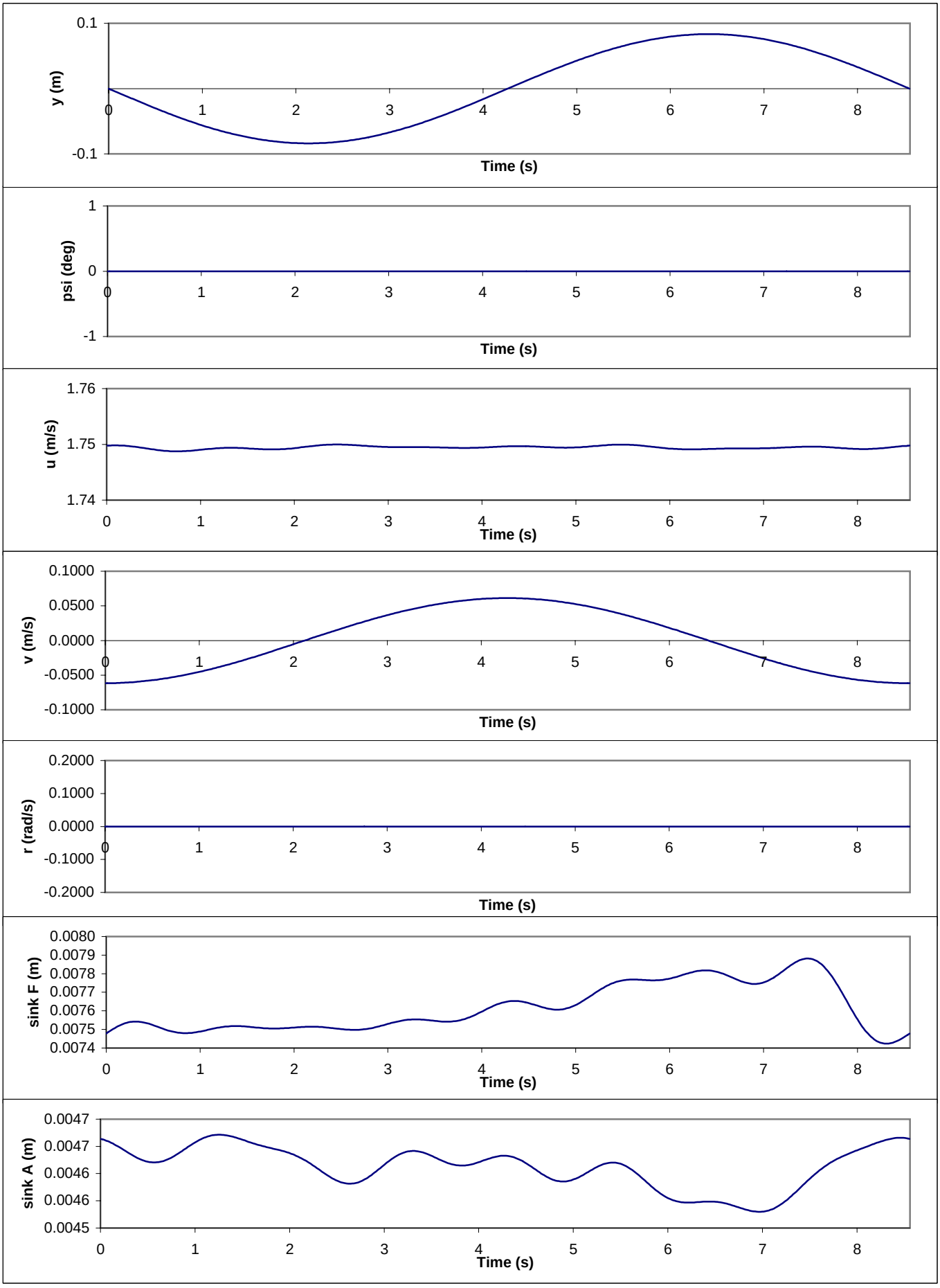
y (m)
0.1
-0.1
0 1 2 3 4 5 6 7 8
Time (s)
psi (deg)
1
0
-1
0 1 2 3 4 5 6 7 8
Time (s)
u (m/s)
1.76
1.75
1.74
0 1 2 3 4 5 6 7 8
Time (s)
v (m/s)
0.1000
0.0500
0.0000
-0.0500
-0.1000
0 1 2 3 4 5 6 7 8
Time (s)
r (rad/s)
0.2000
0.1000
0.0000
-0.1000
-0.2000
0 1 2 3 4 5 6 7 8
Time (s)
sink F (m)
0.0080
0.0079
0.0078
0.0077
0.0076
0.0075
0.0074
0 1 2 3 4 5 6 7 8
Time (s)
sink A (m)
0.0047
0.0047
0.0046
0.0046
0.0045
0 1 2 3 4 5 6 7 8
Time (s)

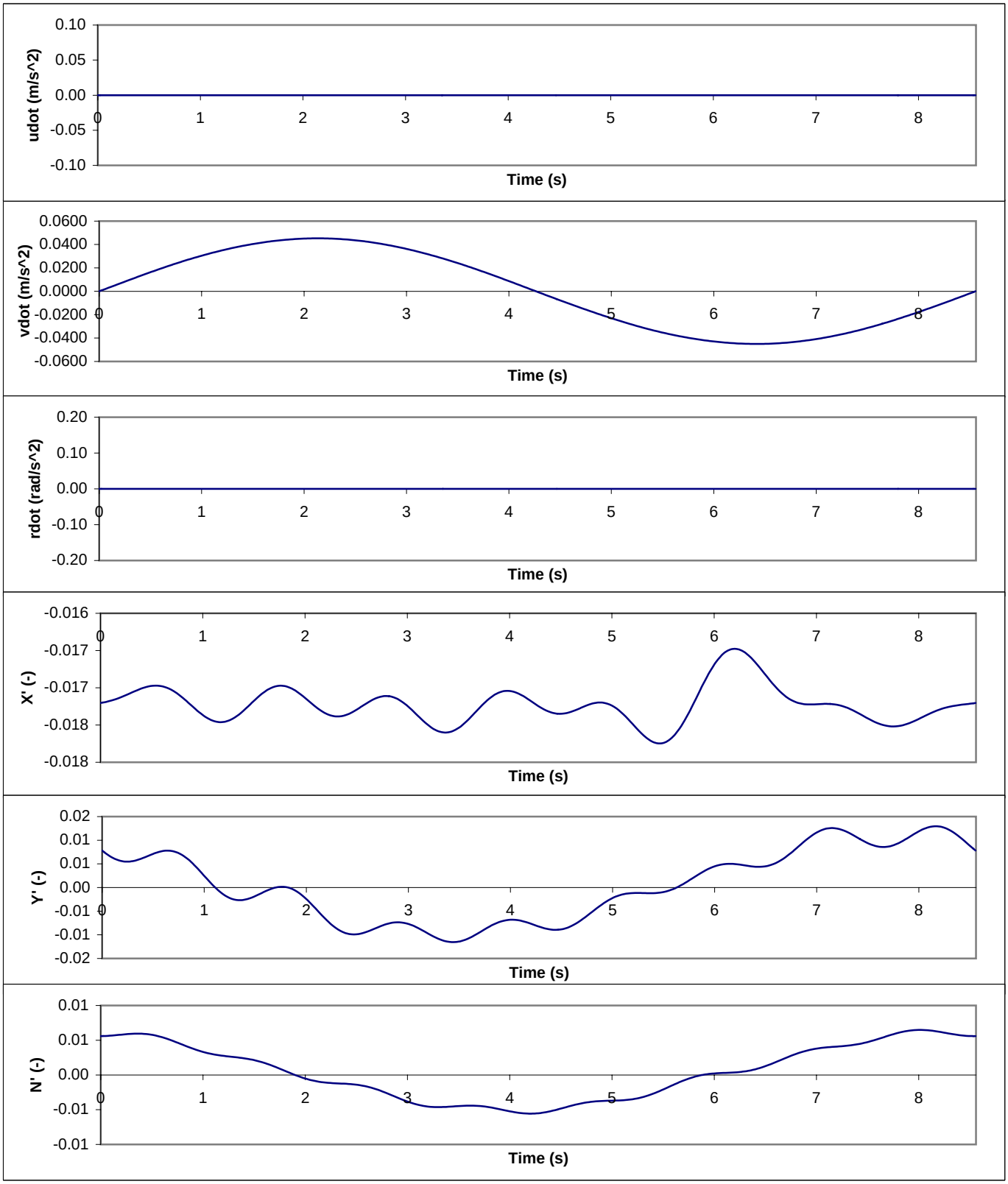
udot (m/s^2)
0.10
0.05
0.00
-0.05
-0.10
0 1 2 3 4 5 6 7 8
Time (s)
vdot (m/s^2)
0.0600
0.0400
0.0200
0.0000
-0.0200
-0.0400
-0.0600
0 1 2 3 4 5 6 7 8
Time (s)
rdot (rad/s^2)
0.20
0.10
0.00
-0.10
-0.20
0 1 2 3 4 5 6 7 8
Time (s)
X' (-)
-0.016
-0.017
-0.017
-0.018
-0.018
0 1 2 3 4 5 6 7 8
Time (s)
Y' (-)
0.02
0.01
0.01
0.00
-0.01
-0.01
-0.02
0 1 2 3 4 5 6 7 8
Time (s)
N' (-)
0.01
0.01
0.00
-0.01
-0.01
0 1 2 3 4 5 6 7 8
Time (s)

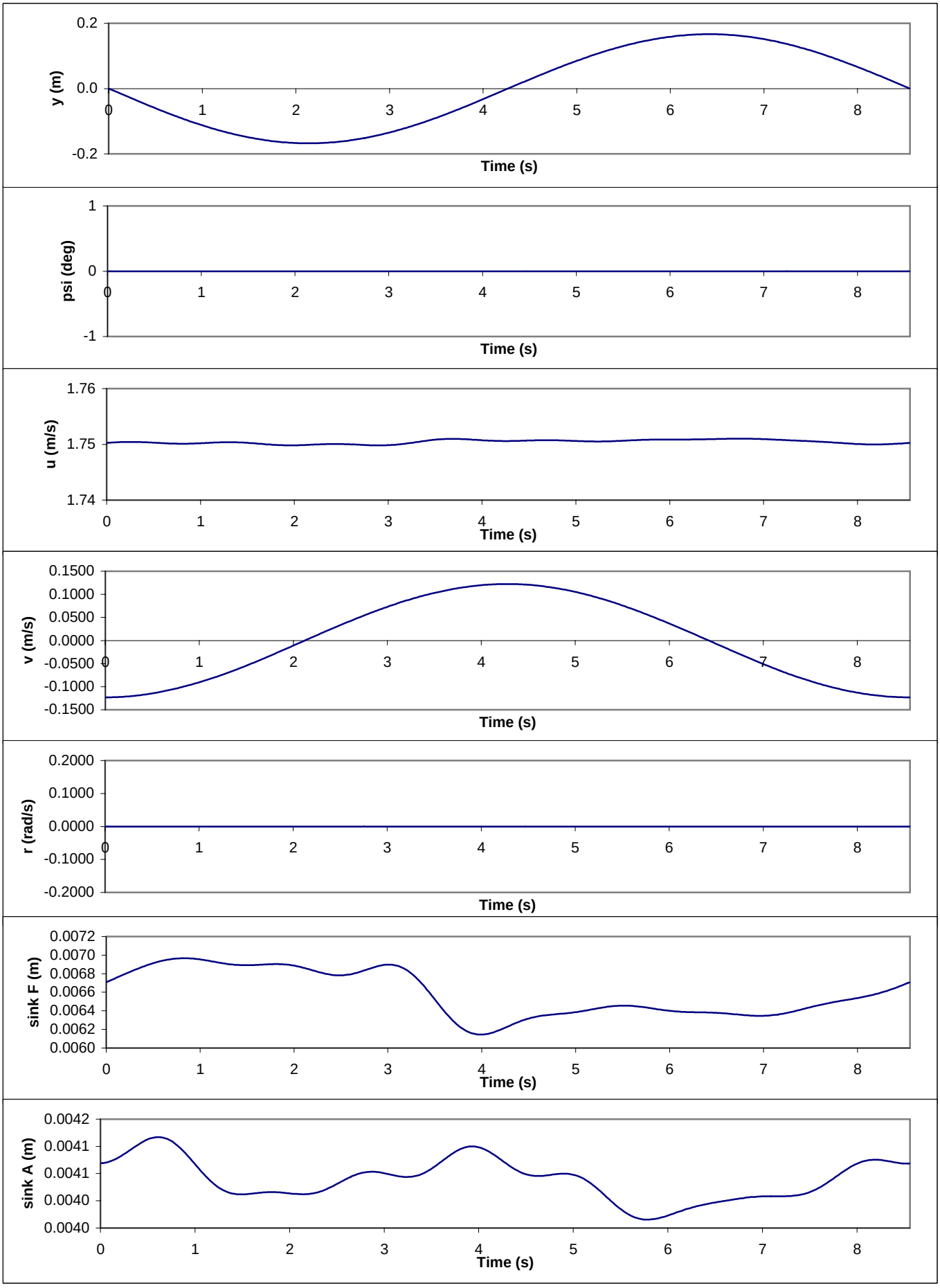

plot of timeseries 1158

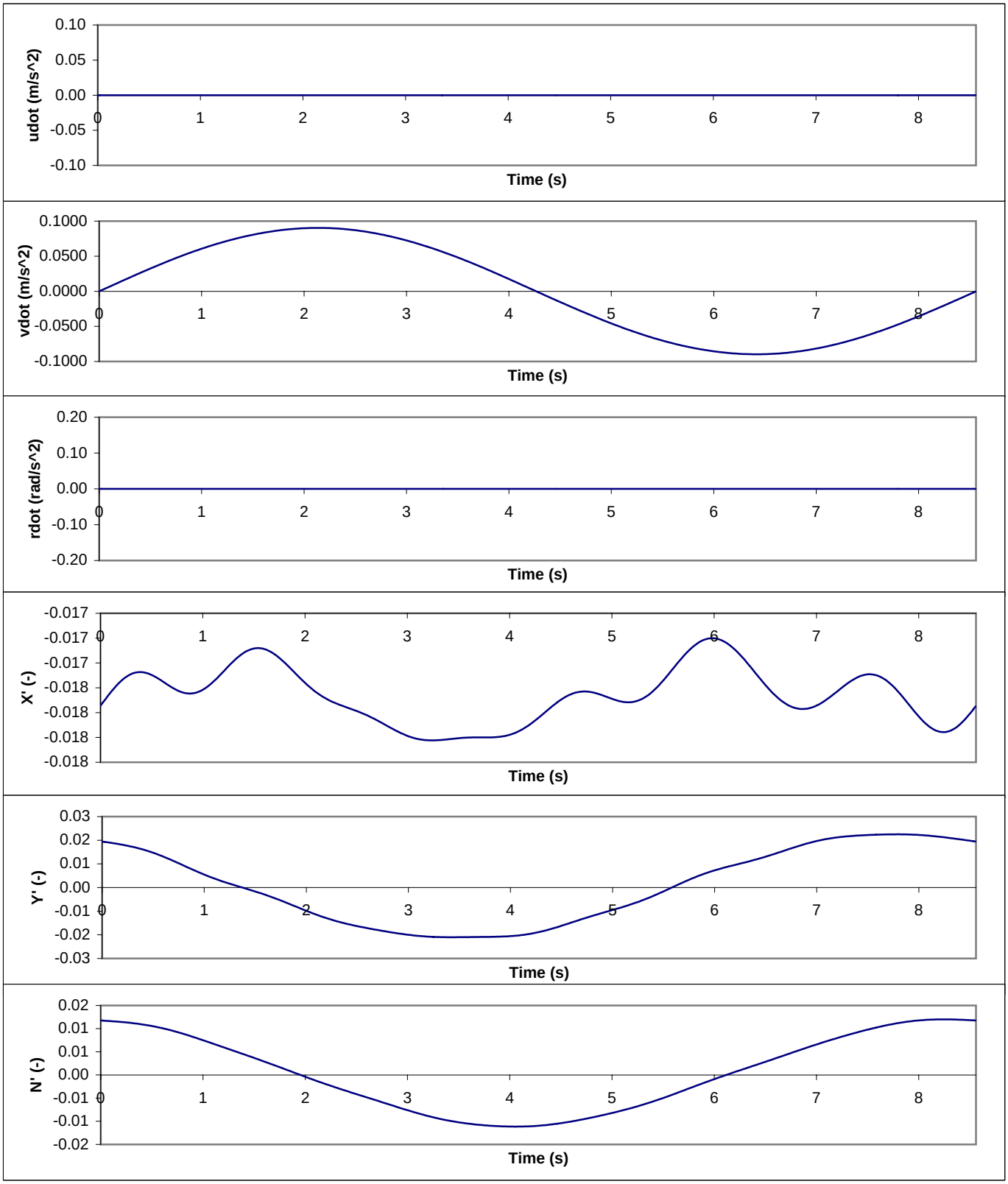
udot (m/s^2)
0.10
0.05
0.00
-0.05
-0.10
0 1 2 3 4 5 6 7 8
Time (s)
vdot (m/s^2)
0.1000
0.0500
0.0000
-0.0500
-0.1000
0 1 2 3 4 5 6 7 8
Time (s)
rdot (rad/s^2)
0.20
0.10
0.00
-0.10
-0.20
0 1 2 3 4 5 6 7 8
Time (s)
X' (-)
-0.017
-0.017
-0.017
-0.018
-0.018
-0.018
-0.018
0 1 2 3 4 5 6 7 8
Time (s)
Y' (-)
0.03
0.02
0.01
0.00
-0.01
-0.02
-0.03
0 1 2 3 4 5 6 7 8
Time (s)
N' (-)
0.02
0.01
0.01
0.00
-0.01
-0.01
-0.02
0 1 2 3 4 5 6 7 8
Time (s)

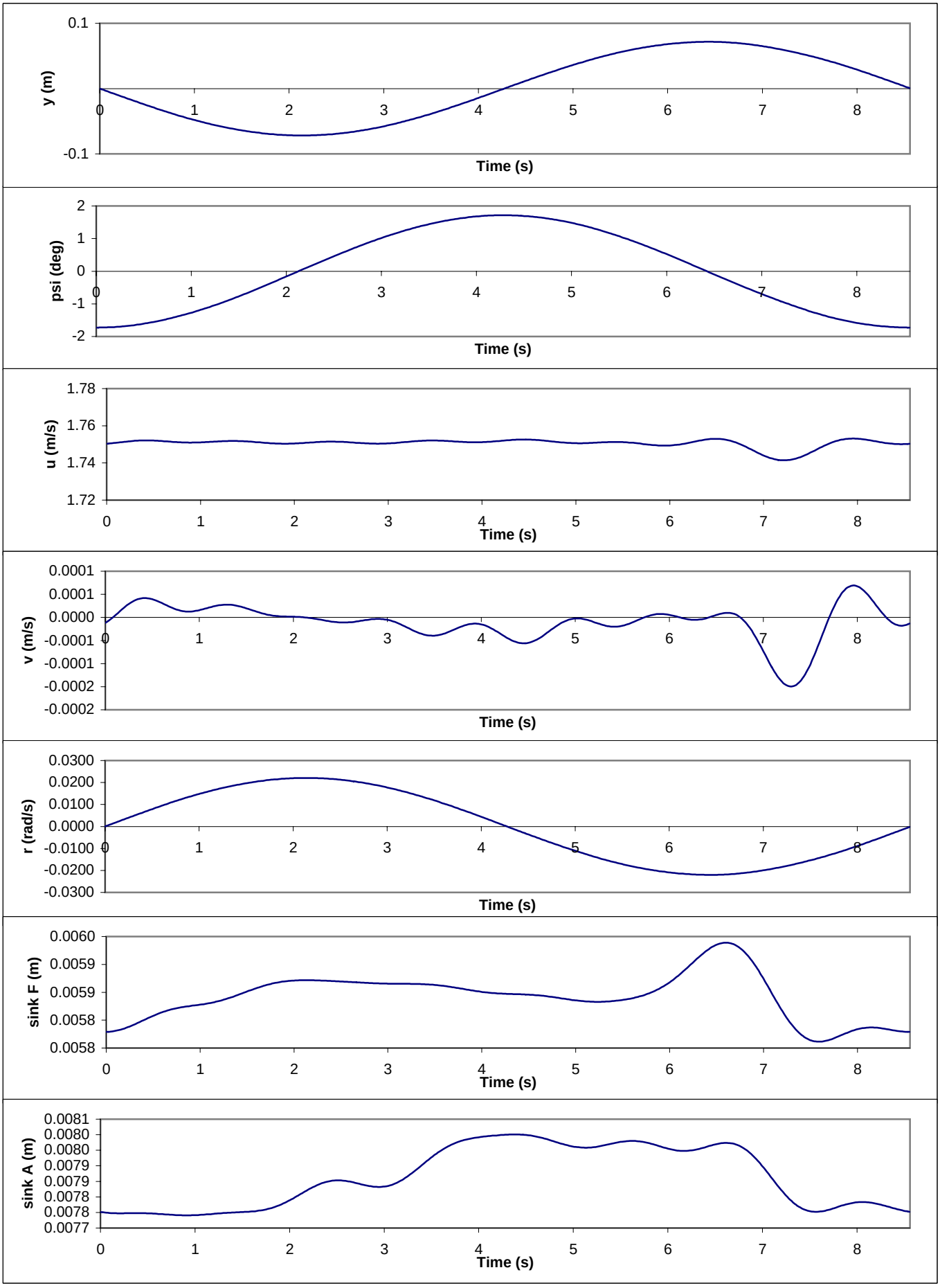

plot of timeseries 1071

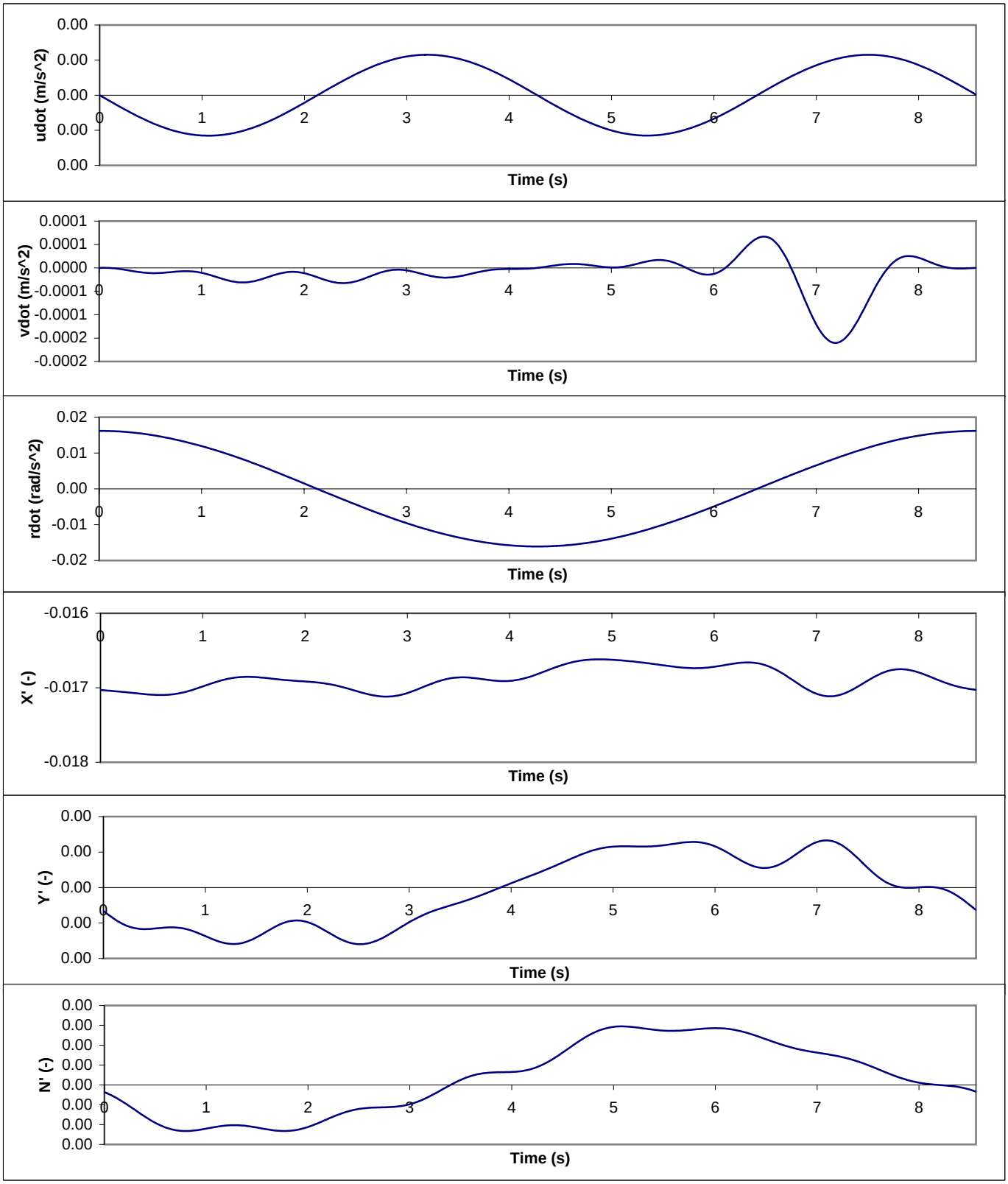
udot (m/s^2)
0.00
0.00
0.00
0.00
0.00
0 1 2 3 4 5 6 7 8
Time (s)
vdot (m/s^2)
0.0001
0.0001
0.0000
-0.0001
-0.0001
-0.0002
-0.0002
0 1 2 3 4 5 6 7 8
Time (s)
rdot (rad/s^2)
0.02
0.01
0.00
-0.01
-0.02
0 1 2 3 4 5 6 7 8
Time (s)
X' (-)
-0.016
-0.017
-0.018
0 1 2 3 4 5 6 7 8
Time (s)
Y' (-)
0.00
0.00
0.00
0.00
0.00
0 1 2 3 4 5 6 7 8
Time (s)
N' (-)
0.00
0.00
0.00
0.00
0.00
0.00
0.00
0.00
0 1 2 3 4 5 6 7 8
Time (s)

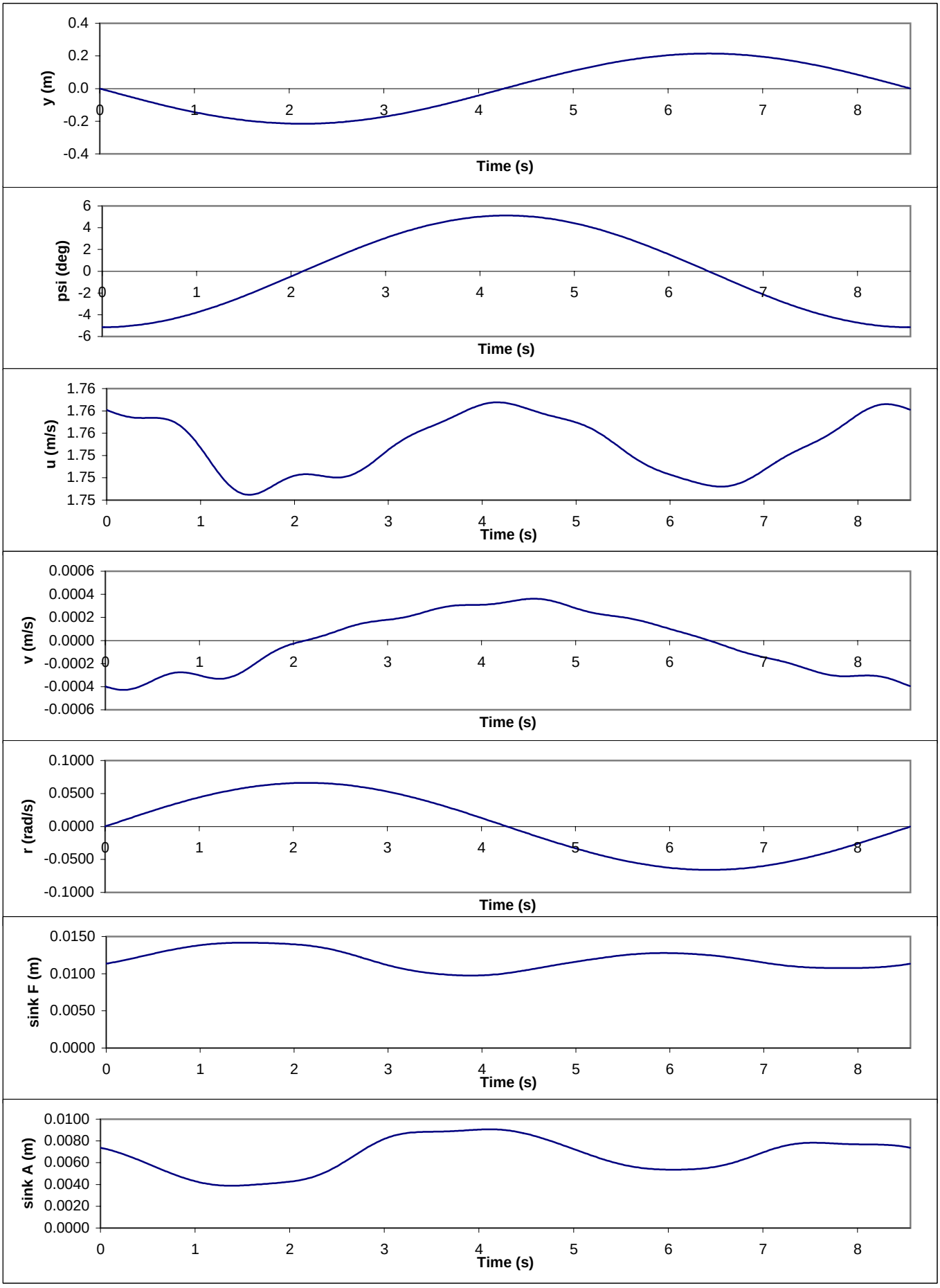
y (m)
0.4
0.2
0.0
-0.2
-0.4
0 1 2 3 4 5 6 7 8
Time (s)
psi (deg)
6
4
2
0
-2
-4
-6
0 1 2 3 4 5 6 7 8
Time (s)
u (m/s)
1.76
1.76
1.76
1.75
1.75
1.75
0 1 2 3 4 5 6 7 8
Time (s)
v (m/s)
0.0006
0.0004
0.0002
0.0000
-0.0002
-0.0004
-0.0006
0 1 2 3 4 5 6 7 8
Time (s)
r (rad/s)
0.1000
0.0500
0.0000
-0.0500
-0.1000
0 1 2 3 4 5 6 7 8
Time (s)
sink F (m)
0.0150
0.0100
0.0050
0.0000
0 1 2 3 4 5 6 7 8
Time (s)
sink A (m)
0.0100
0.0080
0.0060
0.0040
0.0020
0.0000
0 1 2 3 4 5 6 7 8
Time (s)

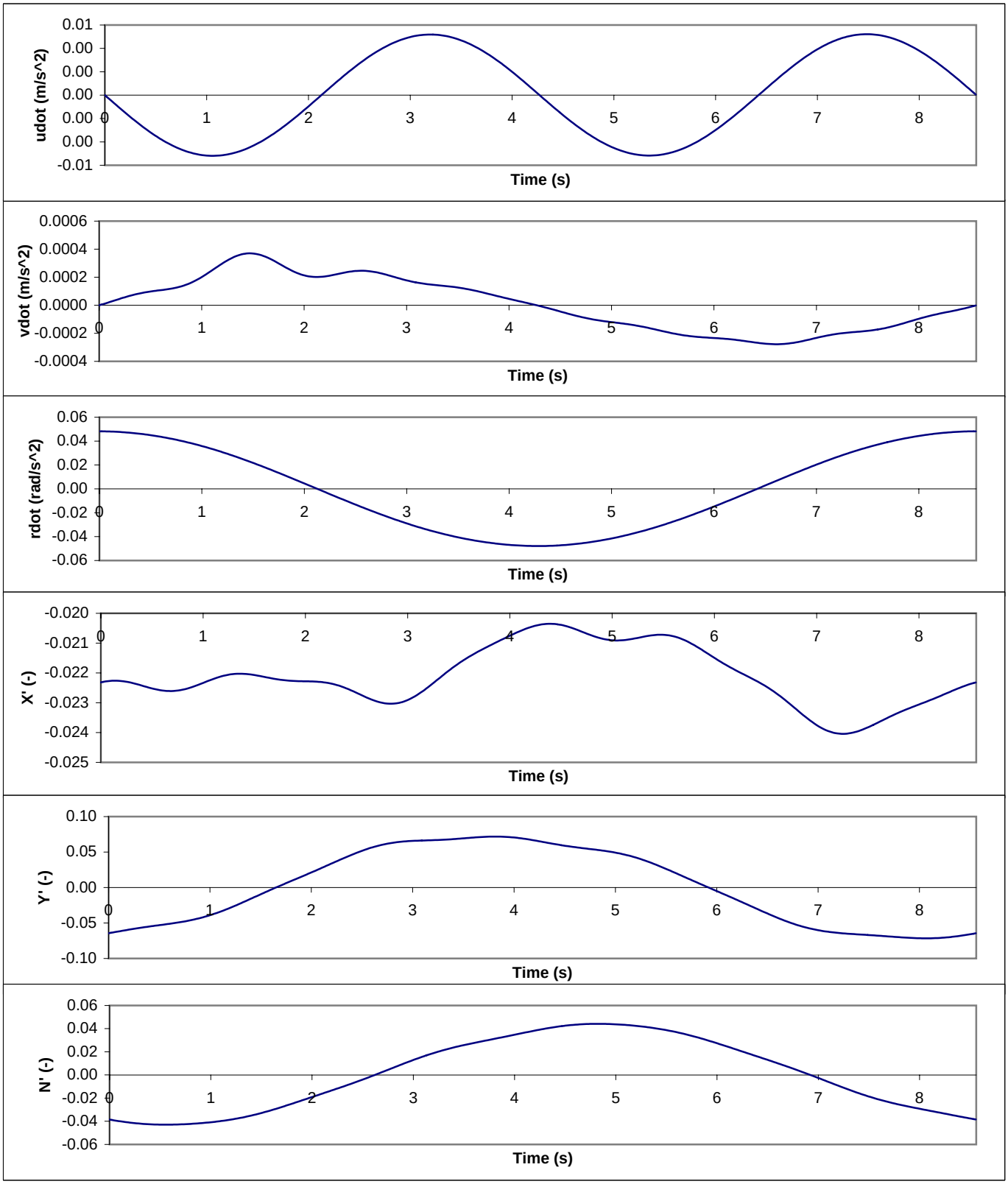
udot (m/s^2)
0.01
0.00
0.00
0.00
0.00
0.00
-0.01
0 1 2 3 4 5 6 7 8
Time (s)
vdot (m/s^2)
0.0006
0.0004
0.0002
0.0000
-0.0002
-0.0004
0 1 2 3 4 5 6 7 8
Time (s)
rdot (rad/s^2)
0.06
0.04
0.02
0.00
-0.02
-0.04
-0.06
0 1 2 3 4 5 6 7 8
Time (s)
X' (-)
-0.020
-0.021
-0.022
-0.023
-0.024
-0.025
0 1 2 3 4 5 6 7 8
Time (s)
Y' (-)
0.10
0.05
0.00
-0.05
-0.10
0 1 2 3 4 5 6 7 8
Time (s)
N' (-)
0.06
0.04
0.02
0.00
-0.02
-0.04
-0.06
0 1 2 3 4 5 6 7 8
Time (s)

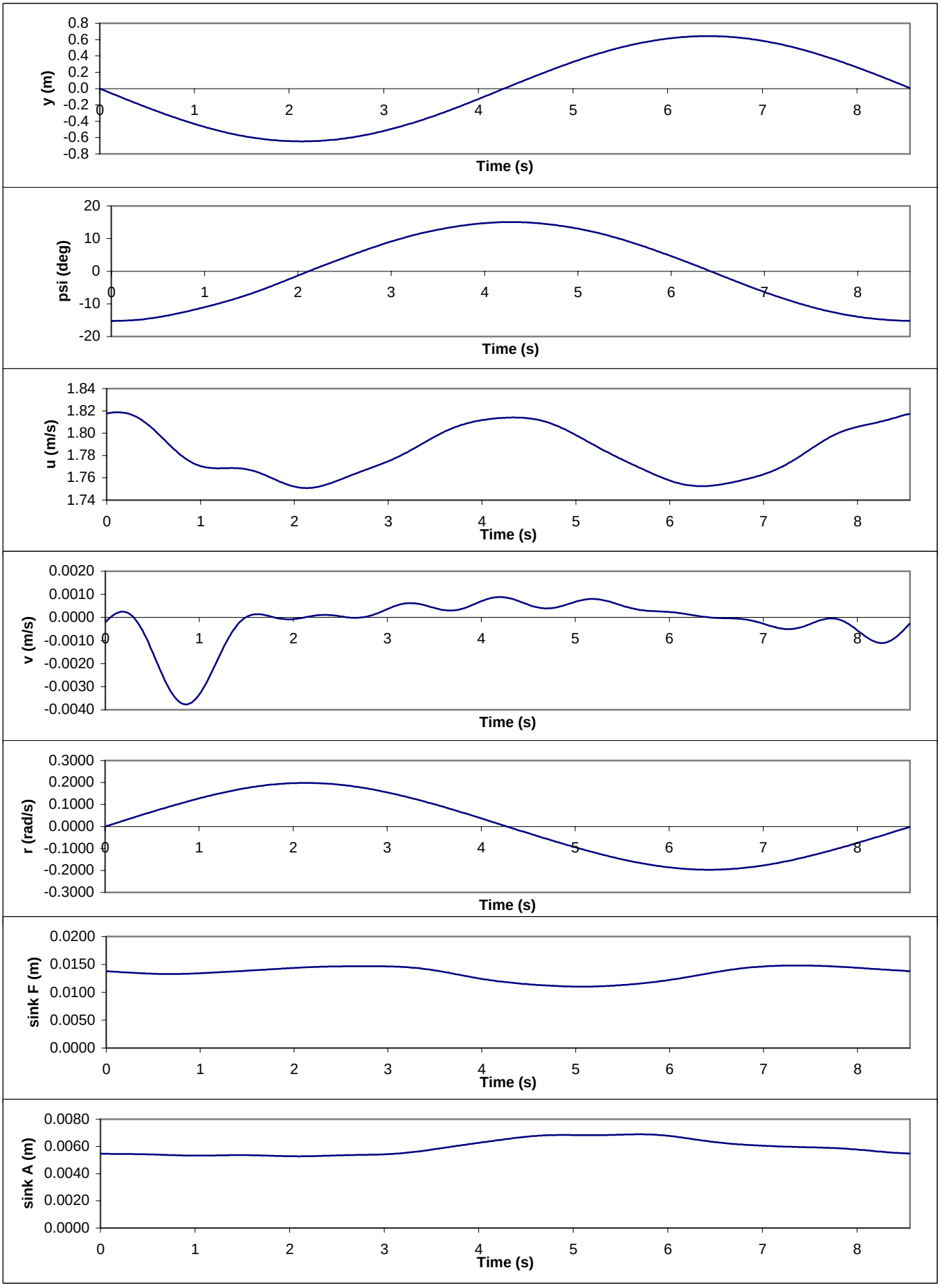
y (m)
0.8
0.6
0.4
0.2
0.0
-0.2
-0.4
-0.6
-0.8
0 1 2 3 4 5 6 7 8
Time (s)
psi (deg)
20
10
0
-10
-20
0 1 2 3 4 5 6 7 8
Time (s)
u (m/s)
1.84
1.82
1.80
1.78
1.76
1.74
0 1 2 3 4 5 6 7 8
Time (s)
v (m/s)
0.0020
0.0010
0.0000
-0.0010
-0.0020
-0.0030
-0.0040
0 1 2 3 4 5 6 7 8
Time (s)
r (rad/s)
0.3000
0.2000
0.1000
0.0000
-0.1000
-0.2000
-0.3000
0 1 2 3 4 5 6 7 8
Time (s)
sink F (m)
0.0200
0.0150
0.0100
0.0050
0.0000
0 1 2 3 4 5 6 7 8
Time (s)
sink A (m)
0.0080
0.0060
0.0040
0.0020
0.0000
0 1 2 3 4 5 6 7 8
Time (s)

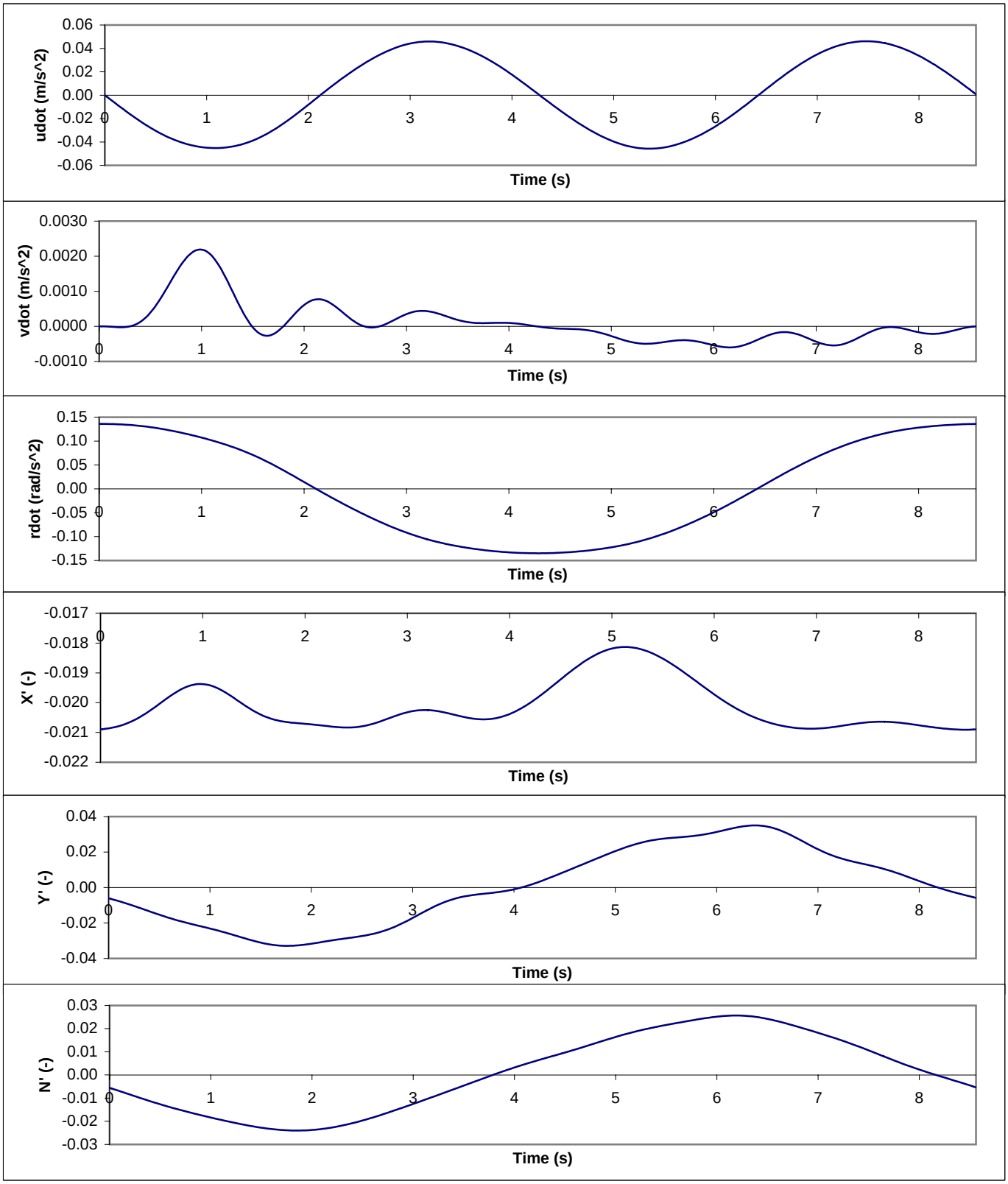
udot (m/s^2)
0.06
0.04
0.02
0.00
-0.02
-0.04
-0.06
0 1 2 3 4 5 6 7 8
Time (s)
vdot (m/s^2)
0.0030
0.0020
0.0010
0.0000
-0.0010
0 1 2 3 4 5 6 7 8
Time (s)
rdot (rad/s^2)
0.15
0.10
0.05
0.00
-0.05
-0.10
-0.15
0 1 2 3 4 5 6 7 8
Time (s)
X' (-)
-0.017
-0.018
-0.019
-0.020
-0.021
-0.022
0 1 2 3 4 5 6 7 8
Time (s)
Y' (-)
0.04
0.02
0.00
-0.02
-0.04
0 1 2 3 4 5 6 7 8
Time (s)
N' (-)
0.03
0.02
0.01
0.00
-0.01
-0.02
-0.03
0 1 2 3 4 5 6 7 8
Time (s)

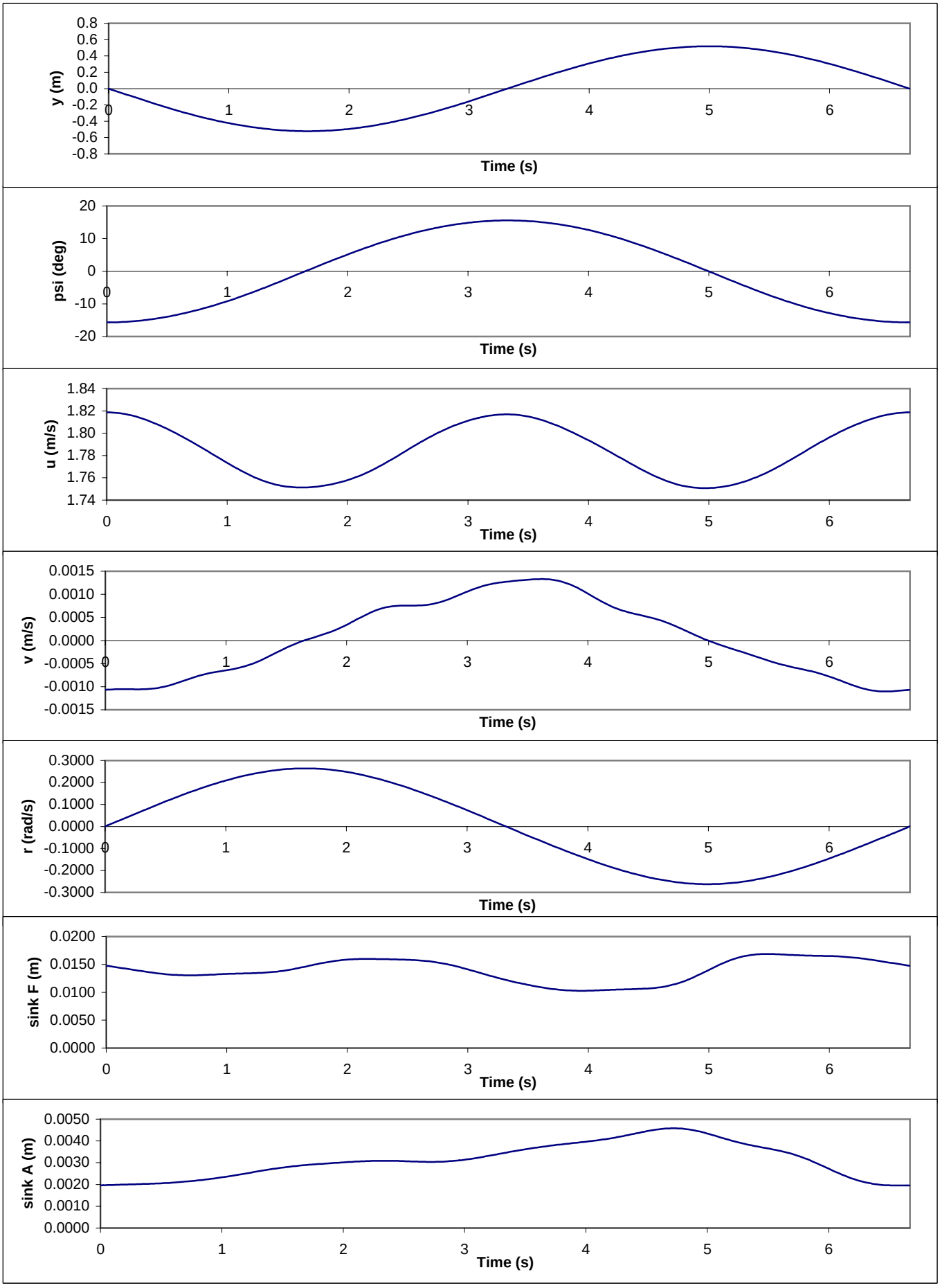
y (m)
0.8
0.6
0.4
0.2
0.0
-0.2
-0.4
-0.6
-0.8
0 1 2 3 4 5 6
Time (s)
psi (deg)
20
10
0
-10
-20
0 1 2 3 4 5 6
Time (s)
u (m/s)
1.84
1.82
1.80
1.78
1.76
1.74
0 1 2 3 4 5 6
Time (s)
v (m/s)
0.0015
0.0010
0.0005
0.0000
-0.0005
-0.0010
-0.0015
0 1 2 3 4 5 6
Time (s)
r (rad/s)
0.3000
0.2000
0.1000
0.0000
-0.1000
-0.2000
-0.3000
0 1 2 3 4 5 6
Time (s)
sink F (m)
0.0200
0.0150
0.0100
0.0050
0.0000
0 1 2 3 4 5 6
Time (s)
sink A (m)
0.0050
0.0040
0.0030
0.0020
0.0010
0.0000
0 1 2 3 4 5 6
Time (s)

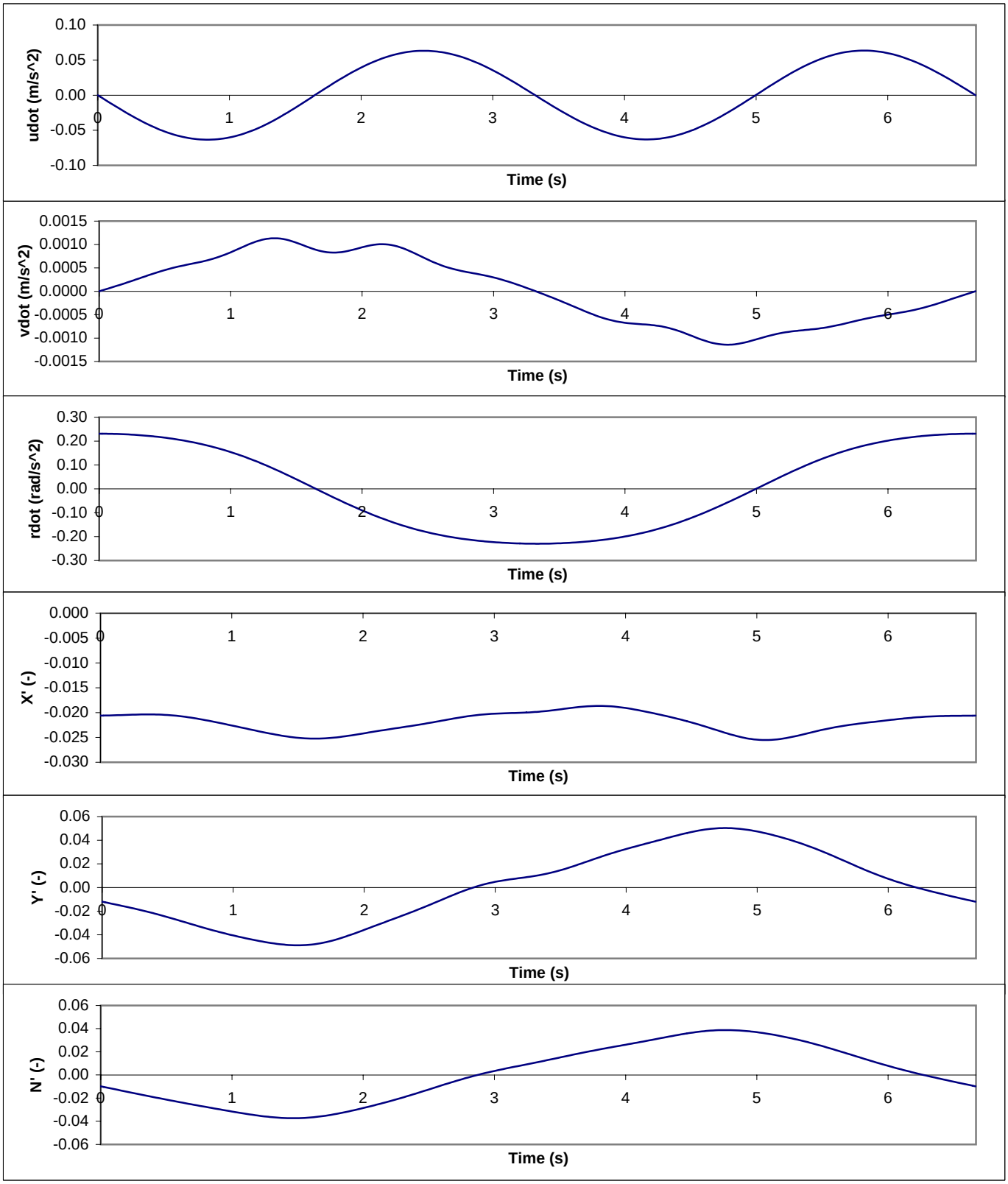
udot (m/s^2)
0.10
0.05
0.00
-0.05
-0.10
0
1
2
3
4
5
6
Time (s)
vdot (m/s^2)
0.0015
0.0010
0.0005
0.0000
-0.0005
-0.0010
-0.0015
Time (s)
rdot (rad/s^2)
0.30
0.20
0.10
0.00
-0.10
-0.20
-0.30
Time (s)
X' (-)
0.000
-0.005
-0.010
-0.015
-0.020
-0.025
-0.030
Time (s)
Y' (-)
0.06
0.04
0.02
0.00
-0.02
-0.04
-0.06
Time (s)
N' (-)
0.06
0.04
0.02
0.00
-0.02
-0.04
-0.06
Time (s)

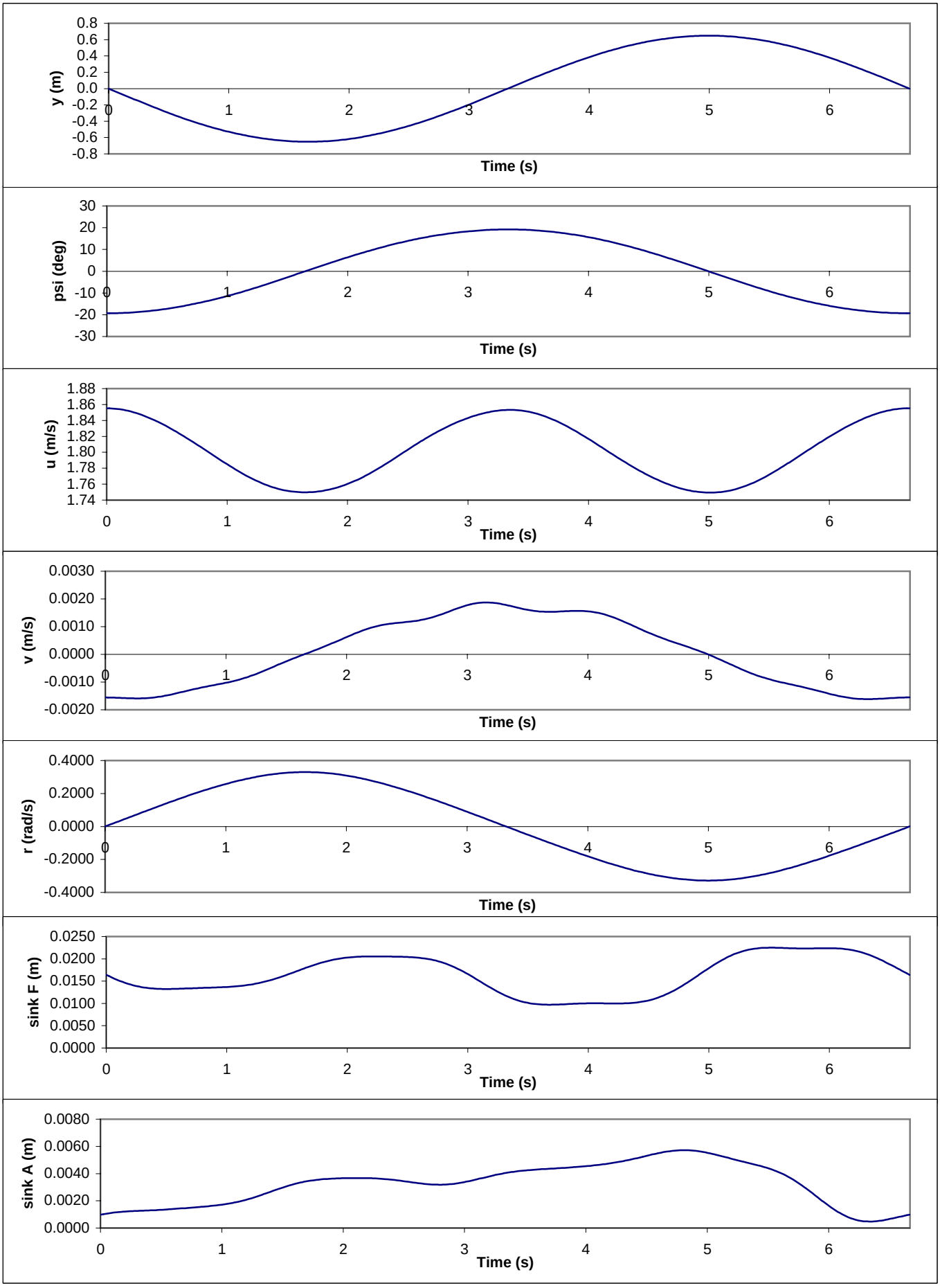
y (m)
0.8
0.6
0.4
0.2
0.0
-0.2
-0.4
-0.6
-0.8
0 1 2 3 4 5 6
Time (s)
psi (deg)
30
20
10
0
-10
-20
-30
0 1 2 3 4 5 6
Time (s)
u (m/s)
1.88
1.86
1.84
1.82
1.80
1.78
1.76
1.74
0 1 2 3 4 5 6
Time (s)
v (m/s)
0.0030
0.0020
0.0010
0.0000
-0.0010
-0.0020
0 1 2 3 4 5 6
Time (s)
r (rad/s)
0.4000
0.2000
0.0000
-0.2000
-0.4000
0 1 2 3 4 5 6
Time (s)
sink F (m)
0.0250
0.0200
0.0150
0.0100
0.0050
0.0000
0 1 2 3 4 5 6
Time (s)
sink A (m)
0.0080
0.0060
0.0040
0.0020
0.0000
0 1 2 3 4 5 6
Time (s)

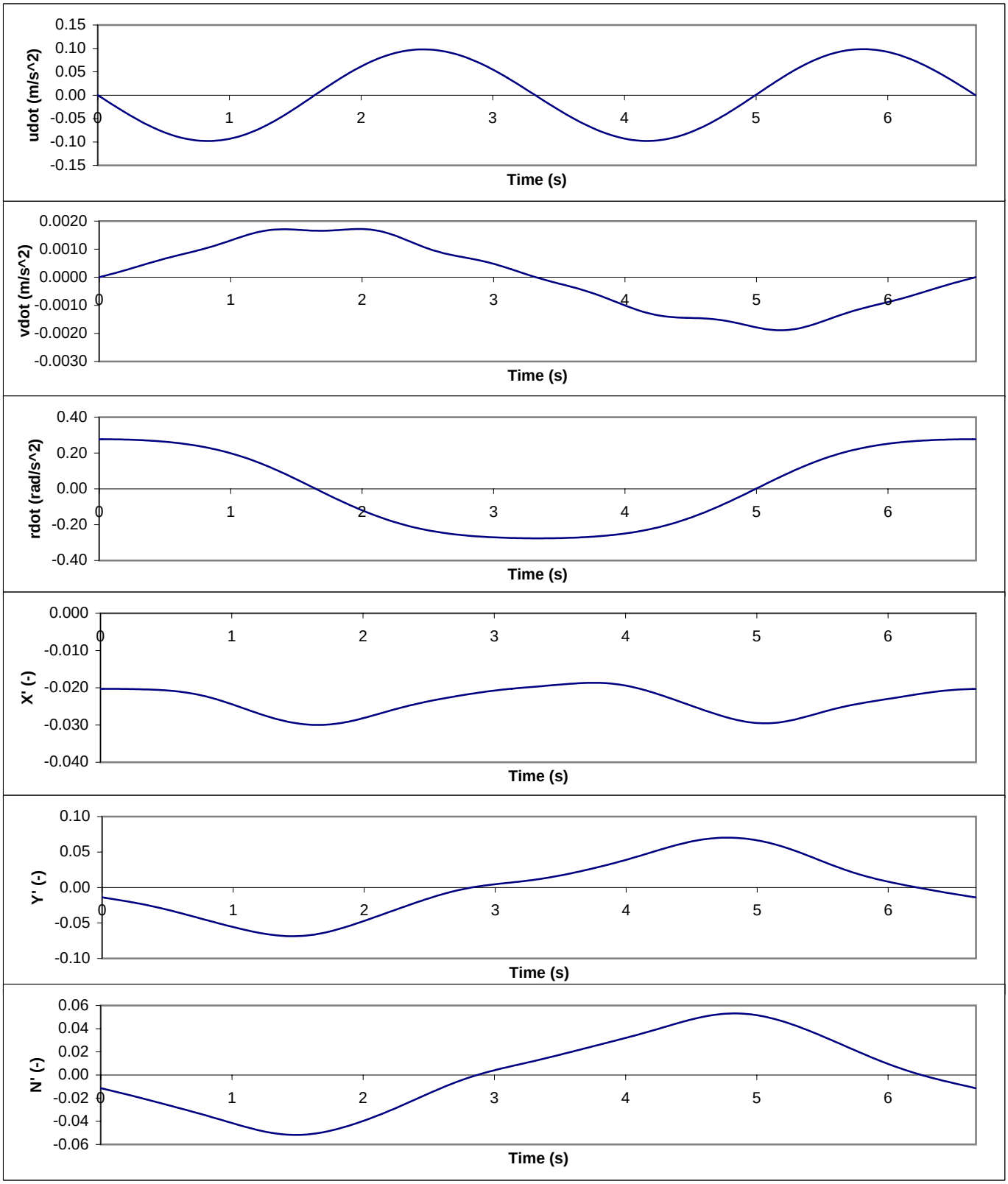
udot (m/s^2)
0.15
0.10
0.05
0.00
-0.05
-0.10
-0.15
0 1 2 3 4 5 6
Time (s)
vdot (m/s^2)
0.0020
0.0010
0.0000
-0.0010
-0.0020
-0.0030
0 1 2 3 4 5 6
Time (s)
rdot (rad/s^2)
0.40
0.20
0.00
-0.20
-0.40
0 1 2 3 4 5 6
Time (s)
X' (-)
0.000
-0.010
-0.020
-0.030
-0.040
0 1 2 3 4 5 6
Time (s)
Y' (-)
0.10
0.05
0.00
-0.05
-0.10
0 1 2 3 4 5 6
Time (s)
N' (-)
0.06
0.04
0.02
0.00
-0.02
-0.04
-0.06
0 1 2 3 4 5 6
Time (s)

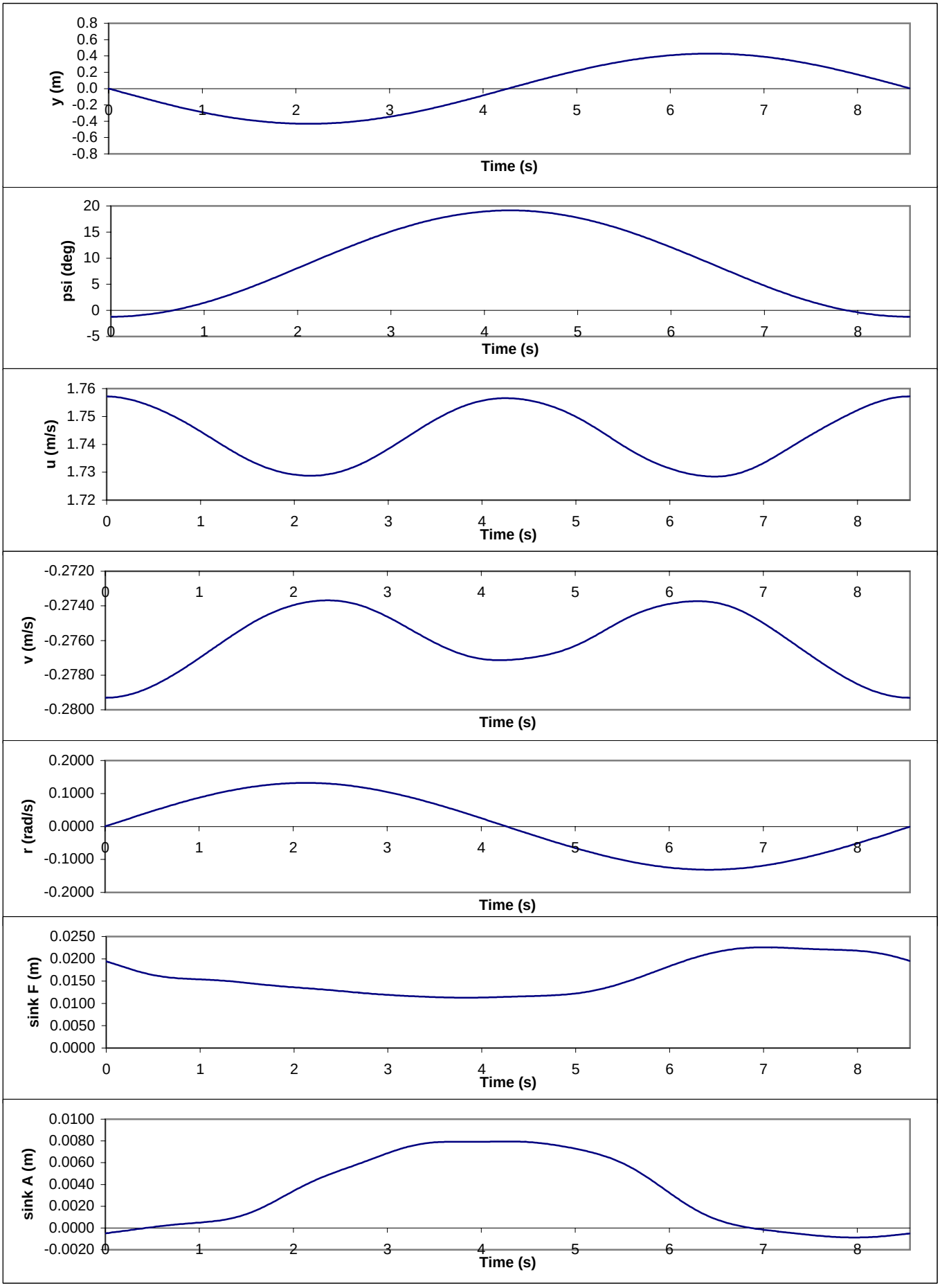
y (m)
0.8
0.6
0.4
0.2
0.0
-0.2
-0.4
-0.6
-0.8
0 1 2 3 4 5 6 7 8
Time (s)
psi (deg)
20
15
10
5
0
-5
0 1 2 3 4 5 6 7 8
Time (s)
u (m/s)
1.76
1.75
1.74
1.73
1.72
0 1 2 3 4 5 6 7 8
Time (s)
v (m/s)
-0.2720
-0.2740
-0.2760
-0.2780
-0.2800
0 1 2 3 4 5 6 7 8
Time (s)
r (rad/s)
0.2000
0.1000
0.0000
-0.1000
-0.2000
0 1 2 3 4 5 6 7 8
Time (s)
sink F (m)
0.0250
0.0200
0.0150
0.0100
0.0050
0.0000
0 1 2 3 4 5 6 7 8
Time (s)
sink A (m)
0.0100
0.0080
0.0060
0.0040
0.0020
0.0000
-0.0020
0 1 2 3 4 5 6 7 8
Time (s)

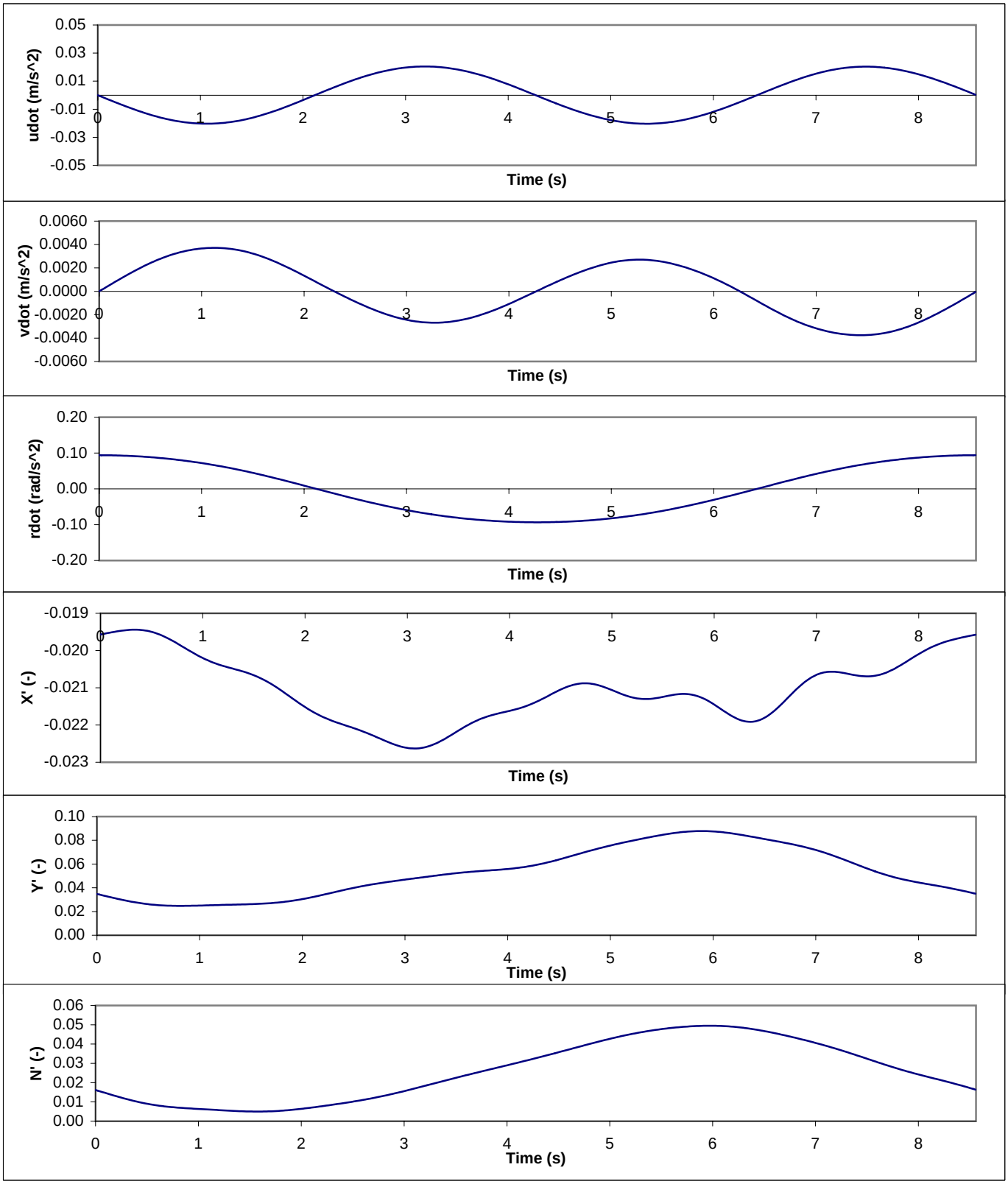
udot (m/s^2)
0.05
0.03
0.01
-0.01
-0.03
-0.05
0 1 2 3 4 5 6 7 8
Time (s)
vdot (m/s^2)
0.0060
0.0040
0.0020
0.0000
-0.0020
-0.0040
-0.0060
0 1 2 3 4 5 6 7 8
Time (s)
rdot (rad/s^2)
0.20
0.10
0.00
-0.10
-0.20
0 1 2 3 4 5 6 7 8
Time (s)
X' (-)
-0.019
-0.020
-0.021
-0.022
-0.023
0 1 2 3 4 5 6 7 8
Time (s)
Y' (-)
0.10
0.08
0.06
0.04
0.02
0.00
0 1 2 3 4 5 6 7 8
Time (s)
N' (-)
0.06
0.05
0.04
0.03
0.02
0.01
0.00
0 1 2 3 4 5 6 7 8
Time (s)

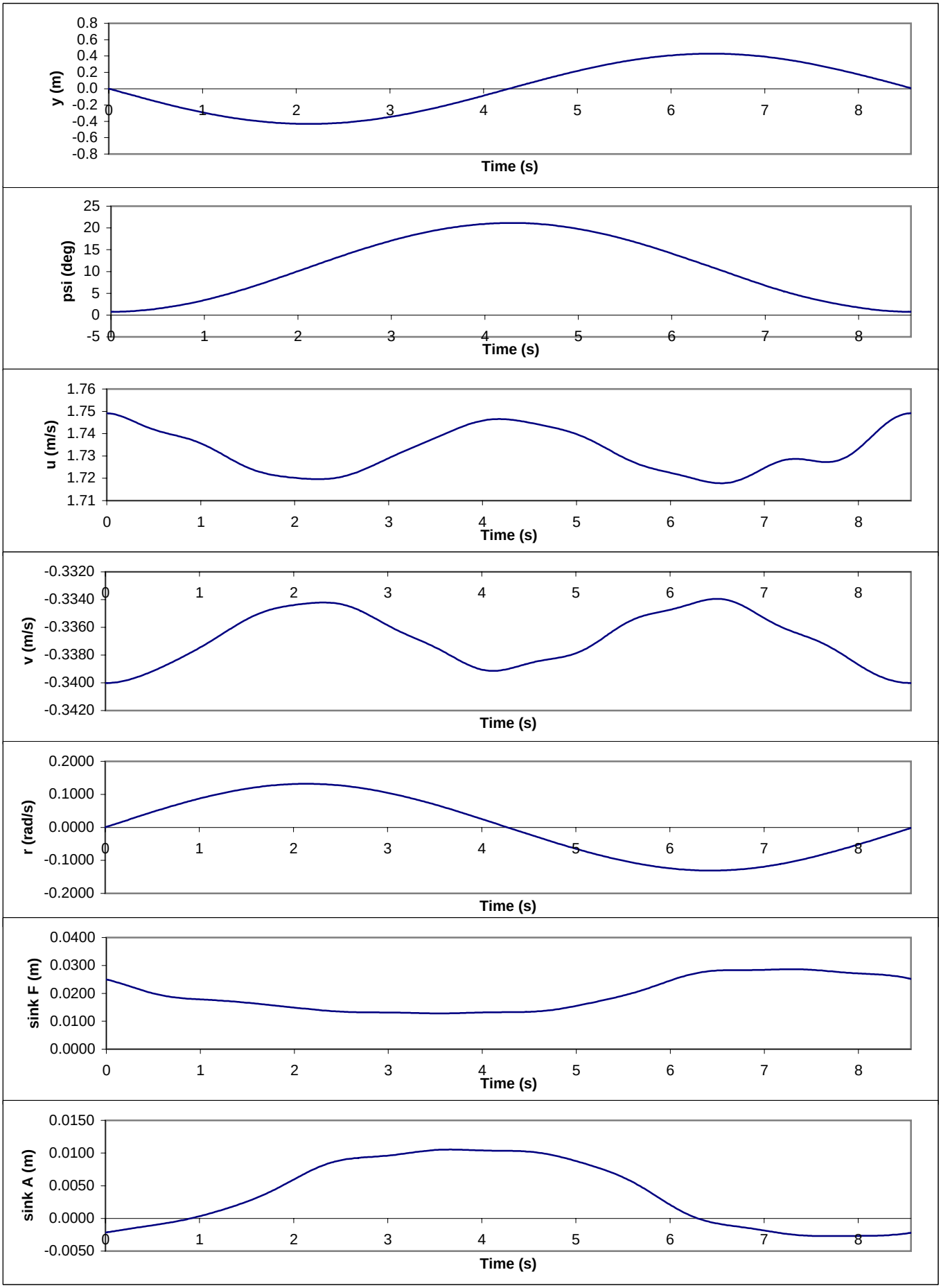
y (m)
0.8
0.6
0.4
0.2
0.0
-0.2
-0.4
-0.6
-0.8
0 1 2 3 4 5 6 7 8
Time (s)
psi (deg)
25
20
15
10
5
0
-5
0 1 2 3 4 5 6 7 8
Time (s)
u (m/s)
1.76
1.75
1.74
1.73
1.72
1.71
0 1 2 3 4 5 6 7 8
Time (s)
v (m/s)
-0.3320
-0.3340
-0.3360
-0.3380
-0.3400
-0.3420
0 1 2 3 4 5 6 7 8
Time (s)
r (rad/s)
0.2000
0.1000
0.0000
-0.1000
-0.2000
0 1 2 3 4 5 6 7 8
Time (s)
sink F (m)
0.0400
0.0300
0.0200
0.0100
0.0000
0 1 2 3 4 5 6 7 8
Time (s)
sink A (m)
0.0150
0.0100
0.0050
0.0000
-0.0050
0 1 2 3 4 5 6 7 8
Time (s)

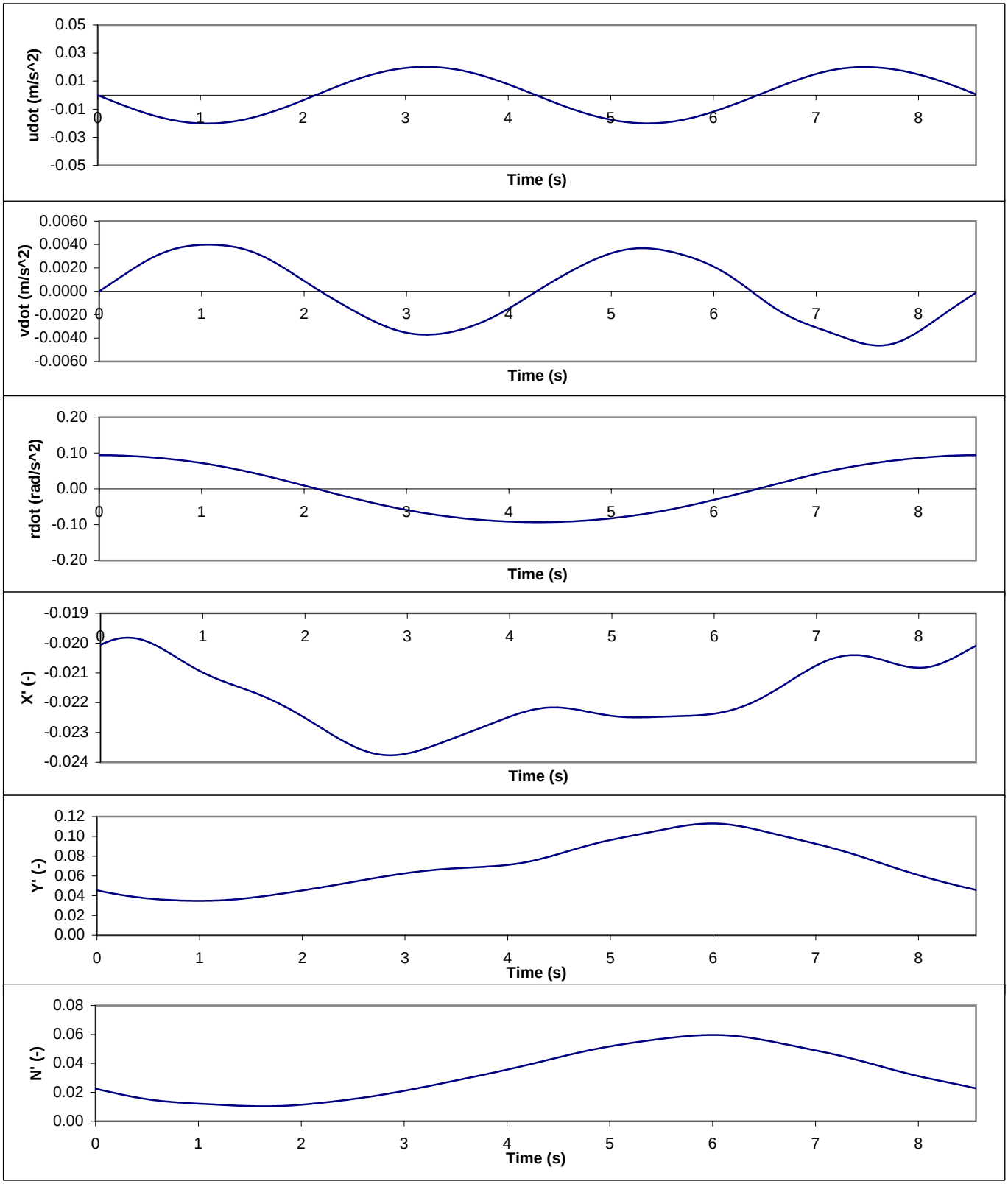
udot (m/s^2)
0.05
0.03
0.01
-0.01
-0.03
-0.05
0 1 2 3 4 5 6 7 8
Time (s)
vdot (m/s^2)
0.0060
0.0040
0.0020
0.0000
-0.0020
-0.0040
-0.0060
0 1 2 3 4 5 6 7 8
Time (s)
rdot (rad/s^2)
0.20
0.10
0.00
-0.10
-0.20
0 1 2 3 4 5 6 7 8
Time (s)
X' (-)
-0.019
-0.020
-0.021
-0.022
-0.023
-0.024
0 1 2 3 4 5 6 7 8
Time (s)
Y' (-)
0.12
0.10
0.08
0.06
0.04
0.02
0.00
0 1 2 3 4 5 6 7 8
Time (s)
N' (-)
0.08
0.06
0.04
0.02
0.00
0 1 2 3 4 5 6 7 8
Time (s)

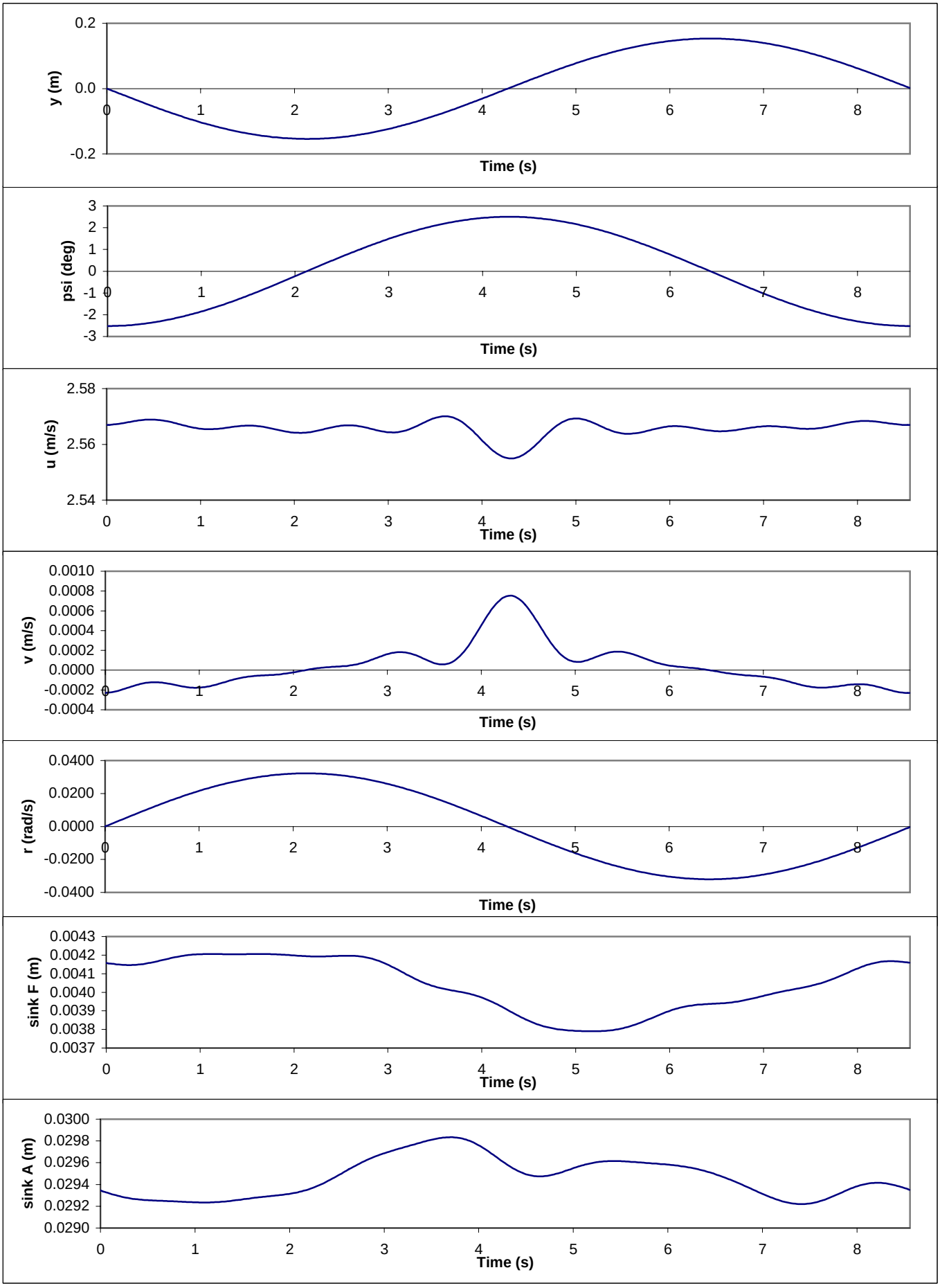
y (m)
0.2
0.0
-0.2
0 1 2 3 4 5 6 7 8
Time (s)
psi (deg)
3 2 1 0 -1 -2 -3
0 1 2 3 4 5 6 7 8
Time (s)
u (m/s)
2.58
2.56
2.54
0 1 2 3 4 5 6 7 8
Time (s)
v (m/s)
0.0010 0.0008 0.0006 0.0004 0.0002 0.0000 -0.0002 -0.0004
0 1 2 3 4 5 6 7 8
Time (s)
r (rad/s)
0.0400 0.0200 0.0000 -0.0200 -0.0400
0 1 2 3 4 5 6 7 8
Time (s)
sink F (m)
0.0043 0.0042 0.0041 0.0040 0.0039 0.0038 0.0037
0 1 2 3 4 5 6 7 8
Time (s)
sink A (m)
0.0300 0.0298 0.0296 0.0294 0.0292 0.0290
0 1 2 3 4 5 6 7 8
Time (s)

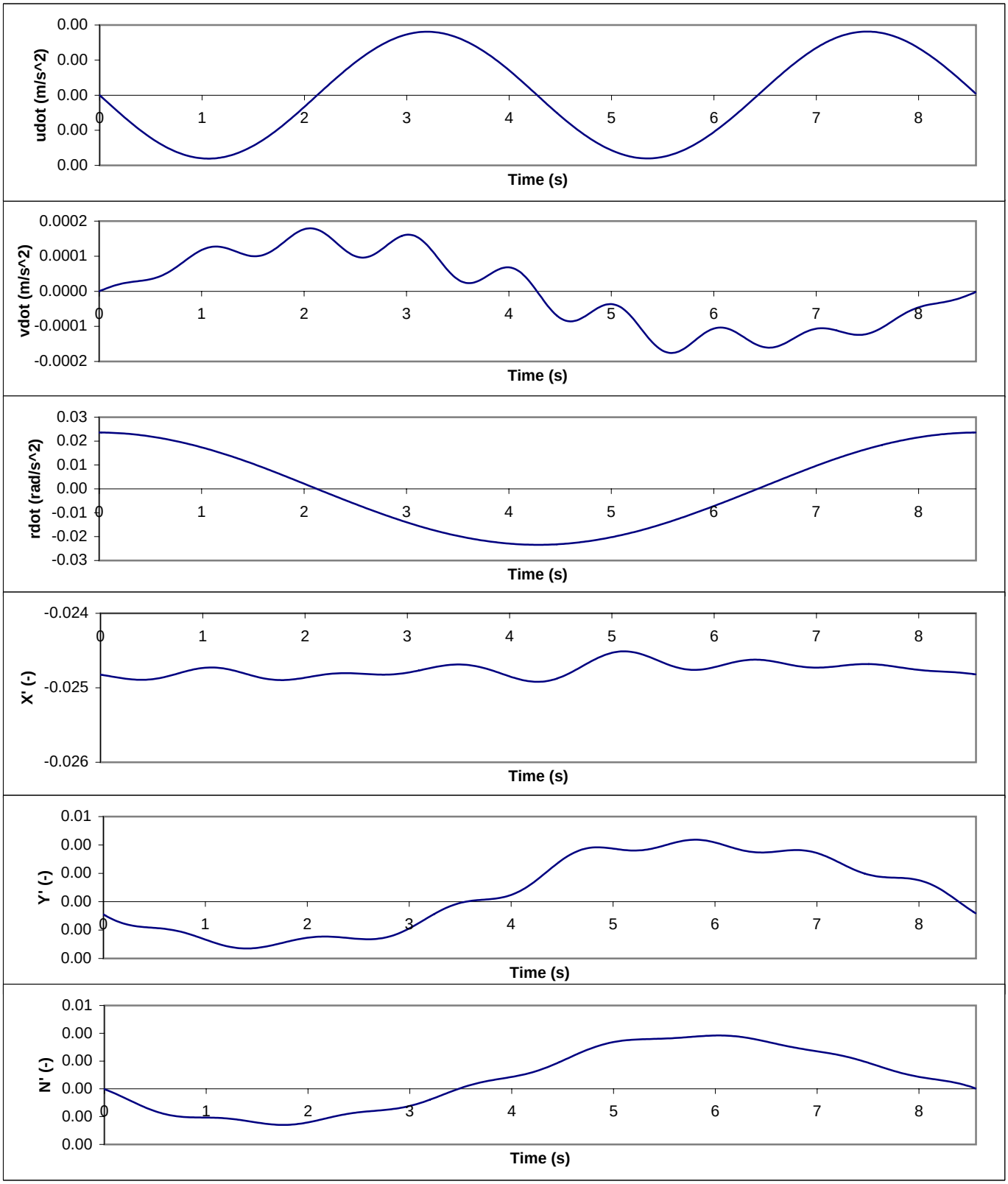
udot (m/s^2)
0.00
0.00
0.00
0.00
0.00
0 1 2 3 4 5 6 7 8
Time (s)
vdot (m/s^2)
0.0002
0.0001
0.0000
-0.0001
-0.0002
0 1 2 3 4 5 6 7 8
Time (s)
rdot (rad/s^2)
0.03
0.02
0.01
0.00
-0.01
-0.02
-0.03
0 1 2 3 4 5 6 7 8
Time (s)
X' (-)
-0.024
-0.025
-0.026
0 1 2 3 4 5 6 7 8
Time (s)
Y' (-)
0.01
0.00
0.00
0.00
0.00
0 1 2 3 4 5 6 7 8
Time (s)
N' (-)
0.01
0.00
0.00
0.00
0.00
0 1 2 3 4 5 6 7 8
Time (s)

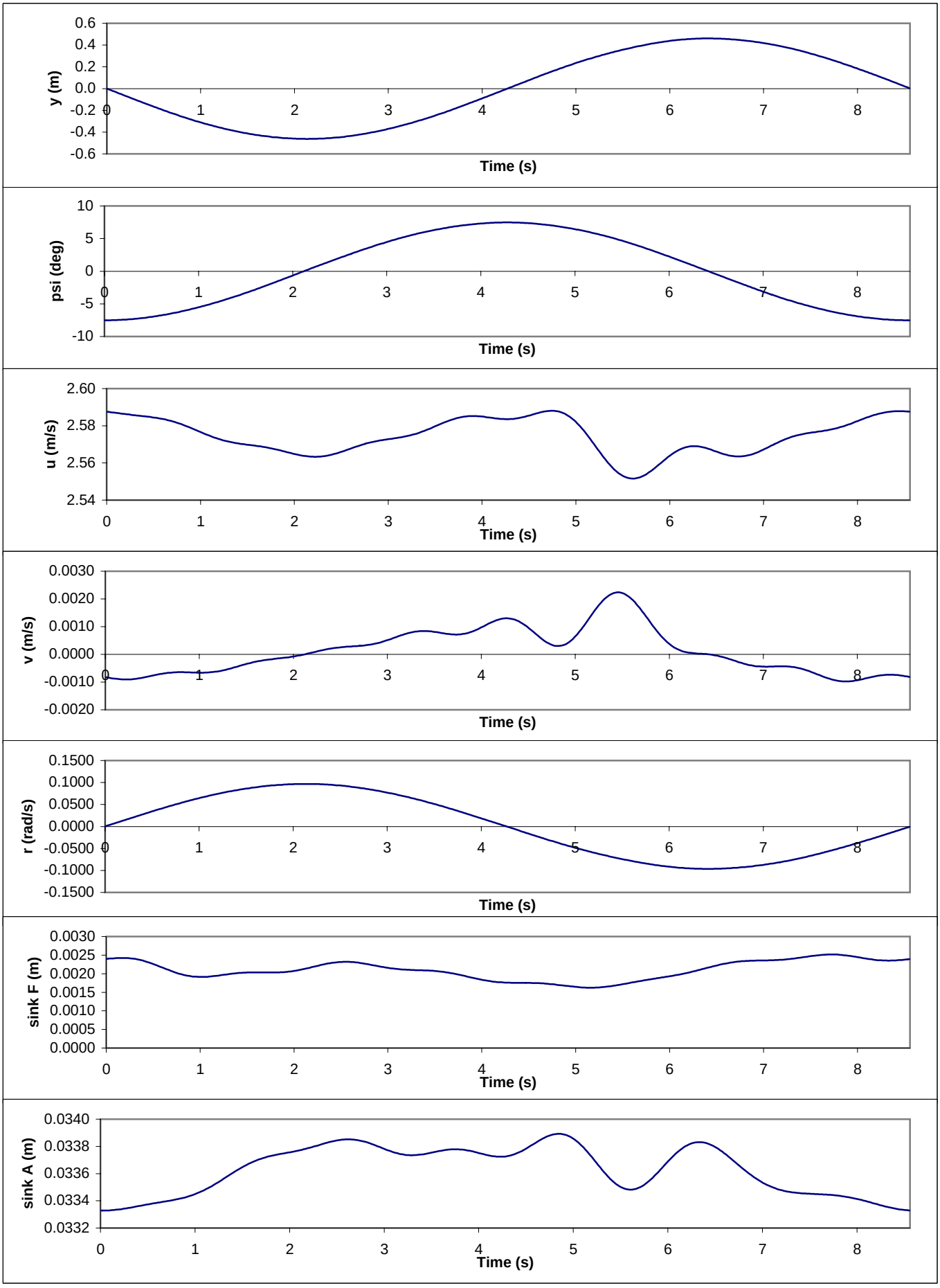
y (m)
0.6
0.4
0.2
0.0
-0.2
-0.4
-0.6
0 1 2 3 4 5 6 7 8
Time (s)
psi (deg)
10
5
0
-5
-10
0 1 2 3 4 5 6 7 8
Time (s)
u (m/s)
2.60
2.58
2.56
2.54
0 1 2 3 4 5 6 7 8
Time (s)
v (m/s)
0.0030
0.0020
0.0010
0.0000
-0.0010
-0.0020
0 1 2 3 4 5 6 7 8
Time (s)
r (rad/s)
0.1500
0.1000
0.0500
0.0000
-0.0500
-0.1000
-0.1500
0 1 2 3 4 5 6 7 8
Time (s)
sink F (m)
0.0030
0.0025
0.0020
0.0015
0.0010
0.0005
0.0000
0 1 2 3 4 5 6 7 8
Time (s)
sink A (m)
0.0340
0.0338
0.0336
0.0334
0.0332
0 1 2 3 4 5 6 7 8
Time (s)

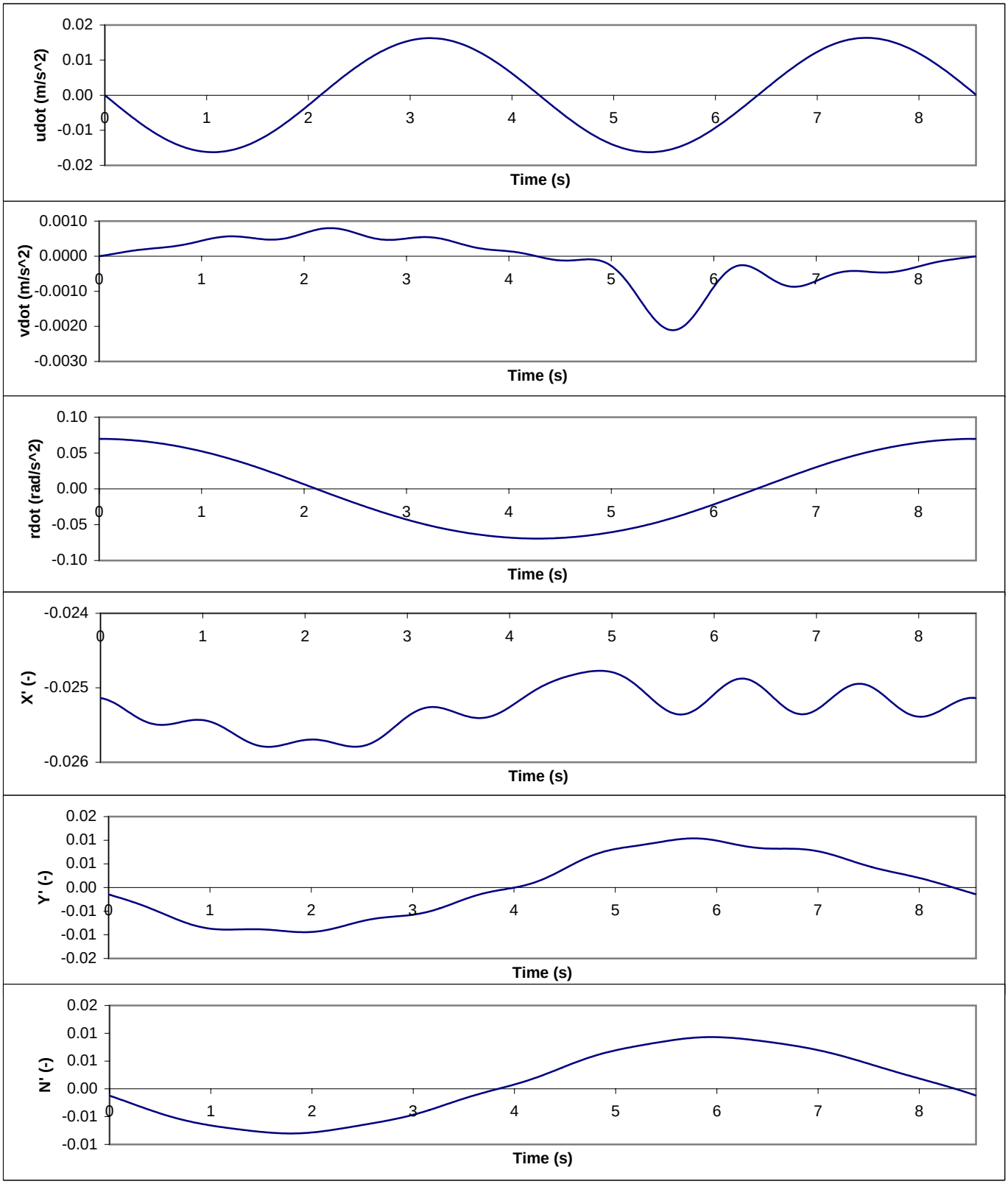
udot (m/s^2)
0.02
0.01
0.00
-0.01
-0.02
0 1 2 3 4 5 6 7 8
Time (s)
vdot (m/s^2)
0.0010
0.0000
-0.0010
-0.0020
-0.0030
0 1 2 3 4 5 6 7 8
Time (s)
rdot (rad/s^2)
0.10
0.05
0.00
-0.05
-0.10
0 1 2 3 4 5 6 7 8
Time (s)
X' (-)
-0.024
-0.025
-0.026
0 1 2 3 4 5 6 7 8
Time (s)
Y' (-)
0.02
0.01
0.01
0.00
-0.01
-0.01
-0.02
0 1 2 3 4 5 6 7 8
Time (s)
N' (-)
0.02
0.01
0.01
0.00
-0.01
-0.01
0 1 2 3 4 5 6 7 8
Time (s)

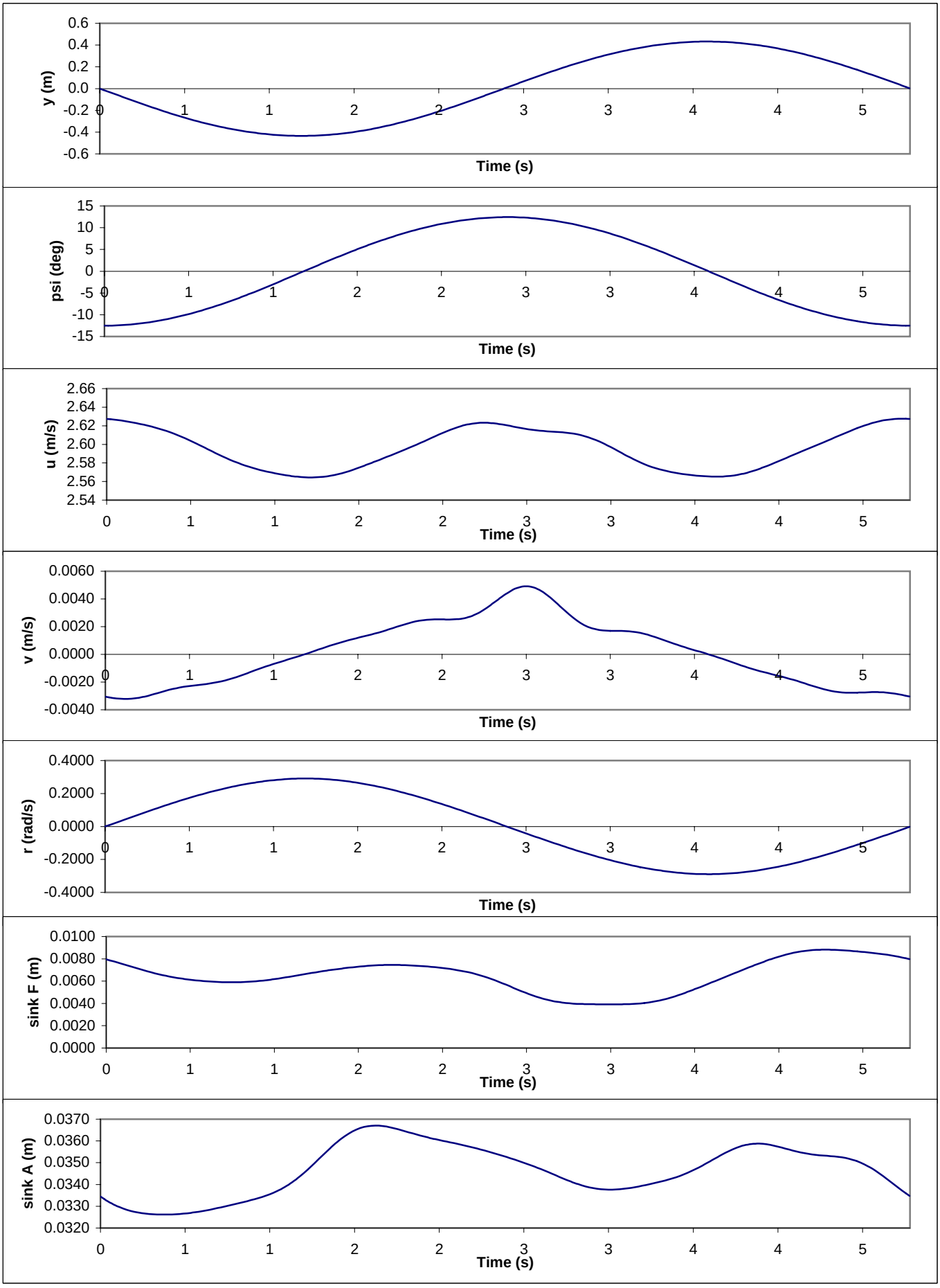
y (m)
0.6
0.4
0.2
0.0
-0.2
-0.4
-0.6
0 1 1 2 2 3 3 4 4 5
Time (s)
psi (deg)
15
10
5
0
-5
-10
-15
0 1 1 2 2 3 3 4 4 5
Time (s)
u (m/s)
2.66
2.64
2.62
2.60
2.58
2.56
2.54
0 1 1 2 2 3 3 4 4 5
Time (s)
v (m/s)
0.0060
0.0040
0.0020
0.0000
-0.0020
-0.0040
0 1 1 2 2 3 3 4 4 5
Time (s)
r (rad/s)
0.4000
0.2000
0.0000
-0.2000
-0.4000
0 1 1 2 2 3 3 4 4 5
Time (s)
sink F (m)
0.0100
0.0080
0.0060
0.0040
0.0020
0.0000
0 1 1 2 2 3 3 4 4 5
Time (s)
sink A (m)
0.0370
0.0360
0.0350
0.0340
0.0330
0.0320
0 1 1 2 2 3 3 4 4 5
Time (s)

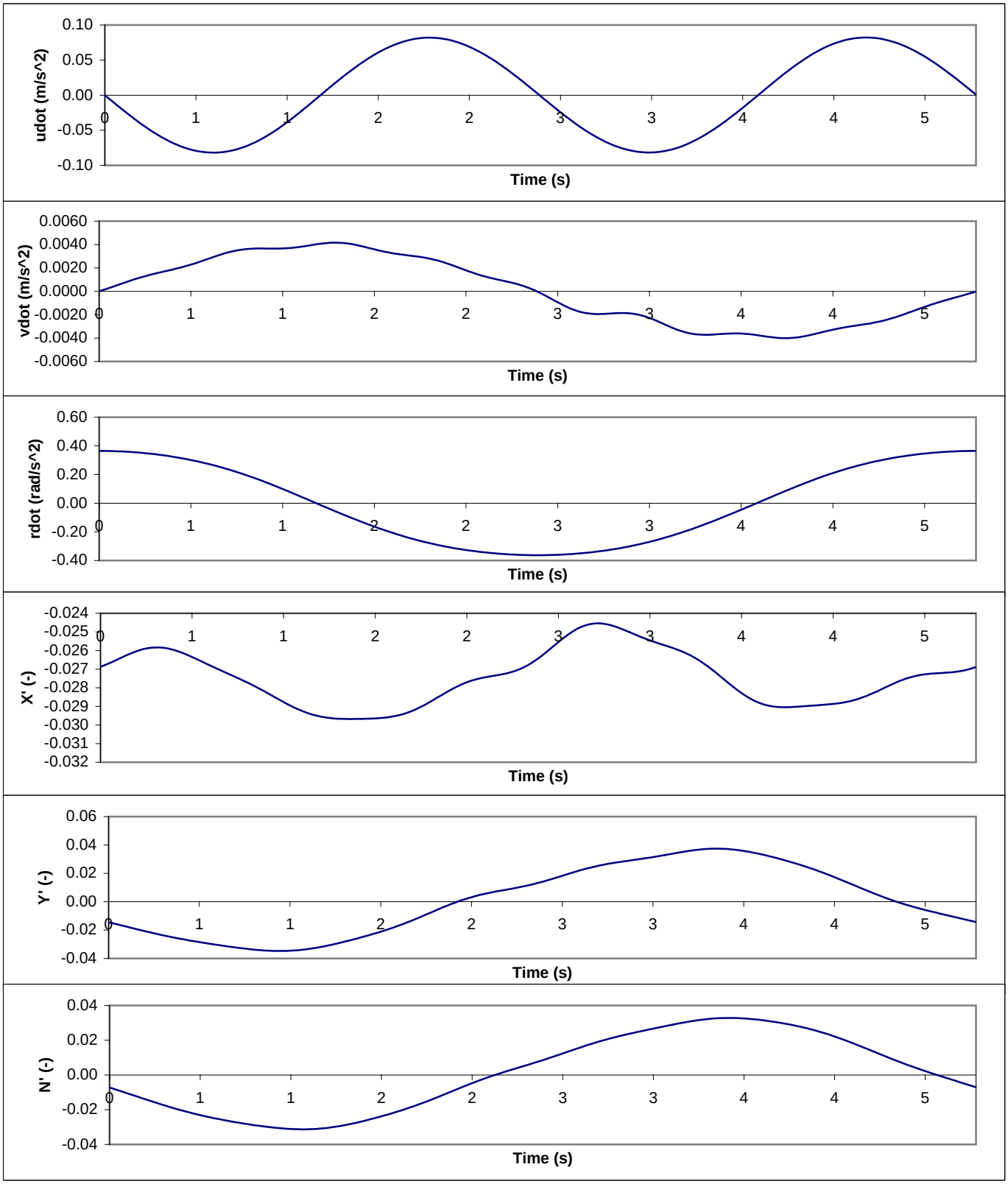
udot (m/s^2)
0.10
0.05
0.00
-0.05
-0.10
0 1 1 2 2 3 3 4 4 5
Time (s)
vdot (m/s^2)
0.0060
0.0040
0.0020
0.0000
-0.0020
-0.0040
-0.0060
0 1 1 2 2 3 3 4 4 5
Time (s)
rdot (rad/s^2)
0.60
0.40
0.20
0.00
-0.20
-0.40
0 1 1 2 2 3 3 4 4 5
Time (s)
X' (-)
-0.024
-0.025
-0.026
-0.027
-0.028
-0.029
-0.030
-0.031
-0.032
0 1 1 2 2 3 3 4 4 5
Time (s)
Y' (-)
0.06
0.04
0.02
0.00
-0.02
-0.04
0 1 1 2 2 3 3 4 4 5
Time (s)
N' (-)
0.04
0.02
0.00
-0.02
-0.04
0 1 1 2 2 3 3 4 4 5
Time (s)